PARTITIONING OF BIOMOLECULES IN TWO-PHASE AQUEOUS MICELLAR SYSTEMS

by

Chia-Li Liu

B.S., National Taiwan University, Taipei, Taiwan (1988)
M.S.C.E.P., Massachusetts Institute of Technology (1995)

Submitted to the Department of Chemical Engineering
in partial fulfillment of the requirements for the degree of

DOCTOR OF PHILOSOPHY IN CHEMICAL ENGINEERING

at the

MASSACHUSETTS INSTITUTE OF TECHNOLOGY

September 1995

Author .....
Department of Chemical Engineering
July 5, 1995

Certified by .....
Daniel Blankschtein
Associate Professor
Thesis Supervisor

Accepted by .....
Robert E. Cohen
Chairman, Committee for Graduate Students

PARTITIONING OF BIOMOLECULES IN TWO-PHASE AQUEOUS MICELLAR SYSTEMS

by

Chia-Li Liu

Submitted to the Department of Chemical Engineering
on July 5, 1995, in partial fulfillment of the
requirements for the degree of
DOCTOR OF PHILOSOPHY IN CHEMICAL ENGINEERING

Abstract

The work presented in this thesis constitutes the first systematic experimental, theoretical, and practical investigation on the partitioning of biomolecules (hydrophilic proteins and viruses) in two-phase aqueous micellar systems.

The partitioning behavior of five hydrophilic proteins (cytochrome c, soybean trypsin inhibitor, ovalbumin, bovine serum albumin, and catalase) in two-phase aqueous micellar systems, composed of the nonionic surfactant $C_{10}E_4$ or the zwitterionic surfactant C_8-lecithin, was investigated. The partition coefficients of these proteins, K_p, which is the ratio of the protein concentrations in the two coexisting micellar solution phases and constitutes a quantitative measure of the partitioning behavior, were found to be of order 1. The protein partitioning results suggested that the observed partitioning phenomenon is driven primarily by excluded-volume interactions between the partitioned biomolecules and the non-charged micelles. A theoretical formulation based on an excluded-volume description of micelle-protein interactions was developed, and the theoretically predicted partitioning behavior was found to be in good agreement with the experimental protein partitioning results.

The partitioning behavior of three bacteriophages (ϕX174, P22, T4) in the two-phase aqueous $C_{10}E_4$ micellar system was subsequently investigated, and the partition coefficients of these viruses, K_v, were found to be of order 10^{-3}, indicating the much more extreme partitioning behavior of virus particles as compared to that of proteins. A theoretical formulation, based on an excluded-volume description of the interactions between flexible micelles and virus particles, was developed. The theoretical description incorporated explicitly the effect of micellar flexibility on the virus partitioning behavior, since micellar flexibility is expected to play an important role in the case of large virus particles. The new theoretical formulation was found to over-predict the partitioning behavior of the larger virus particles examined when compared with the experimental virus partitioning results.

A preliminary investigation on possible kinetic aspects associated with the partitioning phenomenon revealed that the experimentally observed virus partitioning behavior may actually be complicated by kinetic effects, including the slow diffusion

of virus particles and the convection of the microscopic phase domains that form during phase separation. This may help explain the observed deviations between the theoretically predicted virus partition coefficients, which should represent a true thermodynamic equilibrium condition, and the experimentally measured virus partition coefficients.

The feasibility of utilizing two-phase aqueous micellar systems as a useful and practical separation or concentration method was investigated by simultaneously partitioning a protein (ovalbumin) and a virus (P22) in the two-phase aqueous $C_{10}E_4$ micellar system. It was found that, by manipulating the volume ratio of the two coexisting micellar phases, the desired separation or concentration efficiencies of these two biomolecules can be achieved.

Dynamic light scattering studies were conducted to investigate the underlying solution structure of the $C_{10}E_4$ aqueous micellar system. The crossover surfactant concentrations, X^*, denoting the transition of the micellar solution structure from the dilute to the semidilute (entangled) regimes, at various temperatures, T, were deduced from the light scattering results. The light scattering results also suggested that the solution structure of the two coexisting micellar phases in the two-phase aqueous $C_{10}E_4$ micellar system is very different, with the bottom (micelle-poor) phase containing individually dispersed micelles, and the top (micelle-rich) phase containing a transient mesh or net of interpenetrating micelles. This difference in the structure of the two coexisting micellar solution phases may play a role on the observed partitioning behavior of biomolecules in two-phase aqueous micellar systems of this type.

It is hoped that the encouraging results presented in this thesis will stimulate further fundamental as well as practical investigations on the partitioning of solute species (both of biological and non-biological origins) in two-phase aqueous micellar systems. This will lead to an improved understanding on how to better control, optimize, and exploit these fascinating systems as a novel practical methodology for the separation, concentration, and purification of biological and non-biological materials.

Thesis Supervisor: Daniel Blankschtein
Title: Associate Professor

Acknowledgements

I would like to thank my thesis advisor, Prof. Daniel Blankschtein, whose insight, intelligence, and abundant knowledge in the micellar and colloidal area were the most important guidance of this research. His enthusiasm towards research has inspired me to work hard and to achieve the best possible. His concern on students extends beyond scientific dialogues and into students' daily lives. I am lucky to have such a caring and understanding advisor to guide me through my Ph.D. research. He is indeed my mentor in all aspects, and in my heart, he is the role model of an advisor.

I am also grateful to my thesis committee members, including Prof. Charles L. Cooney, Prof. T. Alan Hatton, Prof. Jonathan A. King, and Prof. Daniel I.C. Wang, for their interest in this work. They gave many valuable ideas and generously assisted the progress of this work. Specifically, Prof. King provided viruses and bacteria for my partitioning experiments, and laboratory space for conducting the biological activity assay; Prof. Hatton kindly allowed me to use his UV spectrophotometer; and Prof. Wang recognized the potential of this work and encouraged me to focus on the practical and applicational aspects.

I would like to thank people in my research group. Drs. Sudhakar Puvvada (the "Guru") and Teresa Carale, the first two students in the group, have taught me so much about research as well as how to handle life here. They were important guides when I first came to this country and joined this group. Dr. Nicholas Abbott, who conducted profound studies on two-phase aqueous polymer systems, assisted me in both experimental and theoretical aspects. I especially thank Dr. Yvonne Nikas, a post-doctoral fellow, for helping me develop the theoretical formulation and for being a good friend. Dr. Leo Lue, a young genius, also helped me with the theoretical aspect of this work with his extensive and non-parallel knowledge in statistical mechanics. I am amazed that he is always ready and patient to explain all the details of the derivations.

In addition, Pak-Kai Yuet selflessly shared his knowledge on experimental data analysis and light scattering. Mark Johnson helped me when I was using radioactive

materials. Younger generations in the group, including Anat Shiloach, Nancy Zoeller, Ayal Naor, Ginger Tse, Crist Clark, and Samir Mitragotri, are all good friends. I surely have benefited considerably and enjoyed working in this group!

I would also like to thank several UROP students: Tina Srivastava was conducting preliminary research of this work before I started my research; Loren Baugh and Eric Dong, although with whom I only worked for a short time, helped me greatly in my research. I enjoyed working with them.

I am also grateful to other people in this department. Dr. Brian Kelley (in Profs. Wang and Hatton's group) provided many interesting ideas and materials for my experiments. Drs. Costas Patrikiosis, Paschalis Alexandridis, and Hiroshi Saito are good friends and helped me with experiments.

In addition to people in the Department of Chemical Engineering, I particularly appreciate help from the biology community. In Prof. King's research group, Barrie Greene, Cameron Haase-Pettingell, Margaret Speed, Dr. Anna Mitaki, Dr. Carol Teschke, and Dr. Ann Robinson taught me how to conduct the virus assay, provided their laboratory space for my experiments, and educated me in microbiology. I always appreciate their kindness, patience, and tolerance to a chemical engineer who did not have much biology background. I also received help from biologists in other universities: Prof. Bentley Fane at the University of Arkansas kindly provided the bacteriophage ϕX174 and the host bacteria, and Prof. Edward Goldberg at Tufts University provided the host bacteria of the bacteriophage T4 for my experiments.

I would also like to express my gratitude to people in the physics area. I had many helpful discussions on the light scattering technique with Dr. Henry Thomas in Prof. George Benedek's group in the Department of Physics, and Jyanti Pande (in the same group) taught me how to work and handle proteins. Prof. Sow-Hsin Chen in the Department of Nuclear Engineering and his students (Dan Lee, Jamie Ku, and Yin-Chun Liu) helped me with the neutron scattering experiments, although I could not achieve any neutron scattering measurement. I would like to thank Drs. Fernando García Golding and Mauricio de Lorenzo at Intevep, S.A. (in Venezuela) for their assistance in my light scattering experiments. I was fortunate to be an

"apprentice" of Fernando when I first started the light scattering experiments, and I learned many experimental details from Fernando and Mauricio by communicating with them through e-mails.

Last but definitely not the least, I would like to thank my family and friends for their continuous encouragement and support throughout these years. I am indebted to my parents; it was their love, care, and education which led me to M.I.T. My dear husband, Jeng-Jong Lee, never fails to provide his loving support and tender care to help me in every way, despite his own heavy work as a graduate student at M.I.T. I am indeed lucky to have his company and love in my life. My sister, Margaret Liu, and brother-in-law, Thomas Kao, are always there to listen to me and give me comfort and support. My sister-in-law, Aichu Li, and her husband, Karl Ebner, took good care of me. Miriam Yee (and her dog Veena), with whom I was hanging out during my first year at M.I.T., and Hsiao-Li Chang, my best friend in college, have constantly cheered me up and encouraged me to hang in there. I would like to thank my brother Chiaming Liu, my grandparents and relatives, my parents-in-law and sisters-in-law, as well as all the friends at M.I.T. and old classmates in Taiwan, for their encouragement and support. Finally, I am grateful to my professors at National Taiwan University for the knowledge and education I received from them.

With my experience of graduate study, I realize that no one can complete a Ph.D. study merely by him- or herself. I consider myself lucky to have had so much support and encouragement, for I was always able to find a helping hand when I needed one. To express my deepest gratitude to everybody, I can only say —from the bottom of my heart — THANK YOU!

Contents

List of Figures

List of Tables

Chapter 1

Introduction

1.1 General Considerations

The utilization of two-phase aqueous micellar systems for the separation and purification of biological molecules, particularly proteins, was first considered by Bordier [1] and has received considerable attention ever since [2, 3, 4, 5, 6, 7, 8, 9]. Most of these studies, however, focused on the extraction of *hydrophobic* materials. The investigation presented in this thesis is different from the above mentioned studies in that it focuses on (1) the partitioning of *hydrophilic* biological molecules in two-phase aqueous micellar systems, (2) the development of a theoretical framework to rationalize the observed partitioning behavior, and (3) the implementation of two-phase aqueous micellar systems as a methodology for separation or concentration of *hydrophilic* biological molecules.

The basic concept behind the utilization of two-phase aqueous micellar systems to partition biological molecules is based on recent advances in the following three seemingly unrelated areas:

1. Partitioning of biomolecules in two-phase aqueous polymer systems.
2. Structural characteristics and phase separation behavior of aqueous micellar solutions.
3. Interactions between hydrophilic proteins and surfactants.

A literature review of these three areas is presented in the next section.

1.2 Literature Review

1.2.1 Partitioning of Biomolecules in Two-Phase Aqueous Polymer Systems

Two-phase aqueous polymer systems were first identified by Albertsson in 1955 [10] as novel extractant systems for bioseparations. Since then, these systems have been developed extensively for separation and extraction of biological materials [11, 12]. These two-phase systems can be generated by mixing two species, at least one of which is a polymer, in water under appropriate solution conditions. The two species can be either (1) two polymers, which can be neutral or charged (a polyelectrolyte), such as poly(ethylene oxide) (PEO) and dextran, or (2) one polymer and a low-molecular weight component, such as the PEO-potassium phosphate two-phase system [13]. Systems of type (1) have been studied more extensively, with phase separation resulting from the unfavorable interaction (energy) arising when segments of one polymer contact segments of the other polymer. The solvent (water) molecules also contribute to the phase separation phenomenon by exhibiting the difference and incompatibility in the regions of structured water surrounding the two polymer species, reflecting the difference in the hydration characteristics of each polymer species in aqueous solutions [14]. Typically, the two polymer species are distributed unevenly between the two coexisting phases, with one phase rich in one of the polymers and the other phase rich in the other polymer. An example of the phase compositions in a two-phase aqueous PEO-dextran system is shown in Figure 1-1. Besides the intrinsic incompatibility of the polymers, other factors, such as salt type and concentration and solution pH, can be tuned to manipulate the phase separation behavior. Although, in principle, temperature constitutes a tuning factor as well, its effect on the nature of the two phases is typically small. As a result, the compositions of the two coexisting phases are usually adjusted by changing the overall polymer composition rather than by

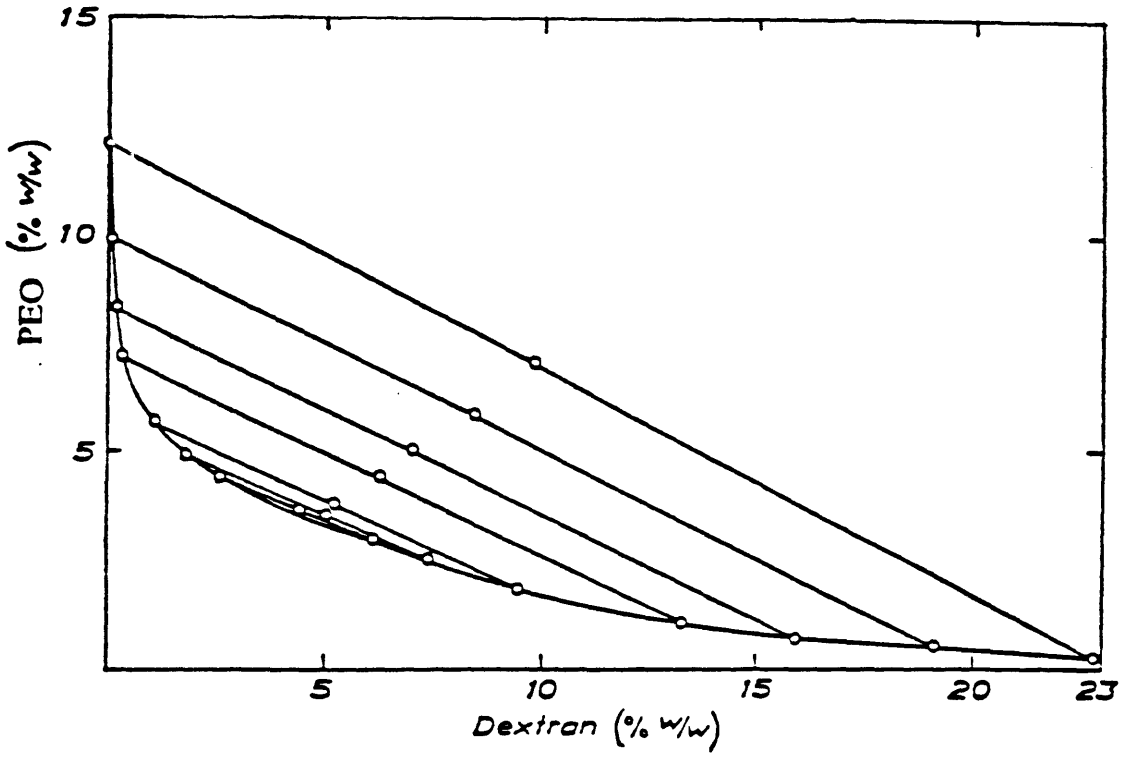

System	Total system			Bottom phase			Top phase		
	Dextran % w/w	PEO % w/w	H_2O % w/w	Dextran % w/w	PEO % w/w	H_2O % w/w	Dextran % w/w	PEO % w/w	H_2O % w/w
A	4.40	3.65	91.95	6.10	2.98	90.92	2.63	4.43	92.94
B	5.00	3.50	91.50	7.34	2.55	90.11	1.80	4.91	93.29
C	5.20	3.80	91.00	9.46	1.85	88.69	1.05	5.70	93.25
D	6.20	4.40	89.40	13.25	1.07	85.68	0.30	7.17	92.53
E	7.00	5.00	88.00	15.89	0.68	83.43	0.14	8.29	91.57
F	8.40	5.80	85.80	19.08	0.52	80.40	0.06	9.93	90.01
G	9.80	7.00	83.20	22.77	0.24	76.99	0.05	12.03	87.92

Figure 1-1: Phase diagram and phase compositions of the poly(ethylene oxide) (PEO)-dextran two-phase aqueous system with Dex48-PEO 6000 at 20°C. Dex48 denotes dextran having an intrinsic viscosity of 48 mL/g and a weight-average molecular weight of 460,000 dalton, and PEO 6000 denotes PEO having a number-average molecular weight in the range of 6,000 - 7,500 dalton (from Reference [13]).

adjusting temperature.

The phase separation behavior of solutions containing two incompatible polymers can be successfully described using the statistical-mechanical treatment of Flory and Huggins [15]. This involves obtaining an expression for the solution Gibbs free energy of mixing, ΔG_m, which is the free-energy change associated with the formation of a polymer solution from the constituent pure components. The chemical potential of each of the three species (two polymers and the solvent), μ_i, can then be calculated from ΔG_m using the conventional methods of thermodynamics. By applying the criteria of phase equilibrium [16], one can compute the resulting coexistence (binodal) curve as well as the critical properties of the system.

From a practical viewpoint, the time required to form the two coexisting phases is an important consideration. In this respect, the rate of phase separation depends strongly on the overall polymer composition in the system as well as on the polymer composition in each phase [17]. In addition, the rate of phase separation can be evaluated qualitatively from knowledge of the polymer compositions on the phase diagram. In general, the rate of phase separation increases with increasing tie-line length, which reflects the difference in the compositions of the two coexisting phases.

The partitioning behavior of biological solutes in two-phase aqueous polymer systems has been studied extensively from both the experimental and theoretical viewpoints [13, 17, 18, 19, 20, 21, 22, 23]. The experimental work was performed primarily at low solute concentrations in order to minimize the effect of solute-solute interactions on the phase separation equilibrium of the aqueous polymer systems, as well as to isolate and study the effect of solute-polymer interactions. Under such conditions, the observed partitioning behavior should only reflect the difference in the interactions between the solute and the phase-forming polymers in the two coexisting phases. It is customary to quantify the partitioning behavior of the solute by introducing the *partition coefficient*, K, defined as

$$K = \frac{C_t}{C_b} \tag{1.1}$$

where C_t and C_b are the solute concentrations in the top and bottom phases respectively. Equation (1.1) indicates that the magnitude of K reflects the distribution of the solute in the two-phase system. By taking proteins as an example, the experimental studies revealed that the protein partition coefficient, K_p, is affected by the following factors [18]:

1. Protein size — The larger the protein molecule, the more unevenly it is distributed between the two coexisting phases.

2. Protein surface properties — Generally, proteins associated with membrane functions in cells tend to be hydrophobic in their surface properties. As a result, their interactions with polymers are usually different from those between polymers and proteins which are not associated with membranes. In addition, the protein surface charge, which depends strongly on the solution pH, also plays an important role, and consequently the partitioning behavior of proteins can be manipulated by varying the solution pH.

3. Polymer molecular weight — It is found that an increase in the molecular weight of one of the phase-forming polymers decreases the tendency of the proteins to partition into the phase which is rich in that polymer. However, an indirect aspect associated with changing the polymer molecular weight is that it may also alter the compositions of the two coexisting phases.

4. Compositions of the two coexisting phases — As the difference in the phase compositions increases, that is, when there is an increase in the the length of the corresponding tie line, the protein partitioning becomes more uneven. In addition to using polymers with different molecular weights, as mentioned in 3 above, the compositions of the two coexisting phases can also be changed by adding salts or by increasing the overall polymer concentration.

5. Salt effects — Different salt types and concentrations have different effects on the two-phase aqueous polymer systems. In general, at low salt concentrations, the salt primarily establishes a bulk-electrical potential difference between the

two coexisting phases. At high salt concentrations (generally higher than 1 M), the effect of salts is attributed primarily to their influence on the structure of water and on the polymer compositions of the two coexisting phases [17]. This influence at high salt concentrations may, in turn, affect the distribution of proteins in the system.

6. Affinity partitioning — By covalently attaching ligands, which have high affinity to specific sites on certain proteins, on one of the phase-forming polymers, the phase rich in that polymer will possess high selectivity with respect to those targeted proteins, and, accordingly, the specificity towards a desired protein can be significantly enhanced.

7. Charged polymers — These polymers interact with proteins through electrostatic interactions, and the strength of these interactions can be manipulated by changing the solution pH and ionic strength. The partitioning behavior of proteins can thus be varied accordingly.

There are several types of theoretical approaches which were developed to rationalize the partitioning behavior of biological molecules in two-phase aqueous polymer systems [18]. Among these, the most relevant to this thesis is the "scaling-thermodynamic" approach [19], which explicitly accounts for the underlying structure of the polymer solution. Specifically, in the PEO-dextran two-phase aqueous system, one can identify a "crossover concentration," C^*, for PEO molecules with a molecular weight M, given by [19]

$$C^* = \frac{3M}{4\pi R_g^3} \tag{1.2}$$

where R_g is the radius of gyration of the PEO molecules. The crossover concentration, C^*, signals a transition in the structure of the polymer solution from the "dilute" to the "entangled" regimes. Such a transition in the polymer solution structure can occur by (1) increasing polymer concentration at a fixed polymer molecular weight, or (2) increasing polymer molecular weight at a fixed polymer concentration. For PEO concentrations $C << C^*$, the solution is in the "dilute" regime, and the polymer

molecules are dispersed as individual coils in the solvent, with the identity of each individual polymer molecule being preserved. Accordingly, in this regime, protein molecules interact with individual polymer coils, each characterized by its radius of gyration, R_g ($=D_p/2$), as shown in Figure 1-2. On the other hand, for PEO concentrations $C >> C^*$, the polymer coils extend and entangle to form a continuous polymer net or mesh. The polymer molecules thus lose their individual identities, and consequently, the polymer molecular weight ceases to be important in this "entangled" regime. In this regime, protein molecules interact with the polymer net or mesh, characterized by the mesh size, ξ_p (see Figure 1-2). This scaling-thermodynamic theoretical approach was found to agree reasonably well with the available experimental observations in the entangled polymer systems [21, 22].

In most of the theoretical approaches developed so far to model the partitioning behavior in two-phase aqueous polymer systems, only *non-specific* solute (protein)-polymer interactions, for example, those of the steric excluded-volume type, are considered. As a result, these approaches are not expected to be accurate in cases where *specific* solute-polymer interactions are known to play an important role, such as in the case of hydrophobic interactions. Nevertheless, these theoretical approaches provide a starting point for developing a better understanding of the interactions between biomolecules and polymers in two-phase aqueous polymer systems, and, as such, they also help to shed light on the partitioning behavior of biological molecules in two-phase aqueous micellar systems.

1.2.2 Structural Characteristics and Phase Separation Behavior of Aqueous Micellar Solutions

Micelles are aggregates of surfactant molecules that form in aqueous environments. A surfactant molecule consists of two distinct chemical moieties [24]: the *hydrophilic* (water-loving) moiety, which is referred to as the "head," and the *hydrophobic* (water-fearing) moiety, which is referred to as the "tail." This duality in a given molecule causes surfactants to display a unique behavior in solutions, particularly of the aque-

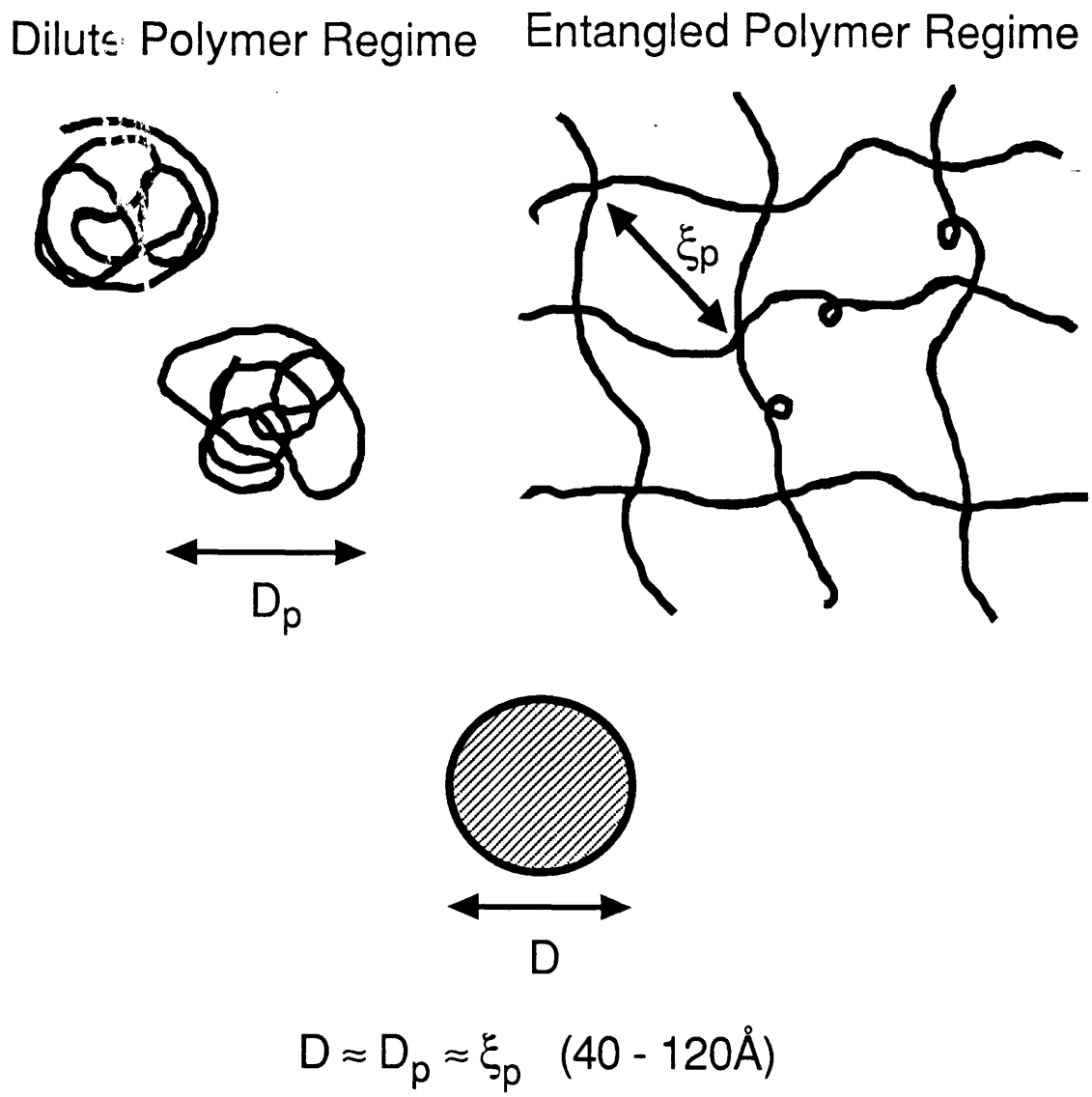

Figure 1-2: Comparison of the length scales (sizes) associated with proteins and polymers, either as individual coils or as a net (mesh). D is the diameter of a protein molecule, D_p is the diameter of a polymer coil, and ξ_p is the mesh size of the polymer net.

ous type. For example, when dissolved in water at low concentrations, surfactant molecules tend to accumulate at the air-water interface, with their hydrophilic heads immersed in water and their hydrophobic tails protruding into air to avoid the unfavorable contact with the water molecules. As the surfactant concentration increases, a threshold concentration — the "critical micelle concentration" (CMC) — is reached, at which surfactant molecules begin to form aggregates (micelles) spontaneously in the bulk solution. Micelles form in such a way that the hydrophobic tails all flock inside to avoid contact with water, while the hydrophilic heads remain outside in favorable contact with water. The onset of micellization at the CMC manifests itself in dramatic changes in many of the physico-chemical properties of the solutions, including the solution surface tension. The CMC usually ranges from 10^{-6} to 10^{-2} M, depending on the molecular structure of the surfactant molecules, such as the type and length of the hydrophobic tail, and the nature of the hydrophilic head (nonionic, ionic, or zwitterionic). The CMC also varies in response to changes in solution conditions, including temperature and the presence of other components, such as salts, in the solution.

Micellization, that is, formation of micelles, actually reflects a delicate balance of intermolecular forces, including van der Waals, steric, electrostatic, and hydrophobic, between surfactant molecules within a self-assembling micellar aggregate [25, 26]. Tanford [25] has given a simple description of micellization by introducing the principle of opposing forces. The forces involved are: (1) the attractive force, arising from the hydrophobic effect acting on the surfactant tails, which favors the aggregation of surfactant molecules, and (2) the repulsive force, arising from the interactions between the surfactant heads, which tends to resist the formation and growth of micelles. For ionic surfactants, the electrostatic repulsion between like charges on the heads constitutes the major repulsive force; for nonionic surfactants, the steric hindrance due to the physical size of the hydrated heads represents the main source of repulsion. A balance between these two opposing forces is necessary for the stabilization of micelles. If the repulsive force dominates, then the surfactant molecules will prefer to be dissolved in water as monomers instead of forming aggregates. On the other hand, if

the attractive force dominates, then the surfactant molecules will prefer to aggregate and form large micelles, or even separate from water and form a new (micelle) phase. Therefore, the stable existence of micelles in an aqueous medium reflects a delicate balance between these two opposing forces.

Micelles can grow one-dimensionally (into cylindrical structures) or two-dimensionally (into disc-like or bilayer structures) with increasing surfactant concentration and variation of solution conditions such as temperature. The micellar size in aqueous solutions depends on the surfactant type and concentration, as well as on solution conditions such as temperature, ionic strength, and pH, and it is found to be primarily controlled by the interactions between the heads, since surfactants possessing smaller heads (for example, those resulting from the dehydration of the poly(ethylene) heads of C_iE_j nonionic surfactants), or surfactants which do not exhibit strong, long-ranged repulsive (electrostatic) interactions between the heads, typically display significant micellar growth. Furthermore, it is often found that micelles do not possess a uniform size but, instead, exhibit a distribution of sizes. In particular, the polydispersity in micellar size depends on the surfactant type and concentration, as well as on the solution conditions. Typically, micelles which can grow significantly exhibit a much higher polydispersity in their size distribution as compared to those which do not grow (and form spherical micelles).

At certain temperatures and surfactant concentrations, an isotropic micellar solution can macroscopically phase separate into two coexisting micellar solution phases, one with a higher and the other with a lower surfactant concentration. The surfactant concentration in each of the two coexisting phases exceeds the CMC, and, hence, *both phases contain micelles.* It is also noteworthy that the average micellar sizes and the micellar size distributions in the two coexisting phases are different, since these micellar characteristics depend on the overall surfactant concentration which is different in each phase [27]. This phase-separation phenomenon of micellar solutions can be represented by a bell-shaped curve, called the binodal or coexistence curve, on a temperature versus surfactant concentration phase diagram [28]. The maximum or minimum of the coexistence curve is called the critical (or conso-

lute) point, and the temperature and surfactant concentration corresponding to this point are referred to as the critical temperature, T_c, and the critical concentration, X_c, respectively. Some surfactant solutions, for example, aqueous solutions of the nonionic surfactant dodecyl hexa(ethylene oxide), $C_{12}E_6$, display a concave-upward coexistence curve which exhibits a lower consolute (critical) point (see Figure 1-3) [29]. Other surfactant solutions, for example, aqueous solutions of the zwitterionic surfactant dioctanoyl phosphatidylcholine (C_8-lecithin), display a concave-downward coexistence curve having an upper consolute (critical) point (see Figure 1-4) [30].

The phase separation behavior results from the competition between the internal-energy effects, which favor separation of micelles from the solvent, and entropic effects, which favor miscibility of micelles in the solvent [24]. The appearance of either a lower or an upper consolute (critical) point results from the difference in the dependence of the internal-energy change, associated with the mixing process and thus related to the type of interactions between solute and solvent molecules, on temperature [28]. For example, for surfactants belonging to the alkyl poly(ethylene oxide), C_iE_j, type, the solubility of micelles in water can be rationalized in terms of hydration of the surfactant head groups, that is, formation of hydrogen bonds between the surfactant heads and water molecules. However, since dehydration of the heads occurs as the surfactant solution is heated up, it follows that this internal-energy effect can eventually overcome the entropic effect which favors miscibility, thus leading to phase separation as temperature is increased [24]. Since, in this case, the phase separation behavior is more pronounced as temperature increases, the resulting coexistence curve possesses a concave-upward shape with a lower consolute (critical) point in the temperature versus surfactant concentration phase diagram (see Figure 1-3) [29].

As shown in Figures 1-3 and 1-4, the two branches of the coexistence curve are stretched in the temperature versus surfactant concentration phase diagram in an asymmetric pattern. Specifically, the branch on the lower-concentration side is very steep while that on the higher-concentration side exhibits a milder slope. In addition, the location of the critical point on the phase diagram can be shifted by adding solution modifiers, such as salts or urea [31]. This feature provides a convenient way

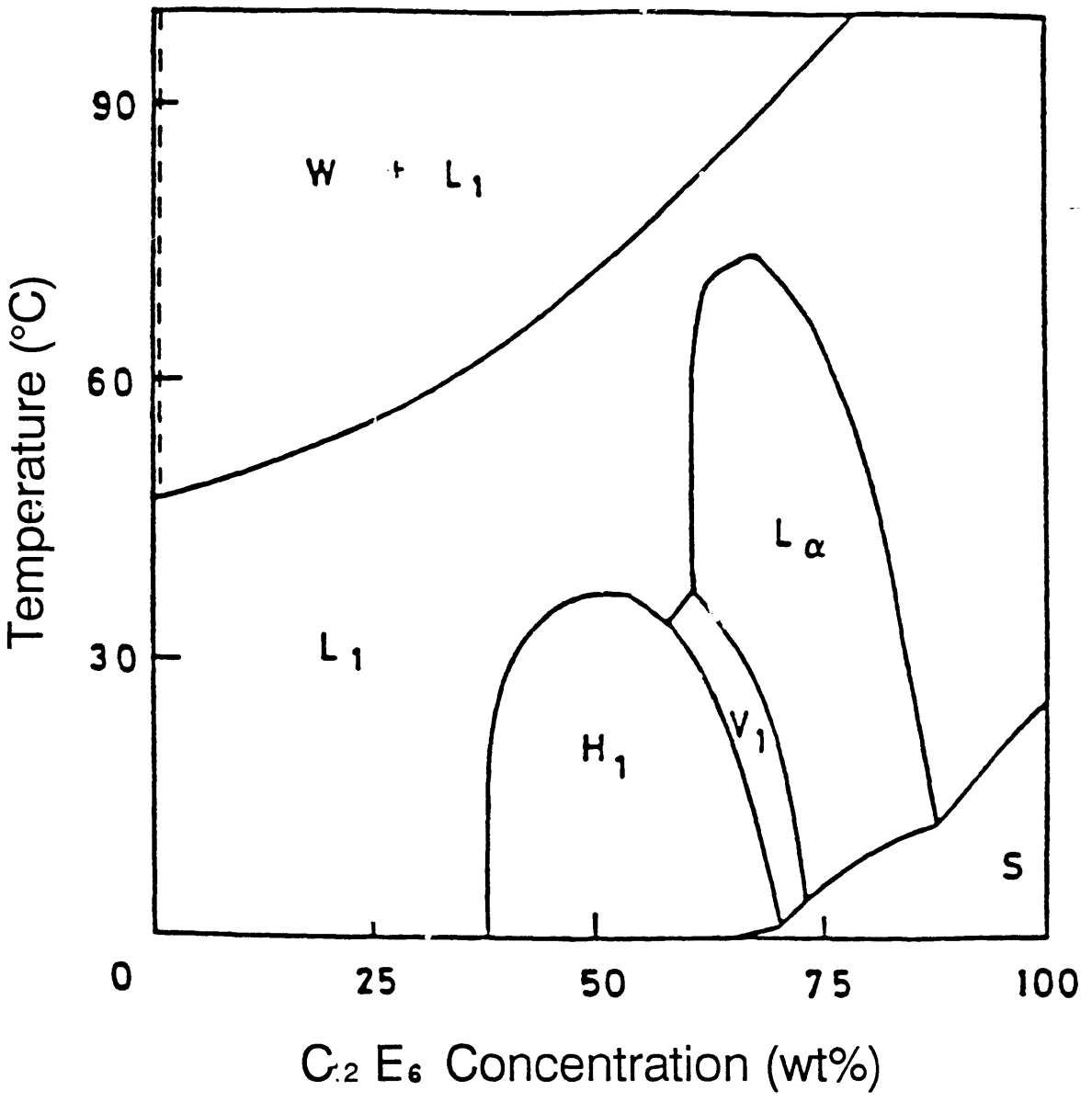

Figure 1-3: Phase diagram of the $C_{12}E_6$-water system. The letters denote various solution structures at different temperatures and surfactant concentrations. W=micellar solution with low surfactant concentration, L_1=micellar solution with high surfactant concentration and continuously connected to W phase. The dashed line and the curve between the (W+L_1) and L_1 regions compose the coexistence curve of the system. Other phases in this system are: H_1=hexagonal phase, L_α=lamellar phase, S=solid surfactant, V_1=normal "bicontinuous" cubic phase (from Reference [29]).

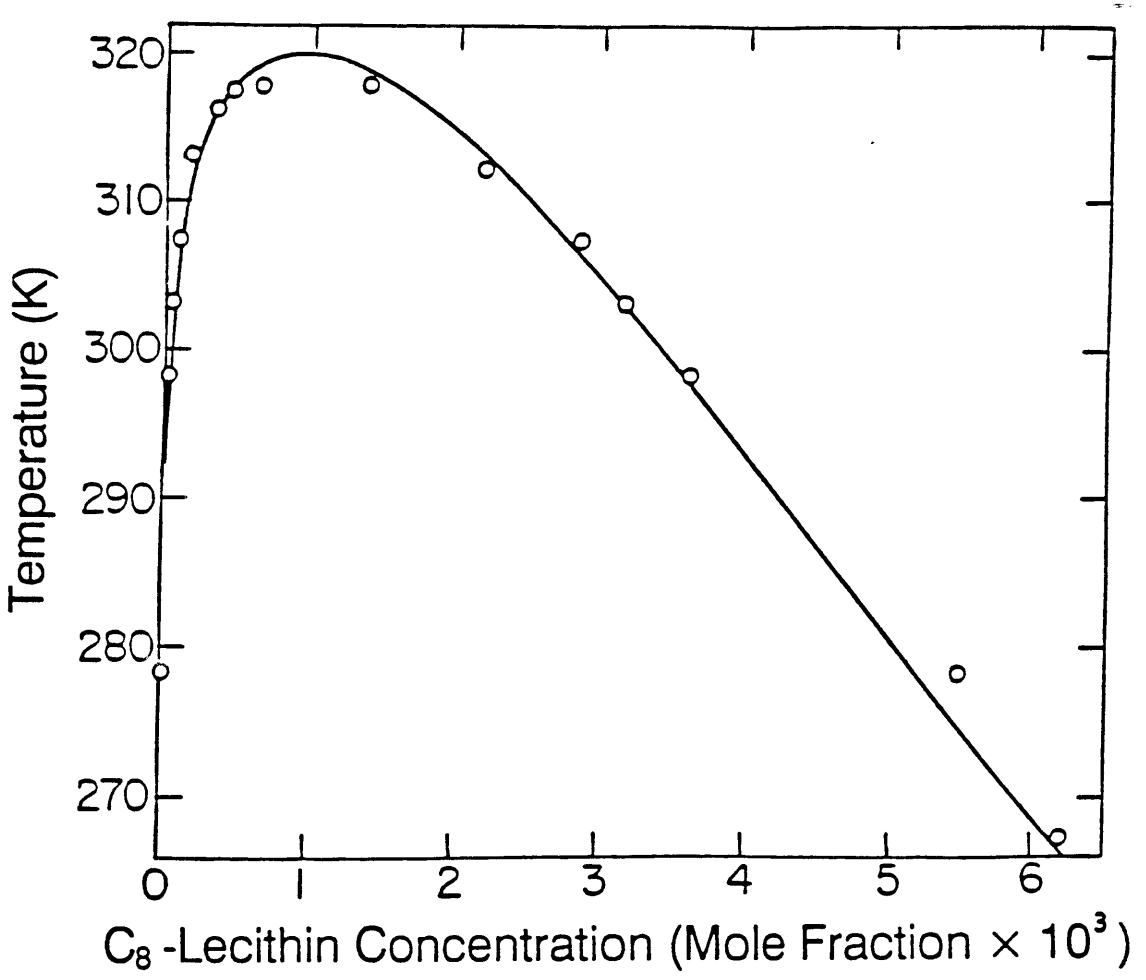

Figure 1-4: Coexistence curve of the C_8-lecithin-water system. The circles denote experimental data, and the solid curve corresponds to a theoretical prediction (from Reference [30]).

to manipulate the phase-separation behavior of aqueous micellar solutions.

Micelles which exhibit one-dimensional growth are usually of cylindrical shape. As the size of these cylindrical micelles exceeds a threshold length scale, known as the persistence length [32], the micelles acquire flexibility and thus resemble polymer molecules in solutions. Moreover, when the surfactant concentration reaches a certain threshold value, known as the "crossover surfactant concentration," X^*, the micelles begin to entangle with each other and form a net or mesh of overlapping micelles, similar to the transition which occurs in aqueous polymer solutions at the crossover concentration, C^* (see Figure 1-2) [33]. In the case of micellar solutions, such a transition can be induced by (1) increasing surfactant concentration at a fixed temperature, or (2) varying temperature at a fixed surfactant concentration. For example, in the C_iE_j micellar solutions, such a transition can be induced by increasing temperature at a fixed surfactant concentration [34, 35]. It was also found [34] that in the $C_{12}E_6$-water system, in which the micelles are of cylindrical shape, the crossover surfactant concentration, X^*, versus temperature curve intersects the coexistence curve in the vicinity of the lower consolute (critical) point, thus bisecting the phase diagram into the "dilute" regime (where micelles are identifiable, single entities) and the "entangled" regime (where micelles overlap and form a net or mesh), as shown in Figure 1-5. In this respect, it is interesting to note that, in the $C_{12}E_6$-water system, the underlying solution structure of the two coexisting micellar phases is different, with the micelle-poor phase containing identifiable micelles and the micelle-rich phase containing an entangled micellar mesh. This observation appears to be generally valid for those C_iE_j-water systems which exhibit significant micellar growth.

A number of theories have been developed to describe and predict the behavior of aqueous surfactant solutions [24, 25, 27, 36]. These predictions include (1) the CMC, (2) the micellar shape, size, and size distribution, (3) the coexistence curve, including the critical concentration, and (4) thermodynamic properties such as the solution osmotic pressure and compressibility.

The fundamental theory of micellization requires that, at thermodynamic equilibrium, the chemical potential of a surfactant molecule in an aggregate (micelle)

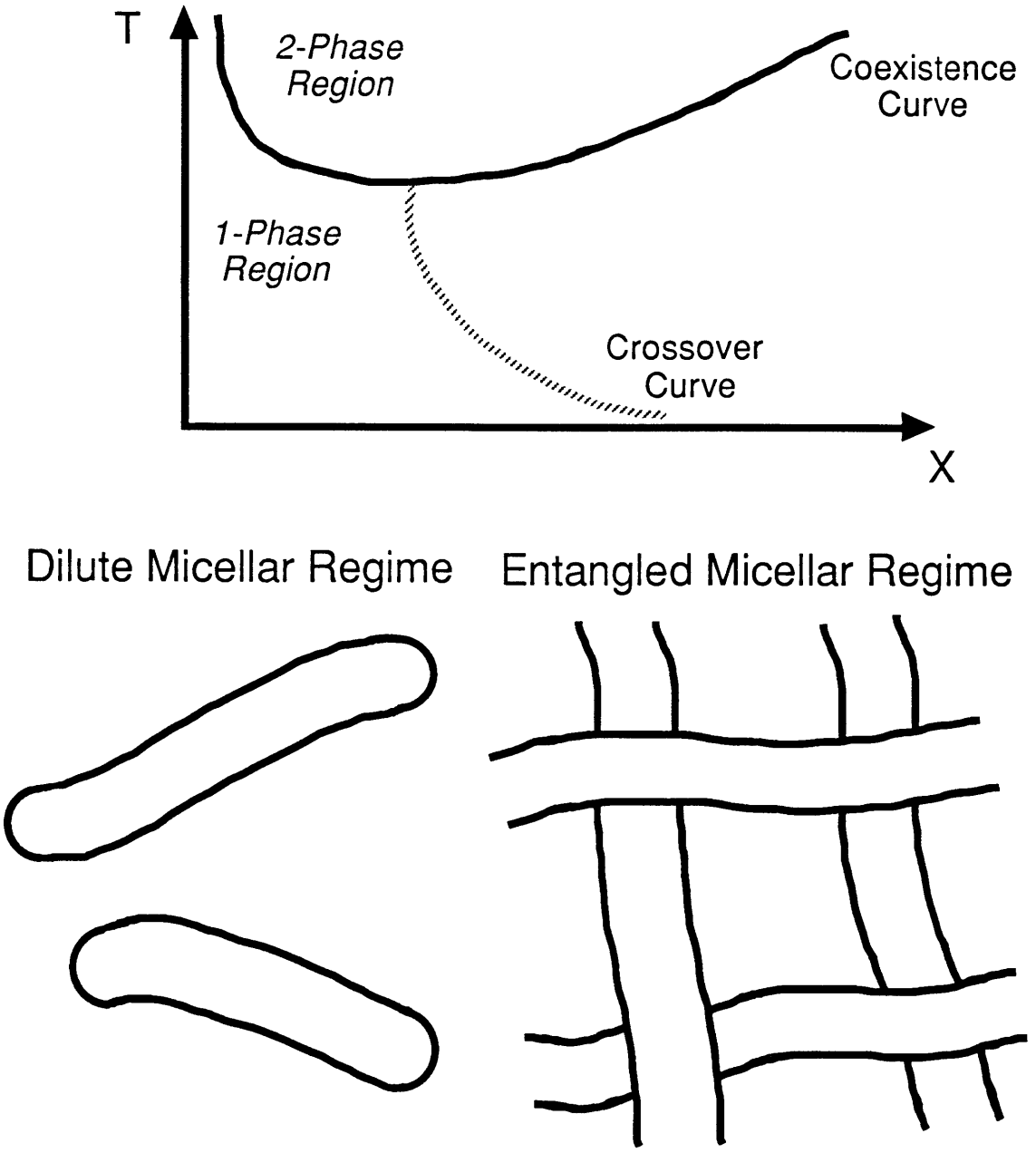

Figure 1-5: Schematic representation of the transition in the underlying structure of aqueous $C_{12}E_6$ micellar solutions. The full concave-upward curve in the T (temperature) versus X (surfactant concentration) phase diagram is the coexistence curve. The dashed curve in the one-phase region is the crossover curve, representing the boundary between the two regimes, dilute and entangled, possessing different underlying solution structure. The structure of the $C_{12}E_6$ micellar solution can thus be changed by varying temperature or surfactant concentration.

of aggregation number n, μ_n/n, should be equal to the chemical potential of a free surfactant monomer, μ_1, for all n's. That is,

$$\frac{\mu_n}{n} = \mu_1 \tag{1.3}$$

In dilute solutions, the chemical potentials, μ_n and μ_1, can be written as [25]

$$\mu_n = \mu_n^0 + k_B T \ln X_n \tag{1.4}$$

$$\text{and} \quad \mu_1 = \mu_1^0 + k_B T \ln X_1 \tag{1.5}$$

where k_B is the Boltzmann constant, T is the absolute temperature, μ_n^0 and μ_1^0 are the standard-state chemical potentials of n-mers and monomers respectively, and X_n and X_1 are the mole fractions (more strictly, the activities) of n-mers and monomers respectively. Using Eqs. (1.4) and (1.5) in Eq. (1.3) yields the following expression for the distribution of micellar sizes, $\{X_n\}$:

$$X_n = (X_1)^n \exp\left[\frac{-(\mu_n^0 - n\mu_1^0)}{k_B T}\right] \tag{1.6}$$

At the CMC, $X_n \approx X_1 \approx$ CMC, and the following approximate expression for the critical micelle concentration can be obtained:

$$\text{CMC} \approx \exp\left[\frac{-(\mu_n^0/n - \mu_1^0)}{k_B T}\right] \tag{1.7}$$

Blankschtein *et al.* [27] developed a theory which provides analytical representations of the equilibrium thermodynamic properties of surfactant-water solutions that exhibit phase separation and critical phenomena. In this theory, the Gibbs free energy, G, of a solution containing N_s surfactant molecules, forming a micellar size distribution, $\{N_n\}$ (where N_n is the number of micelles of aggregation number n), and N_w water molecules in thermodynamic equilibrium at temperature T and pressure P is modeled as the sum of three distinct contributions: G_f, G_m, and G_{int}. The free energy of formation, G_f, summarizes the physico-chemical factors responsible for

the formation of micelles, the free energy of mixing, G_m, models the entropic effects associated with mixing the micellar aggregates, surfactant monomers, and the solvent (water) molecules, and the free energy of interaction, G_{int}, estimates the interactions between the micellar aggregates using a mean-field type approximation. With G_f, G_m, and G_{int} expressed in terms of N_s, N_w, T, and other parameters (such as μ_n^0 and μ_w^0), and $G = G_f + G_m + G_{int}$, the chemical potentials of water and each n-mer can be obtained by differentiation of G, that is, $\mu_w = (\partial G/\partial N_w)_{\{N_n\},T,P}$ and $\mu_n = (\partial G/\partial N_n)_{N_w,\{N_{n'}\},T,P}$ respectively. The osmotic pressure, which is defined as

$$\Pi = \frac{\mu_w^0 - \mu_w}{\Omega_w} \tag{1.8}$$

can thus be calculated, where Ω_w is the effective volume of a water molecule. The osmotic compressibility, $(\partial\Pi/\partial X)_{T,P}^{-1}$, and other thermodynamic properties of the micellar solution, can thus be derived from the expression of Π. The predictions of this theory were found to agree well with many of the experimental observations [27, 30]. Accordingly, this theory will be utilized in this thesis to describe the thermodynamic behavior of the aqueous micellar systems used in the partitioning experiments.

1.2.3 Interactions Between Hydrophilic Proteins and Surfactants

The term, hydrophilic proteins, will refer hereafter to those proteins which are water-soluble and are not directly related to membrane functions. Usually, surfactants, particularly those of the anionic type, are considered as "denaturing agents" of hydrophilic proteins, since they are able to induce unfolding of native protein structure as well as to trigger loss of enzymatic functions [37]. This denaturing effect of surfactants, however, has found its use in biochemistry. For example, sodium dodecyl sulfate (SDS), an anionic surfactant, is used in polyacrylamide gel electrophoresis (PAGE) to determine protein molecular weights. Accordingly, understanding the interactions between hydrophilic proteins and surfactants is a topic of considerable interest in biochemistry.

Research on the interactions between surfactants and proteins is primarily carried out through studies of surfactant binding to protein molecules. Both the binding pattern and the structure of the resulting protein-surfactant complexes have been studied. The binding of ionic surfactants, particularly that of sodium dodecyl sulfate (SDS), has received considerable attention. The ability of SDS to unfold the protein structure was found to be induced by the cooperative binding of SDS molecules onto the protein molecules, and the binding is primarily hydrophobic in nature [37]. Reynolds and Tanford [38] found that a variety of proteins bind identical amounts of SDS on a gram/gram basis at equilibrium SDS monomer concentrations exceeding 0.5 mM, lower than the CMC of SDS, which is about 1.3 mM. The authors accordingly concluded [38] that only the monomeric form, rather than the micellar form, of SDS binds to proteins. These authors also investigated the structure of the resulting protein-SDS complexes [39]. They found that the complexes had a rod-like structure, and that the proteins in the complexes, although denatured, were not in a random-coil state, with some of their secondary structure still preserved. The authors also provided a theoretical basis for using SDS gel electrophoresis in protein molecular weight determination [39]. Since (1) the high level of SDS binding to proteins and the constant binding ratio assure a constant charge per unit mass of the protein-SDS complexes, and (2) the hydrodynamic properties of protein-SDS complexes are a unique function of the polypeptide chain length, it follows that the mobility of protein-SDS complexes in the electrophoretic gel is proportional to the polypeptide chain length, or, equivalently, to the protein molecular weight.

Some proteins, however, are found to have specific binding sites for amphiphilic molecules. For example, some studies [40, 41] revealed that a native bovine serum albumin (BSA) molecule possesses five high-affinity binding sites, which are visualized as hydrophobic patches on the surface of the protein, for organic anionic and neutral amphiphilic molecules. This is in accordance with the major physiological function of this protein, which is to transport fatty acid anions in the circulatory system. However, as the concentration of the ionic surfactant increases, another type of binding — the cooperative binding of surfactant molecules to proteins, causing denaturation

of protein molecules — still takes place.

Similar research on protein-surfactant interactions has also been conducted for cationic surfactants. Nozaki *et al.* [42] studied the binding of a cationic surfactant, tetradecyl trimethylammonium chloride ($C_{14}NMe_3^+$ Cl^-), to various proteins. This cationic surfactant was found to behave qualitatively like SDS, showing the cooperative binding mode accompanied by denaturation of protein molecules, but at a monomer concentration which is ten-fold higher than that required in the SDS case. In addition, this cooperative binding was found to occur at surfactant concentrations very close to the CMC, and consequently saturation of protein molecules with the cationic surfactant cannot be achieved due to the onset of micelle formation. These authors suggested that the difference in the binding of cationic surfactants to proteins, as compared to that of anionic surfactants, is generic, and that this may limit the potential of replacing SDS by cationic surfactants in biochemical applications such as PAGE.

A few binding studies involving nonionic or "mild" surfactants were also conducted. Helenius and Simons [43] studied the binding of Triton X-100 (a nonionic surfactant) and deoxycholate (DOC^-, a bile salt, considered as a "mild" anionic surfactant) on certain hydrophilic and lipophilic proteins. These two surfactants are usually used for extracting membrane components in biochemistry and are supposed to be "mild" towards biomaterials. In addition, they are generally used at concentrations exceeding their CMC's. These authors found that very little or no Triton X-100 or DOC^- bound to hydrophilic proteins. Makino *et al.* [44] conducted similar studies on the proteins BSA and ovalbumin and obtained similar results. Accordingly, these authors proposed that these observed phenomena are due to the low CMC's of Triton X-100 or DOC^- (see Table 1.1).

However, there is also some evidence [45] suggesting that the "mild" surfactant, Triton X-100, may actually induce conformational changes of protein molecules. Whether these changes in protein conformations induced by a "mild" surfactant are restricted only to certain proteins is still unknown.

From the observations summarized above, one can conclude that the denaturation

Table 1.1: Concentrations of amphiphiles required to bind to proteins, as compared to their CMC's. All the concentrations are in mM. DOC^- is the short form for deoxycholate. All the CMC values correspond to an ionic strength of 0.1, except that of Triton X-100, which corresponds to pure water (from Reference [44]).

	$C_{12}SO_4^-Na^+$ (SDS)	$C_8SO_4^-Na^+$	DOC^-	TX-100
50% Saturation of affinity binding sites of native BSA	1×10^{-3}	1.5×10^{-3}	1.5×10^{-2}	5×10^{-2}
Critical concentration for major cooperative binding	0.3	5	(Not observed)	(Not observed)
CMC	1.3	100	3	0.3

of proteins by surfactants is essentially caused by the cooperative binding of ionic surfactants to protein molecules. The so-called "mild" surfactants are mainly those of the nonionic type. It is thus concluded [46] that the charged heads and flexible nonpolar tails constitute required features of denaturing surfactants. This recognition served as the basis for selecting *non-charged* (nonionic) surfactants to generate the two-phase aqueous surfactant systems utilized in the studies reported in this thesis.

1.3 Motivation

When compared to the two-phase aqueous *polymer* systems described in Section 1.2.1, which have been studied extensively and implemented for the separation and extraction of biomaterials, two-phase aqueous *micellar* systems share many similarities with, but also offer certain advantages over, their polymer counterpart. A detailed comparison between these two-phase aqueous systems is presented below:

1. Only a binary surfactant-water system is needed to generate the two-phase aqueous micellar system. This is chemically simpler than in the two-phase aqueous polymer systems, which typically require at least three components — polymer 1-polymer 2-water or polymer-salt-water — in order to generate the two-phase systems.

2. The aqueous surfactant solutions can phase separate at low overall surfactant concentrations, typically 1-2 wt%. When compared with aqueous polymer systems, in which phase separation occurs at polymer concentrations of about 10 wt%, the surfactant systems provide a potentially economical advantage. In addition, surfactants can generally be easily and uniformly dissolved in water, while, in the polymer case, sometimes it is found that phase separation of the polymer systems does not occur as expected due to improper dissolution of the polymers [47]. This easily-dissolved feature of surfactants certainly provides convenience in preparing the two-phase systems.

3. The difference in the association forces — physical forces, such as hydrophobic interactions [25], for micelles, versus chemical bonding for polymers — implies that the two microstructures should display different characters. Indeed, micelles display a self-assembling, labile nature which offers many additional degrees of freedom for manipulating the aqueous surfactant system, while this feature is absent in the polymer case. For example, the micellar size, which is analogous to the polymer molecular weight, can be *tuned in situ* by varying the overall surfactant concentration, temperature, or the salt type and concentration. This unique feature is not available in the polymer case because the polymer molecular weight is fixed upon synthesis. Accordingly, if polymers with different molecular weights are needed, each polymer has to be synthesized separately, which is time-consuming and expensive. Furthermore, by diluting the micellar system with water, the micelles will decrease in size or may even be "broken apart" and dissociate into free surfactant monomers. This feature, which is absent in the polymer case, suggests an interesting and potentially useful method to remove surfactants from biomaterials by filtering the resulting mixture of surfactant monomers and biomaterial after separation or extraction of a desired biomaterial using two-phase aqueous micellar systems.

4. Because a micelle possesses both a hydrophobic interior and a hydrophilic exterior, this microstructure can offer a dual environment to biomaterials, one

possessing a hydrophobic character and the other possessing a hydrophilic character. In contrast, the properties of (homo)polymers considered here depend on the nature of the constituent monomers and can therefore only offer a single environment to biomaterials. In view of this, proteins which are predominantly hydrophilic or hydrophobic are expected to exhibit different partitioning behavior in the two-phase aqueous micellar systems. Specifically, hydrophilic (hydrophobic) proteins are expected to partition more extremely into the micelle-poor (micelle-rich) phase of the two-phase aqueous micellar systems [1, 2, 3, 4, 9]. Clearly, such a differentiation in the partitioning behavior of hydrophilic and hydrophobic proteins will not occur to the same extent in the two-phase aqueous polymer systems.

5. The length scales associated with micelles and polymers are very different when "viewed" by a typical protein molecule. For example, the diameter of a typical globular protein molecule ranges from 40Å to 120Å. The persistence length, which is a measure of flexibility [32], of micelles is about 50 - 100Å [34], while the persistence length of polymers, which is comparable to the length of a polymer segment, is only about 3 - 4Å. In the case of protein partitioning, a protein molecule can thus "feel" simultaneously many segments belonging to one polymer molecule, so that polymers appear highly flexible and diffuse to protein molecules. In contrast, on the length scale of a protein molecule, micelles appear rigid and compact due to their relatively large persistence lengths.

6. Aqueous solutions of polymers (such as PEO) and micelles (for example, composed of C_iE_j nonionic surfactants) can exhibit a transition in the underlying solution structure from the dilute to the entangled regimes [19, 22, 34]. In the dilute regime, the solution contains individually dispersed phase-forming entities (polymer coils or micelles), while in the entangled regime, the solution contains an overlapping net or mesh of polymers or micelles. In spite of these qualitative structural similarities, the length scales associated with each solution regime, as "viewed" by a biological molecule, can be very different in the

polymer and micellar cases, as mentioned in 5 above. As an illustration, for a typical hydrophilic protein molecule with a radius of 20 - 60Å, the characteristic sizes of the protein, the polymer coil, and the mesh size are all comparable [19], as shown in Figure 1-2. As a result, the hydrophilic protein can "sense" the change in the underlying structure of the polymer solution "evolving" from the dilute to the entangled regimes, and this can manifest itself at the macroscopic level in the observed partitioning behavior of hydrophilic proteins [19].

In contrast, in the micellar case, the typical micellar size in the dilute regime is in the range of 1000's of Å, and the mesh size in the entangled regime is about 200 - 300Å, as estimated from simple geometric considerations (see Section 3.5.1) [7]. Hence, both of these length scales are much larger than that of a typical protein (see Figure 1-6). This suggests that the dilute-to-entangled structural transition taking place in the micellar solution can only be "sensed" by particles whose sizes are much larger than that of typical hydrophilic proteins. Accordingly, the partitioning behavior of hydrophilic proteins is expected to be different in two-phase aqueous micellar systems as compared to that observed in the polymer case.

7. By mixing different surfactant species, for example, nonionic and ionic, it should be possible to generate *in situ* a mixed-micellar system in which the mixed micelles resemble polyelectrolyte molecules containing both charged and non-charged units. Moreover, by mixing a surfactant-type ligand with a surfactant, one can generate *in situ* a mixed-micellar system whose selectivity and specificity of extraction will be greatly enhanced.

In view of the discussion presented above, two-phase aqueous micellar systems not only have the potential of being utilized to partition biological molecules, similar to their polymer counterpart, but also exhibit certain advantages and convenient features which are not available in two-phase aqueous polymer systems. In addition, given the mild interactions between non-charged surfactants and biological molecules, as well as the low interfacial tension between the two coexisting micellar phases [48], two-

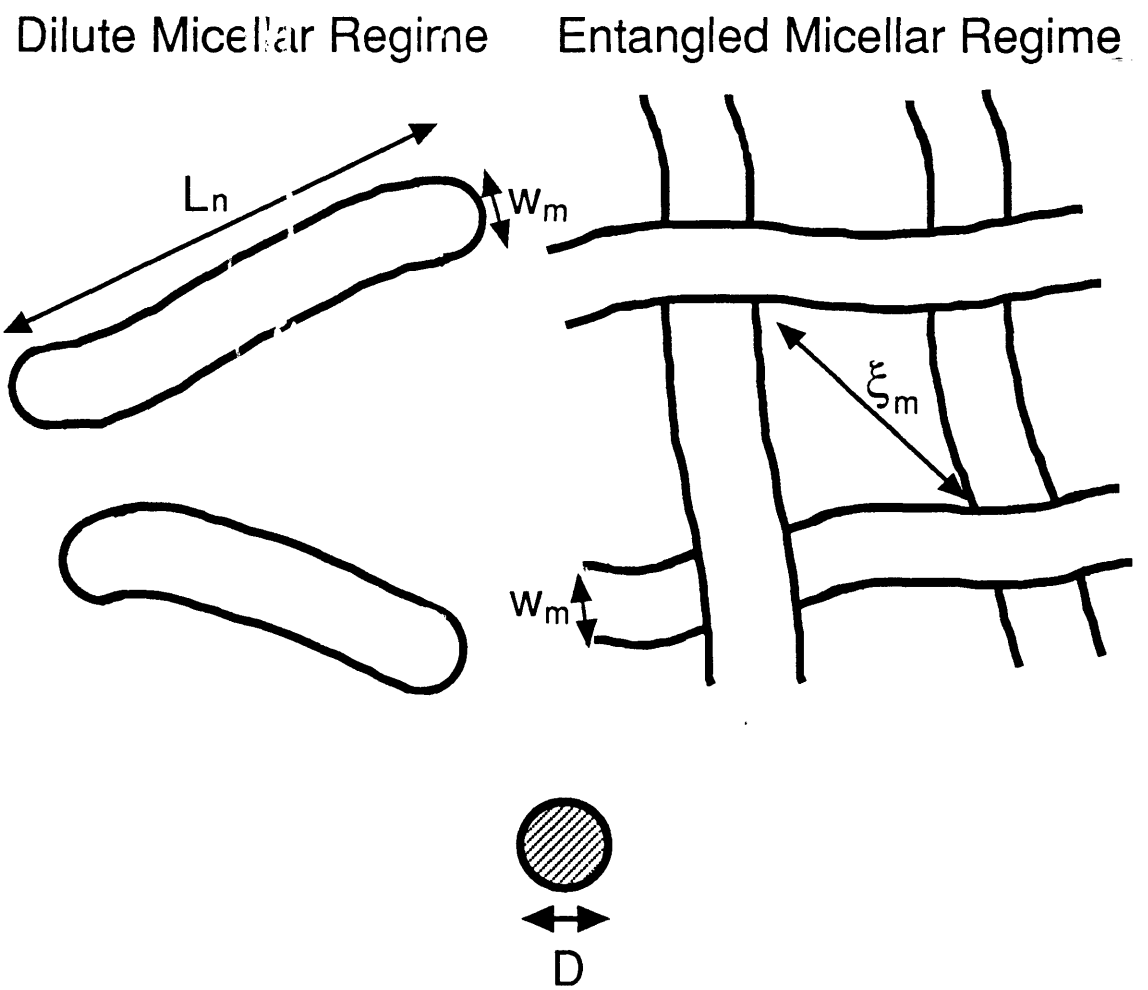

Figure 1-6: A comparison of the length scales associated with hydrophilic proteins and cylindrical micelles. D is the diameter of a protein molecule, $W_m = 2R_0$ is the thickness of a micelle (R_0 is the cross-sectional radius of the cylindrical micelles), L_n is the length of an individual micelle of aggregation number n, and ξ_m is the mesh size of the micellar net or mesh.

phase aqueous micellar systems can indeed provide a mild and friendly environment to biomolecules. As such, two-phase aqueous micellar systems may provide a promising, convenient, and practical methodology for partitioning, separating, or concentrating biomolecules.

The studies reported in this thesis involve the partitioning behavior of biomolecules in two-phase aqueous *micellar* systems. Similar to the case of biomolecule partitioning in two-phase aqueous *polymer* systems, several factors may affect the partitioning behavior in two-phase aqueous *micellar* systems. In the studies reported in this thesis, two important factors — temperature and the size of the partitioned biomolecules —were investigated regarding their effects on the observed partitioning behavior. The reason for choosing temperature as a controlling factor is that, as described in Section 1.2.2, in two-phase aqueous micellar systems, varying temperature will not only change the condition of phase equilibrium by changing the surfactant concentrations in the two coexisting phases, but will also alter the sizes of the micelles present in these two phases (recall that the size distribution of micelles which exhibit one-dimensional growth is strongly dependent on the overall surfactant concentration [27]). Consequently, changing temperature in two-phase aqueous micellar systems is analogous to changing polymer molecular weight in two-phase aqueous polymer systems. In addition, the experimental partitioning results to be presented in the next chapter indicate that the dominant interaction between a hydrophilic entity (protein) and a non-charged micelle is of the excluded-volume type (see Section 2.2.4.3). Accordingly, the partitioning behavior of biomolecules with different sizes is expected to be different due to the difference in their excluded-volume interactions with micelles. In view of this, the size of the biomolecules was chosen as an additional controlling factor in the partitioning experiments reported in this thesis.

When compared and contrasted with two-phase aqueous *polymer* systems which have been studied extensively, many facets associated with two-phase aqueous *micellar* systems, such as the underlying micellar solution structure and its effect on the partitioning behavior, as well as the theoretical basis of biomolecule partitioning, need to be investigated in order to elucidate and enhance our fundamental under-

standing of the partitioning behavior in these systems. This, in turn, will also assist in the practical implementation of two-phase aqueous micellar systems as a useful new technique for the separation or concentration of biomolecules.

1.4 Research Objective and Method of Approach

The central goal of this thesis is to *investigate the partitioning behavior of hydrophilic biological molecules in two-phase aqueous micellar systems.* Specific objectives include:

- To investigate the interactions between micelles and hydrophilic biological molecules responsible for the observed partitioning behavior.
- To develop a theoretical formulation for rationalizing and quantitatively predicting the partitioning behavior of hydrophilic biological molecules.
- To investigate the underlying structure of the micellar solution, and the possible influence of this structure on the partitioning behavior of biological molecules.
- To evaluate the feasibility of utilizing two-phase aqueous micellar systems as a novel practical separation and concentration methodology.

The method of approach to accomplish these objectives is outlined below:

1. To achieve the first objective, partitioning experiments were conducted, using two-phase aqueous micellar systems composed of a nonionic surfactant ($C_{10}E_4$) or a zwitterionic surfactant (C_8-lecithin). Two types of biomolecules — hydrophilic proteins and viruses — were chosen as the partitioned entities, with a total of five proteins and three bacteriophages, all different in size, utilized in the partitioning experiments (see Sections 2.2 and 3.3 for details).
2. To achieve the second objective, a theoretical formulation based on a description of excluded-volume interactions between biomolecules (proteins or viruses) and micelles (cylindrical or spherical) was developed. The flexibility of the

cylindrical micelles was explicitly accounted for in the theoretical formulation describing the partitioning behavior of virus particles. The theoretical predictions were compared with the experimental partitioning results (see Sections 2.3 and 3.4 for details).

3. To achieve the third objective, dynamic light scattering measurements were conducted to investigate the underlying micellar solution structure, and the results were used to help rationalize the observed partitioning behavior of biomolecules (see Chapter 5 for details).

4. To achieve the fourth objective, experiments involving simultaneous partitioning of a protein (ovalbumin) and a virus (P22) at various volume ratios of the two coexisting micellar phases were conducted in order to optimize the separation or concentration efficiencies of the biomolecules in two-phase aqueous micellar systems (see Chapter 4 for details).

1.5 Overview of Thesis

The remainder of the thesis is structured as follows. Chapter 2 presents the partitioning work on hydrophilic proteins in two-phase aqueous micellar systems. This includes the experimental approach, the theoretical formulation to describe the protein partitioning behavior, and a comparison between the theoretical predictions and the experimental results. Chapter 3 describes the partitioning work on virus particles, including experimental results, the theoretical formulation, a comparison between the experimental results and the theoretical predictions, and a preliminary study on kinetic aspects of the partitioning phenomenon. Chapter 4 describes the implementation of two-phase aqueous micellar systems for separation or concentration of biomolecules including proteins and viruses. A comparison of two-phase aqueous micellar systems with other separation methodologies which are currently used in biotechnology is also presented. Chapter 5 presents dynamic light scattering studies aimed at elucidating the underlying solution structure of the $C_{10}E_4$ micellar system.

Finally, Chapter 6 presents a summary and possible extensions of the work presented in this thesis.

Chapter 2

Protein Partitioning in Two-Phase Aqueous Micellar Systems

2.1 Introduction

In this chapter, experimental and theoretical work on the partitioning of hydrophilic proteins in two-phase aqueous micellar systems is reported. As indicated in Chapter 1, this part of the work was inspired by related protein partitioning work in two-phase aqueous polymer systems [19, 20, 21, 22]. Two types of surfactants were used to generate the two-phase aqueous micellar systems, and the partitioning behavior of a total of five hydrophilic proteins was investigated. The protein partition coefficient, K_p, which provides a quantitative measure of the protein partitioning behavior, is defined as

$$K_p = \frac{C_{p,t}}{C_{p,b}} \tag{2.1}$$

where $C_{p,t}$ and $C_{p,b}$ are the protein concentrations in the top and bottom phases respectively, and they were determined using UV/visible light absorbance measurements after partitioning was completed.

This chapter is organized as follows. Section 2.2 presents the experimental study on protein partitioning in two-phase aqueous micellar systems, including the materials, experimental procedures, and results. Section 2.3 presents the theoretical formu-

lation based on a description of the excluded-volume interactions between hydrophilic proteins and micelles, aimed at quantitatively predicting the observed partitioning behavior, as well as a comparison of the theoretical predictions with experimental partitioning data. Finally, Section 2.4 presents concluding remarks on the work reported in this chapter.

2.2 Experimental Approach

2.2.1 Materials

The materials required for the experimental work include surfactants, hydrophilic proteins, and buffer solutions. Below, each material is discussed separately.

2.2.1.1 Surfactants

The criteria for selecting the surfactant include:

- It should be non-destructive to protein molecules. This implies the absence of overall charges on the surfactant heads which may induce protein denaturation, as described in Section 1.2.3.

- It should form a two-phase aqueous micellar system over a convenient temperature range, desirably between 15 - 35°C, such that the integrity of most proteins may be preserved as the proteins are partitioned in the two-phase systems.

- It should be available in high purity, that is, it should be chemically homogeneous. This will reduce artifacts associated with the surfactant chemical heterogeneity. In this case, the resulting surfactant-water micellar solutions will be well characterized, and the comparison between the theoretical predictions and the experimental results will be more precise and devoid of artifacts.

- It should not interfere significantly with the detection methods used to determine protein concentrations.

Specifically, in this study, protein concentrations were measured using the UV/visible absorbance method, and thus the surfactants used should not exhibit absorbance of light in the UV/visible range. Accordingly, surfactants containing phenyl groups (such as those belonging to the Triton series) were not considered appropriate, because the phenyl group has a strong absorbance of light at a wavelength of about 260 nm and can cause interference in the protein concentration measurements, which are usually conducted at 280 nm.

In view of all of the above, the surfactants selected in this study include (1) a nonionic surfactant, decyl tetra(ethylene oxide) ($C_{10}E_4$), and (2) a zwitterionic surfactant, dioctanoyl phosphatidylcholine (C_8-lecithin). Details of their properties are summarized below:

1. **Nonionic Surfactant — $C_{10}E_4$**

   Homogeneous $C_{10}E_4$ (lot no. 1006) was obtained from Nikko Chemicals (Tokyo) and was used as received. This surfactant belongs to the family of alkyl poly(ethylene oxide) nonionic surfactants, C_iE_j, which possess a polar head consisting of j ethylene oxide ($E = OCH_2CH_2$) units and a linear saturated hydrocarbon tail consisting of i carbon atoms. In other words, the surfactant $C_{10}E_4$ has the following chemical formula:

   $$CH_3\text{-}(CH_2)_9\text{ -}(OCH_2CH_2)_4\text{-}OH$$

   The CMC of $C_{10}E_4$ aqueous solutions is 6.4×10^{-4} M at 20.5°C. The $C_{10}E_4$ aqueous micellar system exhibits a lower consolute point, that is, phase separation in this system occurs upon heating. The critical temperature, T_c, of the $C_{10}E_4$-water system is about 20°C in pure water, and about 19°C in pH 7 McIlvaine buffer (see Section 2.2.1.3 for details) at a critical surfactant concentration of about 2.5 wt%. Hence, phase separation in the $C_{10}E_4$-water system occurs over a convenient temperature range for protein partitioning. In addition, $C_{10}E_4$ micelles also exhibit significant one-dimensional growth into cylindrical structures. Therefore, the $C_{10}E_4$-water system is expected to have a transition in

the solution structure from the "dilute" to the "entangled" regimes, similar to that observed in the $C_{12}E_6$-water system (see Figure 1-5).

Note that the absolute values of critical properties, T_c and X_c, as well as of other micellar solution properties such as the CMC, of aqueous C_iE_j surfactant solutions may depend on the particular surfactant lot used in the experiments due to the possible presence of impurities. For the $C_{10}E_4$ surfactant used in this study, the high purity of the surfactant lot (No. 1006) was tested and proved by the manufacturer, and all the $C_{10}E_4$ surfactant utilized in the experiments reported hereafter belonged to this lot (lot no. 1006).

2. **Zwitterionic Surfactant — C_8-Lecithin**

C_8-lecithin powder (lot no. 80PC-34) was obtained from Avanti Polar Lipids, Inc. (Alabaster, Alabama) and was used as received. Its molecular structure is shown in Figure 2-1, indicating that the hydrophobic part consists of two saturated hydrocarbon chains, each having eight carbons and being attached to a glycerol moiety. The hydrophilic phosphatidylcholine group is zwitterionic in the pH range 3 - 11, which implies that over this pH range the head possesses two opposite charges, and the net charge is therefore zero. The structure of the C_8-lecithin molecule is quite similar to that of the phospholipids found in membranes of living organisms, but its hydrocarbon chains are only half as long as those typically found in biological phospholipids.

The CMC of C_8-lecithin in water is 2.5×10^{-4} M at 48°C. The aqueous micellar system of C_8-lecithin exhibits an upper consolute point, and phase separation is thus induced by lowering the temperature. The critical point of the C_8-lecithin-water micellar system is characterized by $T_c \approx 47.5$°C and $X_c = 9.3 \times 10^{-4}$ (mole fraction) = 2.77 wt% in pure water [49]. As in the $C_{10}E_4$-water system, micelles of C_8-lecithin exhibit significant one-dimensional growth into cylindrical structures [27, 49], and a transition from the "dilute" to the "entangled" regimes is also expected in the C_8-lecithin-water system.

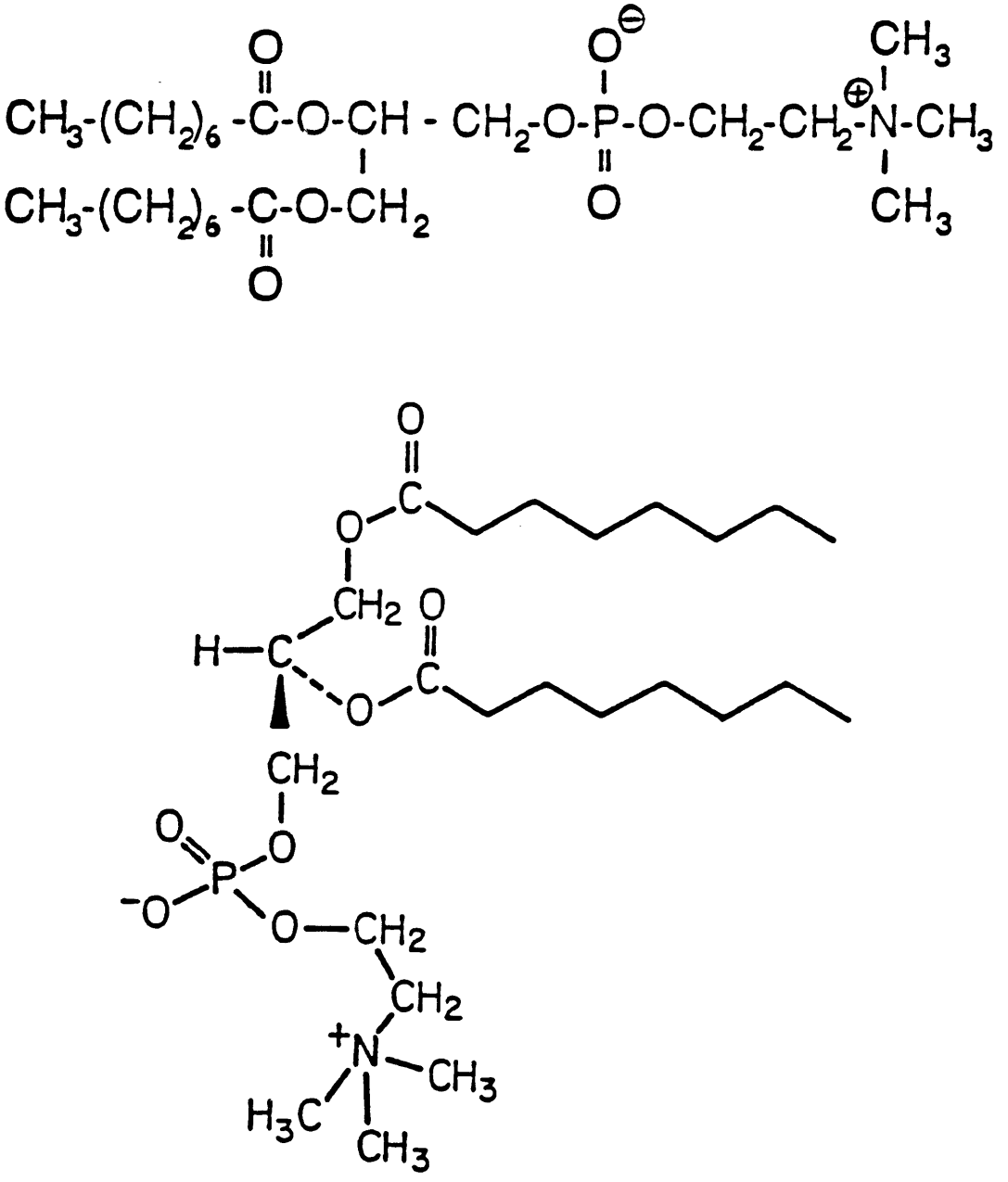

Figure 2-1: Chemical formula and molecular structure of C_8-lecithin (from Reference [49]).

2.2.1.2 Hydrophilic Proteins

Five hydrophilic proteins with different molecular weights (sizes) were selected, since the protein size (molecular weight) was chosen as one of the controlling factors in the present study. The five hydrophilic proteins, cytochrome *c* (from horse heart), soybean trypsin inhibitor (type I-S), ovalbumin, bovine serum albumin, and catalase (from bovine liver), were obtained from Sigma Chemicals (St. Louis, Missouri) and were used as received. Their properties are listed in Table 2.1 [50, 51, 52].

Table 2.1: The five hydrophilic proteins used in this study and some of their characteristic properties.

Protein	Molecular Weight	Isoelectric Point, pI	Hydrodynamic Radius, R_p (Å)
Cytochrome *c*	12,400	10.6	19
Soybean Trypsin Inhibitor	24,000	4.5	22
Ovalbumin	44,000	4.6	29
Bovine Serum Albumin	66,000	4.8	36
Catalase	232,000	5.6	52

An additional useful property of cytochrome *c* and catalase is that they contain a heme group in their molecular structures, and hence they absorb light in the visible range. This makes their concentration measurements easier and more accurate than those for other proteins which do not absorb visible light when the UV/visible light absorbance method is used for protein concentration determination. In the case of cytochrome *c*, since it is typically oxidized when being exposed to air and thus exhibits a different absorbance pattern from that of its reduced form, sodium ascorbate was added into all cytochrome *c* solutions in order to convert cytochrome *c* molecules to the reduced form before measuring the cytochrome *c* concentrations using the UV/visible absorbance method.

The overall protein concentrations used in the partitioning studies were kept low because, under this condition, (1) the interactions between protein molecules are weak and can therefore be neglected, and (2) the micellar structures and size distributions,

as well as the phase separation behavior of the micellar solutions, can be assumed not to be perturbed to any significant extent by the presence of the protein. The overall protein concentrations used in the partitioning experiments were 0.5 g/L or lower.

2.2.1.3 Buffer Solution

The purpose of using buffer is to maintain the solution pH stable and constant. McIlvaine buffer at pH 7, which is composed of citric acid and disodium phosphate aqueous solutions, was used in all experiments. The buffer was prepared by mixing 18.15 mL of 0.1 M citric acid solution with 81.85 mL of 0.2 M disodium phosphate solution in order to obtain a solution pH of 7, and then diluting this mixture by adding water to make the final volume 1 L in order to reduce the salt concentrations and the salt effects on the proteins and the micellar system.

The molecular weights and trade names of the citric acid and disodium phosphate salt used for preparing the McIlvaine buffer are as follows:

- Citric Acid — $H_3C_6H_5O_7 \cdot H_2O$, Formula weight = 210.14 g/mol, Malinckrodt, No. 0616.
- Disodium Phosphate — $Na_2HPO_4 \cdot 7H_2O$, Formula weight = 268.07 g/mol, Fisher Scientific.

Deionized water purified by a Milli-Q ion-exchange system was used to prepare all the salt solutions as well as for dilution. The final buffer solution also contained 0.02% sodium azide to prevent bacterial growth.

2.2.2 Coexistence (Cloud-Point) Curve Measurement

The purpose of this measurement is (1) to obtain the coexistence curve of the aqueous micellar system, as well as to identify the temperature range for the partitioning experiments, and (2) to observe any effects induced by the presence of proteins on the phase separation equilibrium of the (protein-free) aqueous micellar system.

The method adopted for this measurement is the cloud-point measurement, in which the cloud-point temperature, T_{cloud}, of a micellar solution of a specific concen-

tration is measured. The cloud-point temperature is the temperature at which phase separation of the solution begins to occur. As the temperature approaches T_{cloud}, the solution becomes cloudy and turbid. Hence, T_{cloud} can be detected visually as the solution turns cloudy. A plot of the experimentally determined cloud-point temperature, T_{cloud}, as a function of surfactant concentration, X, yields the coexistence curve. This measurement was performed on aqueous micellar solutions without and with a protein present in the solutions in order to investigate whether the presence of proteins affected the phase separation behavior of the micellar system.

As stated in Section 1.2.2, some aqueous micellar systems exhibit lower consolute (coexistence) curves, such as the C_iE_j-water systems (see Figure 1-3 for an example), and hence the phase separation phenomenon occurs when the micellar solutions are heated up. For the aqueous micellar systems exhibiting upper consolute (coexistence) curves, such as the C_8-lecithin-water system (see Figure 1-4), phase separation occurs when the micellar solutions are cooled down.

2.2.2.1 Apparatus

The apparatus used to measure the cloud-point temperature, T_{cloud}, consists of a transparent water cell constructed from plexi-glass, as shown in Figure 2-2. This cell has eight holes on the top for inserting the test tubes containing surfactant solutions, and the transparent cell permits visual inspection of the onset of phase separation in the surfactant solutions. The water cell is connected to a water bath (Neslab RTE-110) by insulated rubber tubings, and the inflow and outflow of water in the cell can be controlled by two stopcocks on the rubber tubings. The temperature of the water in the cell, as well as that of the solutions in the test tubes, is controlled by the water bath, whose temperature control is precise to within 0.1°C. A temperature probe (Omega Thermistor Thermometer) is inserted in a test tube filled with water, as shown in Figure 2-2, for measuring *in situ* the actual water temperature in the cell. The box is placed on a magnetic stirrer (Thermolyne Nuova II), and each of the solutions in the test tubes contains a small magnetic bar which can rotate, as induced by the magnetic stirrer, in order to aid mass and heat transfer in the solution. A piece

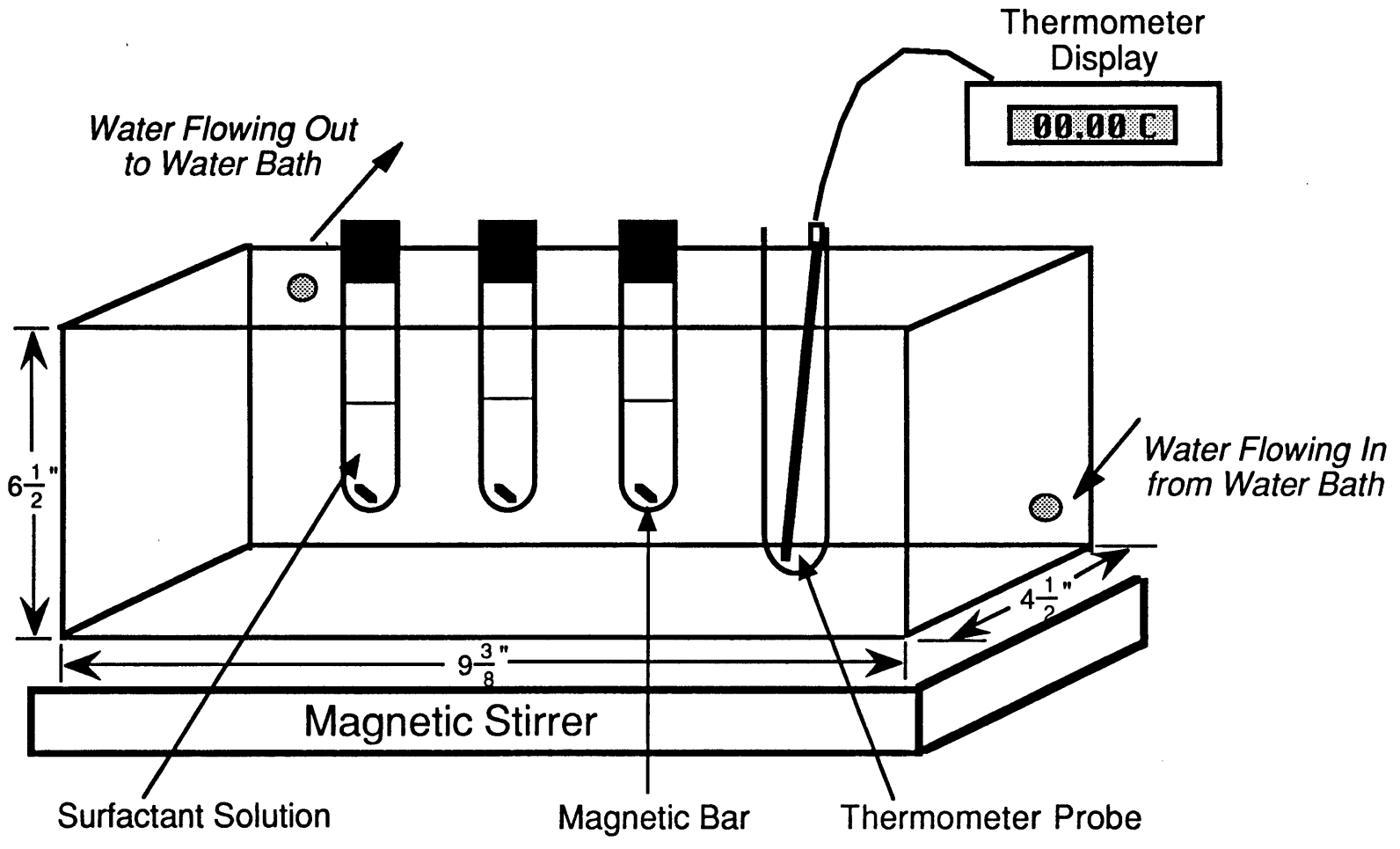

Figure 2-2: Schematic description of the experimental apparatus used to measure the coexistence (cloud-point) curves of aqueous micellar solutions. Note that there are four more holes on the top of the actual water cell used in the experiments.

of black paper, with the words "clear" written in white, is attached to the back of the cell, with the words "clear" arranged in such a way that they can be seen through the solutions in the test tubes. The cloud-point temperature of a micellar solution is then identified as the temperature at which the solution turns cloudy enough so that the word "clear" just disappears when seen through the solution.

2.2.2.2 Experimental Procedures

The following procedures were implemented to measure the cloud-point temperatures. For the sake of illustration, the measurement of T_{cloud} in the $C_{10}E_4$-water system is considered. Similar procedures were also implemented in the C_8-lecithin-water system, with the only difference being that the temperature was lowered instead of being raised.

1. 1.5 - 2 mL of surfactant solutions of a given surfactant concentration (in the range of 0.25 - 11 wt% for the $C_{10}E_4$-water system) were prepared in the McIlvaine buffer at pH 7 in screw-top test tubes. A small teflon magnetic bar was then introduced in each test tube.

2. The test tubes containing surfactant solutions were placed in the water cell. Each solution in the water cell was initially cooled to a temperature low enough such that it exhibited a single, clear, homogeneous phase. The temperature in the water cell was then raised in small increments (of about 0.02 - 0.03°C) by adjusting the temperature of the water bath until the solution began to become cloudy at a temperature T_{heat}. Subsequently, the temperature was lowered in small steps (of about 0.02 - 0.03°C) until cloudiness in the solution disappeared at a temperature T_{cool}. Note that, at each heating-up or cooling-down step, the solution was first stirred thoroughly by turning on the magnetic stirrer to ensure temperature and concentration homogeneity, and subsequently observed for any signs of change in cloudiness with the stirrer turned off. The entire heating-up and cooling-down procedures were repeated for several times to ensure reproducibility and reversibility of the observed clouding behavior. The cloud-point

temperature, T_{cloud}, was then determined by taking the average of the T_{heat}'s and T_{cool}'s, with the measured T_{heat}'s and T_{cool}'s generally reproducible to within 0.03°C.

3. The cloud-point curves of the $C_{10}E_4$ micellar system in the presence of proteins were then measured. First, a protein solution containing 0.5 g/L protein was prepared in McIlvaine buffer (the protein concentration was 0.25 g/L in the case of cytochrome *c*), and then 1.5 - 2 mL of surfactant solution was prepared from this protein solution. Step 2 was subsequently followed to determine the corresponding cloud-point temperature, T_{cloud}.

4. T_{cloud} versus surfactant concentration was then plotted to yield the cloud-point (coexistence) curve.

2.2.2.3 Results and Discussion

Figure 2-3 shows the experimental cloud-point curves of aqueous $C_{10}E_4$ surfactant solutions without protein (○), and with 0.25 g/L cytochrome *c* (△), 0.5 g/L ovalbumin (∗), and 0.5 g/L catalase (□) in McIlvaine buffer at pH 7. From Figure 2-3, one finds that the critical temperature, T_c, and the critical surfactant concentration, X_c, are 18.81°C and 2 wt% respectively, with or without protein. This figure indicates that, over the range of surfactant concentrations examined, the added proteins have a negligible effect on the phase separation behavior of the $C_{10}E_4$ solutions. This important finding will be utilized in the theoretical formulation (presented in Section 2.3.1) to decouple the description of the protein partitioning from that of the surfactant solution phase separation.

Shown in Figure 2-4 is the cloud-point curve of the C_8-lecithin-buffer micellar system. Due to the high cost of this material, only the cloud-point curve without protein was measured. However, the finding from Figure 2-3 that the presence of proteins does not affect the phase separation equilibrium of the $C_{10}E_4$ micellar solutions should also be applicable to the C_8-lecithin-buffer micellar system.

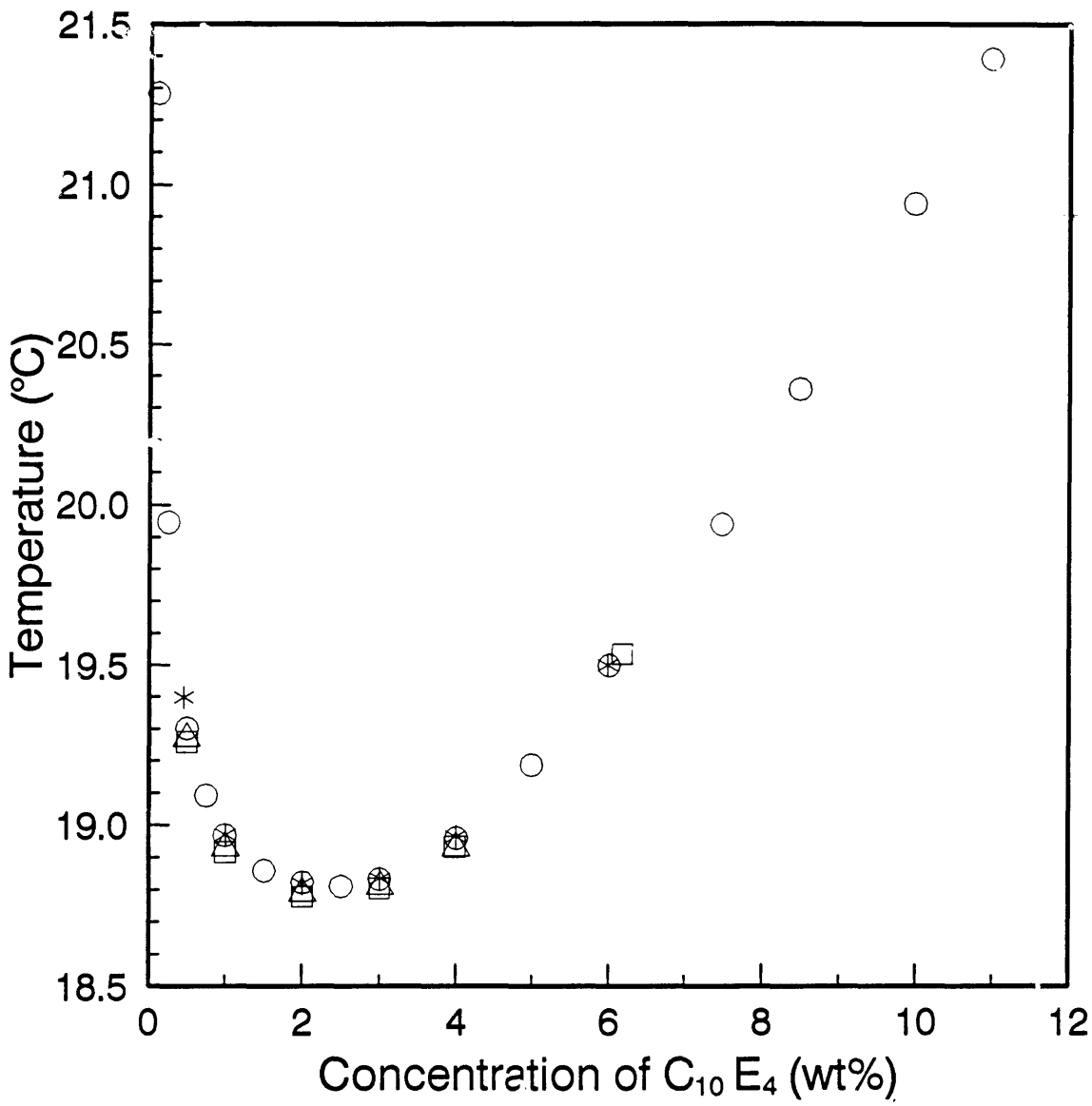

Figure 2-3: Experimentally measured cloud-point (coexistence) curves of the $C_{10}E_4$ micellar system in pH 7 McIlvaine buffer without protein (○) and with 0.25 g/L cytochrome c (△), 0.5 g/L ovalbumin (∗), and 0.5 g/L catalase (□). The area above the data-point curve is the two-phase region, in which the partitioning experiments were conducted.

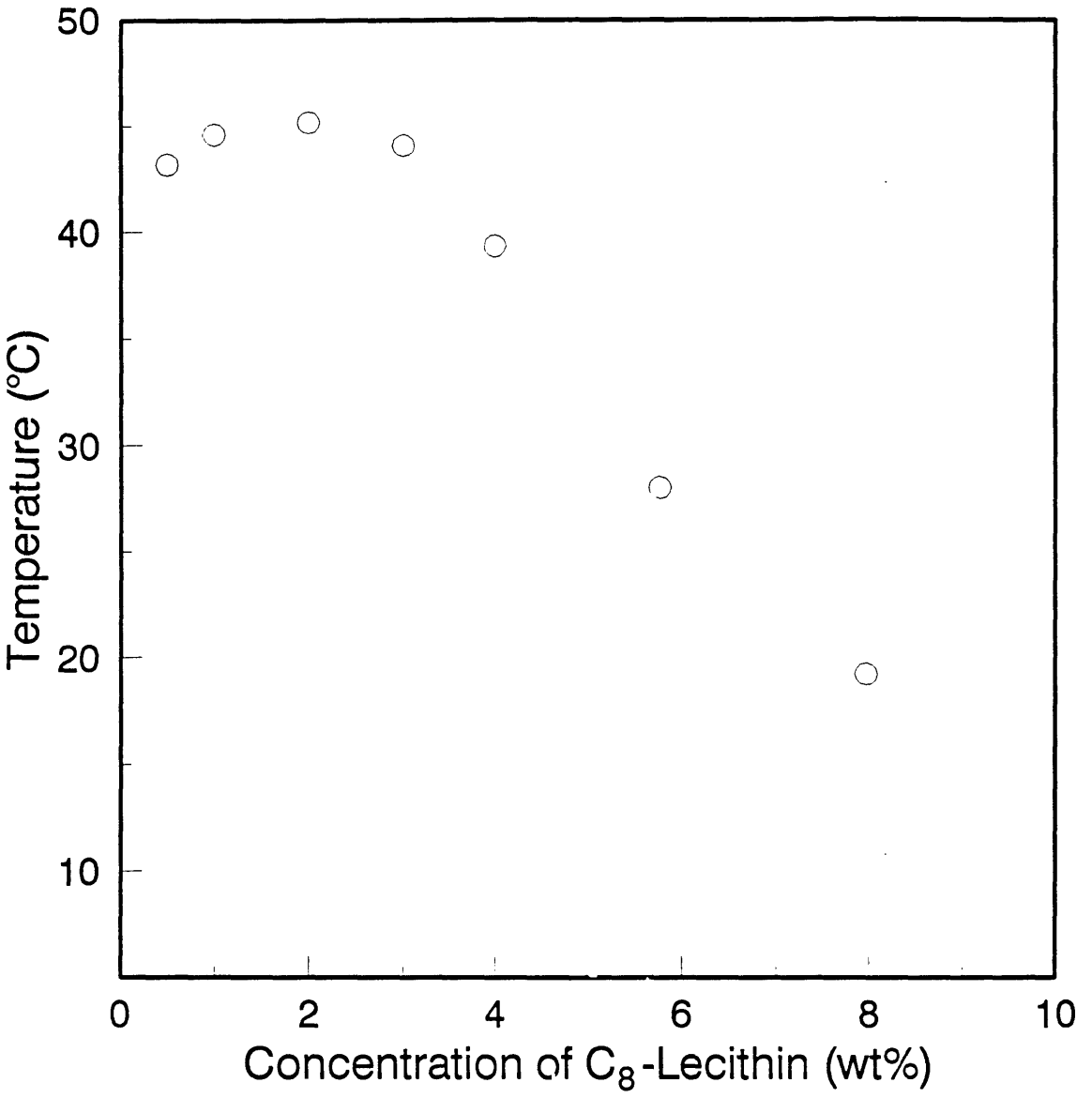

Figure 2-4: Experimentally measured cloud-point (coexistence) curve of the C_8-lecithin micellar system in pH 7 McIlvaine buffer without protein (○). The area beneath the data-point curve is the two-phase region, in which the partitioning experiments were conducted.

2.2.3 Correlation Plots of Proteins

In the partitioning experiments, protein concentrations were determined using UV/visible absorbance measurements. The reason for choosing this method for determination of protein concentrations is that, when compared to other assaying methods, including the Biuret and Lowry methods [53], the UV/visible absorbance measurement is relatively straightforward and convenient to perform, and, if done properly, is devoid of possible side effects associated with the presence of surfactant.

The protein correlation plots display the correlation between the protein concentrations and the UV/visible absorbance of the protein solutions at a specific wavelength, when the UV/visible absorbance technique is used to measure protein concentrations. Typically, all the protein molecules have an absorbance band at about 280 nm, which is proportional to the protein concentration in solutions, with different proportionality constants for different protein species. As a result, the absorbance at 280 nm is generally adopted as an index of protein concentrations in solutions.

The purpose of this measurement is to examine whether the presence of micelles in the protein solutions will interfere with the protein concentration measurement utilizing the UV/visible absorbance method, that is, whether the linear relationship between the protein concentration and the UV/visible absorbance reading exists for protein solutions with and without surfactants (micelles), since micelles coexisted with proteins in the solutions to be examined. Although, as stated earlier, the surfactants ($C_{10}E_4$ and C_8-lecithin) were selected because they do not absorb light in the UV/visible range, the micelles present in solutions can scatter light due to their large sizes. Since the spectrophotometer, the instrument used for measuring the absorbance, measures the intensity of the transmitted beam through the solution, and it assumes that the portion of light not being transmitted is all being "absorbed" by the solution, even though this portion of light may actually be scattered instead of being absorbed. It follows that the scattering of light by micelles can definitely interfere with the protein concentration measurement. It is therefore important to find a method to properly remove the interfering effect of the micelle scattering in

order to obtain a high accuracy in protein concentration measurements. In addition, since the scattered light intensity increases with decreasing wavelength ("Rayleigh scattering" [54]), the interference of micelle scattering with the protein concentration measurement should be more pronounced at lower wavelengths. In view of this, those proteins which have absorbance bands at higher wavelengths, particularly in the visible range, are more favorable, since their concentration measurements will be affected to a smaller extent by the micelle scattering. Proteins containing heme groups in their molecular structure, such as cytochrome c and catalase, fall in this category.

It is also noteworthy that the micellar solutions undergoing phase separation will become cloudy and turbid, a feature which will hinder the UV/visible absorbance measurements. It is therefore necessary to keep the solutions at temperatures at which each of the solutions exists as a clear and single phase in the UV/visible absorbance measurements. The change of temperature does not affect the protein concentration measurement since the UV/visible absorbance of proteins is not dependent on the temperature. For the $C_{10}E_4$-buffer micellar system, whose critical temperature is about 19°C, the temperature at which the UV/visible absorbance was measured was about 15°C, 4°C below T_c; for the C_8-lecithin-buffer system, a temperature which was 3°C higher than that corresponding to the cloud point of the surfactant solution was adopted. For example, for a C_8-lecithin solution with $T_{cloud} = 10$°C, the protein concentration was determined at 13°C.

2.2.3.1 Equipment

A Shimadzu UV-160V double-beam spectrophotometer was used for the UV/visible absorbance measurements. The cell holders in the spectrophotometer were connected to a water bath (Neslab RTE-110), whose temperature control was precise to within 0.1°C, in order to adjust the temperature of the solutions placed in the cell holders. Semi-micro quartz cuvettes were used in order to achieve high accuracy and consistency in the measurements.

2.2.3.2 Experimental Procedures

A. Correlation Plots of Protein Solutions Without Surfactant

1. Protein solutions of various concentrations (0 - 1 g/L) were prepared in pH 7 McIlvaine buffer.

2. The protein solutions were poured into quartz cuvettes, and the UV/visible absorbance of the solutions was measured with the spectrophotometer, using the buffer solution as the reference. The absorbance at 280 nm was measured for most of the proteins, 410 nm for catalase, and 549.5 nm for cytochrome *c* after cytochrome *c* solutions were reduced by adding sodium ascorbate.

3. The UV/visible absorbance readings versus protein concentrations were then plotted for each protein to yield the correlation plot. A linear relationship was obtained.

B. Correlation Plots of Protein Solutions in the Presence of $C_{10}E_4$

1. Protein solutions of various concentrations (0 - 1 g/L) were prepared as described in A.1, followed by the addition of $C_{10}E_4$ into each of the protein solutions. A solution containing only surfactant and buffer, but without protein, was also prepared as the "standard" solution. All the solutions prepared had the same surfactant concentration but different protein concentrations.

2. The UV/visible absorbance measurements were conducted at 15°C. The absorbance measurements were conducted after the solutions were kept in the cell holders in the spectrophotometer at this temperature for at least 40 minutes, and the solutions were totally clear and uniform. In addition to the absorbance at the wavelength of 280 nm (or 410 nm for catalase and 549.5 nm for cytochrome *c*), the absorbance at a higher wavelength, at which no significant absorbance band was located, such as 400 nm (and 600 nm for catalase and cytochrome *c*), was also measured for comparing and calculating the micelle light scattering effect.

3. All the absorbance readings were measured with a buffer solution as the reference. The absorbance of protein in a solution was obtained by subtracting the readings of the surfactant solution without protein (the "standard") to eliminate the micelle light scattering effect. Specifically, using the following notation,

   A^0_{280}, A^0_{400} = Absorbance readings of the "standard" solution at 280 nm and 400 nm respectively,

   A_{280}, A_{400} = Absorbance readings of the solution containing both protein and surfactant at 280 nm and 400 nm respectively,

   A^*_{280} = Absorbance of protein in the solution at 280 nm, which reflects the contribution of protein absorbance solely and therefore should be proportional to the protein concentration,

   A^*_{280} was calculated according to the following equation:

$$A^*_{280} = A_{280} - A_{400} - (A^0_{280} - A^0_{400}) \tag{2.2}$$

   Note that A_{280}, A_{400}, etc. were replaced in Eq. (2.2) by $A_{549.5}$, A_{600}, etc. in the case of cytochrome c solutions, and by A_{410}, A_{600}, etc. in the case of catalase.

4. A^*_{280} data were plotted as a function of the protein concentration. The resulting correlation plot was compared to that obtained without surfactant present in the solutions.

2.2.3.3 Results and Discussion

Figure 2-5 is an example of the correlation plot of ovalbumin at different $C_{10}E_4$ concentrations in pH 7 McIlvaine buffer. The correlation curves of the other proteins were also found to exhibit a similar pattern. This figure indicates that, after subtracting the micelle scattering effect, as in Eq. (2.2), the presence of micelles does not seem to affect the protein concentration measurement to any significant extent. In addition, from the linear relation displayed in the correlation plots, such as the one shown in Figure 2-5 corresponding to ovalbumin, the actual protein concentration

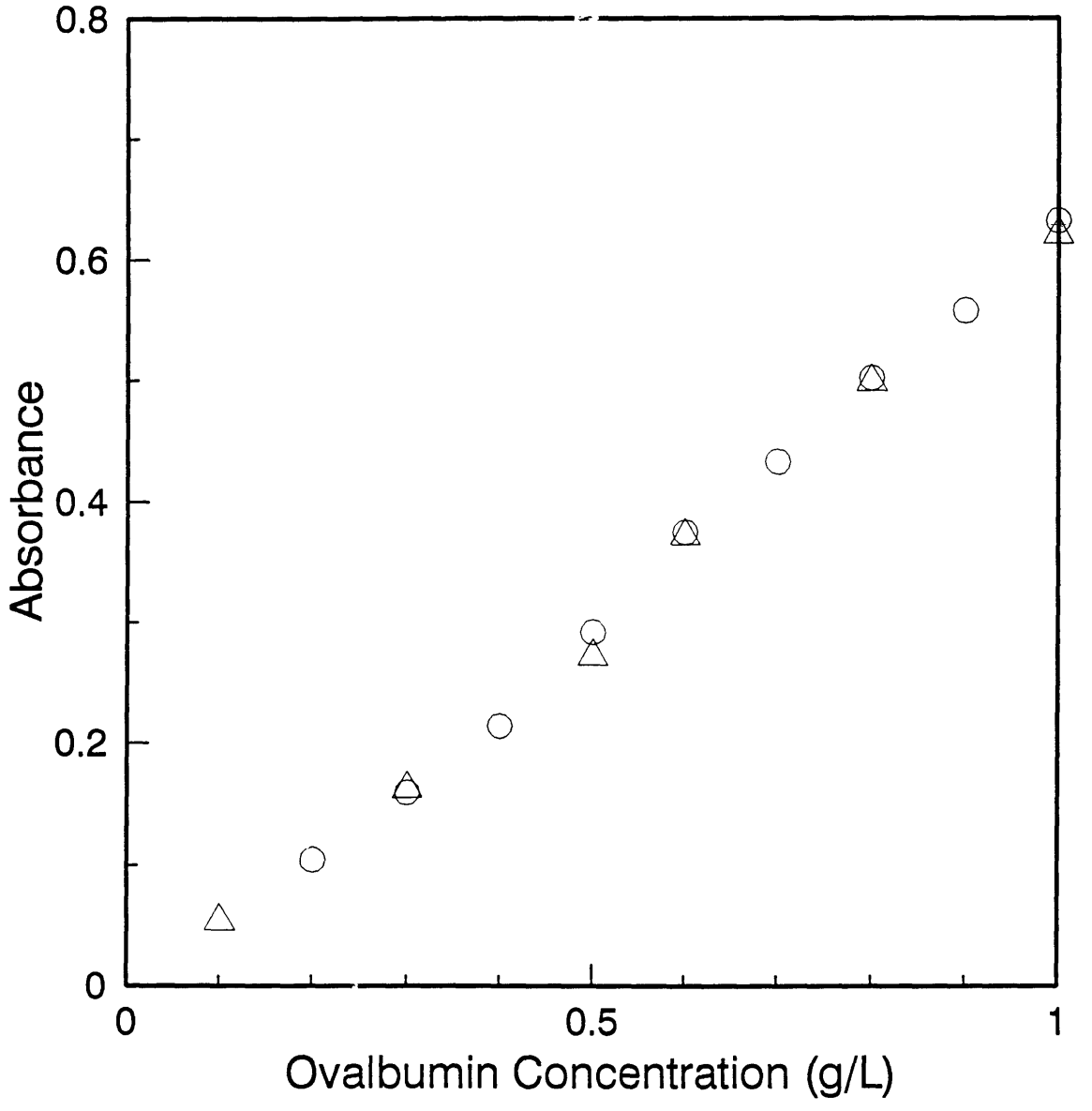

Figure 2-5: Correlation plot of ovalbumin with 0 (◯) and 4 wt% (△) $C_{10}E_4$ in pH 7 McIlvaine buffer.

in the solution can be calculated from the measured absorbance if the solution does not contain surfactant, or it can be calculated from the A^*_{280} values if the solution contains surfactant.

2.2.4 Protein Partition Coefficient Measurement

The protein partition coefficient, K_p, as defined in Eq. (2.1), was measured and calculated from the protein concentrations in the top and bottom phases after partitioning was completed. Each partitioning experiment was conducted at a specific temperature at which the micellar system exhibited phase separation behavior, and only one protein species was partitioned in one phase-separated system.

2.2.4.1 Equipment

The apparatus used in the partitioning experiments was the same as the one described in Section 2.2.2.1 and shown in Figure 2-2, except that the magnetic stirrer and small magnetic bars were not needed. 1-cc Syringes and needles were used to extract the phase solutions after partitioning was completed. The Shimadzu UV-160V double-beam spectrophotometer and quartz cuvettes were used to measure protein concentrations, as described in Sections 2.2.3.1 and 2.2.3.2.

2.2.4.2 Experimental Procedures

1. At least three surfactant solutions containing 0.5 g/L of a protein species (0.25 g/L when cytochrome *c* was partitioned) in pH 7 McIlvaine buffer were prepared. The total surfactant concentration in each of the solutions was chosen to yield approximately equal volumes of the two phases at each temperature, that is, the total surfactant concentration corresponded to the mid-point of the tie-line at the experimental temperature, as determined from the temperature versus concentration coexistence (cloud-point) curve. Another solution with the same total surfactant concentration, but without protein, was also prepared in pH 7 McIlvaine buffer as the "reference" solution. All the solutions were well mixed

by shaking gently and were kept at a temperature at which the solutions exhibited a clear, single phase.

2. Once the water temperature in the cell was set and maintained at the desired temperature, the solutions prepared in step 1 were placed in the water cell and allowed to equilibrate for at least 6 hours. The temperature in the cell was kept constant and was monitored using the thermometer probe during this period of time.

3. Following equilibration, the two phases in each solution were withdrawn with great care using syringe and needle sets in order to ensure that no mixing of the two phases occurred. One syringe and needle set was used exclusively for withdrawing one phase solution.

4. UV/visible absorbance measurements were conducted on all phase solutions in order to measure protein concentrations. Equation (2.2) was applied to subtract the effect of micelle light scattering, using the two phases of the "reference" solution as the "standard" of the top and bottom phases. The protein concentration in each of the phase solutions was then calculated according to the linear relation obtained from the correlation plot of the corresponding protein.

5. The protein partition coefficient, K_p, was calculated according to Eq. (2.1). A mass balance calculation on the amount of protein before and after partitioning was performed in order to assess the accuracy of the measured protein concentrations.

2.2.4.3 Results and Discussion

Figure 2-6 shows the experimentally measured partition coefficients, K_p, of cytochrome c (▲), ovalbumin (●), and catalase (■) as a function of temperature over the range 18.8 - 21.2°C in two-phase aqueous $C_{10}E_4$ systems containing 0.25 g/L cytochrome c, 0.5 g/L ovalbumin, and 0.5 g/L catalase, respectively, in pH 7 McIlvaine buffer. The fact that $K_p < 1$ indicates that these three hydrophilic proteins

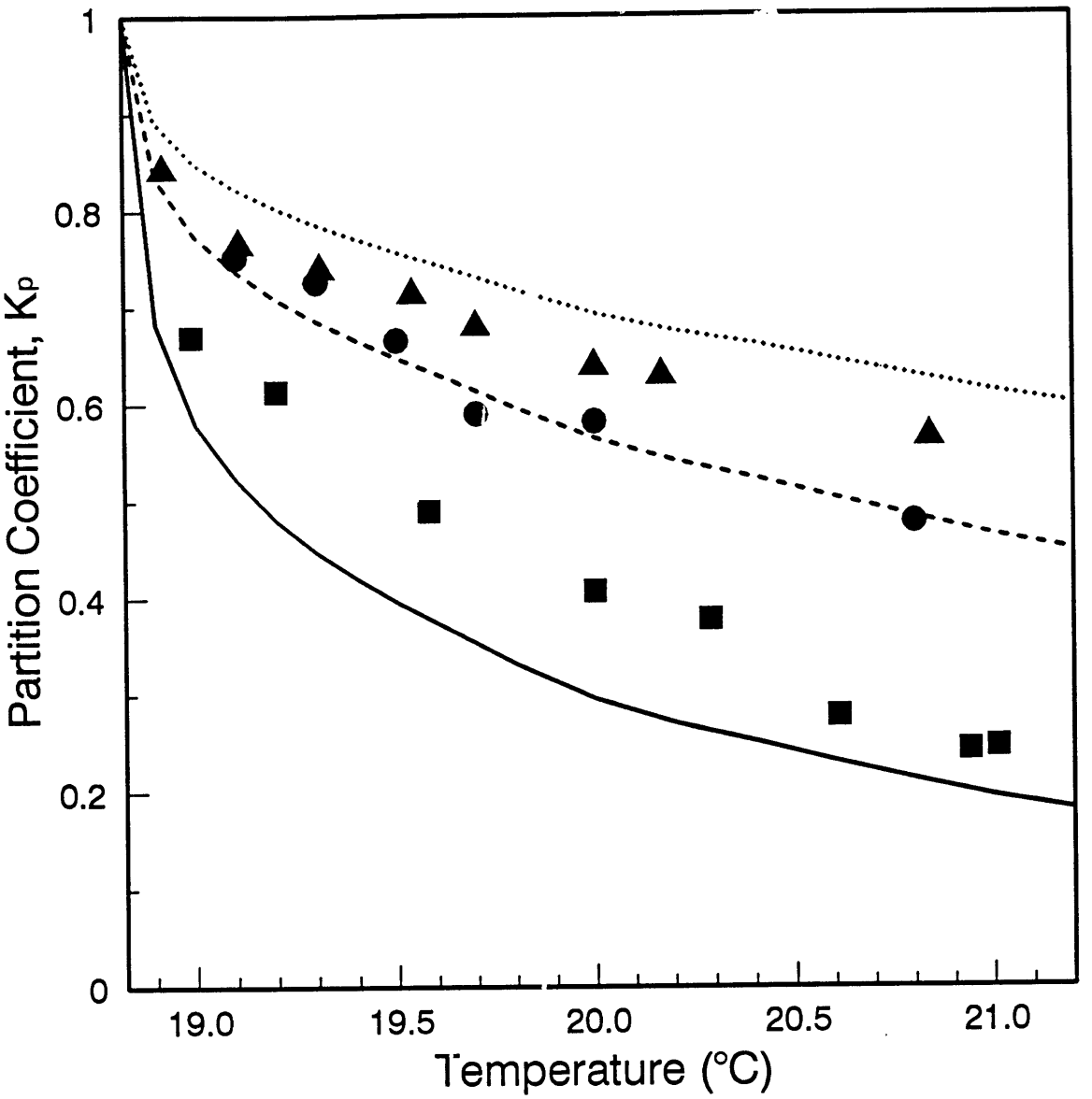

Figure 2-6: Experimentally measured partition coefficients, K_p, of cytochrome c (▲), ovalbumin (●), and catalase (■) in the temperature range of 18.8 - 21.2°C in the two-phase aqueous $C_{10}E_4$ micellar system. Also shown are the predicted partition coefficients K_p of cytochrome c (···), ovalbumin (– –), and catalase (—) as a function of temperature.

partition preferentially into the *bottom micelle-poor phase.* At the critical point, T_c= 18.81°C, which corresponds to the minimum of the coexistence curve in Figure 2-3, the partition coefficients should approach unity since the two coexisting micellar phases become identical at this point. As the temperature increases away from the critical temperature, K_p decreases and deviates further from unity for all the three proteins. These observations suggest that (1) proteins are pushed into the phase which has a larger available free volume (which, in this case, is the bottom micelle-poor phase), and (2) this tendency becomes stronger as $(T - T_c)$ increases, that is, with increasing difference in the surfactant concentrations (or the volume fractions occupied by micelles) of the two coexisting phases (see Figure 2-3). One can also observe from Figure 2-6 that, at a fixed temperature, the extent of the protein partitioning into the bottom micelle-poor phase increases in the order cytochrome $c <$ ovalbumin $<$ catalase. These observed trends are consistent with the notion that excluded-volume interactions between proteins and $C_{10}E_4$ micelles play the dominant role in determining the observed partitioning behavior, since catalase has the largest size (M.W.=232 000 Da), followed by ovalbumin (M.W.=44 000 Da), and cytochrome c (M.W.=12 400 Da). The errors of the mass balance calculation were small (generally within $\pm$10%), indicating that no significant loss of materials had occurred, and that the proteins did not accumulate at the interface between the two phases (this was also observed by visual inspection of the interface).

Some partitioning results in the C_8-lecithin micellar system are presented in Figure 2-9 (see Section 2.3.2 for details).

2.3 Theoretical Approach

2.3.1 Theoretical Formulation

Results of various experimental and theoretical studies have shown [27, 55, 56] that, under appropriate solution conditions, $C_{10}E_4$ and C_8-lecithin can form long, flexible, and polydisperse cylindrical micelles. The average length of a $C_{10}E_4$ or C_8-lecithin

micelle greatly exceeds the hydrodynamic radius of a typical hydrophilic protein (20 - 60Å), and the micelles appear rigid on the scale of a typical protein molecule, as discussed in Section 1.3. As stated in Section 1.2.3, experimental results indicate [43, 44] that hydrophilic proteins do not bind nonionic and zwitterionic surfactants of the type used in this study to any significant extent. In addition, the coexistence (cloud-point) curve measurements, such as those reported in Figure 2-3, reveal that the effect of these hydrophilic proteins on micellar characteristics, including phase separation behavior, is negligible. In view of these observations, it is reasonable to assume that, to a first approximation, hydrophilic proteins and $C_{10}E_4$ or C_8-lecithin micelles behave as mutually non-associating entities interacting primarily through short-ranged, repulsive, excluded-volume interactions. In addition, the micellar solutions in the two coexisting phases are assumed to be at θ-solvent conditions [15, 57]. Under such conditions, the excluded-volume interactions and the attractive interactions (primarily of the van der Waals type) between the micelles exactly cancel each other. Therefore, the non-charged cylindrical micelles can be modeled as non-interacting, mutually penetrable, polydisperse, hard spherocylinders, and the globular hydrophilic proteins are modeled as non-interacting hard spheres [7]. Geometric models of the micelles and the proteins are shown in Figure 2-7.

As stated earlier, the protein partition coefficient is defined in Eq. (2.1) as

$$K_p = \frac{C_{p,t}}{C_{p,b}} \tag{2.3}$$

where $C_{p,t}$ and $C_{p,b}$ are the protein concentrations in the top (t) and bottom (b) phases respectively. Under conditions of low protein concentration, non-charged surfactants, and low salt concentration, the assumption that protein molecules and micelles interact as hard particles can be justified. In Appendix A, it is shown that K_p is given by

$$K_p = \frac{\Omega_t}{\Omega_b} \tag{2.4}$$

Model Cylindrical Micelle

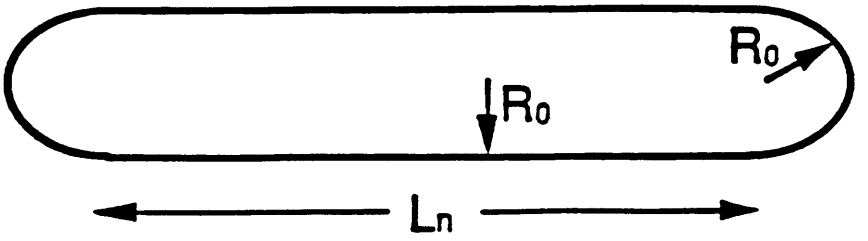

$$V_n = \pi R_0^2 (L_n + 4R_0/3)$$

Model Globular Protein

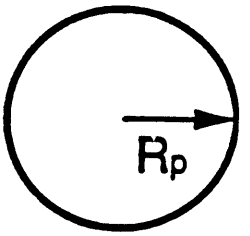

$$V_p = 4\pi R_p^3/3$$

Figure 2-7: Geometric models of the cylindrical micelles and the globular hydrophilic protein molecules assumed in the excluded-volume theoretical approach. The cylindrical micelles are modeled as hard spherocylinders, with hemispherical caps on both ends of the cylinders, and the protein molecules are modeled as hard spheres.

where Ω is given by

$$\Omega = \exp\,(-\sum_n N_n U_{n,p}/V) \tag{2.5}$$

where $U_{n,p}$ is the excluded volume between a protein molecule and a micelle of aggregation number n, N_n is the number of micelles of aggregation number n, and V is the volume of the phase. Using Eq. (2.5) in Eq. (2.4) yields

$$K_p = \exp\,[\,-\sum_n U_{n,p}\left(\frac{N_{n,t}}{V_t} - \frac{N_{n,b}}{V_b}\right)\,] \tag{2.6}$$

The interested reader is referred to Appendix A for a detailed derivation of Eqs. (2.4), (2.5), and (2.6).

The excluded volume, $U_{n,p}$, between a protein molecule (sphere) and a micelle (spherocylinder with hemispherical ends) is given by [7]

$$U_{n,p} = 4\pi(R_n + R_p)^3/3 + \pi(R_n + R_p)^2 L_n \tag{2.7}$$

where R_n and L_n are the cross-sectional radius and length of the cylindrical part of a spherocylindrical micelle of aggregation number n, and R_p is the radius of the protein molecule, as indicated in Figure 2-7. The value of R_n is determined by the "length" of the constituent surfactant monomers and is hence independent of the micellar aggregation number, n. Therefore, one can write $R_n = R_0$. On the other hand, the value of L_n increases linearly with n and is related to the total volume of the micelle, nv_s, where v_s is the volume that a surfactant monomer occupies in the micelle (note that v_s *may not* be the same as the actual physical volume of the surfactant molecule, see Section 2.3.2), by

$$nv_s = \pi R_0^2 L_n + 4\pi R_0^3/3 \tag{2.8}$$

where $4\pi R_0^3/3$ is the volume of the two hemispherical caps of a spherocylindrical micelle. Using Eq. (2.8) in Eq. (2.7), we obtain the following expression for $U_{n,p}$:

$$U_{n,p} = nv_s(1 + R_p/R_0)^2 + V_p(1 + R_0/R_p)^2 \tag{2.9}$$

where $V_p = 4\pi R_p^3/3$ is the volume of the protein molecule. Substituting the expression of $U_{n,p}$ given in Eq. (2.9) in Eq. (2.5) and carrying out the summation yields

$$\Omega = \exp\{-[(1 + R_0/R_p)^2 \rho V_p + (1 + R_p/R_0)^2 \phi]\} \tag{2.10}$$

where $\rho = \sum_n N_n/V$ is the number density of micelles, and $\phi = N_s v_s/V$ is the total volume fraction occupied by micelles, with $N_s = \sum_n nN_n$ being the total number of surfactant molecules. Note that the surfactant monomer concentration is ignored here because it is very close to the critical micelle concentration [25] and hence is nearly equal in the top and bottom micellar solution phases. Accordingly, the presence of the monomers has little effect on the protein partitioning behavior. On the other hand, ϕ represents the fraction of the solution volume which is actually occupied by micelles, and it depends on the volume occupied by a surfactant molecule in a micelle, v_s. Consequently, ϕ *may not* correspond to the actual total volume fraction of surfactant (see Section 2.3.2 for details).

The number density of micelles, ρ, in Eq. (2.10) is determined by the size distribution, $\{N_n\}$, of the micelles. When the micelles grow into long cylinders (which is the case of interest here since both $C_{10}E_4$ and C_8-lecithin form long, cylindrical micelles), ρV_p can be shown [7, 27] to be much smaller than ϕ. In that case, Ω in Eq. (2.10) is given approximately by

$$\Omega = \exp[-\phi(1 + R_p/R_0)^2] \tag{2.11}$$

Using Eq. (2.11) for the top (t) and bottom (b) phases respectively in Eq. (2.4), one obtains the following remarkably simple expression for the protein partition coefficient in a two-phase aqueous surfactant system containing long cylindrical micelles:

$$K_p = \exp[-(\phi_t - \phi_b)(1 + R_p/R_0)^2] \tag{2.12}$$

where ϕ_t and ϕ_b denote the *volume fractions occupied by micelles* in the top and bottom phases respectively.

Although not relevant to the experimental systems considered in this study, it

is interesting to derive the partition coefficient in systems containing monodisperse spherical micelles. In this case, all the micelles are of the same size and have the same aggregation number, n_0, and the number of micelles is $N_{n_0} = N_s v_s / V_{n_0}$, where $V_{n_0} = 4\pi R_0^3/3$ is the volume of a micelle. The number density of micelles is $\rho = N_{n_0}/V$. Using this expression in Eq. (2.10) for Ω yields

$$\Omega = \exp\left[-\phi \left(1 + R_p/R_0\right)^3 \right] \tag{2.13}$$

and the associated protein partition coefficient in a two-phase aqueous surfactant system containing spherical micelles is given by

$$K_p = \exp\left[-(\phi_t - \phi_b)(1 + R_p/R_0)^3 \right] \tag{2.14}$$

Equations (2.12) and (2.14) indicate that the uneven partitioning of a hydrophilic protein in the two-phase aqueous non-charged surfactant systems considered here is a direct consequence of the difference in the volume fractions that micelles occupy in the two coexisting micellar solution phases, $(\phi_t - \phi_b)$. In addition, the value of the partition coefficient depends on the relative sizes of micelles and proteins, as reflected in the values of R_0 and R_p. Specifically, as the protein size increases, the protein will partition more unevenly into the micelle-poor phase of the two-phase aqueous surfactant system. By comparing Eqs. (2.12) and (2.14), one observes that the shape of the micelles also plays an important role on the predicted partitioning behavior. Particularly, the power 3 on the $(1 + R_p/R_0)$ term in Eq. (2.14), relative to the power 2 on the $(1 + R_p/R_0)$ term in Eq. (2.12), suggests that partitioning will be more uneven in the two-phase micellar systems containing spherical (rather than cylindrical) micelles for a specific partitioned biomolecule, if the R_0 value is approximately the same.

2.3.2 Comparison of the Theoretical and Experimental Partitioning Results

In order to predict the variation of K_p with temperature, values of R_0 and R_p and of $(\phi_t - \phi_b)$ as a function of temperature are needed. In general, R_0 is approximately equal to the length of the surfactant molecule in a micelle and can therefore be written as the sum of the cross-sectional radius of the hydrocarbon core, l_c, and the length of the surfactant hydrophilic moiety (referred to as "head"), l_h, that is, $R_0 = l_c + l_h$.

Calculations based on a recently developed molecular model of micellization [55, 58] yield $l_c \approx 12$Å and 10Å for $C_{10}E_4$ and C_8-lecithin micelles respectively. The value of l_h depends on the average conformation adopted by the surfactant head, which is a tetra(ethylene oxide) chain in the case of $C_{10}E_4$ and a phosphatidylcholine group in the case of C_8-lecithin. As a first approximation, it is assumed that the unperturbed tetra(ethylene oxide) chains of $C_{10}E_4$ micelles behave as Gaussian chains with one end attached to a wall (to mimic the micellar surface). This results in a value of $l_h \approx 9$Å [59]. The phosphatidylcholine group in a C_8-lecithin micelle is assumed to be fully extended and oriented perpendicular to the micelle surface, in which case its length is estimated to be 11Å. Therefore, the cross-sectional radii of $C_{10}E_4$ and C_8-lecithin micelles are both approximately R_0 =21Å. The hydrodynamic radii of cytochrome c, ovalbumin, and catalase are R_p =19Å, 29Å, and 52Å, respectively, as listed in Table 2.1.

As stated in Section 2.3.1, the volume fractions of micelles in the top and bottom phases, ϕ_t and ϕ_b, in the case of $C_{10}E_4$ micelles, may be different from the total volume fractions of surfactants, ϕ'_t and ϕ'_b, as determined from Figure 2-3. This is due to the substantial water penetration into the region containing surfactant heads when the tetra(ethylene oxide) chains adopt a Gaussian conformation. In this case, the "wet" volume occupied by a surfactant molecule in a micelle, v_s, can be larger than the actual "dry" volume of a surfactant molecule, v'_s. When there is no water penetration into the region containing the heads, the length of the "dry" surfactant head in a cylindrical micelle, l'_h, is given by $l'_h = l_c[(v'_s/v_c)^{1/2} - 1]$, where v'_s and

v_c are the actual "dry" volumes of the surfactant molecule and its hydrocarbon tail respectively. For $C_{10}E_4$ micelles, v_s' =580Å^3 [7], and v_c =269Å^3 [25, 55], which yields l_h' =5.8Å.

When the head region is highly hydrated, such that $l_h > l_h'$, the volume of a cylindrical micelle is greater than the total physical "dry" volume occupied by the constituent surfactant molecules, and should therefore be scaled by a correction factor $[(l_c + l_h)/(l_c + l_h')]^2$. Accordingly, the actual micelle volume fraction in the solution ϕ_t (ϕ_b) can be calculated from ϕ_t' (ϕ_b'), the "dry" volume ratios (which can be determined from the amount of $C_{10}E_4$ put into a solution when preparing the solution), by multiplying ϕ_t' (ϕ_b') by the correction factor given above.

In the case of C_8-lecithin micelles, the heads are more compact than in the $C_{10}E_4$ case, and the extent of water penetration is expected to be less pronounced. Accordingly, as an approximation, the volume of a C_8-lecithin micelle is assumed to be equal to the total physical "dry" volume occupied by the surfactant molecules constituting the micelle, and the correction factor is taken as 1 for C_8-lecithin micelles.

The values of ϕ_t' and ϕ_b' at various temperatures can be obtained from the experimentally measured coexistence curves of aqueous solutions of $C_{10}E_4$ and C_8-lecithin, such as Figures 2-3 and 2-4. At a given temperature, ϕ_t' and ϕ_b' are given by the intersections of the horizontal tie line corresponding to that temperature with the surfactant-rich and surfactant-poor branches of the coexistence curve respectively. Using the known values of l_c, l_h, and l_h' given earlier, the correction factor for $C_{10}E_4$ can be calculated (it is unity for C_8-lecithin), which, when multiplied by $(\phi_t' - \phi_b')$, yields the values of $(\phi_t - \phi_b)$ to be used in Eq. (2.12).

Figure 2-6 shows the predicted variation of K_p with temperature in the two-phase aqueous $C_{10}E_4$ system for cytochrome c ($\cdots$), ovalbumin ($--$), and catalase (—) corresponding to the $(\phi_t' - \phi_b')$ values determined from Figure 2-3. $R_0 \approx 21$Å, and the R_p values listed above. As can be seen, there is good agreement with the experimentally measured K_p values.

The dependence of the partition coefficient, K_p, on protein size, R_p, can be seen clearly by plotting K_p as a function of the ratio R_p/R_0, at a fixed temperature, or

equivalently, at a fixed value of $(\phi_t' - \phi_b')$. For $C_{10}E_4$ at 21°C, $\phi_t' - \phi_b' \approx 10\%$ (see Figure 2-3). Figure 2-8 shows the predicted variation of K_p as a function of R_p/R_0 (full line), together with the experimental K_p values corresponding to cytochrome c (▲), soybean trypsin inhibitor (◆), ovalbumin (●), bovine serum albumin (▼), and catalase (■). This figure indicates that as R_p increases relative to R_0, the value of K_p decreases and can become vanishingly small for $R_p/R_0 > 5$.

It is also noteworthy that, for bovine serum albumin (BSA), which is known to possess high-affinity binding sites to amphiphilic molecules, as mentioned in Section 1.2.3, the experimentally obtained K_p value agrees well with the theoretical prediction. This suggests that the affinity binding sites of BSA do not bind to the surfactant $C_{10}E_4$, and that the BSA molecules interact with $C_{10}E_4$ micelles mainly through excluded-volume interactions, similar to the other proteins examined.

In the case of C_8-lecithin, $(\phi_b' - \phi_t') \approx 10\%$ at 10°C (see Figure 2-4). Note that in the C_8-lecithin case, the bottom phase is *micelle-rich* while the top phase is *micelle-poor*. Accordingly, due to excluded-volume interactions, hydrophilic proteins should partition preferentially into the top micelle-poor phase, namely, the values of K_p should be greater than 1. Figure 2-9 shows the predicted variation of K_p as a function of R_p/R_0 using Eq. (2.12), together with the experimental K_p values corresponding to cytochrome c (▲), ovalbumin (●), and catalase (■). This figure shows that, as expected, $K_p > 1$ and increases as R_p/R_0 increases. One can see from Figures 2-8 and 2-9 that the agreement between theory and experiment is good for both surfactant systems.

2.4 Conclusions

This chapter presented experimental and theoretical studies on the partitioning of several hydrophilic proteins in two-phase aqueous $C_{10}E_4$ and C_8-lecithin surfactant systems. The following conclusions can be reached:

- The partitioning is more uneven for protein molecules possessing larger sizes, or when the difference in the surfactant concentrations of the two coexisting

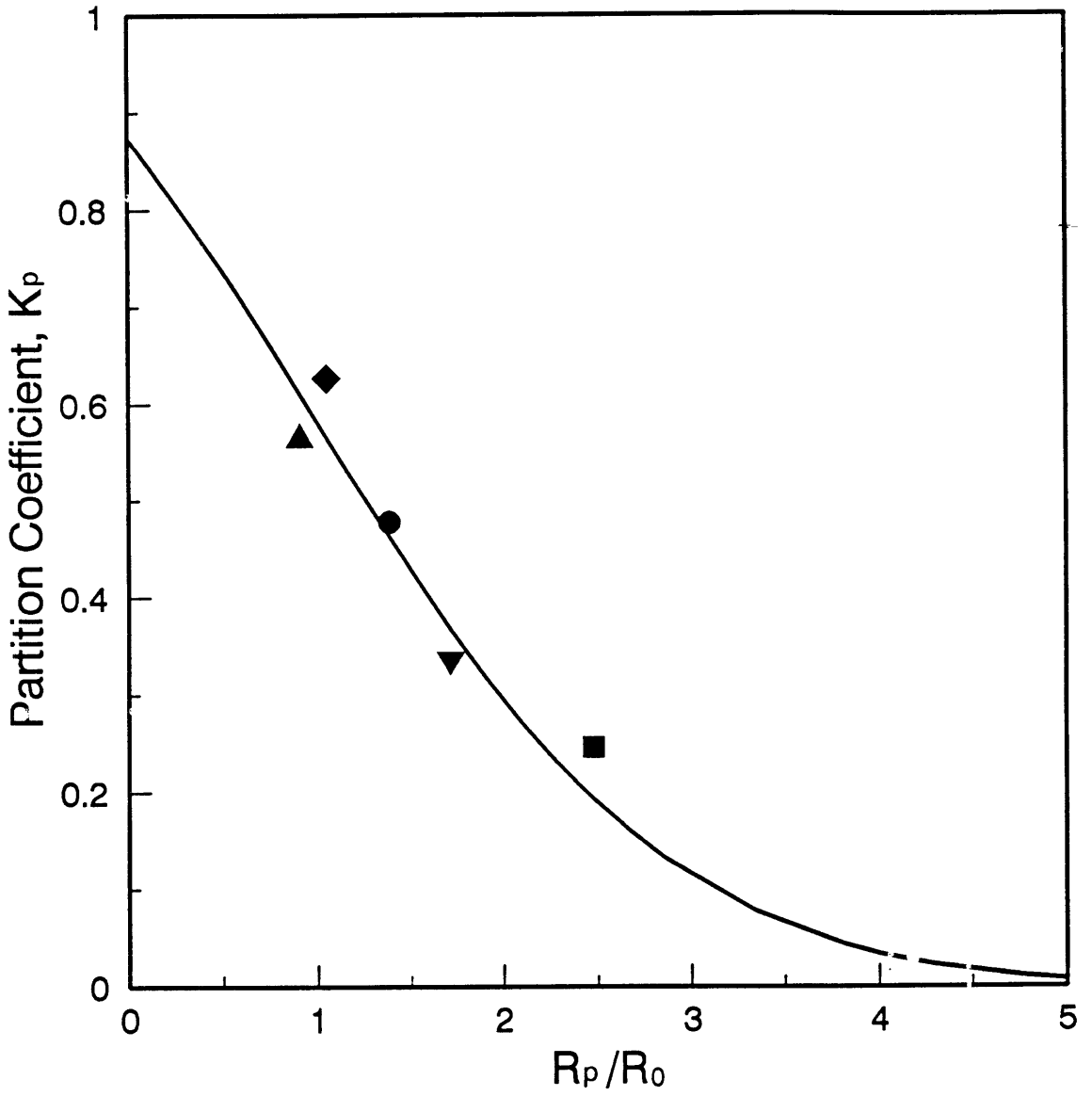

Figure 2-8: Predicted protein partition coefficient, K_p, as a function of the ratio, R_p/R_0, in the two-phase aqueous $C_{10}E_4$ micellar system at 21°C. R_p is the protein hydrodynamic radius, R_0=21Å is the cross-sectional radius of a $C_{10}E_4$ cylindrical micelle, and $\phi_t'-\phi_b'$=10% at 21°C. The various symbols correspond to the experimentally measured K_p values of the following proteins: cytochrome c (▲, R_p=19Å), soybean trypsin inhibitor (◆, R_p=22Å), ovalbumin (●, R_p=29Å), bovine serum albumin (▼, R_p=36Å), and catalase (■, R_p=52Å).

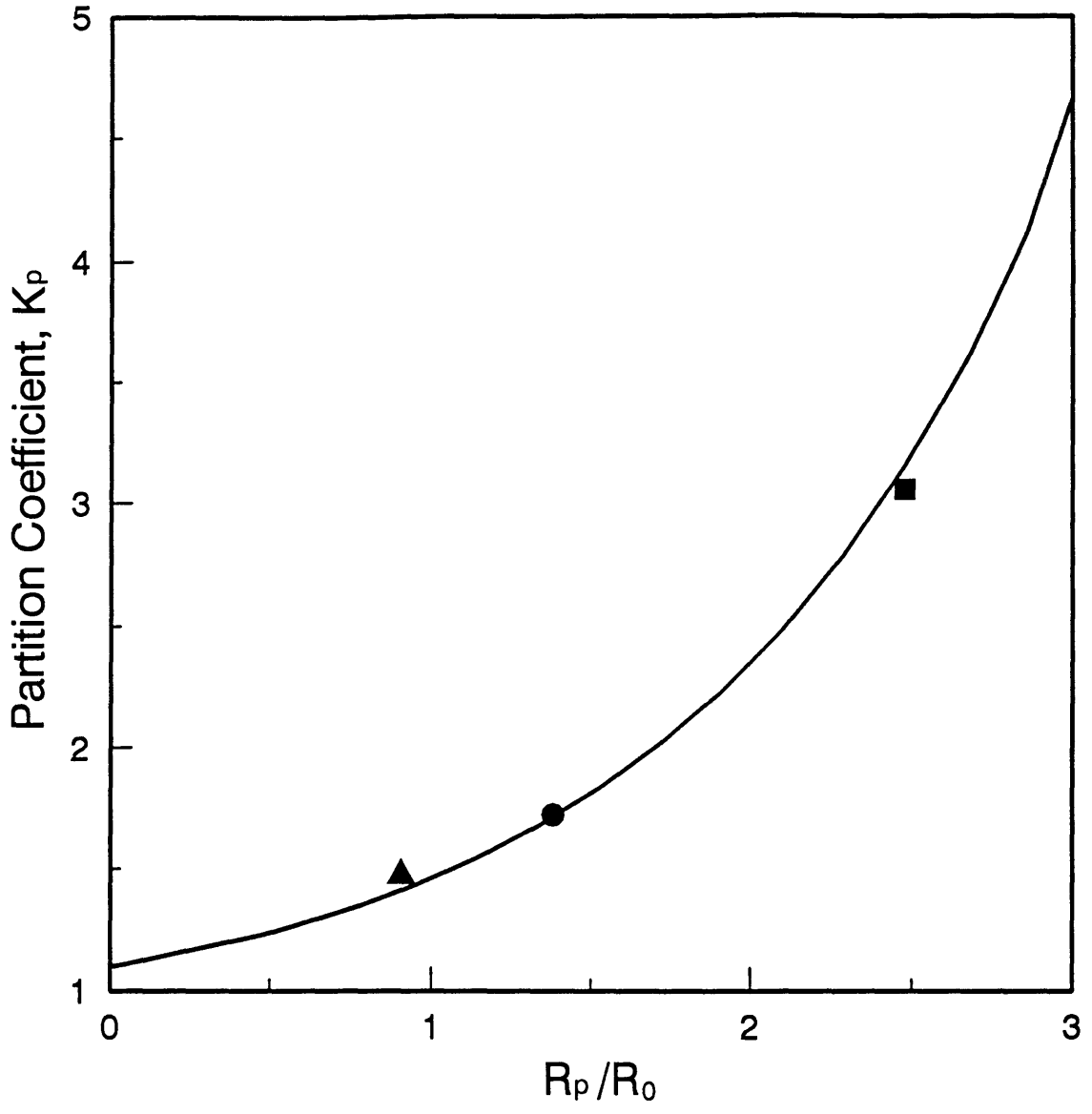

Figure 2-9: Predicted protein partition coefficient, K_p, as a function of the ratio, R_p/R_0, in the two-phase aqueous C_8-lecithin micellar system at 10°C. R_p is the protein hydrodynamic radius, R_0=21Å is the cross-sectional radius of a C_8-lecithin cylindrical micelle, and $\phi'_b - \phi'_t$=10% corresponding to 10°C. The various symbols correspond to the experimentally measured K_p values of the following proteins: cytochrome c (▲, R_p=19Å) , ovalbumin (●, R_p=29Å), and catalase (■, R_p=52Å).

phases is more pronounced. These findings suggest that the interactions between hydrophilic protein molecules and micelles are primarily of the excluded-volume type.

- The good agreement between the theoretical predictions and the experimental results indicates that excluded-volume interactions between proteins and non-charged micelles are indeed the dominant factor controlling the observed protein partitioning behavior.

- Based on the findings in this chapter, it follows that large hydrophilic particles, such as water-soluble colloids, viruses, and cells, should exhibit highly uneven or drastic partitioning behavior in the two-phase aqueous micellar systems. This should be useful in biotechnology for separation or concentration of biological materials.

Accordingly, it appears a natural extension to further investigate the partitioning behavior of larger biological particles in two-phase aqueous micellar systems. An investigation of the partitioning behavior of bacteriophages is presented in the next chapter.

Chapter 3

Partitioning of Virus Particles in the Two-Phase Aqueous $C_{10}E_4$ Micellar System

3.1 Introduction

In the case of protein partitioning in two-phase aqueous micellar systems reported in Chapter 2, the excluded-volume theoretical formulation suggested the extremely uneven partitioning behavior of partitioned entities with radii exceeding about 100Å. Hence, it appears interesting to extend the partitioning work reported in Chapter 2 to the case of larger hydrophilic particles. With this in mind, the partitioning behavior of virus particles, specifically of bacteriophages, was investigated, and the results of this investigation are reported in this chapter.

This chapter is organized as follows. Section 3.2 presents an overview of the properties of virus particles, and the reasons for choosing bacteriophages for the partitioning studies. Section 3.3 describes the experimental approach adopted in the virus partitioning experiments, including a detailed description of the bacteriophages used, the experimental procedures, and results of the partitioning experiments. Section 3.4 presents the theoretical approach for modeling the virus partitioning behavior,

including modifications of the theoretical formulation presented in Section 2.3.1 to incorporate the flexibility of micelles, as well as a comparison of the theoretical predictions with the experimental partitioning results. Section 3.5 describes results of a preliminary study on kinetic aspects associated with the partitioning phenomenon. Finally, Section 3.6 presents concluding remarks on the studies reported in this chapter.

3.2 Overview of Virus Properties

3.2.1 General Properties of Viruses

Viruses are small, transmissible, and potentially pathogenic biological particles. Viruses were not discovered until the end of the 19th century [60] mainly due to their small sizes. Indeed, unlike bacteria, viruses cannot be observed using conventional microscopes. The shape and size of virus particles could not be observed or measured explicitly until the invention of the electron microscope [61].

A unique feature of viruses is that the only metabolic function that they exhibit is reproduction and multiplication through infecting and destroying living cells, with each virus species infecting a specific cell species (which is usually called the "host" cell). The viral behavior of infecting, attacking, and destroying cells is called "lysis." Hence, viruses are parasitic in nature. Viruses can hence be categorized into three classes according to the nature of the host cells: (1) animal viruses, (2) plant viruses, and (3) bacterial viruses or bacteriophages (in short referred to as "phages"). Research on viral properties frequently exploits the lysis phenomenon, which may result in animal or plant virus lesion or formation of bacteriophage plaques [61] (see Section B.1 of Appendix B for details on generating bacteriophage plaques).

The infecting unit of viruses is a virus particle or a "virion." The structure of virus particles typically includes a protein capsid and nucleic acids. The nucleic acids, DNA or RNA, carrying the genetic information of viruses, are packed inside the capsids. The capsids are composed of protein molecules and usually include two types:

(1) helical capsids, for example, in the tobacco mosaic virus (a plant virus), and (2) isometric (quasi-spherical) capsids, for example, in the bacteriophage ϕX174. Some of the viruses belonging to the latter category also possess more complex structures, including spikes on the vertices of the capsids, tails, or tail fibers (for example, in the bacteriophage T4). In the viral capsids, the arrangement of the protein molecules corresponds to the energetically most stable condition. Certain experimental results [61] revealed that the segregated protein molecules can reaggregate into the shape of the original capsid, regardless of whether the nucleic acids are present in the capsid. This indicates that the structure of virus particles is very stable and intact, thus enabling viruses to endure harsh conditions without being destroyed. In addition, some viruses, mostly animal viruses, possess external envelopes composed mainly of phospholipid bilayers. For additional information on virus structures, genetic characteristics, and virus-host interactions, see References [60, 61].

3.2.2 Reasons for Choosing Bacteriophages in the Partitioning Experiments

The reasons for choosing bacteriophages in the partitioning experiments are listed below:

- They possess a suitable size

  The radii of bacteriophage particles are in the range of 100 - 1000Å and, as such, their sizes range from slightly larger to about 1 - 2 orders of magnitude larger than those of protein molecules. Accordingly, the use of bacteriophages significantly increases the size of the partitioned entity beyond that of proteins considered earlier.

- They possess a homogeneous structure

  As stated earlier, virus capsids are built and assembled from small protein subunits in a prescribed pattern. Accordingly, bacteriophages are as homogeneous as protein molecules, with every particle belonging to the same viral species

possessing the same shape, size, and composition [61]. This homogeneity in the virus physical and chemical properties is even higher than that of bacterial or yeast cells from a pure cell culture. This feature also makes viruses more suitable than other synthetic colloidal particles, for example, polystyrene beads, for the partitioning study.

- They possess stable properties

  As mentioned earlier, the structure of the viral capsids corresponds to a state of minimal free energy. As a result, unlike protein molecules whose conformations may be affected by the environment, the structure of virus particles is sturdy and cannot be altered easily. This indicates that the virus particles can remain stable and intact in various environments.

- Their concentration can be reliably measured

  The typical assaying method for determining bacteriophage concentrations involves a biological activity assay (see Sections 3.3.2 and B.1 for details), which is a well-established method and is not easily affected by the presence of other particles. Consequently, results obtained from the biological activity assay are very reliable.

- Bacteriophages are harmless to human beings

  Since bacteriophages only infect bacterial cells and do not harm animal (human) cells, they are harmless to researchers investigating their behavior. In addition, by modifying the genetic characteristics of bacteriophages and their host bacterial cells, biologists are able to control the growth of bacteriophages. Therefore, handling and utilization of bacteriophages is convenient as compared to that of animal or plant viruses.

In view of the reasons listed above, bacteriophages were chosen as the model virus particles for the partitioning experiments. Specifically, three bacteriophages, ϕX174, P22, and T4 (in the order of increasing size), were utilized in the partitioning experiments involving two-phase aqueous $C_{10}E_4$ nonionic micellar systems.

3.3 Experimental Approach

3.3.1 Materials

The materials used in the experiments reported below include: (1) the nonionic surfactant, $C_{10}E_4$, (2) bacteriophages, and (3) pH 7 McIlvaine buffer. $C_{10}E_4$ and the McIlvaine buffer are the same as those used in the protein partitioning experiments described in Sections 2.2.1.1 and 2.2.1.3. A description of the bacteriophages used, ϕX174, P22, and T4, including some of their properties and those of the host bacteria is presented below:

- P22 and its host bacteria, *Salmonella* strand 7136 or 7155, were obtained from the laboratory of Professor Jonathan King in the Department of Biology at M.I.T. P22 is a DNA bacteriophage which consists of an isometric head with short tail spikes. P22 possesses a spherical shape with a radius of 285Å, as measured with x-ray diffraction [62]. P22 was first found as a temperate phage of the bacterium *Salmonella typhimurium* [63] (a "temperate" phage is one which can be incorporated into its host cells without destroying or lysing the host cells). This phage requires the presence of magnesium ions (Mg^{+2}) to remain stable and intact in solutions.

- ϕX174 type am(E)W4 and its host bacteria, *Escherichia coli* strain B (BAF5), were kindly provided by Professor Bentley Fane in the Department of Biological Sciences at the University of Arkansas. ϕX174 is a small bacteriophage consisting of single-stranded DNA and a protein capsid [64]. ϕX174 can thus be viewed as having a spherical shape with a radius of 125Å, as measured with x-ray diffraction [64]. Unlike P22, ϕX174 does not possess tail spikes on the spherical capsids. Due to its simple structure, ϕX174 constitutes an attractive system for biological studies. ϕX174 infects *Escherichia coli* and *Salmonella typhimurium* by binding to lipopolysaccharides present in the outer membranes of these cells. Calcium ions (Ca^{+2}) are required by ϕX174 for successful infection of the host cells.

- T4-D (wild type) was also obtained from Professor King's laboratory, and its host bacteria, *Escherichia coli* strain B (B40), was kindly provided by Professor Edward Goldberg in the Department of Microbiology at Tufts University. T4 is a DNA bacteriophage which has been studied extensively. It possesses a complicated structure, including an isometric capsid, a tail, and tail fibers (see Figure 3-1) [65]. The width of the T4 particles is 850Å as measured with X-ray diffraction [65], and the length of the capsid is 1100Å. The tail sheath can be extended or contracted, with an average length of 980Å. Accordingly, it is appropriate to treat T4 particles as rod-like (rather than spherical) particles, with a total length of about 2000Å. The equivalent particle radius of T4 particles can be estimated using the relation:

$$\frac{4}{3}\pi R_v^3 = \pi(\frac{850}{2})^2 \times 2000 \tag{3.1}$$

which yields $R_v \approx$700Å.

Note that T4 requires magnesium ions (Mg^{+2}) to remain stable in solutions.

3.3.2 Biological Activity Assay

Virus concentrations in solutions were determined using the biological activity assay. The "biological activity" refers to the ability of the bacteriophage particles to infect, destroy, and lyse the host bacterial cells, and is typically signaled by generation of plaques. A "plaque," which is a circular transparent spot developing in a dense bacterial layer in a solid agar plate, is a colony of 10^7 - 10^9 bacteriophage particles descended from a single parent virus. As such, a plaque represents one virus particle originally implanted on the agar plate. Accordingly, this assaying method is based on the assumption that all the virus particles are intact and healthy, so that the number of virus particles exhibiting biological activity is equal to the number of virus particles present in the solution.

The biological activity assay includes: (1) serial dilution of the solution, (2) mixing

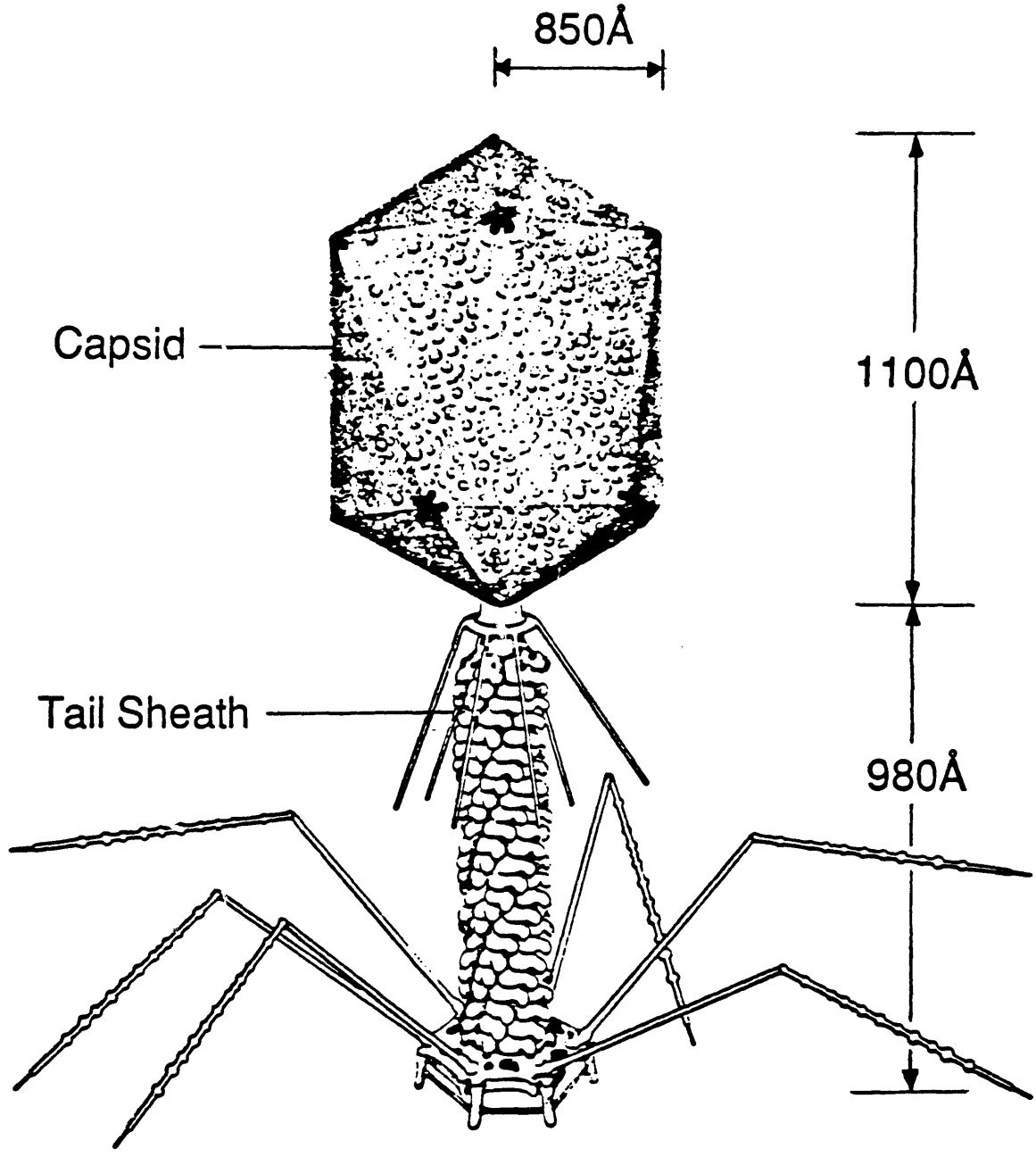

Figure 3-1: Structure of the bacteriophage T4 particle, based on an electron microscopy structural analysis with a resolution of 20 - 30Å. Also shown in the figure are the size of the capsid and the average size of the tail sheath (from Reference [65]).

part of the final diluted solution with the host bacteria, agar, and nutrients, (3) pouring this mixture on an agar plate and incubating the plate overnight at 30°C, and (4) counting the plaques generated on the agar plate. See Section B.1 of Appendix B for a detailed description of the procedures of the biological activity assay.

The purpose of the serial dilution is to ensure that the number of plaques generated in one plate is countable, typically in the range of 50 - 600 plaques/plate, depending on the size of plaques and phage species. A serial dilution consists of conducting a series of dilution steps on a given solution, with each dilution step being either 1:100 or 1:10 dilution. For example, in order to obtain a final $1{:}10^5$ dilution of a solution, two consecutive 1:100 dilution steps followed by one 1:10 dilution step need to be performed on this specific solution. 0.1 mL of the final diluted solution is then extracted to be incubated in an agar plate, and hence the number of plaques generated in one plate represents the number of virus particles present in 0.1 mL of the final diluted solution. Note that this serial dilution procedure enables the biological activity assay method to provide the same accuracy and sensitivity in determining the bacteriophage concentrations in different ranges, or even of different order of magnitude, since serial dilution can systematically bring the virus concentrations down to the range which is measurable by generating plaques in agar plates.

It is noteworthy, however, that the number of dilution steps required for obtaining the appropriate number of countable plaques must be estimated before conducting the serial dilution. Occasionally, one may run into a situation in which the number of plaques generated from the solution in the final dilution step is either too high to be accurately counted or too low to provide statistically-meaningful results. Accordingly, it is often necessary to use more than one (usually two) diluted solutions obtained from the series of dilution steps to generate the plaques. Typically, the two solutions are chosen such that one is a 1:10 dilution of the other, and, hence, the numbers of plaques generated from these two solutions should be different by one order of magnitude. If one plate contains too many or too few plaques, then the other plate should contain plaques whose total number can provide statistically-meaningful results.

The appropriate number of plaques which is usually generated in one plate depends

on the size of one plaque, which varies with the virus species. In general, small viruses tend to generate larger plaques since they diffuse at a faster rate. For example, when incubated at the same temperature for the same time, ϕX174 (the smallest phage examined) generates plaques which are much larger in size than those of T4 (the largest phage examined). Consequently, the appropriate number of ϕX174 plaques in one plate (about 40 - 200) is smaller than that of T4 plaques (about 70 - 600).

When implanting the virus and the host bacteria on the agar plates, nutrients need to be provided to keep the bacteria viable and healthy, but not to be consumed directly by the viruses. This is crucial, since viruses only infect or lyse living cells. The nutrients for bacteria are added in both the "hard agar"(which is poured in the sterilized petri dish for making agar plates) and in the "soft agar" (which is mixed with the virus and bacteria solutions and then poured on the agar plate for incubation) (see steps 1 and 3 in Section B.1 of Appendix B for more details). The bacteria growing on the agar plates usually appear yellowish, opaque, and look like a layer of yellow "lawn" on top of the agar. The purpose of using agar is to retard the diffusional movement of the virus colonies in order to generate clearly visible plaques on the opaque bacteria background. The virus concentration in the original (non-diluted) solution can then be calculated according to the counted number of plaques, and the types and numbers of dilution steps conducted.

Usually, two or three sets of serial dilution were performed on one solution whose virus concentration was to be determined in order to obtain a higher accuracy in determining the virus concentration in that solution.

It is noteworthy that the typical error of the biological activity assay is in the range of 20 - 30%. Therefore, counting results differing by about 10% are usually considered as being the same. See Section B.2 of Appendix B for a discussion on possible sources of error associated with the virus concentration determination.

3.3.3 Virus Stability Test

The virus stability test is essential to ensure an accurate determination of the virus concentrations in the virus partitioning experiments. Results of the virus stability

test provide useful information on how to conduct the virus partitioning experiments in order to ensure the accuracy and reliability of the partitioning results.

The virus stability is related to the "friendliness" of the environment in which the virus is placed, and can be quantified in terms of the variation of the virus concentration with time in a given solution condition. For example, if the test reveals that the virus concentration in the $C_{10}E_4$ solution decreases significantly with time as compared to that in the stable condition, say, it decreases by a factor of 10 after overnight incubation, this implies that this solution condition may be detrimental to the virus. In this case, special precautions should be taken to ensure that the virus remains viable and healthy in the given solution condition. For example, a "stabilizing agent" for the virus, such as Mg^{+2} for P22 and T4, should be included in the surfactant solution to ensure the stability and viability of the virus. On the other hand, if the test reveals that the virus concentration remains steady for, say, 6 hours, and is subsequently followed by a decrease with time, then all the experimental procedures should be completed within the first 6-hour period. Therefore, prior to conducting the virus partitioning experiments, the virus stability in the surfactant solution needs to be examined.

The stability test was conducted by introducing the virus (P22, T4, or ϕX174) into various solution conditions, including the $C_{10}E_4$ solution in McIlvaine buffer, followed by a determination of the virus concentration in each of the solution conditions after certain time intervals. Results of the stability tests of P22, T4, and ϕX174 revealed that the virus concentrations in all the solution conditions examined decreased after overnight incubation. To be specific, the P22 concentrations in various solutions conditions were found to be higher than one half of the initial P22 concentrations, while those of T4 or ϕX174 were found to be lower than one half of the initial T4 or ϕX174 concentrations. It is noteworthy that this observed decay in the virus concentrations by a factor of about 2 after overnight incubation is considered by biologists to be a natural decay. In other words, the observed decay does not reflect any significant damaging effect, and hence should not be viewed as being serious (this was pointed out by Professor King). Moreover, it is expected that, since the

given partitioning result reflects a ratio of virus concentrations in the top and bottom phases, the effect of the virus concentration decay rate should cancel out, thus having a minimal influence on the virus partitioning results.

The results of the stability tests also indicated that P22 possesses a somewhat higher stability than T4 and ϕX174. Consequently, the P22 partitioning experiments were conducted overnight, with the biological activity assay for measuring P22 concentrations conducted on the next day. On the other hand, the time involved in the T4 or ϕX174 partitioning experiments did not exceed 4 - 5 hours. See Appendix C for a detailed description of the experimental procedures associated with the virus stability tests, as well as for a discussion of the test results.

3.3.4 Coexistence Curve Measurement

The coexistence curve of the $C_{10}E_4$ aqueous micellar system in the presence of a bacteriophage was determined using the cloud-point curve measurement. As described in Section 2.2.2, the purpose of this measurement is to examine whether the presence of a bacteriophage will affect the phase separation equilibrium of the micellar solution. The solutions were prepared as in Section 2.2.2.2, with a phage concentration of about 10^8 phages/mL, which is similar to that used in the partitioning experiments (see Section 3.3.5).

Figure 3-2 shows the experimentally measured coexistence (cloud-point) curves of $C_{10}E_4$ surfactant solutions in pH 7 McIlvaine buffer without bacteriophage (○), with P22 at a concentration of 10^8 phage/mL (△), and with T4 at a concentration of 2×10^8 phage/mL (□). Similar to the protein case (see Figure 2-3), Figure 3-2 indicates that the presence of bacteriophages at the concentrations examined has a negligible effect on the phase separation behavior of the $C_{10}E_4$ micellar solutions.

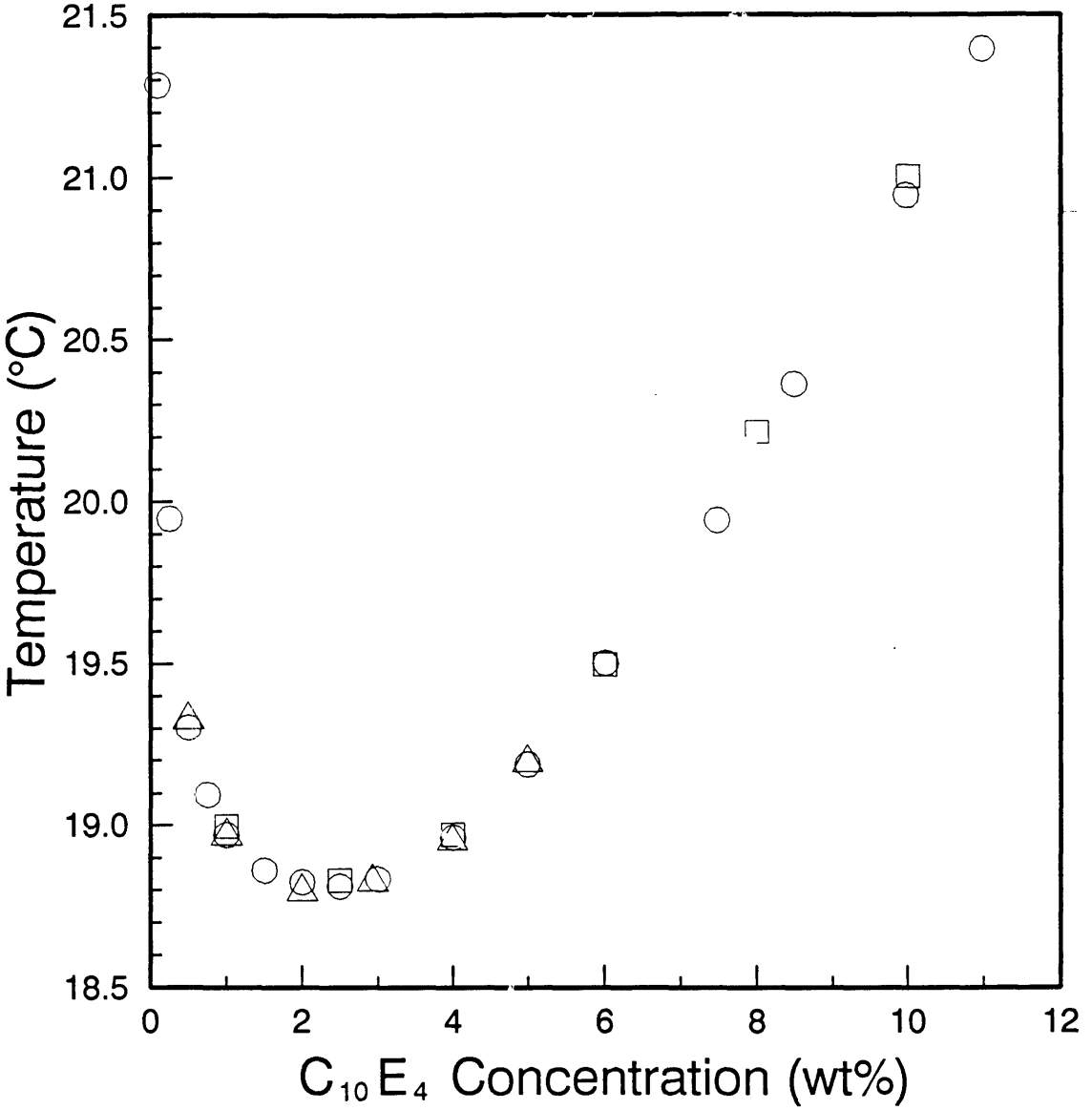

Figure 3-2: Experimentally measured coexistence (cloud-point) curves of the $C_{10}E_4$-buffer micellar system without bacteriophage (○), with P22 at a concentration of 10^8 phage/mL (△), and with T4 at a concentration of 2×10^8 phage/mL (□).

3.3.5 Partitioning Experiments

3.3.5.1 Experimental Procedures

The procedures for conducting the virus partitioning experiments are similar to those for conducting the protein partitioning experiments, as described in Section 2.2.4.2. Three solutions containing a known $C_{10}E_4$ concentration (chosen to yield approximately equal volumes of the two coexisting phases) and one bacteriophage species, with a concentration of about 10^8 phages/mL, were prepared in pH 7 McIlvaine buffer. They were subsequently placed in the water cell (see Figure 2-2) at a constant temperature for an appropriate time period chosen to ensure that equilibrium was indeed reached. Note that the time period depends on the stability of the phages, with the results of the stability tests presented in Section C.3 of Appendix C providing useful information on this issue. Specifically, an equilibration time period of about 8 - 14 hours was adopted for P22, and a 4-hour period was adopted for both ϕX174 and T4. Note that the time needed for the two coexisting micellar phases to appear is usually less than one hour. Hence, phase separation equilibrium should be attainable even within the 4-hour period.

The concentrations of virus particles in the two coexisting phases were determined using the biological activity assay, as described in Section 3.3.2 and Section B.1 of Appendix B. The virus partition coefficient, K_v, which is defined as the ratio of the virus concentration in the top phase, $C_{v,t}$, to that in the bottom phase, $C_{v,b}$, that is, $K_v = C_{v,t}/C_{v,b}$, was calculated as a quantitative measure of the partitioning behavior of the virus particles.

3.3.5.2 Partitioning Results

Figures 3-3, 3-4, and 3-5 show the experimentally measured virus partition coefficients, K_v, drawn in a logarithmic scale, as a function of temperature (in the range of 18.8 - 21.2°C) for the bacteriophages ϕX174, P22, and T4, respectively, in the two-phase $C_{10}E_4$-buffer micellar system. As in the protein case, temperature is used as the controlling factor of partitioning since an increase in temperature corresponds

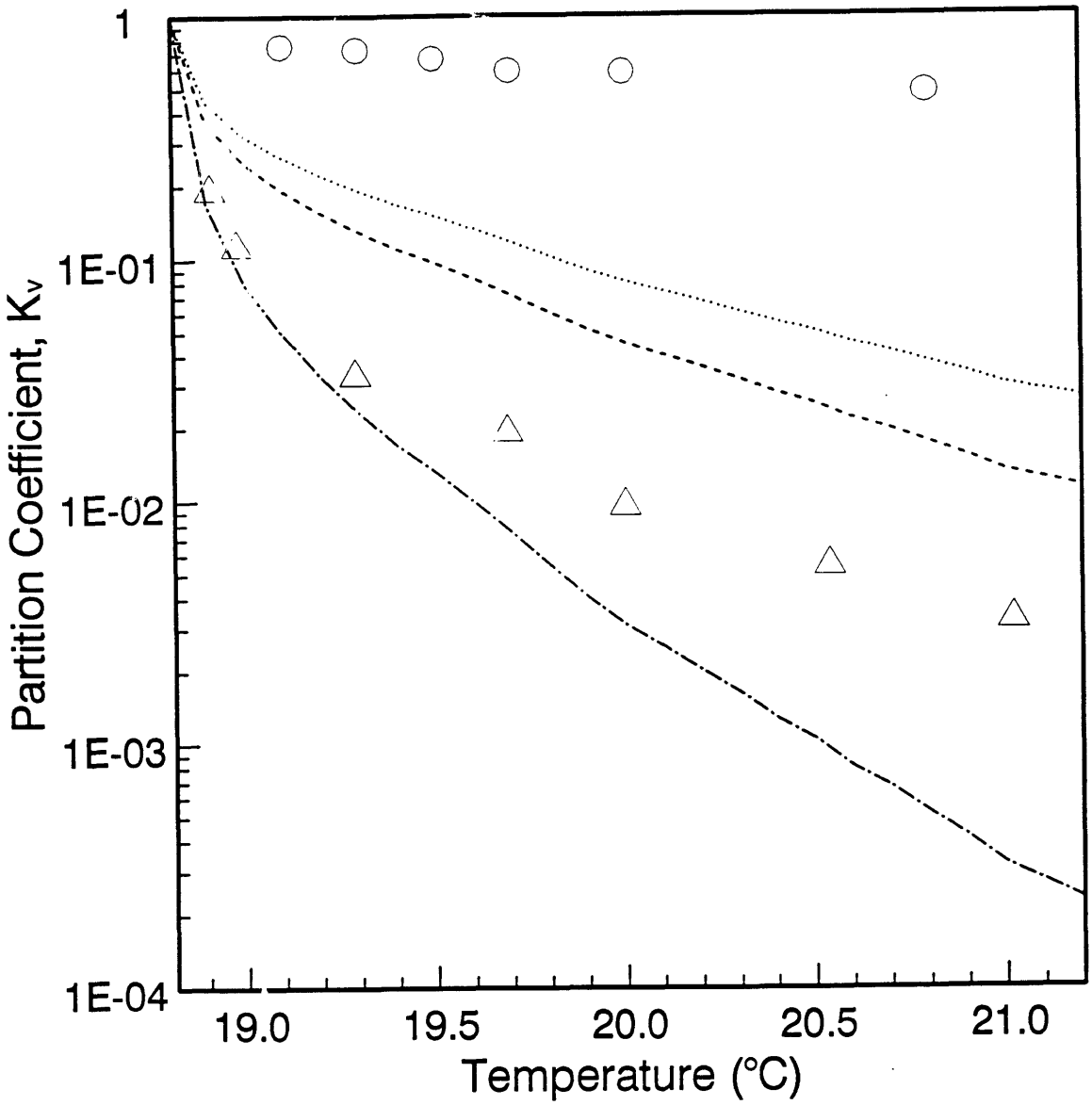

Figure 3-3: Experimentally measured partition coefficient, K_v, of the bacteriophage ϕX174 ($\triangle$) as a function of temperature in the two-phase $C_{10}E_4$-buffer micellar system. The experimentally measured partition coefficient of the protein ovalbumin ($\bigcirc$) is also shown for comparison purposes. Also shown are the predicted partition coefficients based on the assumption that $C_{10}E_4$ micelles are flexible, with a Kuhn length of 100Å ($\cdots$) or 150Å ($- - -$), and that the micelles are rigid (with a Kuhn length $l \to \infty$) ($- \cdot - \cdot -$), see the discussion in Section 3.4.3. The radius of a ϕX174 virus particle is 125Å.

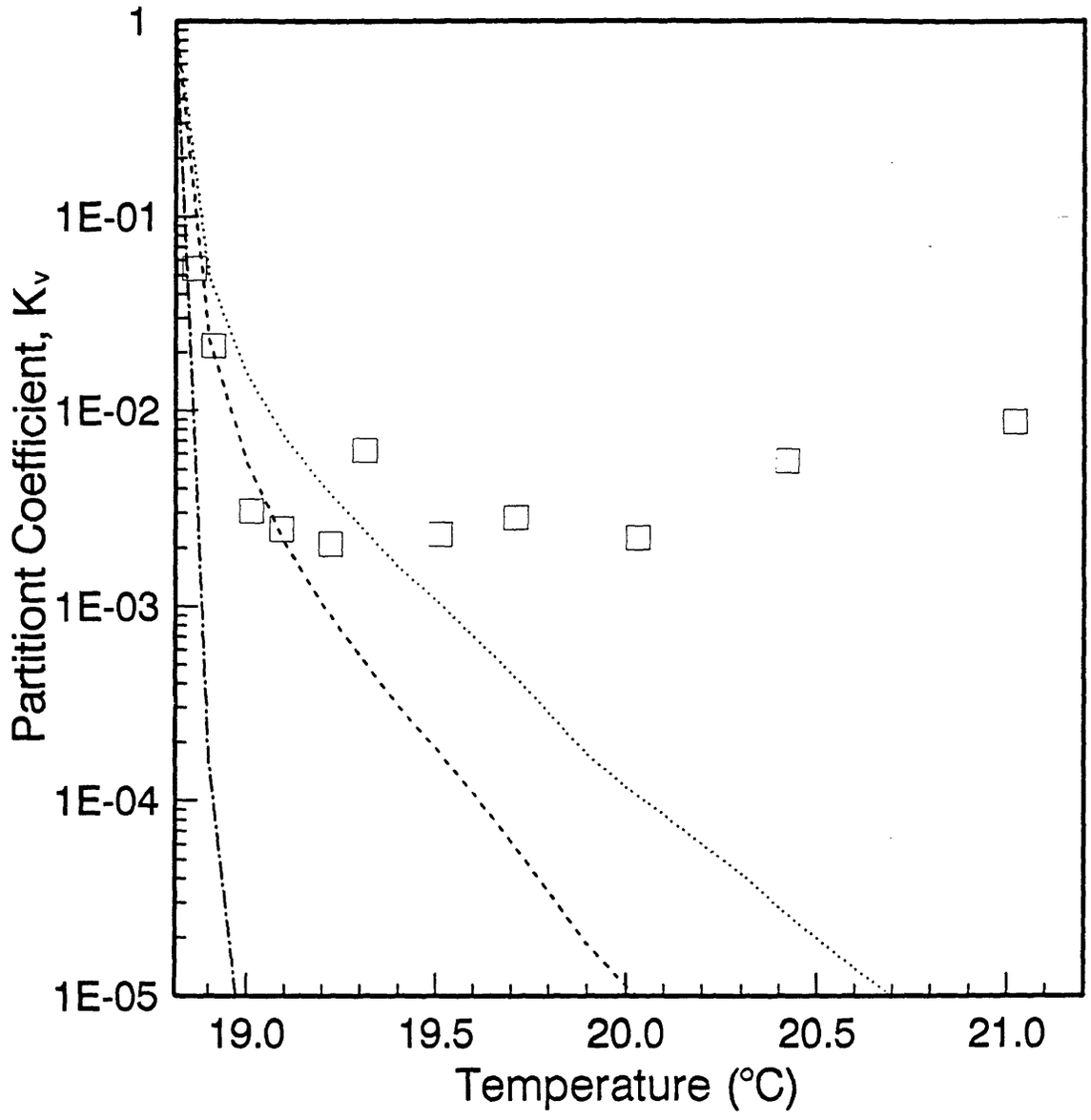

Figure 3-4: Experimentally measured partition coefficient, K_v, of the bacteriophage P22 (□) as a function of temperature in the two-phase $C_{10}E_4$-buffer micellar system. The notation is the same as that in Figure 3-3. The radius of a P22 virus particle is 300Å.

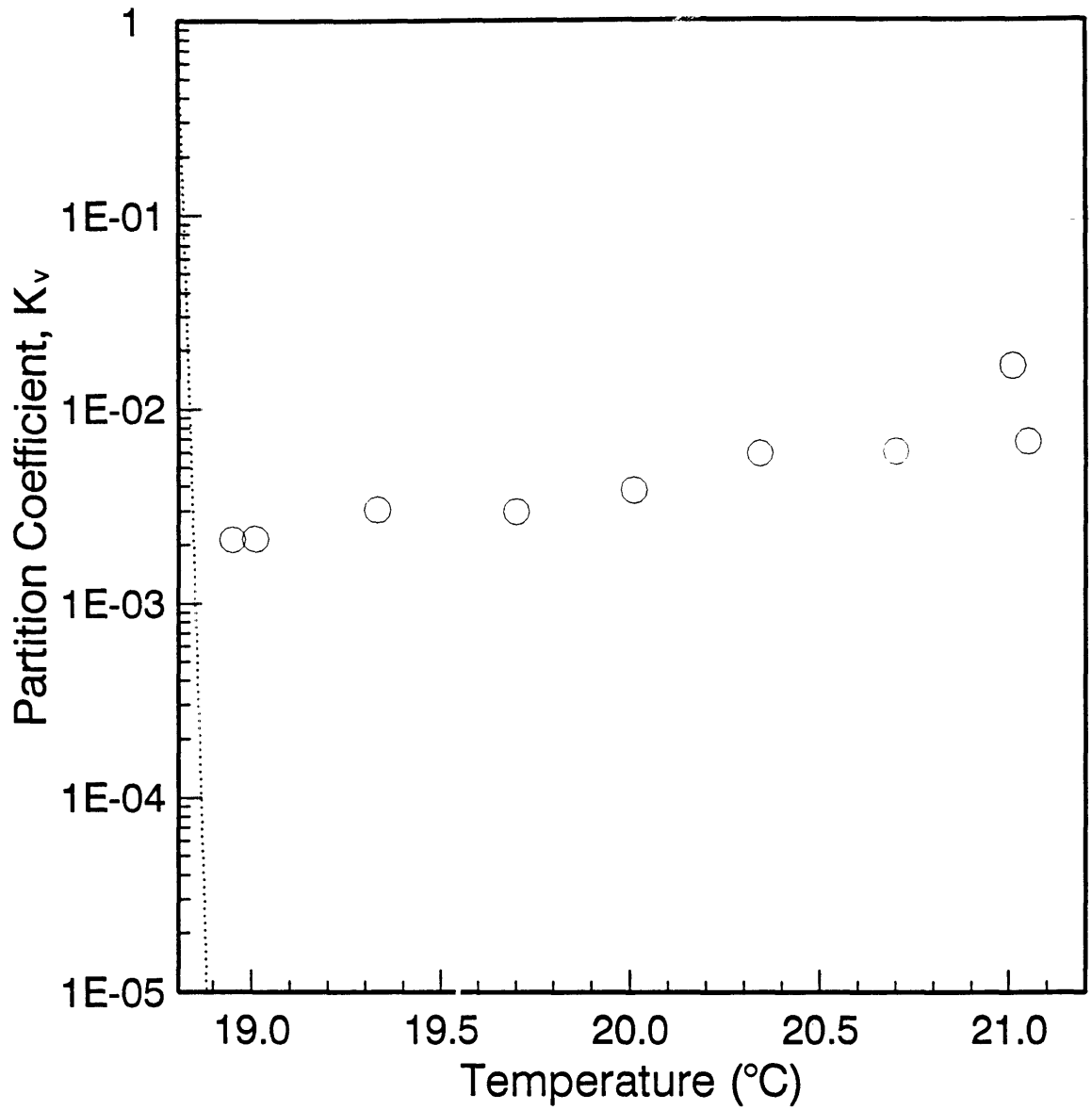

Figure 3-5: Experimentally measured partition coefficient, K_v, of the bacteriophage T4 (○) as a function of temperature in the two-phase $C_{10}E_4$-buffer micellar system. The dotted line is the predicted partition coefficient based on the assumption that the $C_{10}E_4$ micelles are flexible and have a Kuhn length of 100Å, see the discussion in Section 3.4.3. Note that T4 virus particles are rod-like, with an estimated equivalent radius of about 700Å.

to an increase in the difference in the surfactant concentrations of the two coexisting phases in the two-phase aqueous $C_{10}E_4$ micellar system (see Figures 2-3 and 3-2). Note also that the partitioning experiments reported in Figures 3-3, 3-4, and 3-5 were conducted at temperatures above the critical temperature, T_c=18.81°C, indicating the onset of phase separation in the $C_{10}E_4$-buffer micellar system, as discussed in Section 2.2.4.3.

Figure 3-3 shows the partition coefficient, K_v, of ϕX174, which is the smallest virus particle studied in the partitioning experiments (R_v=125Å). As in the protein partitioning case, K_v of ϕX174 decreases with increasing temperature, reaching a value of about 10^{-3} at 21°C. Note that this K_v value is about two orders of magnitude lower than that of ovalbumin (R_p=29Å), which is also shown in Figure 3-3 for comparison purposes. This clearly indicates that, as conjectured from the theoretical formulation (see Sections 2.3.1 and 2.3.2), much more extreme partitioning can indeed be achieved in the case of virus particles which are much larger than typical protein molecules.

In the P22 case ($R_v \approx$300Å), as shown in Figure 3-4, the partition coefficient, K_v, first decreases with increasing temperature, but then levels off and seems to remain at a value of about 10^{-3} as the temperature exceeds 19°C. A closer examination reveals that, for T >19°C, the K_v values increase slightly with increasing temperature, reaching a value of about 10^{-2} at 21°C.

Figure 3-5 shows the partitioning behavior of T4, which is the largest virus particle used in the partitioning experiments (with an equivalent R_v=700Å). The variation of K_v with temperature exhibits a trend similar to that observed in the P22 case for T >19°C. Specifically, K_v exhibits a minimum value of 2×10^{-3} at 18.9°C and then increases gradually to about 10^{-2} at 21°C.

When comparing the partitioning behavior of these three bacteriophages at a given temperature, specifically, for T <19°C, the virus partition coefficient, K_v, exhibits the expected trend of decreasing with increasing virus particle size, that is,

$$K_v(\phi\text{X174}) > K_v(\text{P22}) > K_v(\text{T4}) \tag{3.2}$$

which agrees qualitatively with the theoretical prediction based on the assumption that the interactions between micelles and virus particles are of the excluded-volume type, as described in Section 2.3. On the other hand, for T >19°C, $K_v(\phi X174)$ is still larger than K_v(P22) and K_v(T4), but K_v(P22) and K_v(T4) are about equal, due to the leveling off of the K_v(P22) and K_v(T4) values over this temperature range. This "plateau" phenomenon observed in the partitioning behavior of the bigger virus particles was not observed in the protein cases (see Section 2.2.4), and it is not predicted by the excluded-volume theoretical description presented in Section 2.3.1. This suggests that other approaches may need to be considered in order to provide a better description and further understanding of the partitioning behavior of large virus particles. The following two approaches come to mind: (1) a modification of the current excluded-volume theoretical formulation presented in Section 2.3, and (2) a consideration of other factors, such as possible kinetic aspects of virus partitioning. These two approaches are discussed in the next two sections.

3.4 Theoretical Description of the Virus Partitioning Behavior

3.4.1 Introduction

The theoretical formulation for describing the virus partitioning behavior is a generalization of that for describing the protein partitioning behavior (see Section 2.3.1) aimed at incorporating the relative flexibility of the $C_{10}E_4$ micelles as "probed" by the larger virus particles. As in the protein case, the central assumption is that excluded-volume interactions between the nonionic $C_{10}E_4$ micelles and the virus particles dominate the observed partitioning behavior. Micellar flexibility is included in the virus case because the virus particles are sufficiently large to "sense" the micellar flexibility, while typical protein molecules are too small to do that. Indeed, in the protein case (see the discussions in Section 1.3), a protein molecule is typically smaller (R_p=20 - 60Å) than the Kuhn length or persistence length of a $C_{10}E_4$ or C_8-lecithin

cylindrical micelle ($\sim$ 100Å), and hence the micelle appears as a rigid and infinitely long rod on the scale of the protein. As a result, the excluded volume between a spherical protein and a $C_{10}E_4$ (or C_8-lecithin) micelle can then be modeled as that between a sphere and a rigid long rod, with the micellar flexibility not playing any role. On the other hand, in the virus case, since the size of a virus particle is comparable (R_v=100 - 1000Å) to, or even greater, than the Kuhn or persistence length of the micelle, the virus particle can "probe" the flexibility of the micelle. Consequently, when modeling the excluded volume between a virus particle and a micelle, it appears necessary to incorporate the flexibility of the micelles into the theoretical description.

In Section 2.3.1, based on the excluded-volume theory, the following expression for the partition coefficient, K, was obtained:

$$K = \frac{\Omega_t}{\Omega_b} \tag{3.3}$$

where

$$\Omega = \exp(-\sum_n N_n U_{n,p}/V) \tag{3.4}$$

In Eq. (3.4), N_n is the number of micelles of aggregation number n, $U_{n,p}$ is the excluded volume between a micelle of aggregation number n and a protein molecule, and V is the volume of the phase (see Appendix A for a detailed derivation of Eqs. (3.3) and (3.4)). Using the expression for $U_{n,p}$ given in Eq. (2.7) in Eqs. (3.3) and (3.4), the predicted partition coefficients of proteins were found to agree well with the experimentally measured partition coefficients (see Section 2.3.2 for details). As stated above, in the virus case, the flexibility of the micelles should be accounted for in the calculation of the excluded volume, $U_{n,v}$, between a virus particle and a micelle of aggregation number n. Accordingly, one envisions obtaining a new theoretical model, which can be applied to a wider range of particle sizes and micellar flexibility.

Below, a brief derivation of the new theoretical model, which was developed in collaboration with Dr. Leo Lue [66], is presented. This includes (1) a discussion of the essential elements in the derivation of the new expression for the excluded volume, $U_{n,v}$, between a "big" spherical particle (virus particle) and a flexible micelle

of aggregation number n, and (2) a comparison of the theoretically predicted virus partition coefficients with the experimentally measured ones.

3.4.2 Derivation of the Excluded-Volume Theoretical Model

The system under consideration consists of the partitioned solutes (virus particles) and the micelles, with the aqueous solvent treated as a continuum. It is assumed that virus particles can be modeled as hard spheres with a radius R_v. In addition, a flexible micelle is treated as a freely-jointed chain with a contour length (overall length) L_n (where n denotes the aggregation number of the micelle) and a cross-sectional radius R_0, consisting of N Kuhn segments, each of length l (that is, $Nl = L_n$) (see Figure 3-6 (a)), dispersed in solution at the θ-solvent conditions (see Section 2.3.1) [15, 57]. The excluded volume between these two entities can be shown to be the same as that between an effective sphere of radius $R = R_v + R_0$ and an infinitely thin freely-jointed chain consisting of N Kuhn segments, each of length l (see Figure 3-6 (b)) [66]. Note that the Kuhn length, l, and the persistence length, ξ, are both length scales characterizing the chain flexibility, with $l = 2\xi$ (see Reference [32] for more details on chain flexibility). Note also that this description of the system represents a limiting case in which the excluded volume obtained is a minimum with respect to the shape of the solute particles, which are assumed to be spherical. If the solute particles are cylindrical or rod-like, the resulting excluded volume will be larger than that obtained in the following derivation due to the additional rotational degrees of freedom associated with the cylindrical solute particles.

When the solutes are protein molecules, since the flexibility of micelles is not so significant, the excluded volume, $U_{n,p}$, is given in terms of R_p, R_0, and L_n, as in Eq. (2.7), that is,

$$\begin{aligned} U_{n,p} &= 4\pi(R_0 + R_p)^3/3 + \pi(R_0 + R_p)^2 L_n \\ U_{n,p} &= 4\pi R^3/3 + \pi R^2 L_n \end{aligned} \tag{3.5}$$

where $R = R_0 + R_p$ in Eq. (3.5). On the other hand, when partitioning larger virus

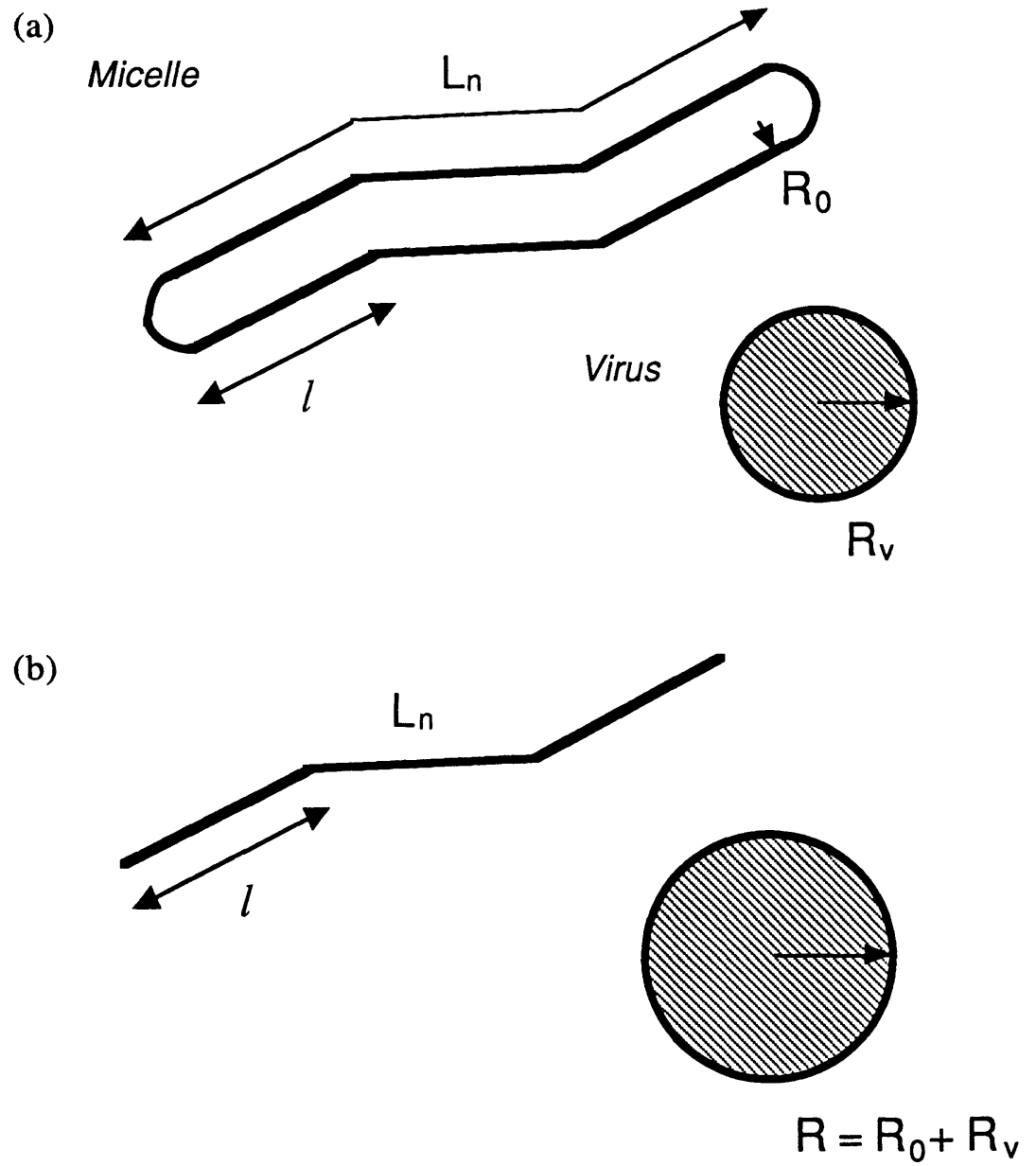

Figure 3-6: Models of a spherical virus particle and a flexible micelle for deriving the excluded volume, $U_{n,v}$, between them.
(a) Illustration of modeling a virus particle and a micelle in a realistic way.
(b) Illustration of an alternative way of modeling the virus particle and the micelle, which yields the same excluded volume, $U_{n,v}$, as in (a).

particles, the micellar flexibility, which is reflected in the Kuhn or persistence length, may play an important role in the observed partitioning behavior. Consequently, the Kuhn length (or persistence length) should be included in the theoretical modeling of the excluded volume. In this case, the excluded volume, $U_{n,v}$, is a function of three length scales — $R = R_0 + R_p$, L_n, and l — which are all interrelated.

In order to reduce the number of independent variables and simplify the expression for $U_{n,v}$, it is convenient to introduce two dimensionless variables associated with the relevant length scales characterizing the system under consideration. Specifically,

$$x = \frac{1}{\sqrt{L_n/l}} = N^{-1/2} \tag{3.6}$$

$$y = \frac{R}{l} \tag{3.7}$$

It is also convenient to define a dimensionless "scaled-excluded volume," U', as

$$U' = \frac{U_{n,v} - \frac{4}{3}\pi R^3}{\pi L_n l^2} \tag{3.8}$$

The term $\frac{4}{3}\pi R^3$ in Eq. (3.8) represents the effective volume of the spherical solute and does not depend on the flexibility of the micelles. Hence, by subtracting this term from $U_{n,v}$, the scaled-excluded volume, U', can best reflect the effect of micellar flexibility on the excluded-volume interactions with the solute particles. The purpose of dividing by the term $\pi L_n l^2$ in Eq. (3.8) is to make U' dimensionless, since, from Eq. (3.5), $U_{n,p} - 4\pi R^3/3 = \pi R^2 L_n$, which is dimensionally equivalent to $\pi L_n l^2$. U', as defined in Eq. (3.8), can thus simplify the derivation when the micellar flexibility is taken into consideration.

First, let us examine the two extreme cases in which the micellar chain has either no flexibility (totally rigid case) or infinite flexibility (totally flexible case) as "viewed" by the spherical solute particles.

1. Totally Rigid Case

In this case, the chain is totally rigid and consists of at most only one Kuhn

segment, that is, $L_n \leq l$ or $x \to 1$. The excluded volume, U_{rigid}, and the scaled-excluded volume between a rigid cylinder and a hard sphere, U'_{rigid}, are given by [67]

$$U_{rigid} = \frac{4}{3}\pi R^3 + \pi R^2 L_n \tag{3.9}$$

$$U'_{rigid} = y^2 \tag{3.10}$$

It is noteworthy that, when the effective radius of the sphere, R, is much smaller than the Kuhn length of the chain, l, that is, when $R \ll l$ or $y \to 0$, the chain will appear rigid to the sphere, and the excluded-volume expressions in this case are also given by Eqs. (3.9) and (3.10). This is precisely the situation in the protein-micelle case, and the U_{rigid} expression given in Eq. (3.9) is therefore exactly the same as that for $U_{n,p}$ given in Eqs. (2.7) or (3.5).

2. Totally Flexible Case

In this case, the effective radius of the sphere, R, is much larger than the Kuhn length of the chain, l, that is, $R \gg l$ or $y \to \infty$, and the number of Kuhn segments on a chain is infinite, that is, $L_n \gg l$ or $x \approx 0$. Therefore, in this limit, the chain can be treated as a Gaussian coil [57]. The excluded volume, U_{gc}, and the scaled-excluded volume, U'_{gc}, between a sphere and a Gaussian coil are given by [67]

$$U_{gc} = \frac{2}{3}\pi R L_n l + 4\left(\frac{2\pi L_n l}{3}\right)^{1/2} R^2 + \frac{4}{3}\pi R^3 \tag{3.11}$$

$$U'_{gc} = \frac{2}{3}y + \alpha x y^2 \tag{3.12}$$

where $\alpha = 4(\frac{2}{3\pi})^{1/2}$.

In summary, the scaled-excluded volume in these two extreme cases is given by

$$U' = \begin{cases} y^2, & \text{as } x \to 1 \text{ or } y \to 0 \\ \frac{2}{3}y + \alpha x y^2, & \text{as } x \to 0 \text{ and } y \to 1 \end{cases} \tag{3.13}$$

Regarding cases which may lie between the two extreme cases discussed above, that is, those in which $0 < x < 1$ and $0 < y < \infty$, a Monte Carlo simulation was conducted to calculate the corresponding excluded volume between a sphere and a chain with finite flexibility. The basic idea behind this simulation is: (1) to randomly generate several chain configurations, and (2) to determine the fraction of these chain configurations which intersect the sphere. The simulation results indicate [66] that both U'_{rigid} and U'_{gc} overestimate the actual scaled-excluded volume, U', over most of the x and y ranges, except in certain limiting cases where U' is very close to either U'_{rigid} or U'_{gc}.

Using the simulation results, an approximate analytical expression was derived for the scaled-excluded volume, U'. Specifically [66],

$$U'(x,y) = \frac{a_0 + a_1 x}{1 + a_2 x} \tag{3.14}$$

where a_0, a_1, and a_2 are functions of y and are given by

$$a_0 = \frac{y^2}{1 + 3y/2} \tag{3.15}$$

$$a_1 = \frac{y^2}{(1 + 3y/2)^2}[2\alpha - 1 + (3\alpha - 1)\frac{3y}{2} + \alpha\left(\frac{3y}{2}\right)^2] \tag{3.16}$$

$$a_2 = \frac{(2\alpha - 1) + (\alpha - 1)3y/2}{1 + 3y/2} \tag{3.17}$$

The actual excluded volume, U, can then be calculated by using Eqs. (3.14) - (3.17) in Eq. (3.8). This yields

$$U(R, l, L_n) = \pi L_n l^2 U'(N^{-1/2}, R/l) + \frac{4}{3}\pi R^3 \tag{3.18}$$

In principle, by using Eqs. (3.18) and (3.13) to replace $U_{n,p}$ in Eq. (3.4), with the micellar size distribution, $\{N_n\}$, the contour length, L_n, and the micellar number density, $\rho_n = N_n/V$, calculated from the surfactant concentrations in the two

coexisting phases [27, 55], followed by summing up the contributions from micelles of various aggregation numbers n, the partition coefficient of the virus particles, K_v, can be calculated from Eq. (3.3).

3.4.3 Calculation of Virus Partition Coefficients and Comparison with Experimental Results

In the calculation of the virus partition coefficient, K_v, using the theoretical model presented in Section 3.4.2, the cross-sectional radius of a $C_{10}E_4$ micelle is taken to be R_0=21Å (see Section 2.3.2), and the radii of the virus particles are R_v=125, 300, and 700Å for the bacteriophages ϕX174, P22, and T4, respectively (see Section 3.3.1). The number density of micelles of aggregation number n, $\rho_n = N_n/V$, and the contour length of such micelles, L_n, are calculated from the surfactant concentrations in the two coexisting phases according to the molecular-thermodynamic approach described in Section 1.2.2 [27]. The contour length, L_n, of $C_{10}E_4$ micelles is typically 1000's of Å. The Kuhn segment length of a $C_{10}E_4$ micelle is not available in the literature. However, in the $C_{12}E_6$ micellar system, which is similar in many respects to the $C_{10}E_4$ micellar system, the Kuhn length was estimated [35] to be about 100 - 150Å in the temperature range (T_c−10°C) - T_c, with $T_c \approx$ 50°C. In view of this, a similar Kuhn length value was adopted in the $C_{10}E_4$ case. Additional evidence substantiating the use of these Kuhn length values for $C_{10}E_4$ micelles will be presented in Chapter 5. The contributions of $C_{10}E_4$ micelles of various aggregation numbers n are then summed up in Eq. (3.4) in order to calculate the virus partition coefficient, K_v, using Eq. (3.3).

Figures 3-3, 3-4, and 3-5 presented earlier show the predicted and the experimentally measured virus partition coefficients of ϕX174, P22, and T4 in the two-phase $C_{10}E_4$-buffer system, respectively. In Figures 3-3 and 3-4, the predicted partition coefficient, $K_{v,l}$, is calculated for various Kuhn length values, l, of a $C_{10}E_4$ micelle, including: (1) l=100Å ($\cdots$), (2) l=150Å ($- - -$), and (3) $l \rightarrow \infty$ (rigid cylinder) ($- \cdot - \cdot -$). Note that curve (3) corresponds to that used previously to describe the protein partitioning case (see Section 2.3.1). In Figure 3-5, only the predicted par-

tition coefficient, $K_{v,l}$, corresponding to a Kuhn length, l=100Å ($\cdots$), is shown. An examination of Figures 3-3 and 3-4 reveals that, for a given virus particle at the same temperature, the predicted partition coefficients, $K_{v,l}$, follow the trend:

$$K_{v,rigid} < K_{v,l=150\text{Å}} < K_{v,l=100\text{Å}} < 1 \tag{3.19}$$

Equation (3.19) indicates that, depending on the micellar flexibility, as reflected in the value of the Kuhn length, l, the new theoretical model predicts a weaker partitioning of the solute particles as compared to the previous model, which assumed rigid micelles. This is expected, since the introduction of micellar flexibility should decrease the excluded-volume interactions between the solute particles and the micelles. Equation (3.19) also indicates that, as the micelles become more flexible, as reflected in a lower l value, the predicted partition coefficients, $K_{v,l}$, attain values closer to unity, indicating a more even partitioning.

When comparing the predicted virus partition coefficients with those measured experimentally, it appears that the inclusion of micellar flexibility in the new theoretical formulation does not always improve the accuracy of the theoretical predictions. For example, for ϕX174 (see Figure 3-3), which is a spherical virus with a radius of 125Å, the predicted K_{rigid} exhibits a trend similar to that observed experimentally, and agrees well with the experimental K_v values in the temperature range 18.8°C $< T <$ 19.3°C. Beyond T=19.3°C, the $K_{v,rigid}$ values are over-predicted (lower) as compared to the experimental K_v values. On the other hand, inclusion of micellar flexibility, as reflected in the predicted values of $K_{v,l=100\text{Å}}$ and $K_{v,l=150\text{Å}}$, results in an under-prediction of the partition coefficient, thus suggesting an under-estimation of the excluded-volume effects in the ϕX174 case.

In the case of P22, which is also spherical with a radius of 300Å, the predicted K_{rigid} values agree with the experimental ones only for T <19.0°C (see Figure 3-4). Inclusion of micellar flexibility, as reflected in the predicted $K_{v,l=100\text{Å}}$ and $K_{v,l=150\text{Å}}$ values, extends the temperature range of agreement to about 19.3°C. However, as shown in Figure 3-4, the experimentally measured P22 partition coefficients reach

a seemingly constant, "plateau" value beyond T >19°C, a feature which cannot be reproduced in the context of the excluded-volume theory developed so far. It is possible that other mechanisms, not accounted for in the theory, may also play a role and lead to the observed "plateau" region.

As in the case of T4, which is rod-like and has an estimated radius of 700Å, Figure 3-5 shows that the trend of the experimentally observed partition coefficients is similar to that in the "plateau" region in Figure 3-4 and, in addition, exhibits a mild increasing trend with increasing temperature, which is contrary to that predicted according to the excluded-volume interactions. Moreover, the predicted partition coefficients, $K_{v,rigid}$, $K_{v,l=150\text{Å}^\circ}$, and $K_{v,l=100\text{Å}^\circ}$, are all many orders of magnitude lower than the experimentally measured K_v and hence over-estimate the T4 partitioning behavior. In fact, the values of the predicted partition coefficients for T4 are so low that only $K_{l=100\text{Å}^\circ}$ can be plotted in Figure 3-5. This indicates that the current theory, which is based solely on excluded-volume interactions, is unable to describe the experimentally observed T4 partitioning behavior.

In Figure 3-7, the experimentally measured partition coefficients at 20°C are plotted as a function of the particle radius, R_p or R_v, of the three proteins—cytochrome c, ovalbumin, and catalase— and the three bacteriophages—ϕX174, P22, and T4, along with a comparison with the predicted partition coefficients. As can be seen, the agreement between the experimental and predicted partition coefficients is reasonably good for the smaller particles, particularly in the protein cases. In addition, the difference between the predicted partition coefficients based on the different micellar flexibility (l=100Å, 150Å, and ∞) are not pronounced for the smaller particles, indicating, as expected, that micellar flexibility is not essential in describing the excluded-volume interactions when the solute particles are small. However, as the particle size increases, the predicted partition coefficients begin to deviate from the experimental data. In particular, there seems to be a "threshold" radius (of about 150 - 200Å) beyond which the partitioning behavior of the solute particles can no longer be described by the excluded-volume theoretical formulation developed here, regardless of the extent of micellar flexibility. This phenomenon requires further examination and

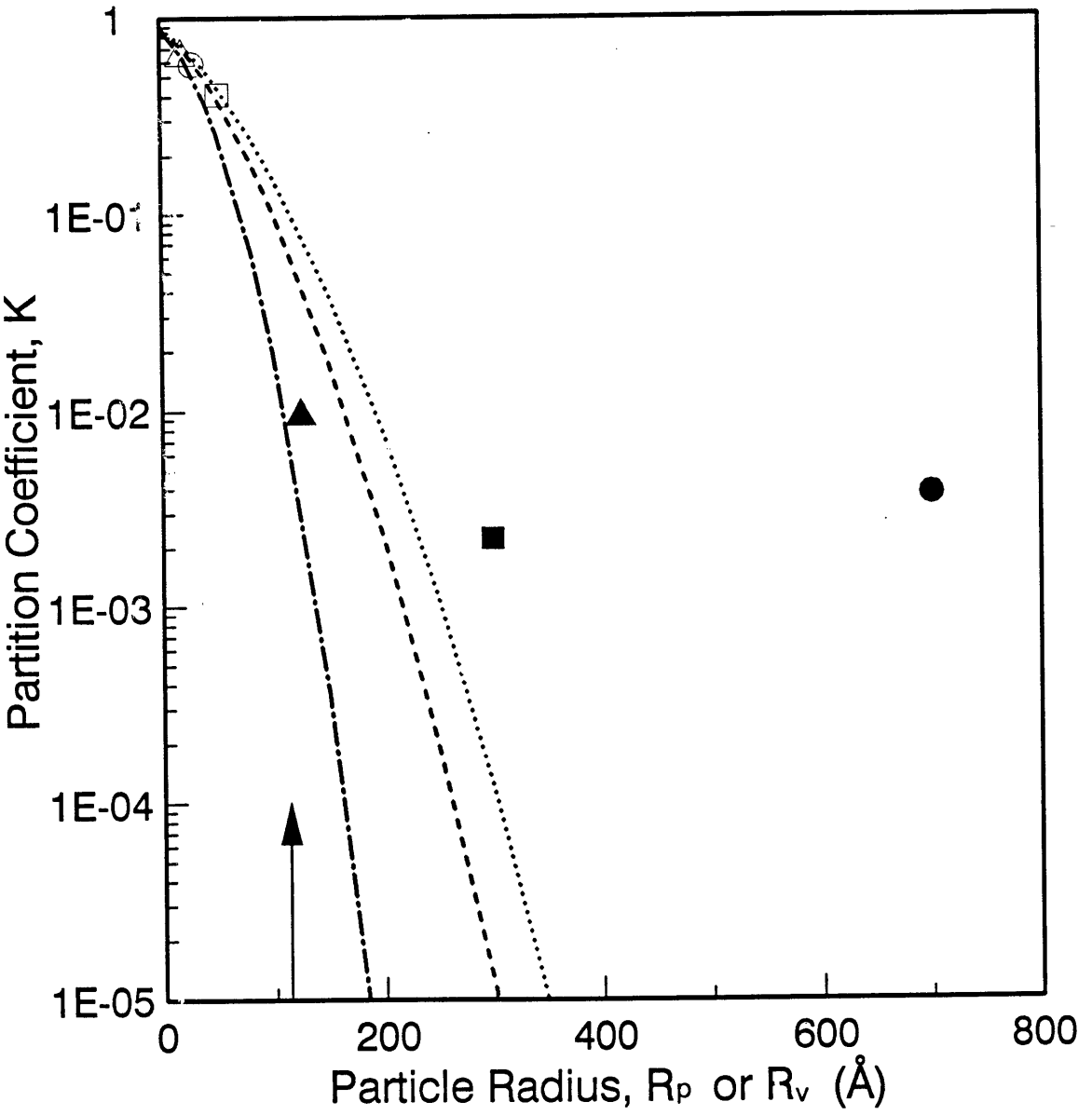

Figure 3-7: Experimentally measured partition coefficients, K, as a function of the particle radius, R_p or R_v, in the two-phase $C_{10}E_4$-buffer micellar system at 20°C. The various symbols represent proteins and bacteriophages: (△) cytochrome c, R_p=19Å, (○) ovalbumin, R_p=29Å, (□) catalase, R_p=52Å, (▲) ϕX174, R_v=125Å, (■) P22, R_v=300Å, and (●) T4, R_v=700Å,. Also shown are the predicted partition coefficients based on the assumption that the $C_{10}E_4$ micelles are flexible and have a Kuhn length of 100Å ($\cdots$), 150Å ($- - -$), or that the micelles are rigid ($l \to \infty$) ($- \cdot - - \cdot -$). The arrow indicates half of the average mesh size, $\xi_m/2$=115Å, as estimated from Eq. (3.21).

investigation.

3.4.4 Discussion of the Deviations Between the Predicted and Experimentally Measured Partition Coefficients

The deviations of the excluded-volume predictions from the experimentally observed partitioning behavior, as presented in the previous section, suggests that inclusion of other mechanisms is needed to explain the observed virus partitioning behavior. The following reasons come to mind in attempting to rationalize the observed deviations:

1. The observed partitioning behavior may not reflect a true thermodynamic equilibrium state, but, instead, may be kinetically driven, since the theoretical predictions are based on the assumption of true thermodynamic equilibrium.

2. The virus particles may have specific interactions with the micelles or surfactant molecules, with these not being explicitly accounted for in the excluded-volume theoretical formulation.

One could argue that reason 2 is not likely to be the major cause of the observed deviations, when the likelihood of interactions other than those of the excluded-volume type are examined more closely. First, since the $C_{10}E_4$ surfactant is nonionic, electrostatic interactions between the virus particles and the $C_{10}E_4$ micelles or the $C_{10}E_4$ monomers should be negligible. Second, hydrophobic interactions between the $C_{10}E_4$ micelles and the virus particles are also unlikely. As mentioned in Sections 3.2.2 and 3.3.1, the virus particles examined are all composed of protein capsids and do not possess phospholipid envelops. Moreover, the protein molecules composing the capsids do not degrade, disentangle, or expose their hydrophobic moieties easily. Accordingly, the virus particles should be quite "inert," thus displaying very little surface activity. As a result, the ability of virus particles to interact with the hydrophobic cores of the $C_{10}E_4$ micelles should be very limited. It appears, therefore, that reason 2 is not very plausible, and, hence, that reason 1 should be pursued and investigated further. A preliminary examination of reason 1 is presented in the next section.

3.5 Preliminary Study on Kinetic Aspects of Partitioning

3.5.1 Evidence of Possible Kinetic Effects

The observed deviations between the theoretical virus partitioning results and the experimental ones may be due to kinetic effects associated with the structure of the top $C_{10}E_4$ micelle-rich phase. Dynamic light scattering measurements seem to indicate that the $C_{10}E_4$ micelles present in the top micelle-rich phase may grow into elongated cylindrical structures capable of forming a transient mesh or net of interpenetrating micelles (see Chapter 5 for details). The mesh size of this net decreases with increasing surfactant concentration and, therefore, with increasing temperature (see the right branch of the temperature versus $C_{10}E_4$ concentration phase diagram in Figure 2-3).

Recent work by Abbott *et al.* on polymer-protein interactions [22] seems to indicate that the diffusion of "big" protein molecules (with radii in the range of 30 - 50Å) through a membrane (having sufficiently large pore sizes, ~300Å, to allow passage of proteins while preventing passage of polymers) into a concentrated PEO solution, in which the PEO molecules entangled and formed a mesh, did not attain equilibrium within the time frame of observation (3-7 days) or before the proteins degraded. This, however, does not happen with relatively small proteins (with radii of about 20Å), and equilibrium of the smaller proteins can be reliably and repeatedly obtained. This suggests that the kinetics involving particle diffusion through the polymer mesh may be strongly dependent on the relative sizes of the polymer mesh and the diffusing particles, with bigger particles taking longer time to diffuse into the mesh. It is tempting to speculate that an analogy may exist between the polymer mesh and the transient micellar mesh present in the top micelle-rich phase, particularly with respect to the diffusion of the large virus particles. From this perspective, true virus partitioning equilibrium may not have been attained within the time frame of the partitioning experiments conducted so far (4-14 hours).

The value of the micellar mesh size can be estimated using geometric arguments [7]. This argument assumes that micelles form a simple cubic net. By assuming that the size of the cube is ξ_m, and that each of the twelve edges of the cube contributes effectively 1/4 of a column with a cross-sectional radius R_0, the volume fraction of surfactant in each cubic cell should be equal to the volume fraction of surfactant in the solution, ϕ. That is,

$$\begin{aligned} \phi &= 12 \times \frac{1}{4}\pi R_0^2 \xi_m / \xi_m^3 \\ \phi &= 3\pi R_0^2 \xi_m / \xi_m^3 \end{aligned} \tag{3.20}$$

The micellar mesh size, ξ_m, can then be derived as

$$\xi_m \approx (\frac{3\pi}{\phi})^{1/2} R_0 \tag{3.21}$$

In the two-phase aqueous $C_{10}E_4$ micellar system, the ξ_m values in the concentrated phase have been estimated using Eq. (3.21) as a function of temperature and are tabulated in Table 3.1. The $C_{10}E_4$ mesh size, ranging from 310Å at 19°C to 200Å at 21°C, is comparable to, or smaller than, the diameters of the viruses examined. In particular, at 20°C, ξ_m ≈230Å and $\xi_m/2$ ≈115Å, which, as shown by the arrow in Figure 3-7, appears to correspond to a threshold size beyond which the theoretical predictions begin to deviate from the experimental observations. This indeed suggests that kinetic effects associated with the diffusion of large virus particles through the mesh-like structure in the concentrated micellar phase may play a role in the observed virus partitioning behavior.

To contrast this with the protein partitioning case, since protein molecules are relatively small (with radii of 20 - 60Å) as compared to: (1) the micellar contour length (1000's of Å), or (2) the micellar mesh size (about 200-300Å), the protein molecules cannot "see" or "sense" the change in the $C_{10}E_4$ micellar solution structure with increasing temperature. Instead, they "see" $C_{10}E_4$ micelles as rigid cylindrical structures under all conditions. Consequently, the protein partitioning behavior should be

Table 3.1: Estimated micellar mesh size, ξ_m, in the concentrated phase of the two-phase aqueous $C_{10}E_4$ micellar system.

Temperature (°C)	Volume Fraction in the Concentrated Phase, ϕ	Mesh Size, ξ_m (Å)
18.9	0.0377	332
19.0	0.0439	308
19.5	0.0624	258
20.0	0.0790	229
20.5	0.0916	213
21.0	0.1052	199

minimally affected by kinetic effects of the type described above. Indeed, the experimental observations (not reported here) indicate that the protein partition coefficients obtained after 2, 6, and 8 hours of partitioning in two-phase aqueous micellar systems are essentially the same (see also Section 3.5.3 and Figure 3-8).

Although kinetic effects may provide a reasonable explanation for the observed protein and virus partitioning behavior, additional work is needed in order to further elucidate and investigate the influence of these kinetic effects. Some preliminary experimental studies in this direction are described next.

3.5.2 Experimental Methods

Two model systems were chosen for examining possible kinetic effects of the partitioning behavior: (1) the hydrophilic protein ovalbumin, and (2) the bacteriophage P22, each partitioning in the two-phase aqueous $C_{10}E_4$ micellar system. This was done in order to compare and contrast the kinetic aspects associated with the partitioning behavior of these two biomolecules which possess very different sizes. All the experiments were conducted at 20.0°C.

Two types of partitioning experiments were conducted:

- Partitioning for different time periods, with the solutions prepared in the regular way, as described in Sections 2.2.4.2 and 3.3.5.1. This experiment was aimed at examining the possible dependence of the partition coefficients on partitioning

time.

- Injection of concentrated solutions of a partitioned entity (either ovalbumin or P22) into one of the two coexisting micellar phases after phase separation had already been established. The aim here was to gain some understanding on the mechanism of partitioning.

The following detailed procedures were adopted:

1. Partitioning in solutions prepared in the regular way for different time periods

   A set of two or three $C_{10}E_4$ solutions, containing either ovalbumin or P22, was prepared in pH 7 McIlvaine buffer, as described in Sections 2.2.4.2 and 3.3.5.1. The ovalbumin and P22 concentrations were 0.5 g/L and 3×10^8 particles/mL respectively. The surfactant concentration in each solution was 3.96 wt% in order to generate two coexisting phases of equal volume at 20.0°C. These solutions were then placed in the water cell (see Figure 2-2) already adjusted to 20°C to initiate phase separation. Each set of solutions was kept at this temperature for different time periods, ranging from 18 hours (overnight) to 3 days for ovalbumin partitioning, and from 5 hours to 2 weeks (14 days) for P22 partitioning. The two coexisting phases were then withdrawn, and the ovalbumin (or P22) concentration in each of the phase solutions was determined using the UV/visible absorbance method, as described in Section 2.2.3 (or the biological activity assay, as described in Sections 3.3.2 and B.1). Mass balance calculations were then conducted to examine whether there was loss of ovalbumin molecules or P22 particles before and after partitioning.

2. Injection of concentrated solutions of a partitioned entity into one of the already-formed micellar phases

   A set of two or three $C_{10}E_4$ solutions in pH 7 McIlvaine buffer, but containing no ovalbumin or P22, was prepared. Each solution had a volume of about 2.4 mL, and the surfactant concentration in each solution was also 3.96 wt% in order to generate two coexisting phases of equal volume at 20.0°C. These solutions were

then placed in the water cell (see Figure 2-2) adjusted to 20.0°C to initiate phase separation. Usually, at this temperature, the two coexisting phases formed and appeared in about 30 minutes. After the solutions were kept in the cell for 1.5 - 2 hours, a concentrated ovalbumin or P22 solution was injected *in situ* into one of the two coexisting phases using a 50-mL microsyringe while the phase solutions were kept in the water cell at 20.0°C. The concentration of the concentrated ovalbumin (or P22) solution and the amount of the concentrated solution injected were monitored such that, after injection, the final overall solute concentration in the solutions was about 0.5 g/L for ovalbumin or 3×10^8 particles/mL for P22, the same as those used when solutions were prepared in the regular way, as described in 1 above.

In the case of ovalbumin, a concentrated ovalbumin solution with 15 g/L was prepared in pH 7 McIlvaine buffer, and 80 μL of it was injected into one of the two coexisting phases. In the case of P22, the concentrated P22 solution with a concentration of about 3×10^{10} particles/mL was prepared in pH 7 McIlvaine buffer, and 24μL of it was injected into one of the two coexisting phases.

The injection was performed slowly and carefully in order to ensure that ovalbumin or P22 was placed exclusively in one of the two phases, and that no disturbance of the two phases was caused by the injection. Details of the injection procedure are described below:

- When injecting into the top phase:

  The needle of the microsyringe was inserted into the top phase. The concentrated solution therein was injected very slowly and, at the same time, mixed thoroughly with the top phase solution using the needle of the syringe. The purpose was to avoid droplets of the injected solution (essentially aqueous) from forming in the top phase, since these droplets fell down quickly into the bottom phase due to their density being higher than that of the top micelle-rich phase. As a result of mixing, the top phase looked turbid after injection.

- When injecting into the bottom phase:

  Before inserting the needle into the solution, some air was taken into the microsyringe in order to have a portion of air in front of the injected solution in the microsyringe. The needle of the microsyringe was then inserted slowly to the very bottom of the bottom phase. Since the needle had to go through the top phase to reach the bottom phase, some components of the top-phase solution could stick on the needle and could be brought down to the bottom phase by the needle. By injecting air bubbles from the microsyringe, these top-phase components can be "knocked out" from the needle and lifted back to the top phase region. Injection of the concentrated solution was not performed until all the phase components had stopped moving around, and the presence of the needle did not seem to perturb the appearance of the two coexisting phases. Injection of the P22 solution was then performed slowly, with the needle fixed at the very bottom of the solution. After injection of the solution was completed, the needle was withdrawn slowly from the solution in order to avoid disturbing the two phases.

In general, the time spent on injection into one solution was about 10 minutes. After the needle of the microsyringe was withdrawn from the solution, the test tubes containing solutions were sealed, and the solutions were kept in the water cell overnight (about 18 hours) before withdrawal of the phase solutions for concentration analysis.

3.5.3 Results and Discussion

Figure 3-8 shows the experimentally measured partition coefficients of ovalbumin at 20.0°C as a function of partitioning time. Three cases were examined: (1) partitioning for different time periods with the solution prepared in the regular way (◯) (denoted as $K_{regular}$), (2) injection into the top phase (△) (denoted as K_{top}), and (3) injection into the bottom phase (□) (denoted as K_{bot}). Figure 3-9 shows the experimentally

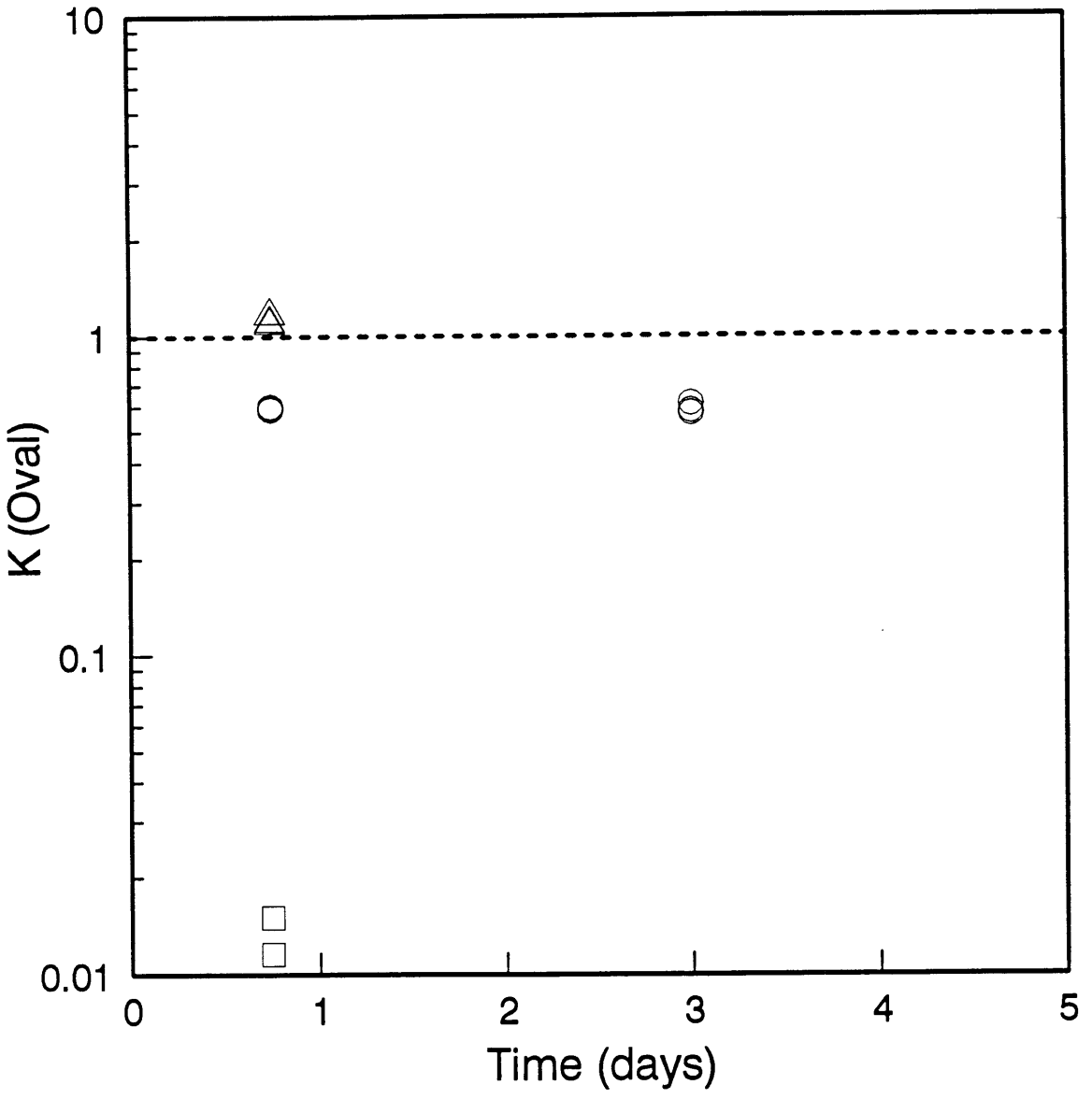

Figure 3-8: Experimentally measured partition coefficient of the protein ovalbumin, $K(Oval)$, as a function of partitioning time in the two-phase aqueous $C_{10}E_4$ micellar system at 20.0°C. The various symbols represent three different experimental conditions: (1) partitioning for various time periods, with the solutions prepared in the regular way, $K_{regular}$ (○), (2) injection of the concentrated ovalbumin solution into the top phase, K_{top} (△), and (3) injection of the concentrated ovalbumin solution into the bottom phase, K_{bot} (□). The dashed line with a $K(Oval)$ value of unity is shown for reference purposes.

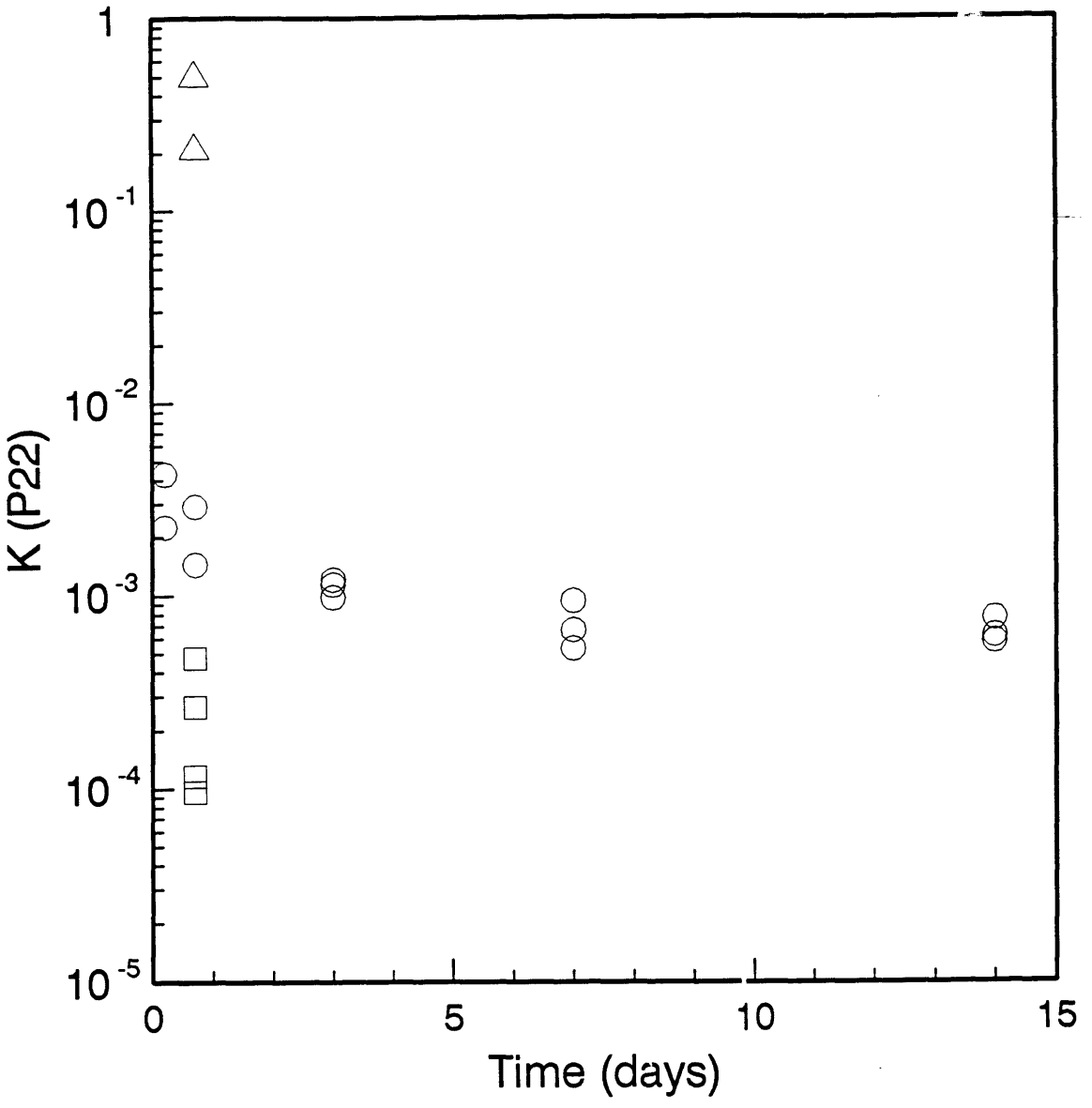

Figure 3-9: Experimentally measured partition coefficient of the bacteriophage P22, $K(P22)$, as a function of partitioning time in the two-phase aqueous $C_{10}E_4$ micellar system at 20.0°C. The notation is the same as that in Figure 3-8.

measured partition coefficients of P22 at 20.0°C as a function of partitioning time, using the same notation as that used in Figure 3-8. In these two figures, the number of symbols at a given partitioning time represents the number of partitioning samples examined.

It is noteworthy that the injection experiments were found to be sensitive to many factors or artifacts, including gravity and the location in a given phase at which the injection was done. With this in mind, the results shown in Figures 3-8 and 3-9 should be qualitatively reliable for deducing information about the possible kinetic aspects of the partitioning phenomenon. A more detailed examination and comparison of the results shown in Figures 3-8 and 3-9 is presented below:

- Comparison between $K_{regular}(Oval)$ and $K_{regular}(P22)$

  An examination of Figure 3-8 indicates that $K_{regular}(Oval)$ remains essentially constant as a function of the partitioning time during 1 to 3 days. This agrees with the earlier findings that the protein partition coefficients do not vary with the partitioning time (see Section 3.5.1). In the case of P22, Figure 3-9 shows that $K_{regular}(P22)$ initially decreases with increasing partitioning time, but appears to gradually reach a constant value ($\sim 6 \times 10^{-4}$) after partitioning for 7 days and remains at this value after partitioning for 14 days. In view of this trend, it does not seem likely that $K_{regular}(P22)$ will continue to decrease by orders of magnitude as the partitioning time is increased further. One can conclude that the P22 partitioning behavior reaches the final K value (6×10^{-4}) at a rate which is much slower than that of ovalbumin partitioning (7 days versus a few hours). However, it should be noted that the mass balance calculation revealed a loss of P22 particles (about 20 - 40%) after partitioning for 7 days or more. Accordingly, the observed reduction in $K_{regular}(P22)$ with increasing partitioning time may also have resulted from the loss of P22 particles during partitioning, and, therefore, the final $K_{regular}(P22)$ value of 6×10^{-4} may not represent the true thermodynamic equilibrium condition.

- Comparison between $K_{regular}$ and K_{top}, K_{bot}

  Both Figures 3-8 and 3-9 indicate that $K_{top} > K_{regular} > K_{bot}$ after overnight partitioning for both ovalbumin and P22. This inequality may reflect the difference in the transport patterns associated with each experimental condition examined. In obtaining K_{top} or K_{bot}, the partitioned solutes (ovalbumin molecules or P22 particles) were injected into one of the two coexisting and pre-equilibrated phases, and partitioning was achieved solely by diffusion of the solute particles within the macroscopic phases and through the interface separating the two phases. On the other hand, in obtaining $K_{regular}$, the solute existed in the solutions prior to the onset of phase separation. After phase separation was initiated (for example, by placing the solutions at 20.0°C), microscopic domains of phase components began to emerge, and the solute particles could more easily diffuse and be exchanged through the boundaries of these small phase domains, with the total interfacial area being much larger than that between the two coexisting macroscopic phases. In addition, the convective movement of the microscopic phase domains to form the two macroscopic phases, induced by the density difference, helped transport the solute particles as well, hence reducing the time required to reach the final partitioning condition. This process is apparently more efficient than diffusion between the two macroscopic phases.

  The above discussions also suggest that K_{top} and K_{bot} may eventually converge to $K_{regular}$ if the allowed partitioning time is sufficiently long. Additional experimental work involving partitioning for times longer than one day is required to further elucidate this issue.

- Comparison of the partitioning behavior of ovalbumin and P22

  It is interesting to compare the partitioning behavior of ovalbumin and P22 through their K_{top} and K_{bot} values. An interesting feature is that $K_{top}(Oval) > 1$ but $K_{top}(P22) < 1$ after overnight partitioning, suggesting that the bigger solute particles (P22) come out of the top micelle-rich phase faster than the

smaller particles (ovalbumin). This has a strong similarity to *size-exclusion chromatography*, in which the smaller particles take longer to come out of the chromatographic column since they can permeate into the small meshes and hence travel by longer routes through the column. This would also be consistent with the notion advanced in this thesis that the interactions between micelles and ovalbumin molecules, or between micelles and P22 particles, are *essentially of the excluded-volume type.*

3.5.4 Qualitative Rationalization of Kinetic Effects on the Partitioning Phenomenon

From the results and discussion presented in the previous section, the following picture can be advanced to rationalize the virus partitioning behavior from a kinetic perspective. Specifically, the interplay between (1) the attainment of phase separation equilibrium of the two-phase aqueous micellar system, and (2) the attainment of partitioning equilibrium of the partitioned solutes in the two-phase aqueous micellar system, is examined below.

In the partitioning experiments conducted in this thesis, phase separation in a micellar system is initiated by changing the solution temperature, and small domains of the two phases begin to appear and move in opposite directions to form the two coexisting macroscopic phases due to density differences, with the partitioning of the solute particles proceeding at the same time. The observed partitioning behavior is primarily driven by the interactions between micelles and solute particles, which are essentially of the excluded-volume type in the cases examined. In principle, these interactions force the bigger partitioned entities (such as P22 virus particles) to be "kicked out" of the top micelle-rich phase domains more extremely than the smaller solutes (such as ovalbumin protein molecules), thus resulting in more uneven and extreme partitioning of the bigger solute particles. In addition, transport of the solute particles is attained via two mechanisms: (1) diffusion of solute particles within the phase domains, and (2) convective motion of microscopic phase domains to form

macroscopic phases.

The influence of these two mechanisms is discussed below:

- Diffusion of solute particles within the phase domains

  As mentioned earlier, the direction in which the solute particles are transported between the two coexisting phases (either microscopic or macroscopic) is driven by interactions between micelles and solute particles, which are primarily of the excluded-volume type in the cases examined so far. However, the solute particles have to travel within the (micelle-rich) phase domains via diffusion to reach the phase boundaries, where they can be exchanged between phase domains in order to reach partitioning equilibrium. According to the Stokes-Einstein relation [68]:

  $$D = \frac{k_B T}{6\pi\eta\xi_h} \tag{3.22}$$

  where D and ξ_h are the diffusion coefficient and the hydrodynamic length of the solute particles respectively, η is the viscosity of the solvent, k_B is the Boltzmann constant, and T is the absolute temperature. Equation (3.22) suggests that solute particles with bigger sizes have smaller diffusion coefficients and hence move more slowly than the smaller ones. Specifically, when comparing P22 (R_v=300Å) with ovalbumin (R_p=29Å), the diffusion coefficient of P22 particles should be (300/29)$\sim$10 times smaller than that of ovalbumin at the same temperature and solvent viscosity. In other words, P22 particles need to spend much longer time than ovalbumin molecules to travel the same distance in a medium. Furthermore, in a more viscous medium, such as the top micelle-rich phase, the diffusivity of the solute particles will be further reduced, and the movement of the bigger solute particles will be further retarded. Consequently, the time needed for the bigger solute particles to reach partitioning equilibrium between the phase domains is expected to be longer than that for smaller solute particles between the same phase domains. This, therefore, results in a transport limitation by this diffusion process.

- Convective motion of microscopic phase domains

  The microscopic domains can carry solute particles and bring these particles into the final macroscopic phases at a faster rate than that related to transport via diffusion only. Another important effect associated with the convection of the phase domains is the entrainment of the solute particles. The entrainment occurs in such a way that solute particles may be dragged along by the micelle-rich phase domains, ending up in the final micelle-rich phase. Alternatively, domains of the micelle-poor phase, having a solute concentration higher than that of the micelle-rich phase (due to excluded-volume interactions), may be entrapped between moving micelle-rich phase domains and end up being incorporated into the final macroscopic micelle-rich phase. This entrainment effect should occur in both directions, with the micelle-rich phase domains being carried into the micelle-poor phase as well, thus resulting in more even partitioning than expected.

  The entrainment effect is expected to be more pronounced when the equilibrium solute concentrations in the two coexisting phases are very different. For example, in the virus partitioning case, the virus concentrations in the two coexisting phases were found to differ by orders of magnitude, and hence the entrainment of a micelle-poor phase domain, which is much more concentrated in virus than the micelle-rich phase, will make the concentration in the final macroscopic micelle-rich phase much higher, thus resulting in more even partitioning than that predicted theoretically. On the other hand, in the protein partitioning case, since the equilibrium protein concentrations in the two coexisting phases are essentially of the same order of magnitude, the entrainment of the phase components will not have a significant influence on the final partitioning result.

It is also interesting to examine the combined effect of the two mechanisms discussed above on solute partitioning during the attainment of phase separation equilibrium. Since the convective motion of phase domains can only take place for a limited time, that is, during the formation of the macroscopic phases, it follows that,

once the macroscopic phases form, the convective motion must cease. For example, in the $C_{10}E_4$ micellar system, as the temperature increases, the difference in the surfactant concentrations, as well as the difference in the densities, of the two coexisting phases becomes more pronounced. As a result, the microscopic phase domains move faster,and it takes shorter time to form the final macroscopic phases. Accordingly, the time available for the small phase domains to be in contact with each other, as well as the time available for the solute particles to be transported via diffusion between the small phase domains, are concomitantly shorter. In addition, the viscosity of the micelle-rich phase increases with increasing surfactant concentration, and hence, with temperature, which provides additional hindrance to the diffusion of the bigger solute particles. Consequently, in the $C_{10}E_4$ micellar system, at higher temperatures, the ability of bigger solute particles to attain *partitioning equilibrium* during the attainment of *phase separation equilibrium* of the micellar system is reduced, which may result in more even partitioning than that predicted theoretically. This, in turn, may explain the "plateau" region and the slightly increasing trend of K_v with temperature for the bigger virus particles, P22 and T4, as shown in Figures 3-4 and 3-5.

In the case of protein molecules, since they are typically about ten times smaller in size than virus particles, they can diffuse ten times faster than the virus particles, according to the Stokes-Einstein relation (see Eq. (3.22)). Therefore, their transport is not so limited by the diffusion process as in the virus partitioning case, and kinetic effects of the type described above are not expected to be pronounced in the protein partitioning case. It is therefore possible to reach *partitioning equilibrium* of protein molecules during the attainment of *phase separation equilibrium* of the micellar system, and the experimental partitioning results can thus reflect a true thermodynamic equilibrium condition. This may help explain the reasonably good agreement found between the experimentally observed and theoretically predicted partitioning behavior, as presented in Section 2.3.2.

The above qualitative rationalization based on kinetic aspects associated with the partitioning phenomenon provides some basis to explain the observed partitioning trend of the bigger virus particles. If this rationalization is correct, it indicates that the

observed P22 and T4 partitioning behavior is actually complicated by kinetic effects. This rationalization also suggests that, in partitioning experiments, *reaching phase separation equilibrium* of the phase-forming entities (micelles or polymers) may not be equivalent to *reaching partitioning equilibrium* of the partitioned solutes (proteins or viruses), particularly when the solute particles possess large sizes. More work, however, is needed to justify the qualitative rationalization presented above. Some ideas about the experiments which may be helpful to further clarify this issue are discussed in Section 6.2.5.

3.6 Conclusions

This chapter presented an investigation on the partitioning behavior of bacteriophages in the two-phase aqueous $C_{10}E_4$ micellar system, including the experimental observations, theoretical formulation, and a preliminary study on kinetic aspects of the partitioning phenomenon. A summary of the central results follows:

- The experimentally measured partition coefficients of bacteriophages in the two-phase aqueous $C_{10}E_4$ micellar system were found to be of order 10^{-3}, reflecting a much more extreme partitioning than in the case of protein molecules. A monotonic decrease of the partition coefficient with increasing temperature was only observed in the case of the smaller virus particles, such as ϕX174. For the larger virus particles, such as P22 and T4, their partition coefficients reached a minimum value ($\approx 10^{-3}$) at a certain threshold temperature and remain at approximately this value at all higher temperatures examined, as shown in Figures 3-4 and 3-5.

- The theoretical formulation based on excluded-volume interactions was modified to include micellar flexibility which can be "sensed" by larger solute particles, such as viruses. However, the predictions based on the new theoretical formulation were unable to reproduce the experimentally observed virus partitioning behavior, particularly in the case of the larger virus particles, such as P22 and

T4, for which a "plateau" region was observed beyond a threshold temperature (see Figures 3-4 and 3-5).

- A preliminary study on kinetic aspects of partitioning was conducted to shed light on the observed deviations between $K_{v,expt}$ and $K_{v,theo}$, as well as to help explain the "plateau" phenomenon in the K_v versus temperature plots of P22 and T4, as shown in Figures 3-4 and 3-5. A qualitative rationalization was presented in which the observed partitioning behavior ofaller than that of ovalbumin at the same temperature and solvent viscosity. In other words, P22 particles need to spend much longer time than ovalbumin molecules to travel the same distance in a medium. Furthermore, in a more viscous medium, such as the top micelle-rich phase, the diffusivity of the solute particles will be further reduced, and the movement of the bigger solute particles will be further retarded. Consequently, the time needed for the bigger solute particles to reach partitioning equilibrium between the phase domains is expected to be longer than that for smaller solute particles between the same phase domains. This, therefore, results in a transport limitation by this diffusion process.

Chapter 4

Utilization of Two-Phase Aqueous Micellar Systems as a Practical Separation or Concentration Method

4.1 Introduction and Motivation

Based on the studies and results reported in Chapters 1, 2, and 3, two-phase aqueous micellar systems can potentially be utilized as a practical separation or concentration method for the following reasons:

1. The partitioning results obtained in Chapters 2 and 3 indicate that biomolecules having different sizes, such as hydrophilic proteins and viruses, exhibit very different partitioning behavior in two-phase aqueous micellar systems. In particular, in the $C_{10}E_4$ two-phase aqueous micellar system, both the hydrophilic proteins and the viruses tend to partition preferentially into the bottom micelle-poor phase, but to very different extents. Specifically, the measured partition coefficients of proteins were found to be of order 1 (see Section 2.2.4.3 and Figures 2-6 and 2-8), while those of viruses were found to be of order 10^{-3} (see

Section 3.3.5.2 and Figure 3-6). This indicates a much more extreme partitioning of the viruses (the larger biomolecule), which clearly suggests the potential of achieving an efficient separation of biomolecules, based on the size of the solute particles, with the use of two-phase aqueous micellar systems.

2. As described in Section 1.2.3, the non-charged surfactants do not bind to protein molecules or induce loss of enzymatic activity. In addition, the stability test results presented in Section 3.3.3 demonstrated indirectly that the presence of micelles in the solution does not have detrimental effects on the viability of the viruses. It can therefore be concluded that two-phase aqueous micellar systems composed of nonionic (and zwitterionic) surfactants can indeed provide friendly and non-harmful environments to biological materials.

3. Two-phase aqueous micellar systems constitute a liquid-liquid extraction method and, therefore, have the potential of being scaled up with relative ease.

In view of these encouraging reasons, the utilization of two-phase aqueous micellar systems as a separation or concentration method was investigated, with the results of this investigation presented in this chapter.

In the studies reported in Chapters 2 and 3, temperature, which indirectly controls the surfactant (micellar) concentrations in the two coexisting phases, as well as the micellar size, was the key factor tuned to control the partitioning behavior of a specific biomolecule in the two-phase aqueous micellar systems. Although tuning other factors, such as salt type and concentration and solution pH, was not attempted, the partitioning results obtained so far seem to suggest the implementation of certain strategies in order to enhance the separation efficiency associated with the use of two-phase aqueous micellar systems. Specifically, as explained below, it appears promising to vary the volume ratio of the two coexisting micellar phases as a means of increasing the separation or concentration efficiencies.

In the partitioning work reported in Chapters 2 and 3, the partitioning experiments were all conducted utilizing two-phase systems having approximately equal volumes of the two coexisting micellar phases. As first pointed out by Albertsson [69],

the partition coefficient is an intensive thermodynamic property. As such, it should not depend on the overall concentration of the partitioned solute (biomolecules), as well as on the volumes (or the volume ratio) of the two coexisting phases. In other words, a mere manipulation of the volume ratio of the two coexisting phases should not change the partition coefficients of solutes (biomolecules). On the other hand, as shown below, the manipulation of this volume ratio can have a pronounced effect on improving the efficiency of separation or concentration of the biomolecules.

Following the "one-step procedure" proposed by Albertsson [69] in the case of two-phase aqueous polymer systems, one can "force" the volume of one of the two coexisting phases to be much larger than that of the other in order to achieve the desired separation or concentration efficiencies. More specifically, in the two-phase aqueous $C_{10}E_4$ nonionic micellar system, both the hydrophilic proteins and the viruses partition preferentially into the bottom (micelle-poor) phase. However, since, as mentioned earlier, the virus particles exhibit much more extreme partitioning behavior than proteins, concentration of virus particles in the bottom phase can be achieved by making $V_t/V_b > 1$, where V_t and V_b are the volumes of the top and bottom phases respectively. In addition, using the same strategy, most of the proteins can be retrieved from the top phase, with relatively few viruses remaining in the top phase. Accordingly, it is proposed that, by partitioning hydrophilic proteins and viruses simultaneously in a two-phase aqueous micellar system having $V_t/V_b > 1$, one can accomplish the tasks of separation and concentration at the same time.

The volume ratio of the two coexisting micellar phases can be tuned by varying the total surfactant concentration of the solution at a given temperature. More specifically, from knowledge of the surfactant concentrations in the two coexisting phases at a certain temperature, as obtained from the measured coexistence (cloud-point) curve on the temperature versus surfactant concentration phase diagram (see, for example, Figures 2-3 and 2-4), the total surfactant concentration needed to achieve the desired final volume ratio, V_t/V_b, at the temperature of interest can be calculated according to the lever rule. However, since the desired total surfactant concentration may be very close to one of the ends of the tie line drawn across the coexistence (cloud-

point) curve at the temperature of interest, the corresponding micellar solution may be close to, or possibly, even inside the metastable region of the phase diagram. In this case, the solution condition is close to equilibrium, and the rate of change towards equilibrium usually becomes very slow as equilibrium is approached [70]. As a results, the time required to attain phase separation equilibrium is longer than that required in the case of equal-volume partitioning.

The remainder of this chapter is organized as follows. Section 4.2 presents general considerations concerning the unequal-volume partitioning strategy, including a brief discussion of the lever rule and the definition of two useful parameters for assessing the separation or concentration efficiencies. Section 4.3 presents the experimental details associated with the unequal-volume partitioning. Section 4.4 presents a brief comparison between partitioning in two-phase aqueous (micellar or polymer) systems and other separation methodologies which are commonly used in biotechnology. Finally, Section 4.5 summarizes the results presented in this chapter, including some concluding remarks.

4.2 General Considerations Associated with the Unequal-Volume Partitioning Strategy

The partition coefficient of a biomolecule, K, in the two-phase system was defined in Chapter 2 and is given by

$$K = \frac{C_t}{C_b} \tag{4.1}$$

where C_t and C_b are the biomolecule concentrations in the top and bottom phases respectively. The following mass-balance relation is generally valid:

$$C_0 V_0 = C_0(V_t + V_b) = C_t V_t + C_b V_b \tag{4.2}$$

where C_0 is the initial total biomolecule concentration, V_0 is the initial total volume of the solution, including the volume of the surfactant (the phase-forming material),

and V_t and V_b are the volumes of the top and bottom phases respectively. Note that under the reasonable approximation that the total volume of the solution does not change upon partitioning, it follows that $V_0 = V_t + V_b$.

Equations (4.1) and (4.2) are valid under all conditions. Specifically, as mentioned earlier, the partition coefficient is an intensive thermodynamic property, and, as such, should be independent of the overall solute concentration and the volume ratio of the two coexisting phases [69]. Consequently, in principle, the final volume ratio, V_t/V_b, required to achieve a desired partitioning result can be calculated before the partitioning experiment is conducted, with the associated partition coefficients obtained from the equal-volume partitioning experiments.

4.2.1 The Lever Rule

The lever rule provides a simple tool to calculate the volume ratio of the two coexisting phases in phase-separated one-component or multi-component systems [71]. For example, in the case of one-component systems, the phase diagram consists of a pressure versus molar volume relationship, while in the case of binary systems at a fixed pressure, it consists of a temperature versus composition relationship.

Figure 4-1 provides an illustration of the various elements which need to be assigned to apply the lever rule in the case of the $C_{10}E_4$-water binary micellar system. The tie line (dashed line in Figure 4-1) connects two points on the coexistence curve which represent the compositions of the two coexisting phases at a certain temperature (and pressure) condition. For example, in Figure 4-1, the tie line at a given temperature $T°$ intersects the coexistence curve at point A, having a $C_{10}E_4$ concentration C_A, and at point B, having a $C_{10}E_4$ concentration C_B. If a solution with an overall $C_{10}E_4$ concentration C_O is prepared at the temperature $T°$, as represented by point O in Figure 4-1, such a solution will separate into two phases, since point O lies within the two-phase region. After separation equilibrium is attained, the resulting two coexisting phases will have compositions C_A and C_B. This type of *qualitative* information can be obtained by a simple inspection of the phase diagram. The lever rule provides a tool to *quantify* this information. Let V_A and V_B be the final volumes

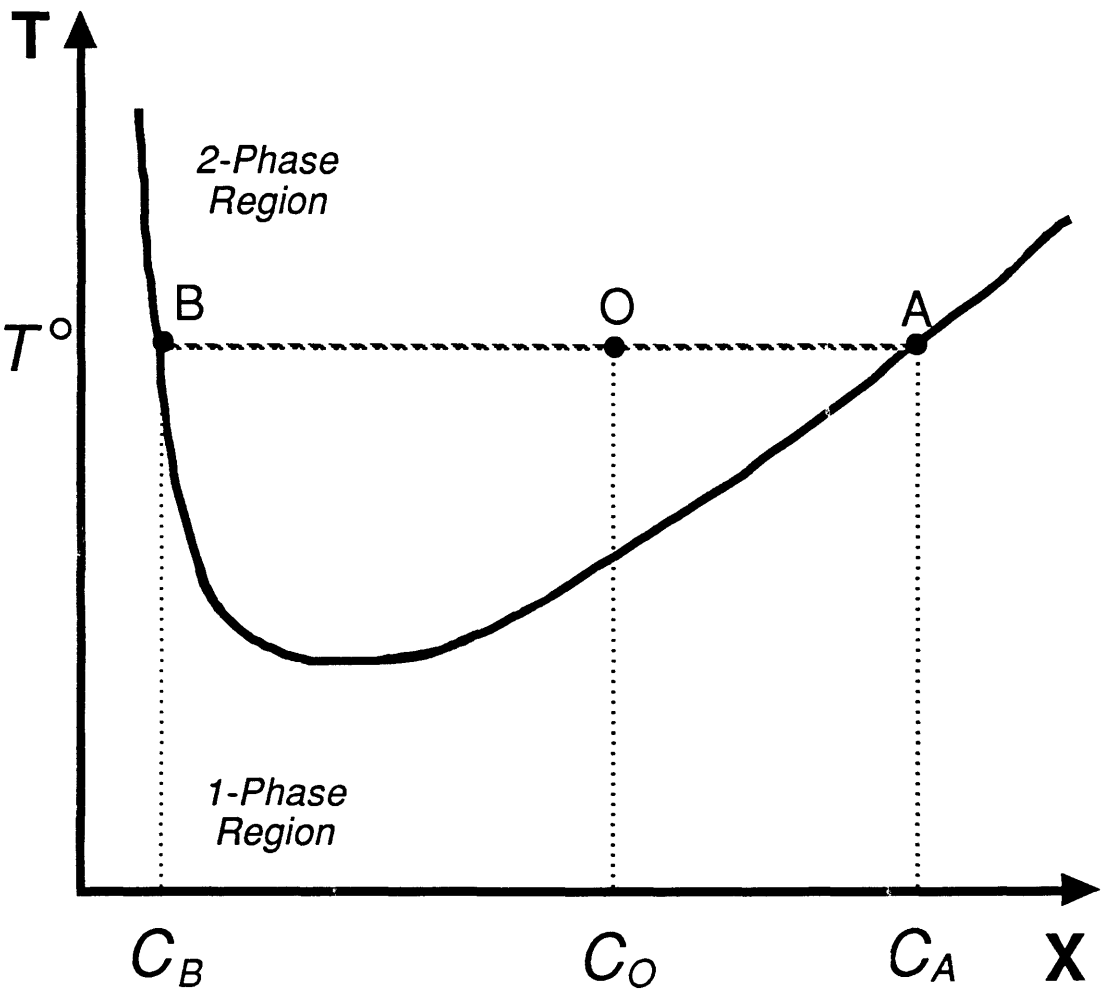

Figure 4-1: Illustration of the various elements which need to be assigned to apply the lever rule in the case of the $C_{10}E_4$-water binary micellar system. In the temperature (T) versus $C_{10}E_4$ concentration (X) phase diagram, the solid curve is the coexistence (cloud-point) curve separating the one-phase and two-phase regions, and the dashed line is the tie line at temperature $T°$. C_B, C_O, and C_A are the $C_{10}E_4$ concentrations corresponding to points B, O, and A, respectively.

of phases A and B respectively. The following expression then follows from a mass balance on the initial and final amounts of $C_{10}E_4$ in the solution:

$$C_O(V_A + V_B) = C_A V_A + C_B V_B \tag{4.3}$$

Rearranging Eq. (4.3) yields

$$(C_A - C_O)V_A = (C_O - C_B)V_B$$

$$\frac{V_A}{V_B} = \frac{C_O - C_B}{C_A - C_O} \tag{4.4}$$

$$\text{or} \quad \frac{V_A}{V_B} = \frac{OB}{OA} \tag{4.5}$$

where $OB = C_O - C_B$ and $OA = C_A - C_O$. In other words, the volume ratio of the two coexisting phases, V_A/V_B, is given by the ratio of the lengths of the tie-line segments OB and OA. Since the mathematical relation given in Eq. (4.5) is similar in structure to that corresponding to a lever derived in classical mechanics, it is referred to as the "lever rule."

In the $C_{10}E_4$ aqueous micellar system, the top phase is micelle-rich and is therefore located on the right branch of the coexistence curve, illustrated by point A in Figure 4-1, while the bottom phase is micelle-poor and is therefore located on the left branch of the coexistence curve, illustrated by point B in Figure 4-1. The volume ratio of the two coexisting micellar phases is hence given by

$$\frac{V_t}{V_b} = \frac{OB}{OA} \tag{4.6}$$

Equation (4.6) clearly indicates that, in order to make the value of V_t/V_b much greater than unity, point O (representing the total $C_{10}E_4$ concentration) should be chosen as close as possible to point A. In other words, the total surfactant concentration must be fairly high in order to obtain a large V_t/V_b value. As point O approaches point A, it may penetrate into the metastable region of the phase diagram, thus resulting

in a longer equilibration time (see discussion in Section 4.1). Consequently, the time required to attain phase-separation equilibrium depends on the desired final volume ratio, and is expected to be longer in the case of larger final volume ratios.

4.2.2 Definition of Two Useful Parameters for Assessing Separation and Concentration Efficiencies

Two useful parameters are defined in this section in order to quantitatively assess the efficiency of separation and concentration using two-phase aqueous micellar systems. These are (1) the yield in the top phase, Y, and (2) the concentration factor in the bottom phase, α.

1. **Yield in the Top Phase, Y**

   The parameter Y is defined as the amount of a desired solute which can be retrieved from the top phase (C_tV_t) relative to the total amount of this solute in the solution ($C_tV_t + C_bV_b$), that is,

   $$Y(\%) = \frac{C_tV_t}{C_tV_t + C_bV_b} \times 100\% \tag{4.7}$$

   Using the partition coefficient definition given in Eq. (4.1) in Eq. (4.7) yields the following alternative expression for Y:

   $$Y(\%) = \frac{K\left(\frac{V_t}{V_b}\right)}{1 + K\left(\frac{V_t}{V_b}\right)} \times 100\% \tag{4.8}$$

   It is interesting to examine Eq. (4.8) to learn how the yield, Y, varies with the volume ratio, V_t/V_b, particularly when $V_t/V_b > 1$. For a fixed K value (which, as stated above, is independent of the V_t/V_b value), Y increases as V_t/V_b increases, and, for a fixed V_t/V_b value, Y is lower for smaller K values. Recall that in the case of partitioning in the two-phase aqueous $C_{10}E_4$ micellar system, K was found to be of order 1 for hydrophilic proteins and of order 10^{-3} for viruses, the latter being much smaller than unity. Accordingly, it is expected that, by

increasing the volume ratio, V_t/V_b, the yield of the proteins in the top phase should increase significantly, while that of the viruses should not. As will be shown below, this is indeed the case, and it constitutes a very useful feature for removal of viruses with concomitant purification of proteins.

2. Concentration Factor in the Bottom Phase, α

The parameter α is defined as the ratio of the concentration of a solute in the bottom phase, C_b, and the initial total solute concentration, C_0, that is,

$$\alpha = \frac{C_b}{C_0} \tag{4.9}$$

Combining Eqs. (4.2) and (4.1), it follows that

$$C_0 = \frac{C_t V_t + C_b V_b}{(V_t + V_b)} \tag{4.10}$$

$$\text{or} \quad C_0 = \frac{C_b(KV_t + V_b)}{(V_t + V_b)} \tag{4.11}$$

Using Eq. (4.11) in Eq. (4.9), and rearranging, yields

$$\alpha = \frac{V_t + V_b}{KV_t + V_b} \tag{4.12}$$

$$\text{or} \quad \alpha = \frac{1 + \left(\frac{V_t}{V_b}\right)}{1 + K\left(\frac{V_t}{V_b}\right)} \tag{4.13}$$

An examination of Eq. (4.13) reveals that, for a constant K value, α increases with an increase in the volume ratio, V_t/V_b. In addition, for a fixed V_t/V_b value, α increases as K decreases, reaching a maximum value of

$$\alpha_{max} \approx 1 + \frac{V_t}{V_b}, \tag{4.14}$$

when $K \to 0$. Note that α_{max} is indeed very large when V_t/V_b is very large. Since the partition coefficients of hydrophilic proteins, K_p, and those of virus

particles, K_v, are both smaller than unity in the $C_{10}E_4$ two-phase aqueous micellar system, and K_v's were found to be at least two orders of magnitude smaller than K_p's, it follows that the virus concentration factors, α_v, should increase more significantly with increasing volume ratio, V_t/V_b, than the protein concentration factors, α_p. Accordingly, significant concentration of viruses in the bottom phase of the $C_{10}E_4$ two-phase aqueous micellar system should be accomplished by using large V_t/V_b values.

The highest V_t/V_b value which was obtained so far in two-phase aqueous polymer systems is about 100 [72, 73, 74]. If this maximal V_t/V_b value can indeed be reached in two-phase aqueous micellar systems, the derivations presented above clearly indicate that the efficiency of separation and concentration operations may be greatly enhanced.

4.3 Experimental Approach

4.3.1 Materials

The materials used in these studies included the nonionic surfactant $C_{10}E_4$ (as described in Section 2.2.1.1), the hydrophilic protein ovalbumin (as described in Section 2.2.1.2), and the bacteriophage P22 (as described in Section 3.3.1). As in the previous two chapters, all the solutions were buffered with pH 7 McIlvaine buffer.

4.3.2 Experimental Methods

Two types of partitioning experiments were conducted, both utilizing volume ratios V_t/V_b greater than unity. The first type involved an examination of the effect of increasing the volume ratio, V_t/V_b, on the partitioning efficiency of either ovalbumin or P22, with the V_t/V_b values ranging from 1 to 6. The second type involved simultaneous partitioning of ovalbumin and P22 at a volume ratio of 14.5 in order to assess the separation efficiencies of these biomolecules when a higher volume ratio was used. Details of these studies are presented below:

1. Final volume ratios V_t/V_b=1 - 6

The partitioning of a bimolecular species (either the protein ovalbumin or the bacteriophage P22) at various final volume ratios, V_t/V_b=1 - 6, and at a fixed temperature of 19.3°C was conducted. Solutions containing the surfactant $C_{10}E_4$ and either ovalbumin or P22 were prepared in pH 7 McIlvaine buffer, as described in Sections 2.2.4.2 and 3.3.5.1. Note that in the experiments reported here, the total surfactant concentrations used were different from those used in Sections 2.2.4.2 and 3.3.5.1, which were chosen to yield V_t/V_b=1, in order to obtain final volume ratios V_t/V_b larger than unity. The total surfactant concentration in a given solution needed for reaching a desired volume ratio at the end of partitioning was calculated according to the lever rule (see Section 4.2.1). In the temperature versus $C_{10}E_4$ concentration phase diagram (see Figure 2-3), the 19.3°C tie line intersects the coexistence curve at $C_t \approx$5.4 wt% and $C_b \approx$0.5 wt%, representing the surfactant concentrations in the top and bottom phases respectively after phase separation equilibrium is attained. In order to calculate the total surfactant concentration, C_O, required to obtain a final volume ratio of, for example, V_t/V_b=3, the lever rule result given in Eq. (4.6) can be utilized. Expressing the surfactant concentration in wt% yields

$$\frac{V_t}{V_b} = 3 = \frac{C_O - 0.5}{5.4 - C_O} \tag{4.15}$$

from which a value of C_O=4.18wt% is obtained. Following the same procedure, C_O=4.7 wt% for reaching a final volume ratio V_t/V_b=6, and C_O=2.95 wt% in the case of equal-volume partitioning, that is, for reaching a final volume ratio V_t/V_b=1.

At least three surfactant solutions, each containing either 0.5 g/L ovalbumin or $\sim 10^8$ particles/mL P22, were prepared in pH 7 McIlvaine buffer, with the total $C_{10}E_4$ concentration, C_O, in each solution in the range of 3.0 - 4.7 wt%, depending on the desired final volume ratio. These solutions were prepared in test tubes with graduations, so that the final volumes of the two coexisting

phases could be easily measured. The total volume of each solution was about [(desired V_t/V_b)+1] mL in order to obtain a final V_b of 1 mL, since at least 1 mL of solution was needed for protein concentration determination. After being well mixed and cooled down in the refrigerator, the solutions were placed in the water cell (see Figure 2-2), whose temperature was already adjusted to 19.3°C, for about 13 - 14 hours (overnight) to ensure that the systems reached thermodynamic equilibrium. Since the resulting final volume ratios in each solution may not be exactly the same as those calculated from Eq. (4.6) due to the possible inaccuracy in the determination of the intersections of the tie line with the coexistence curve in the phase diagram, the actual final volumes of the two coexisting phases were recorded at the end of each partitioning experiment, and the corresponding actual volume ratios were calculated. The two coexisting phases were then withdrawn with syringe and needle sets, and the ovalbumin (or P22) concentrations were determined using the UV absorbance measurements described in Section 2.2.3 (or the biological activity assay described in Section 3.3.2). The corresponding partition coefficient, K, the yield in the top phase, $Y(\%)$, and the concentration factor in the bottom phase, α, were then calculated according to Eqs. (4.1), (4.7), and (4.9), respectively.

2. Final volume ratio V_t/V_b=14.5

The simultaneous partitioning of ovalbumin and P22 at a larger final volume ratio V_t/V_b=14.5 was then conducted at 20°C. Prior to conducting this partitioning experiment, it was tested and found that, although ovalbumin and P22 coexisted in the solutions, there was essentially no interference in the concentration determination of one type of biomolecule by the presence of the other. This is due to the fact that the P22 concentrations (in the range of 10^5 - 10^8 particles/mL) were not sufficiently high to induce strong absorbance or scattering which could have interfered with the UV absorbance measurements used to determine the ovalbumin concentrations. On the other hand, the biological activity assay used for determining P22 concentrations is not sensitive to the

presence of inert proteins which do not perform enzymatic functions on P22 particles, such as ovalbumin. Consequently, the concentrations of the protein and the virus can still be measured accurately using the UV/visible absorbance and biological activity assay respectively.

At 20.0°C, the surfactant concentrations in the top and bottom phases are C_t ≈7.6 wt% and C_b ≈0.24 wt% respectively, as deduced from the intersections of the 20.0°C tie line with the $C_{10}E_4$ coexistence curve (see Figure 2-3). Three surfactant solutions containing both ovalbumin and P22 (with concentrations of 0.5 g/L and $\sim 10^8$ particles/mL respectively), and with a total $C_{10}E_4$ concentration of 7.5wt% in order to reach a final volume ratio V_t/V_b=20, were prepared. The amount of each solution was about 21 mL (21 g) such that the final volume of the bottom phase was about 1 mL. These solutions were prepared in pear-shaped flasks with graduations. These flasks were used in this experiment because (1) typical test tubes cannot accommodate 21 mL of liquid, and (2) such flasks are wide on the top and narrow on the bottom and, hence, can facilitate withdrawal of the small bottom phase. In addition to these solutions, a 2.5 mL solution with a total $C_{10}E_4$ concentration of 3.96 wt% (in order to achieve equal-volume partitioning at 20.0°C), but without ovalbumin or P22, was also prepared in order to have the resulting two phases serve as the "reference" for the ovalbumin concentration measurement (see Section 2.2.4). These solutions were placed in the water cell set at about 20.0°C for about 24 hours. The final volumes of the two coexisting phases were measured from the graduations on the flasks, and the corresponding actual final volume ratios were then calculated.

The two phases were then withdrawn with syringe and needle sets, and the ovalbumin and P22 concentrations in each of the two phases were determined using the UV absorbance measurement and the biological activity assay respectively. The resulting partition coefficients of ovalbumin and P22, K, as well as their yields in the top phase, $Y(\%)$, and concentration factors in the bottom phase,

α, were then calculated according to Eqs. (4.1), (4.7), and (4.9).

4.3.3 Results and Discussion

Figure 4-2 shows the measured partition coefficients, K, of ovalbumin and P22 as a function of the actual final volume ratio of the two coexisting phases, V_t/V_b, in the two-phase aqueous $C_{10}E_4$ micellar system at 19.3°C. The circles and triangles denote the experimental data points from the ovalbumin and P22 partitioning experiments respectively, and the lines, which are drawn to guide the eye, connect the averages of the data points corresponding to each V_t/V_b value. As shown in Figure 4-2, the partition coefficient of ovalbumin (◯) remains approximately constant with increasing volume ratio. On the other hand, the average partition coefficient of P22 (– – –) increases only slightly, from about 2×10^{-3} to about 4×10^{-3}, as the volume ratio increases from 1 to 5.5, thus essentially remaining at the same order of magnitude. This is consistent with the expectation [69] that there should be no dependence of the partition coefficients on the volume ratio.

Figure 4-3 shows the yields in the top phase, $Y(\%)$, defined in Eq. (4.7), of ovalbumin and P22 as a function of the final volume ratio, V_t/V_b. The notation is the same as that in Figure 4-2. Figure 4-3 shows that the experimental Y values of ovalbumin (◯) exhibit a significant increase with increasing V_t/V_b, reaching a value of about 80% for $V_t/V_b \approx 5$. On the other hand, the Y values of P22 (△) are low and do not increase considerably with increasing V_t/V_b. Figure 4-4 shows the concentration factors in the bottom phase, α, defined in Eq. (4.9), of ovalbumin and P22 as a function of the final volume ratio, V_t/V_b. The notation is the same as that in Figure 4-2. Figure 4-4 indicates that α of P22 (△) increases significantly with increasing V_t/V_b, reaching a value of $\alpha \approx 7$ at $V_t/V_b \approx 5.5$, while α of ovalbumin (◯) remains essentially constant. Figures 4-3 and 4-4 clearly suggest that it is very promising to increase the volume ratio, V_t/V_b, for the purposes of both retrieving proteins from the top phase and concentrating viruses in the bottom phase in the two-phase aqueous $C_{10}E_4$ micellar system.

The experimental results obtained from the simultaneous partitioning of ovalbu-

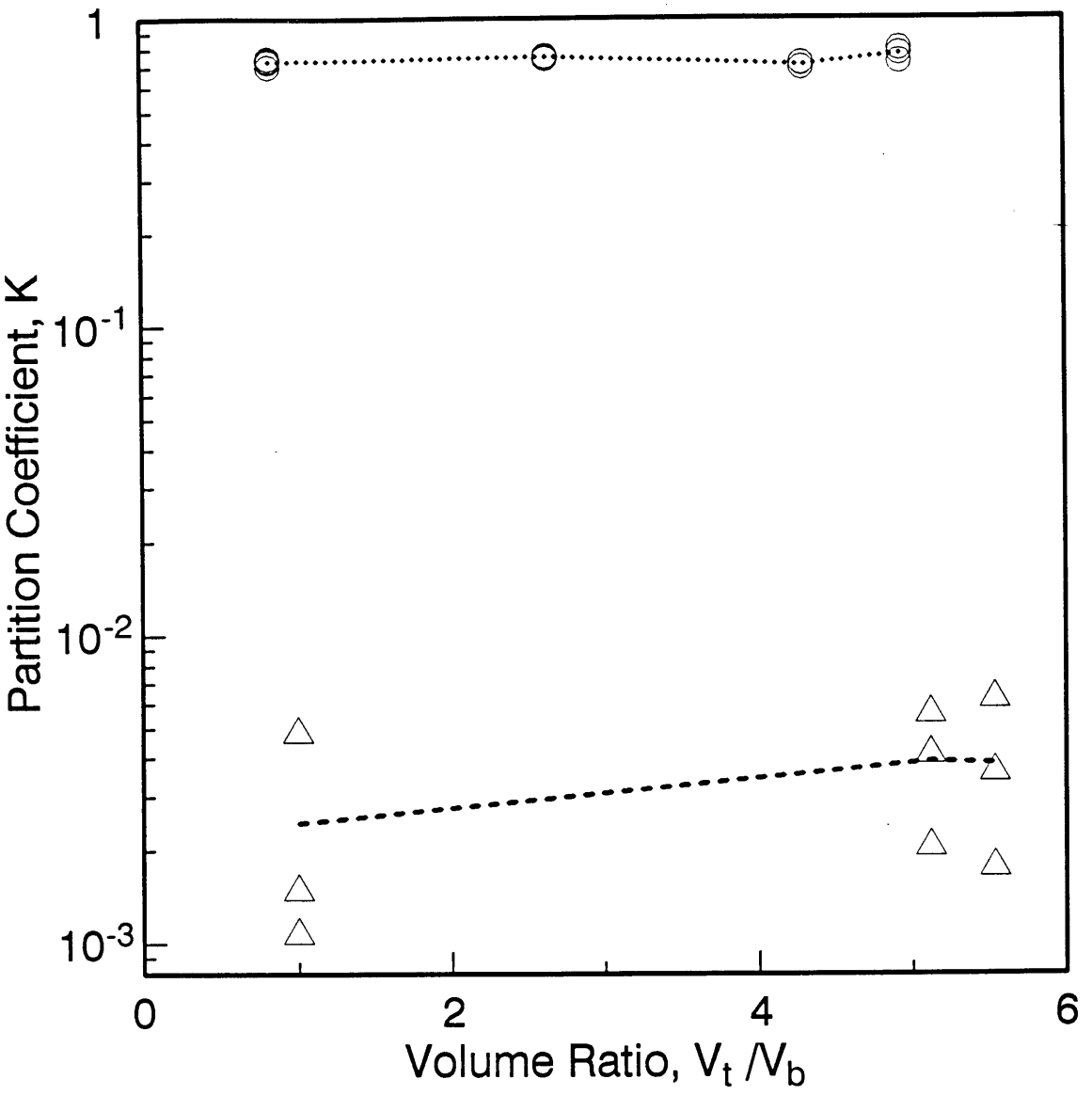

Figure 4-2: Experimentally measured partition coefficients of the protein ovalbumin (○) and the bacteriophage P22 (△) as a function of the actual final volume ratio, V_t/V_b (between 1 - 6), in the two-phase aqueous $C_{10}E_4$ micellar system at 19.3°C. The lines, which connect the average values of the partition coefficients of ovalbumin (···) and P22 (– – –) corresponding to each V_t/V_b value, are drawn to guide the eye.

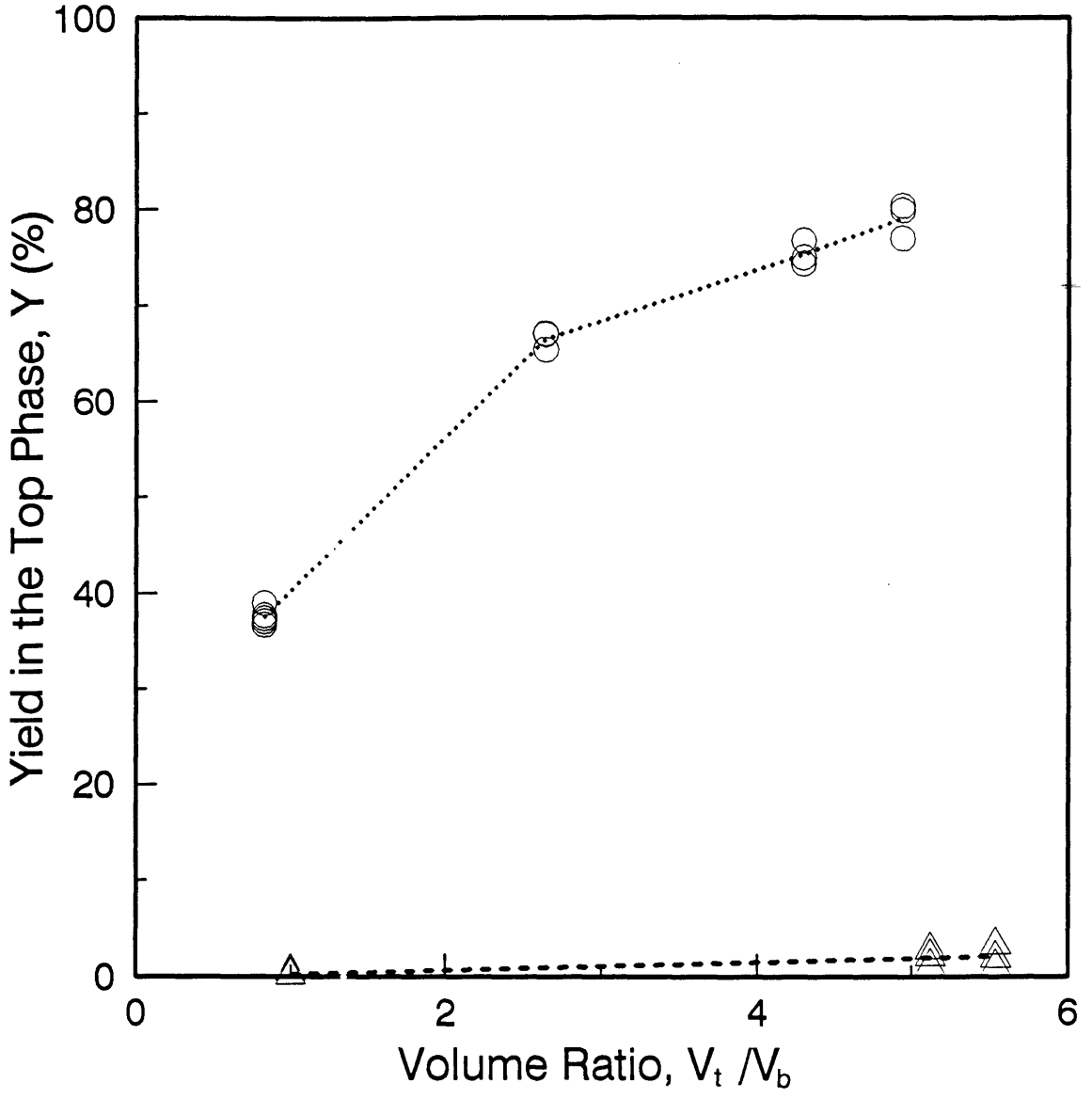

Figure 4-3: Yield in the top phase, $Y(\%)$, as a function of the actual final volume ratio, V_t/V_b, in the two-phase aqueous $C_{10}E_4$ micellar system at 19.3°C. The notation is the same as that in Figure 4-2.

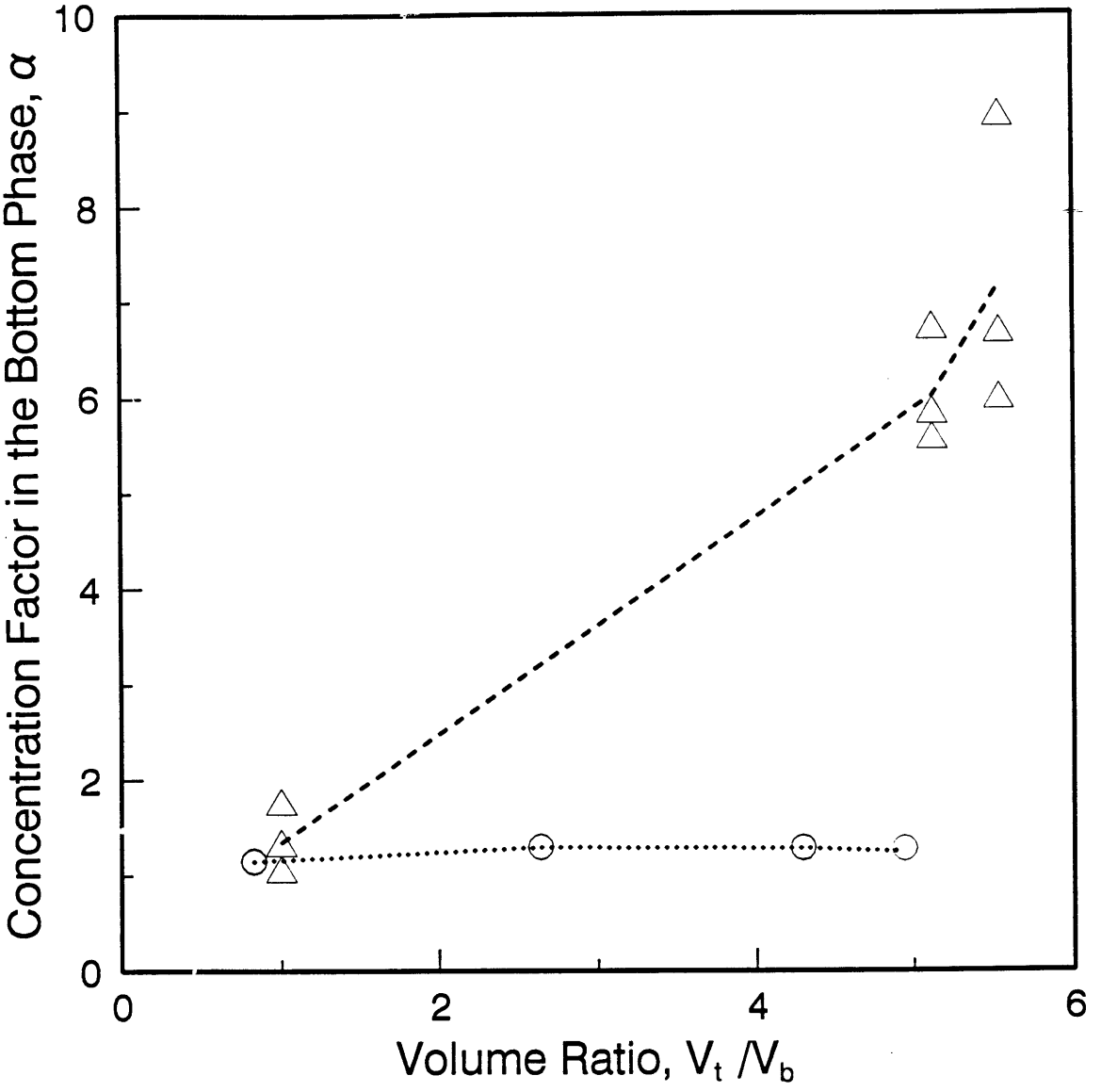

Figure 4-4: Concentration factor in the bottom phase, α, as a function of the actual final volume ratio, V_t/V_b, in the two-phase aqueous $C_{10}E_4$ micellar system at 19.3°C. The notation is the same as that in Figure 4-2. Note that one circle (representing ovalbumin data) is actually the overlap of three data points.

Table 4.1: Summary of the experimental results of the unequal-volume partitioning of ovalbumin and P22 in the two-phase aqueous $C_{10}E_4$ micellar system conducted at 20.0°C.

- Experimental Conditions

Temperature	20.11 ±0.02	°C
Total $C_{10}E_4$ Concentration	7.5	wt%
Equilibration Time	21	Hours
Final Volume Ratio, V_t/V_b	14.5/1	

- Results

	Ovalbumin	P22
Original Concentration	0.62 g/L	4.7×10^7 ϕ/mL
Final Concentration: Top	0.54 g/L	3.7×10^6 ϕ/mL
Final Concentration: Bottom	1.05 g/L	6.7×10^8 ϕ/mL
Partition Coefficient, K	**0.51**	**5.7×10^{-3}**
Yield in the Top Phase, Y (%)	**84.48**	**7.64**
Concentration Factor in the Bottom Phase, α	**1.68**	**14.05**

min and P22 at 20°C are schematically illustrated in Figure 4-5 and tabulated in Table 4.1. In this partitioning experiment, the temperature control was very steady, fluctuating solely within ±0.02°C during the entire partitioning period. The final volume ratio obtained was V_t/V_b=14.5, which is higher than in the experiments conducted at 19.3°C, the results of which are reported in Figures 4-2, 4-3, and 4-4. However, this volume ratio is still lower than the expected value (about 20), which was calculated according to the lever rule using the surfactant concentrations, C_t and C_b, obtained from the phase diagram, as described in Section 4.3.2. This is probably due to the inaccuracy associated with determining the concentrations C_t and C_b from the intersections of the 20.0°C tie line with the coexistence curve.

In Table 4.1, the partition coefficients obtained at these conditions are 0.51 for ovalbumin and 5.7×10^{-3} for P22. When compared with the partition coefficient values obtained from the equal-volume partitioning at 20.0°C (see Sections 2.2.4.3 and 3.3.5.2), which are 0.58 for ovalbumin and 2.24×10^{-3} for P22, it appears that the partition coefficient values are essentially not affected to a significant extent by

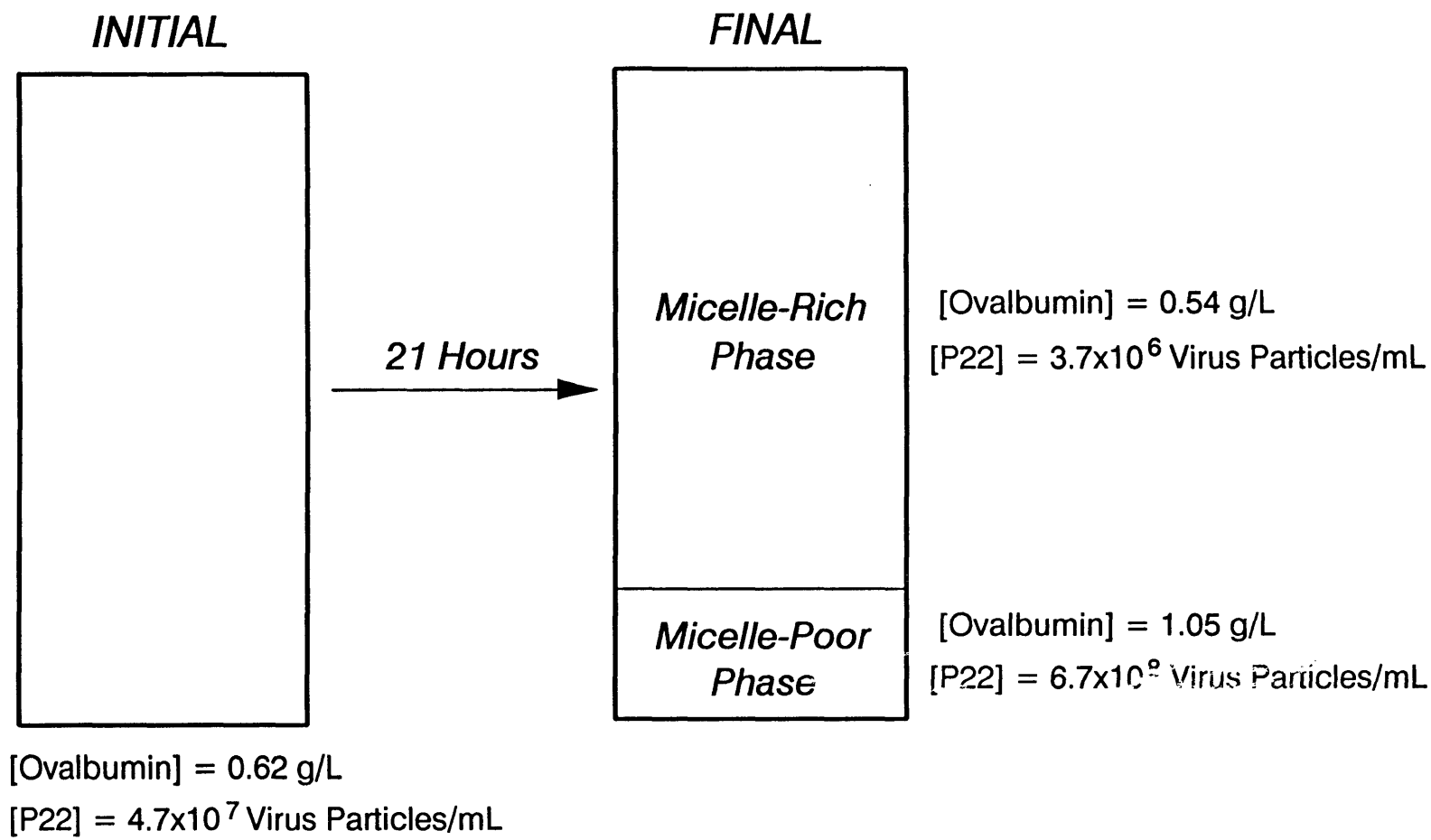

Figure 4-5: Schematic illustration of the unequal-volume partitioning experiment conducted at 20°C, in which the final volume ratio obtained was $V_t/V_b \approx 14.5$.

the volume ratio used. The yields in the top phase, $Y(\%)$, indicate that more than 80% of the total protein ovalbumin can be retrieved from the top phase, with only 7.6% of the virus P22 remaining in that phase, since most of the virus particles (about 92% in this case) partitioned into the bottom phase. This suggests that, by increasing the volume ratio in the two-phase aqueous micellar systems, one can indeed remove viruses from the desired protein while retrieving as much protein as possible.

The concentration factors in the bottom phase, α, indicate that the P22 concentration in the bottom phase is 14 times higher than its original concentration, while the concentration of the protein ovalbumin is only increased by a small factor (lower than 2). Furthermore, the value of $\alpha \approx 14$ for P22 is close to the maximum α value that can be attained at a volume ratio of 14.5, as predicted by Eq. (4.14). This suggests that virus particles such as P22, whose partition coefficient is of order 10^{-3}, can be efficiently concentrated and purified using unequal-volume partitioning in the two-phase aqueous $C_{10}E_4$ micellar systems. In other words, it is also promising to utilize two-phase aqueous micellar systems with high volume ratios for the purpose of concentrating large biomolecules, such as viruses and cells.

Although the highest volume ratio obtained in the experiments reported above was 14.5, it is still possible to achieve even higher volume ratios in two-phase aqueous micellar systems. For example, if a final volume ratio of 100 could be achieved in the experiments illustrated in Figure 4-5, the corresponding yields in the top phase, Y, and concentration factors in the bottom phase, α, of ovalbumin and P22 could be calculated according to Eqs. (4.8) and (4.13), assuming that the K values are the same as those listed in Table 4.1:

	Ovalbumin	P22
Partition Coefficient, K	0.51	5.7×10^{-3}
Yield in the Top Phase, $Y(\%)$	98.08	36.31
Concentration Factor in the Bottom Phase, α	1.94	64.33

A comparison of the new $Y(\%)$ and α values with those reported in Table 4.1 shows

that $Y(\%)$ and α of both ovalbumin and P22 increase. Although this is desirable regarding Y_{oval} and α_{P22}, which should be as high as possible in order to maximize the purification of ovalbumin in the top phase and the concentration of P22 in the bottom phase, it is undesirable regarding Y_{P22} and α_{oval}, which should be as low as possible to minimize the presence of ovalbumin in the bottom phase and the presence of P22 in the top phase. Consequently, a "trade-off" is needed when selecting the optimal volume ratio, V_t/V_b, which will result in the desired Y_{oval} and α_{P22} values while yielding tolerable Y_{P22} and α_{oval} values.

4.4 Comparison with Other Separation Methods

Table 4.2 presents a comparison of two-phase aqueous (micellar or polymer) systems with other separation methodologies commonly used in biotechnology, including centrifugation, chromatography, and membrane filtration. This comparison is based on the general operation of these methodologies, particularly with respect to the following five aspects:

- Friendliness and mildness towards biological materials
- Ease of operation
- Capability to be scaled up
- Separation efficiency
- Speed

Note, however, that since the operations of these methodologies are based on different principles, the comparison of the advantages and disadvantages listed in Table 4.2 is not an absolute one under all conditions, but can still provide useful guidelines.

As shown in Table 4.2, each separation methodology has some advantages and disadvantages. Nevertheless, two-phase aqueous systems are superior to the other separation methodologies in several aspects summarized below:

Table 4.2: Comparison of various separation methodologies.

Methodology	Operation Principle	Advantages	Disadvantages
Centrifugation (with Density Gradient)	Density	• Fast • High separation efficiency with density gradient	• May disrupt native structures of biomolecules [75, 76] • Capability to be scaled up is limited
Chromatography - Gel Filtration - Ion Exchange - Affinity	Size, Electrostatic, Specific Interactions	• High separation efficiency	• May not be applicable to all types of biomolecules [75] • Not easily scaled up • Preparation procedures are tedious
Membrane Filtration	Size	• Easy to operate • May be scaled up • High selectivity in sizes	• May need to apply pressure, which is not favorable for certain biomolecules
Two-Phase Aqueous Systems	Size, Affinity	• Mild and gentle to biomolecules • Can be applied to all types of biomolecules • Easy to generate systems • Can be scaled up with relative ease • High separation efficiency • Fast	• Phase-forming materials may need to be removed after completion of biomolecule separation

1. Two-phase aqueous systems can provide a mild and friendly environment due to their higher water content, and no harsh operation is required when using these systems. These features make two-phase aqueous systems better than (1) centrifugation, which may have detrimental effects on virus particles, causing loss of structural integrity and biological functions [75, 76], and (2) membrane filtration, which involves applying pressure and is thus not favorable to certain biomolecules.

2. In utilizing two-phase aqueous systems, there is no limitation on the sizes or properties of the biomolecules. This is to be contrasted with ion exchange or affinity chromatography methodologies, which are not suitable for large assemblies, such as virus particles, due to the size-exclusion effect of the resins in the chromatographic columns [75].

3. Two-phase aqueous systems are relatively easy to generate and operate. In this respect, two-phase aqueous micellar systems are even easier to generate than their polymer counterpart, since surfactants are more easily dissolved in water than polymers (see discussions in Section 1.3). Hence, two-phase aqueous systems are more convenient as compared to (1) chromatography, which requires tedious procedures to prepare elution solutions and to pack the columns, and (2) centrifugation with density gradient, in which the density gradient has to be accurately built.

4. The ability of two-phase aqueous systems to be scaled up is a feature which cannot be surpassed by any of the other separation methodologies listed in Table 4.2. Two-phase aqueous systems are able to perform the separation operation in a large scale and hence enhance the operational efficiency.

5. As presented in Section 4.3.3, the separation or concentration efficiency of proteins and viruses using the two-phase aqueous $C_{10}E_4$ micellar systems is fairly high. The separation reported in Section 4.3.3 is based on the size-exclusion principle, but separation using these systems can also be accomplished by exploiting other types of interactions, such as the hydrophobic ones. Indeed, there is experimental evidence [1, 2, 3, 4, 6, 9] which indicates that desirable separation efficiencies can be obtained using two-phase aqueous micellar systems based on differences in the hydrophobicity of the partitioned entities.

6. Phase separation in two-phase aqueous systems can be completed fairly fast, with the final products obtained in hours, depending on the selection of the final volume ratio, V_t/V_b. Accordingly, in addition to the ease of operation, two-

phase aqueous systems can achieve separation faster than the other separation methodologies.

In view of the above, two-phase aqueous systems, particularly those of the micellar type considered in this thesis, display many advantages as compared to other separation methodologies and, hence, possess the potential to be developed and exploited in biotechnology. Possible directions for future work in this area are discussed in the next section.

4.5 Conclusions and Potential of Utilizing Two-Phase Aqueous Micellar Systems as a Practical Separation or Concentration Method

In view of the studies reported in this chapter, two-phase aqueous micellar systems are indeed potentially useful as a separation or concentration method in biotechnology. Some conclusions, as well as possible extensions of the work described above are discussed below:

- The results reported in Section 4.3.3 indicate that the separation efficiency can indeed be enhanced by solely manipulating the volume ratio of the two coexisting phases, V_t/V_b, and, in the case of the $C_{10}E_4$ aqueous micellar system, a more desirable separation efficiency can be achieved as the volume ratio is increased. Although the highest volume ratio obtained in the experiments reported in Section 4.3.3 was 14.5, it is still possible to achieve even higher volume ratios. It appears that the major problem in reaching higher volume ratios is the inaccuracy in determining the surfactant concentrations of the two coexisting phases, C_t and C_b, at a given temperature from the coexistence curve on the phase diagram. This problem can be overcome by a more careful measurement of the coexistence (cloud-point) curve of the $C_{10}E_4$ aqueous micellar system.

With more reliable C_t and C_b data at hand, the desired higher final volume ratios may be actually reached in the experiments. However, as described in Section 4.3.3, a "trade-off" is needed in selecting the optimal V_t/V_b value to ensure a minimal loss of the desired biomaterials.

- The single-step operation associated with the unequal-volume partitioning in two-phase aqueous micellar systems is indeed promising for the purposes of viral removal as well as concentration of viruses. In principle, it is possible to combine and repeat the single-step operation described in Section 4.3 to generate a multi-stage process capable of enhancing the efficiency of separation or concentration. However, one should keep in mind that, after each partitioning step, some of the materials will be lost in the other "undesired" phase, which is the bottom phase in the case of viral removal from proteins, and the top phase in the case of concentrating viruses. If the desired material is valuable, additional work may be required to retrieve the material "lost" in the "undesired" phase.

- In addition to the unequal-volume and multi-stage operations, two-phase aqueous micellar systems can further be developed into a continuous process, such as a counter-current operation, similar to what was done in the two-phase aqueous polymer systems [11, 12]. However, two-phase aqueous micellar systems are more sensitive to temperature changes as compared to their polymer counterpart. For example, in the $C_{10}E_4$ two-phase aqueous micellar system, a small temperature variation will induce a large change in the concentration in the top micelle-rich phase. Consequently, it may be necessary to maintain the whole process at a constant temperature condition in order to achieve good control over the performance of the process. An interesting alternative is to utilize surfactants whose two-phase aqueous micellar systems are less sensitive to temperature than the $C_{10}E_4$ system. An example of such surfactants is C_8-lecithin, since, as shown in its phase diagram (see Figures 1-4 and 2-4), the slope of the right branch of the coexistence (cloud-point) curve is steep as compared to that of $C_{10}E_4$, thus suggesting that the C_8-lecithin two-phase aqueous micellar

system is less sensitive to temperature variations than the $C_{10}E_4$ one.

- In addition to varying the volume ratio of the two coexisting phases, manipulation of other factors, including addition of salts, variation of solution pH, or addition of affinity ligands, may also induce changes in the partitioning behavior of biomolecules in two-phase aqueous micellar systems. In fact, variation of these factors can add more degrees of freedom and flexibility for achieving desired separation results. Details on this possibility will be discussed further in Section 6.2.1.

- As stressed in Section 2.3.1, the excluded-volume theoretical formulation indicates that, as the difference in the surfactant concentrations of the two coexisting micellar phases increases, that is, as the value of $|\phi_t - \phi_b|$ in Eqs. (2.12) and (2.14) increases, the partitioning behavior of biomolecules will become more uneven. In addition, as discussed in Section 2.3.1, a comparison between Eqs. (2.12) and (2.14) suggests that partitioning will be more uneven in two-phase aqueous micellar systems containing spherical rather than cylindrical micelles. These findings indicate that other surfactant systems, particularly those which may yield high $|\phi_t - \phi_b|$ values over a convenient temperature range (15 - 35°C), or which contain spherical micelles, should be exploited for partitioning of biomolecules in order to achieve more extreme partitioning as well as more favorable separation efficiencies.

In the next chapter, dynamic light scattering studies aimed at elucidating the underlying micellar solution structure of the $C_{10}E_4$ aqueous micellar system are presented.

Chapter 5

Dynamic Light Scattering Studies of the $C_{10}E_4$ Aqueous Micellar System

5.1 Motivation

In the studies on protein and virus partitioning in the two-phase aqueous $C_{10}E_4$ micellar system presented in Chapters 2 and 3, the underlying structure of the top (micelle-rich) phase was assumed to be semidilute (entangled), while that of the bottom (micelle-poor) phase was assumed to be dilute. This assumption was based on: (1) an analogy with the previously studied $C_{12}E_6$ aqueous micellar system [34], and (2) light scattering results which are presented in this chapter. Specifically, dynamic light scattering was utilized to investigate the underlying structure of the aqueous $C_{10}E_4$ micellar system, as well as the possibility of observing a transition of the solution structure from the dilute to the semidilute micellar solution regimes.

This chapter is organized as follows. Section 5.2 presents a brief overview of the basic principles of dynamic light scattering, the experimental principles, and the data-analysis technique used. Section 5.3 describes the experimental methods, including sample preparation, the light scattering equipment, and the experimental procedures.

Section 5.4 presents the experimental results and a discussion of these results. Finally, Section 5.5 presents some concluding remarks.

5.2 Basic Principles of Dynamic Light Scattering

Light scattering is a powerful experimental technique which can provide information regarding particle shape and size, solution structure, and inter-particle interactions in solutions. In this section, the principles of dynamic light scattering, including the theoretical background and the experimental principles, are briefly discussed. For a comprehensive discussion on dynamic light scattering, see References [68, 77].

5.2.1 Theoretical Background

Light is an electromagnetic wave consisting of electric and magnetic fields oscillating in directions perpendicular to that of the propagating wave. The electric field of the light wave can accelerate a charge in a periodically oscillating pattern, which, according to the classical electromagnetic theory, induces emmision of radiation and is the source of the scattered light [54].

In dynamic light scattering from a solution, the scattered light from a sample solution is measured as a function of time, and the correlation of the scattered light, which is associated with the solution properties and the interactions between the solute particles, is then calculated.

Usually, homodyne (or self-beat) dynamic light scattering experiments are conducted, yielding the time autocorrelation function of the scattered light. The autocorrelation function is defined as [68]

$$< I(0)I(\tau) >= \lim_{T\to 0} \frac{1}{T} \int_{t_0}^{t_0+T} I(t)I(t+\tau)dt \tag{5.1}$$

where $I(t)$ and $I(t+\tau)$ are the scattered light intensities measured at times t and $t+\tau$ respectively, and T is the total measuring time during which the scattering data are collected. Note that for a sufficiently large T, the integral in Eq. (5.1) is independent

of the starting time t_0.

Since the scattered light intensity is proportional to the square of the scattered electric field, E, that is, $I(t) \propto |E(t)|^2$ [68, 54, 78], and E can be assumed to be a random variable distributed according to a Gaussian distribution [68], it follows that the autocorrelation function is given by [68]

$$< I(0)I(\tau) >= B < I >^2 \left(1 + f(A)[g(\tau)]^2\right) \tag{5.2}$$

where B is a proportionality constant which is associated with the efficiency of the scattered light detector, $B < I >^2$ denotes the baseline of the autocorrelation function, $f(A)$ is a spatial coherence factor which depends on the number of coherence areas viewed, and $g(\tau)$ denotes the decay of the correlation function with time and is given by

$$g(\tau) = \frac{|I_1(\tau)|}{|I_1(0)|} \tag{5.3}$$

where $I_1(\tau)$, the first scattered-field autocorrelation function, is defined as

$$I_1(\tau) \equiv < E^*(0)E(\tau) > \tag{5.4}$$

where $E^*(0)$ denotes the complex conjugate of the scattered electric field $E(0)$.

$I_1(\tau)$ is related to the fluctuation of the solute concentration in the solution, $\delta c(\vec{\mathbf{q}}, \tau)$, that is, [68]

$$I_1(\tau) \propto < \delta c(\vec{\mathbf{q}}, \tau)\delta c(\vec{\mathbf{q}}, 0) > \tag{5.5}$$

Using Eqs. (5.4) and (5.5) in Eq. (5.3) yields

$$g(\tau) = \frac{< \delta c(\vec{\mathbf{q}}, \tau)\delta c(\vec{\mathbf{q}}, 0) >}{< |\delta c|^2 >} \tag{5.6}$$

In Eqs. (5.5) and (5.6), $\vec{\mathbf{q}}$ is the *scattering vector* and is defined as (see Figure 5-1)

$$\vec{\mathbf{q}} = \vec{\mathbf{k}}_i - \vec{\mathbf{k}}_f \tag{5.7}$$

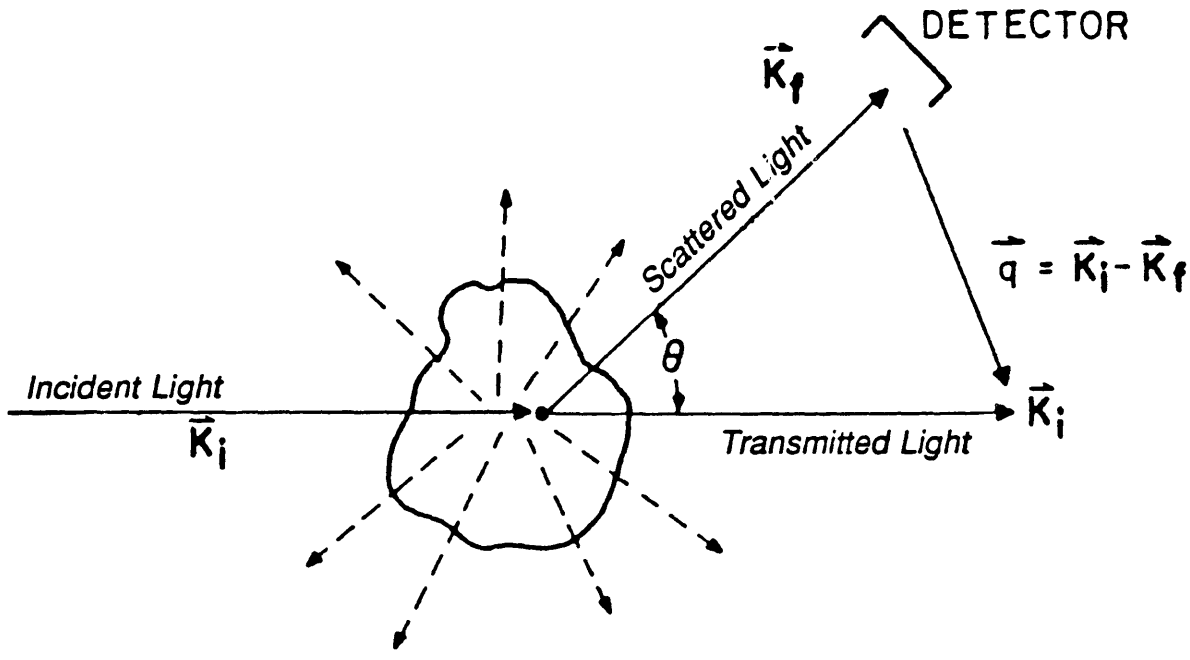

Figure 5-1: Illustration of the light scattered from a region in the sample in all directions. The incident and transmitted light have the same wave vector $\vec{k}_i$. Only the scattered light with the wave vector $\vec{k}_f$ can be detected by the detector. The scattering vector is defined as $\vec{q} = \vec{k}_i - \vec{k}_f$. The magnitude of $\vec{q}$ is obtained using geometry as $q = 2|\vec{k}_i| \sin\frac{\theta}{2} = \frac{4\pi n}{\lambda_0} \sin\frac{\theta}{2}$, where θ is the scattering angle between the two wave vectors $\vec{k}_i$ and $\vec{k}_f$ (from Reference [68]).

where $\vec{\mathbf{k}}_i$ is the wave vector in the direction of the incident and transmitted light beam, and $\vec{\mathbf{k}}_f$ is that denoting the position of the detector. Since, when the scattering is elastic,

$$|\vec{\mathbf{k}}_i| \approx |\vec{\mathbf{k}}_f| = \frac{2\pi n}{\lambda_0} \tag{5.8}$$

where n is the refractive index of the sample solution and λ_0 is the wavelength of light in vacuum, the magnitude of $\vec{\mathbf{q}}$ is given by

$$q = 2|\vec{\mathbf{k}}_i| \sin\frac{\theta}{2} = \frac{4\pi n}{\lambda_0} \sin\frac{\theta}{2} \tag{5.9}$$

where θ is the scattering angle between the two wave vectors $\vec{\mathbf{k}}_i$ and $\vec{\mathbf{k}}_f$ (see Figure 5-1). Hence, q reflects both the scattering angle, θ, and the wavelength of light, λ_0.

Assuming that the solute particles undergo Brownian motion in the solution, their motion should obey the diffusion equation (Fick's second law), and, consequently, the fluctuation of the solute concentration in the solution should obey the diffusion equation as well [68], that is,

$$\frac{\partial}{\partial\tau} < \delta c(\vec{\mathbf{q}},\tau)\delta c(\vec{\mathbf{q}},0) >= D\nabla^2 < \delta c(\vec{\mathbf{q}},\tau)\delta c(\vec{\mathbf{q}},0) > \tag{5.10}$$

where D is the self-diffusion coefficient of the solute particles. Integrating Eq. (5.10) yields

$$< \delta c(\vec{\mathbf{q}},\tau)\delta c(\vec{\mathbf{q}},0) >=< |\delta c|^2 > \exp(-\Gamma\tau) \tag{5.11}$$

A comparison between Eqs. (5.6) and (5.11) shows that

$$g(\tau) = \exp(-\Gamma\tau) \tag{5.12}$$

where Γ is the decay rate and is related to the self-diffusion coefficient, D, as

$$\Gamma = Dq^2 \tag{5.13}$$

When the solute particles are of uniform size, the diffusion coefficient of the so-

lute particles can be obtained from the particle size according to the Stokes-Einstein relation:

$$D = \frac{k_B T}{6\pi\eta\xi_h} \tag{5.14}$$

where k_B is the Boltzmann constant, T is the absolute temperature, η is the viscosity of the solvent, and ξ_h is the hydrodynamic length of the solute particles, which is equal to the hydrodynamic radius of the solute particles, R_h [68]. The size of the solute particles, as reflected in ξ_h, can therefore be obtained from the dynamic light scattering results (see Eq. (5.14)).

If the sizes of the solute particles are not uniform but, instead, exhibit a size distribution, which is the case for the micelles in the $C_{10}E_4$ aqueous micellar system, $g(\tau)$ should reflect the superposition of various decay rates of particles with different sizes. Specifically [77],

$$g(\tau) = \sum_i G(\Gamma_i)\exp(-\Gamma_i\tau) \tag{5.15}$$

$$\text{or} \quad g(\tau) = \int_0^\infty G(\Gamma)\exp(-\Gamma\tau)d\Gamma \tag{5.16}$$

where $G(\Gamma_i)$ is the distribution function and denotes the contribution of the decay rate Γ_i by the particles with size $\xi_{h,i}$. The distribution function, $G(\Gamma)$, needs to be calculated from $g(\tau)$ in order to derive the average decay rate Γ, as well as the average hydrodynamic length ξ_h (see the next section for details).

5.2.2 Experimental Principles and Data-Analysis Technique

In the actual light scattering measurements, the incident light has a single wavelength, and the scattered light intensity is measured as a photon-counting process by the photomultiplier detector (or photomultiplier tube). In the dynamic light scattering measurements, the scattered photons are collected during a very short time interval Δt (in the microsecond range) at a fixed angle. Let n_i denote the number of photons counted between the time $i\Delta t$ and $(i+1)\Delta t$, with n_i equivalent to the scattered light intensity measured at time $t = i\Delta t$, that is, $I(t) = I(i\Delta t)$. Let us also define the

correlation time by $\tau = a\Delta t$, and the total measuring time by $T = N_s\Delta t$, where N_s is the total number of samples (countings) taken. In this case,

$$I(t)I(t+\tau) = I(i\Delta t)I((i+a)\Delta t) = n_i\ n_{i+a} \tag{5.17}$$

and the time autocorrelation function is obtained from experiments as [68]

$$< I(0)I(\tau) > = \frac{1}{T}\sum_i n_i\ n_{i+a} \tag{5.18}$$

$$= \frac{1}{N_s\Delta t}\sum_i n_i\ n_{i+a} \tag{5.19}$$

In the case of polydisperse systems, in order to solve for the unknown $G(\Gamma)$ according to Eq. (5.16), a Laplace inversion is conducted on the experimentally obtained $g(\tau)$. There are several data-analysis techniques, with the most commonly used being the *cumulant expansion* [79]. In the cumulant expansion, the logarithm of $g(\tau)$ is expanded in terms of τ:

$$\ln|g(\tau)| = -\overline{\Gamma}\tau + \frac{1}{2!}\mu_2\tau^2 - \frac{1}{3!}\mu_3\tau^3 + \frac{1}{4!}(\mu_4 - 3\mu_2)\tau^4 - .... \tag{5.20}$$

where

$$\overline{\Gamma} = \int_0^\infty \Gamma G(\Gamma)d\Gamma \tag{5.21}$$

$$\mu_j = \int_0^\infty (\Gamma - \overline{\Gamma})^j G(\Gamma)d\Gamma \tag{5.22}$$

and

$$\ln|g(\tau)| = \sum_1^\infty K_m(\Gamma)(-\tau)^m/m! \tag{5.23}$$

where $K_m(\Gamma)$ is the mth cumulant, and $K_1 = \overline{\Gamma}$, $K_2 = \mu_2$, $K_3 = \mu_3$, ... Note that Eqs. (5.21) - (5.23) reveal that all the cumulants are calculated from the distribution function $G(\Gamma)$, and hence the Γ values derived from the cumulants represent certain types of averages of the true Γ's.

Generally speaking, the cumulant expansion is valid for small τ values and a sufficiently narrow distribution function $G(\Gamma)$ [79]. This analysis technique is fast and relatively simple to implement, and its results are often used as a starting point for a more detailed data analysis. For details of other data-analysis techniques, including the double-exponential distribution and the method of regularization (usually known as CONTIN), see Reference [79].

The solution of $G(\Gamma)$ derived from a certain $g(\tau)$, however, is usually not unique due to the noise in the experimental data, which results from the measuring error and the round-off error in the photon-counting process. In addition, $g(\tau)$ is strongly dependent on the time increment Δt. Hence, obtaining $G(\Gamma)$ from $g(\tau)$ is an ill-posed problem, and a small error in the measurement of the autocorrelation function may result in a large error in $G(\Gamma)$. Typically, it is recommended to increase the total number of samples, N_s, and the incident light intensity in order to decrease the noise level when measuring the autocorrelation function [79].

5.3 Experimental Approach

A micellar system composed of $C_{10}E_4$ and pure water was examined. The reason for using pure water, instead of the McIlvaine buffer solution (as in Chapters 2 and 3), to generate the micellar system is to eliminate possible effects of the buffering salts on the properties of the micellar system [80]. The critical temperature T_c of the $C_{10}E_4$-water system is about 19.8°C, which is 1°C higher than that of the $C_{10}E_4$-buffer system (see Figure 2-3), with a corresponding critical concentration of about 2.5 wt%, which is approximately the same as that of the $C_{10}E_4$-buffer system. The scattering experiments were therefore conducted at temperatures lower than 19.8°C, a range over which aqueous $C_{10}E_4$ micellar solutions exhibit a clear and uniform phase.

5.3.1 Equipment

The light scattering instrument consists of the BI-200SM goniometer system (Brookhaven Instrument Company, NY) and a laser beam source (Lexel Model 95 Argon Ion Laser

with a maximal power of 2 Watts). The goniometer includes a photomultiplier tube which can be moved circularly around the sample holder to reach any specified angle for measuring the scattered light intensity. The goniometer system is also equipped with a BI-9000AT Digital Correlator for dynamic light scattering data analysis. An unpolarized laser beam with a wavelength of 514.5 nm was used as the light source. Decalin (decahydronaphthalene, *cis* and *trans*) was used as the index-matching fluid to match the refractive index of the glass sample cell. The sample temperature was controlled using a water bath connected to the brass tubes surrounding the sample holder. Note that the actual temperature of the sample may be different from that displayed on the water bath and, therefore, its precise value needs to be measured separately.

5.3.2 Experimental Procedures

5.3.2.1 Sample Preparation

Samples for the light scattering measurements were prepared with the surfactant $C_{10}E_4$ (lot no. 1006, as described in Section 2.2.1.1) and water which was fed through a Milli-Q water purification system. The resulting solutions were vortexed to achieve thorough mixing. Dust in the solutions was removed by filtration for at least six times using Millex-GS Filters (Millipore, Bedford, MA) with a pore size of 0.22μm. Note that centrifugation was not utilized to remove dust since the $C_{10}E_4$ solutions phase separate at room temperature, and centrifugation is usually conducted at room temperature and may therefore result in phase separation of the $C_{10}E_4$ micellar solutions.

5.3.2.2 Light Scattering Measurement

Light scattering measurements were conducted at 7.0, 10.0, 13.0, 16.0, and 18.0°C, as displayed on the water bath. Scattering measurements could not be conducted at even lower temperatures because the index-matching fluid (decalin) was found to become turbid as the temperature was further reduced, thus hindering the measurement of light scattering from the sample solution. A possible reason for the observed turbidity

of decalin may be the condensation and nucleation of absorbed water vapor in decalin as the temperature is reduced towards 0°C. Note that since the melting point of decalin is about -40°C, the observed turbidity in decalin at temperatures lower than 7.0°C should not result from the crystallization of decalin.

The experimental procedures for conducting the dynamic light scattering experiments on a given sample solution are described below:

1. The water bath was set at a desired experimental temperature.

2. Before being inserted into the sample holder, the outer surface of the sample cell was rinsed with acetone. After inserting the sample into the sample holder, decalin was filtered for at least 30 minutes in order to remove dust. Filtration of decalin was performed intermittently, that is, decalin was filtered for 10 minutes, followed by turning off the decalin filtration pump for 5 minutes in order to cool down the sample by the circulation of cold water from the water bath. This procedure was adopted in order to prevent phase separation in the sample which may be induced by introducing warm decalin during the filtration step. This procedure was repeated until the total filtration time exceeded 30 minutes.

3. After completing decalin filtration, the sample and decalin were maintained at this temperature condition for at least 30 minutes prior to the light scattering measurement in order to ensure that the sample had reached thermal equilibrium.

4. Prior to conducting the actual light scattering measurements at the scattering angle θ=90°, a "control" measurement was conducted at a lower angle (θ = 30° or 45°) in order to detect the possible existence of dust either in the sample solution or in decalin. This exploited the fact that the correlation function of the scattered light at lower angles is very sensitive to the presence of large particles such as dust. If the presence of dust was detected, which was typically indicated by the large difference between the measured and calculated baselines provided by the Digital Correlator, the dust was then visually located by observing the

strong scattering due to the dust in either the sample solution or decalin. In this case, filtration of the sample solution, as described in Section 5.3.2.1 (or decalin, as described in step 2 above) was repeated if the dust was found in the sample solution (or in decalin), followed by an additional attempt to detect the presence of dust using dynamic light scattering at $\theta = 30°$ or $45°$.

5. The actual dynamic light scattering measurements were conducted at $\theta = 90°$. For each sample at each temperature of interest, at least six measurements were performed during the same sample time. The resulting autocorrelation functions were subsequently analyzed using the cumulant expansion (discussed in Section 5.2.2), which was built in as a program in the BI-9000AT Digital Correlator.

6. After completing a dynamic light scattering measurement at a given temperature, the temperature of the water bath was adjusted to a new value, and the sample and decalin were maintained at this temperature condition for at least 30 minutes to ensure thermal equilibration of the sample before conducting the measurement, as stated in step 5.

The actual temperature of the sample corresponding to that displayed on the water bath was measured using a thermometer probe (Omega Thermistor Thermometer). This measured temperature was then used in all subsequent data analyses, including the calculation of the solvent viscosity (see Table 5.1 and Section 5.3.3).

5.3.3 Analysis of the Experimental Results

As mentioned in the previous section, at each $C_{10}E_4$ concentration and temperature examined, the measured autocorrelation function was analyzed using a cumulant expansion. The third cumulant was used in further calculations, since it usually yields the lowest root-mean square error, as compared to the other cumulants.

Since all the measurements were conducted at $\theta = 90°$, the magnitude of the scattering vector, q, defined in Eq. (5.9), was essentially constant under the reasonable

Table 5.1: Water viscosity at various temperatures examined in the light scattering measurements. The viscosity values were calculated by interpolating the water viscosity versus temperature data given in Reference [81] to the actual sample temperature (see the second column).

Temperature Display on Water Bath (°C)	Actual Temperature of the Sample (°C)	Water Viscosity (cp)
18	18.1	1.048
16	16.3	1.101
13	13.4	1.193
10	10.6	1.287
7	7.7	1.419

assumption that, at the relatively dilute $C_{10}E_4$ concentrations and the narrow temperature range examined, the refractive index of the solutions, n, was about the same as that of pure water and remained approximately constant with temperature. At each $C_{10}E_4$ concentration and temperature examined, the average value of the decay rate, Γ, was obtained from the third cumulant, as in Eq. (5.22), and subsequently used in Eq. (5.13) to calculate the diffusion coefficient, D. Note that the solvent (water) viscosity, η, at each temperature examined was obtained by interpolating the water viscosity versus temperature data [81] to the temperature examined (see Table 5.1).

It is useful to introduce a "scaled diffusion coefficient," D^*, as follows [33]:

$$D^* \equiv \frac{D\eta_T}{\eta_{20°C}} \tag{5.24}$$

where η_T and $\eta_{20°C}$ are the water viscosity at temperatures T and 20°C respectively, with $\eta_{20°C}$=1.002 cp [81]. Note that the scaled diffusion coefficient, D^*, is the diffusion coefficient (see Eq. (5.14)) corrected for the change of solvent viscosity with temperature with respect to a standard condition (20°C in this case) [33]. As discussed in the next section, a plot of log D^* versus log X ($C_{10}E_4$ concentration) can provide information on the solution structure at various surfactant concentrations [33].

5.4 Results and Discussion

Figure 5-2 shows a log-log plot of the measured scaled diffusion coefficient, D^*, versus $C_{10}E_4$ concentration (in molar) at various temperatures: 7.7°C (○), 10.6°C (△), 13.4°C (□), 16.3°C (●), and 18.1°C (▲). Figure 5-2 reveals that, at each temperature examined, there is a minimum value of D^*, with the minimum becoming more pronounced as the temperature increases. It is possible to relate the occurrence of such a minimum to a transition of the underlying micellar solution structure from the dilute to the semidilute (entangled) regimes. In this picture, the surfactant concentration at which D^* attains its minimum value corresponds to the "crossover surfactant concentration," X^*, which denotes the onset of the structural transition, as discussed in Sections 1.2.2 and 1.3. This follows from the fact that D^* is inversely proportional to the average hydrodynamic length of the micelles, ξ_h (see Eq. (5.14)). More specifically, when the surfactant concentration, X, is lower than X^*, the measured hydrodynamic length ξ_h denotes the average size of *individual* micelles, with the average micellar size ξ_h increasing with surfactant concentration. In other words, for $X < X^*$, D^* decreases with increasing X (recall that $D^* \sim \frac{1}{\xi_h}$). On the other hand, when the surfactant concentration is higher than X^*, micelles in the solution entangle with each other and form a transient mesh or net, which becomes denser as the surfactant concentration increases, and, therefore, the measured ξ_h actually represents the mesh size of the micellar net, which decreases with increasing surfactant concentration (see Figure 1-5). In other words, for $X > X^*$, D^* increases with increasing X. Clearly, the behavior of D^* versus X for $X < X^*$ and $X > X^*$ indicates the existence of a minimum D^* value.

To obtain the exact minimum of D^* at each temperature examined from the experimental results shown in Figure 5-2, each set of D^* data was fitted using a linear regression to the 6th order, and the minimum of D^*, as well as the corresponding $C_{10}E_4$ concentration, were calculated accordingly. The results of the linear regression analysis are depicted by various lines in Figure 5-2, and the corresponding minimum on each line is marked by an asterisk ($*$). In view of the discussion above, the

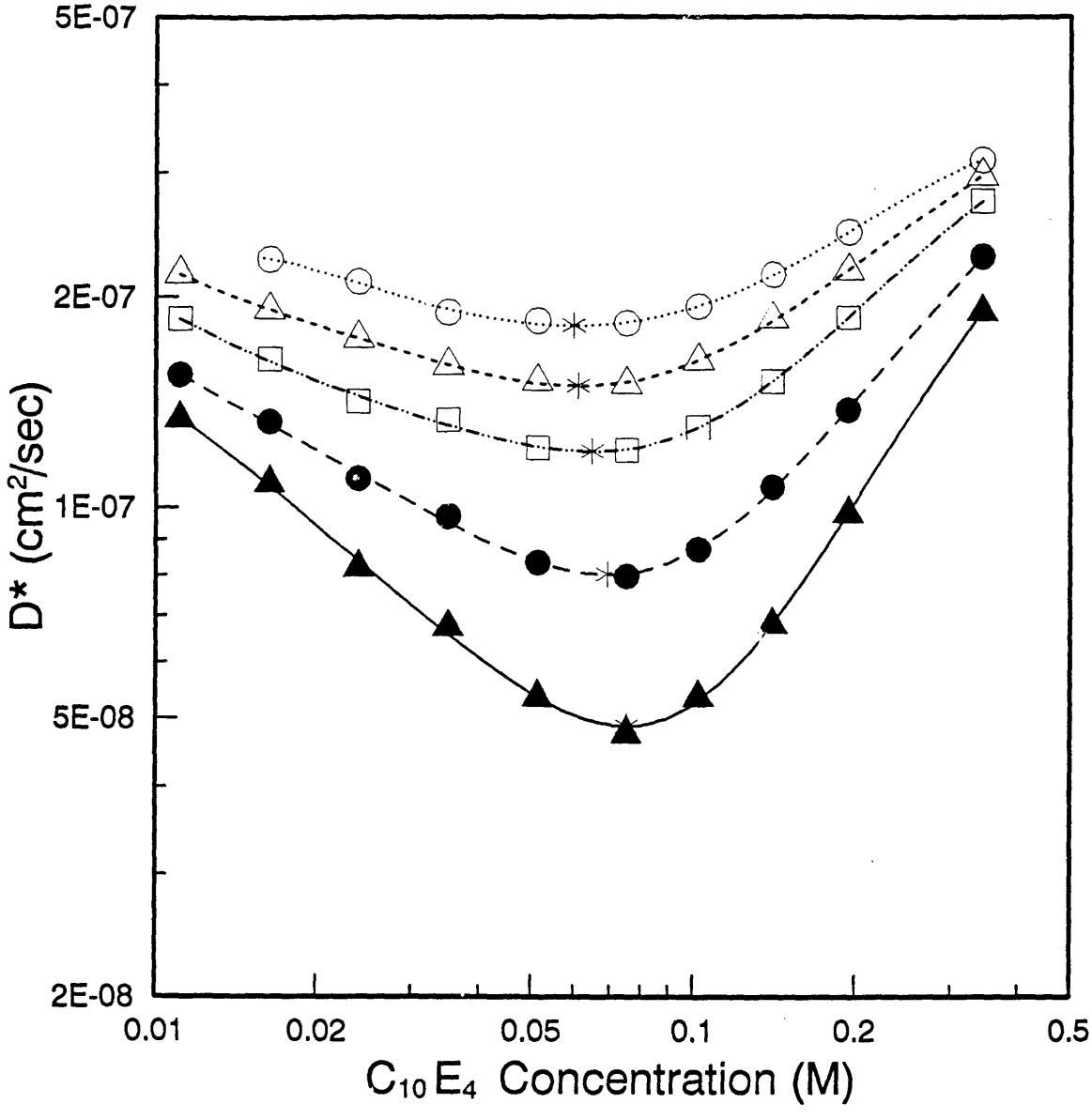

Figure 5-2: Log-log plot of the experimentally measured scaled diffusion coefficient, D^*, versus $C_{10}E_4$ concentration (in molar) at various temperatures: 7.7°C (○), 10.6°C (△), 13.4°C (□), 16.3°C (●), and 18.1°C (▲). The lines are the results of a linear regression on the data points of 7.7°C (· · ·), 10.6°C (- - -), 13.4°C (— · · —), 16.3°C (— — —), and 18.1°C (—), respectively. The asterisk on each line denotes the minimum D^* value at that temperature, as calculated from the linear regression.

surfactant concentration corresponding to an asterisk can be viewed as the crossover surfactant concentration, X^*, at each specific temperature.

One can also rationalize the observed variation of D^* *with temperature* shown in Figure 5-2 as follows: When the surfactant concentration is lower than X^*, that is, on the left-hand side of Figure 5-2, the observed decrease of D^* with increasing temperature reflects the fact that the average $C_{10}E_4$ micellar size increases (micellar growth, see Section 1.2.2) with increasing temperature. When the surfactant concentration is higher than X^*, that is, on the right-hand side of Figure 5-2, the trend that D^* decreases with increasing temperature is also observed, denoting the fact that the micellar mesh size also increases with increasing temperature. Nevertheless, as the surfactant concentration increases further, the observed D^* values at all the temperatures examined seem to converge, indicating that, at high surfactant concentrations, the mesh size becomes independent of temperature. This has indeed been observed in other micellar systems in which the micelles also exhibit significant growth into long, rod-like micelles [33, 82]. In addition, at high surfactant concentrations, the variation of D^* versus surfactant concentration was found to obey a simple scaling law by exploiting an analogy with polymer solutions [83]. This scaling law relates the mesh size, ξ_m, to the surfactant concentration, X, as follows:

$$\xi_m \sim X^{-0.77} \tag{5.25}$$

$$D \propto \frac{1}{\xi_m} \sim X^{0.77} \tag{5.26}$$

Equation (5.26) implies that, at high surfactant concentrations, the structure of these micellar systems resembles that of a flexible polymer net. Extrapolation of the experimental data shown in Figure 5-2 to higher $C_{10}E_4$ concentrations indicates that the variation of D^* with X ranges from $D^* \sim X^{0.42}$ at 7.7°C to $D^* \sim X^{1.15}$ at 18.1°C. Hence, it is possible that the D^* values at each of the temperatures examined will indeed converge to $D^* \sim X^{0.77}$ as X is increased further.

It is also interesting to plot the X^* values obtained from the linear regression at the various temperatures examined on the temperature versus $C_{10}E_4$ concentration

phase diagram. Figure 5-3 shows the X^* values obtained from the linear regression as asterisks ($*$), together with the coexistence (cloud-point) curve (the solid curve), and the critical point (the black dot). Figure 5-3 indicates that the extension of these X^* values to higher temperatures appears to approach the critical point, thus bisecting the one-phase region of the phase diagram into the dilute regime (on the left-hand side of the asterisks) and the semidilute (entangled) regime (on the right-hand side of the asterisks). This suggests that the two coexisting micellar phases of the two-phase aqueous $C_{10}E_4$ micellar system indeed possess different solution structure, with the top (micelle-rich) phase containing a transient micellar mesh or net, and the bottom (micelle-poor) phase containing individually dispersed micelles. This finding leads support to the conjecture made in Section 1.2.2 about the underlying structure of the top and bottom phases in the two-phase aqueous $C_{10}E_4$ micellar system, which was also based on the analogy to the $C_{12}E_5$ aqueous micellar system [34].

It is noteworthy that the variation of the crossover concentration, X^*, with temperature can actually be calculated using a recently-developed molecular-thermodynamic approach [27, 55], if the Kuhn length of the micelles (a measure of micellar flexibility) [32] is known. The crossover concentrations of the $C_{10}E_4$ aqueous micellar system corresponding to Kuhn lengths of l=100Å and 150Å in the temperature range 5 - 19.5°C were calculated [27, 55] and are also shown in Figure 5-3 as dashed and dotted lines respectively. As can be seen, the X^* values obtained from the linear regression (the asterisks in Figure 5-3) are found to be located between the two theoretically calculated lines, indicating that the actual Kuhn length of $C_{10}E_4$ micelles in this temperature range is indeed between 100 - 150Å. Note that the Kuhn length is actually a function of temperature and is expected to decrease with increasing temperature in the $C_{10}E_4$ micellar system, similar to what is found in the $C_{12}E_6$ aqueous micellar system [35]. This also implies that 100 - 150Å is a reasonable estimation of the Kuhn length of the $C_{10}E_4$ micelles in this temperature range. Recall that this range of Kuhn length values was also used for calculating the excluded volume between virus particles and flexible micelles (see Section 3.4.3).

The results of the dynamic light scattering studies presented in this chapter are

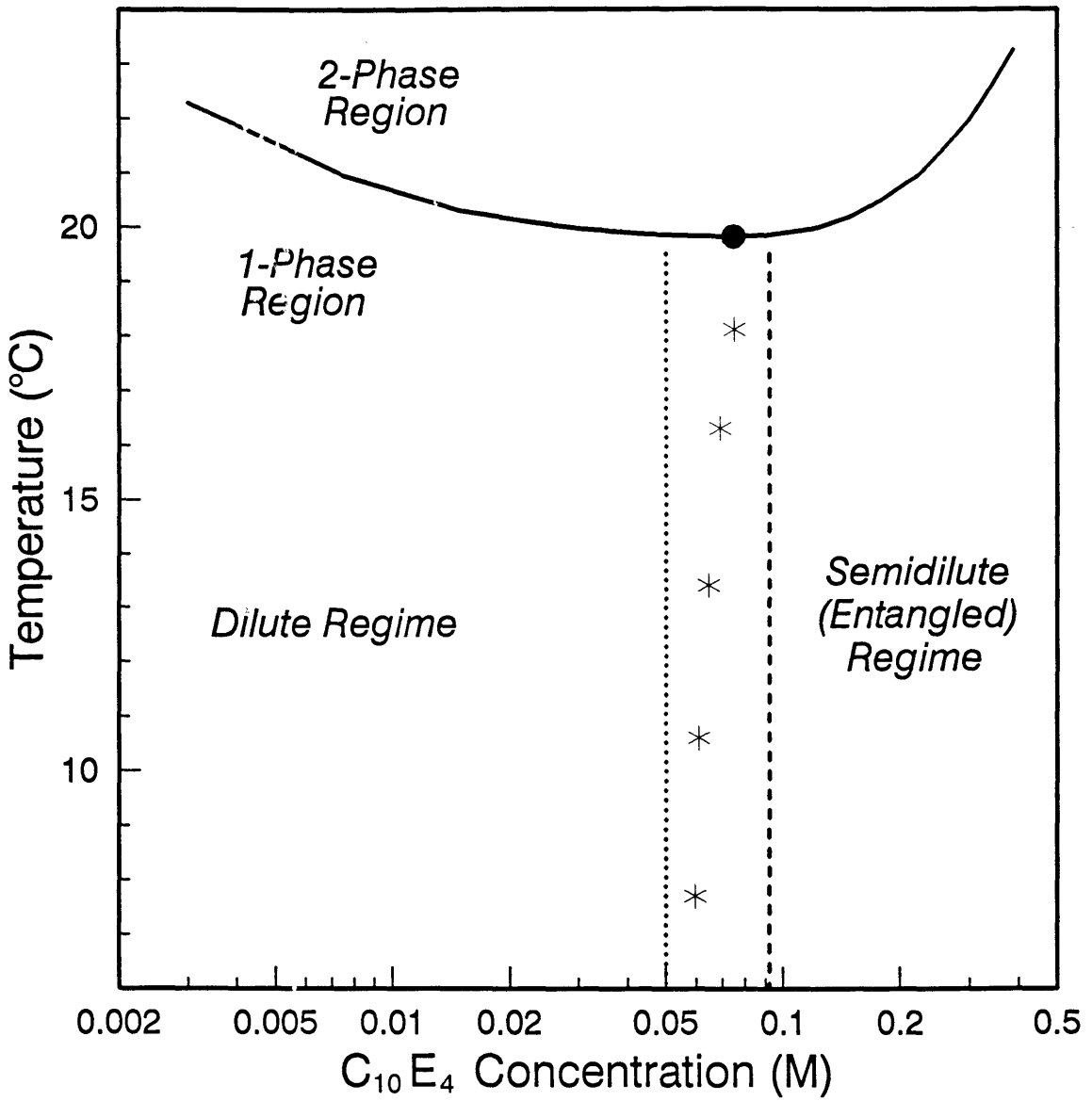

Figure 5-3: The location of the crossover concentration, X^* $(*)$, on the temperature versus concentration phase diagram of the $C_{10}E_4$ aqueous micellar system. The solid curve is the coexistence (cloud-point) curve which separates the phase diagram into the one-phase and two-phase regions, and the black dot on the curve denotes the critical point. The dashed and dotted lines are theoretically predicted crossover concentrations at Kuhn length of 100Å $(- - -)$ and 150Å $(\cdots)$ respectively. The left-hand side corresponds to the dilute regime, in which $C_{10}E_4$ micelles are individually dispersed in the solution, while the right-hand side corresponds to the semidilute (entangled) regime, in which a transient micellar mesh or net forms.

consistent with the occurrence of the crossover phenomenon in the $C_{10}E_4$ micellar system. In order to obtain a more complete picture of the micellar solution structure, including the average molecular weight and the Kuhn length of micelles, other experimental methods, such as static light scattering, should be conducted. However, it is well-known that the results of light scattering experiments can be strongly affected by intermicellar interactions and critical fluctuations [84, 85]. Consequently, extreme caution should be exercised when interpreting the light scattering results. In addition, other experimental methods which are not as sensitive to these complicating factors, such as viscosity measurements, should also be considered for investigating the micellar solution structure in order to obtain a more accurate description of the $C_{10}E_4$ micellar system. It is also noteworthy that, unlike a conventional phase transition, the transition of the solution structure from the dilute to the semidilute regimes is not a sharp one. Accordingly, the crossover concentrations deduced using different experimental techniques may be somewhat different.

5.5 Conclusions

This chapter described dynamic light scattering measurements aimed at elucidating the underlying structure of the $C_{10}E_4$ aqueous micellar system. The following conclusions follow:

- Useful information about the transition in the micellar solution structure from the dilute to the semidilute regimes can be obtained from the dynamic light scattering measurements. The crossover surfactant concentrations of the $C_{10}E_4$ micellar system, X^*, which were obtained from the linear regression of the experimental data at various temperatures, appear to bisect the one-phase region of the temperature versus $C_{10}E_4$ concentration phase diagram into a dilute regime, consisting of individually dispersed $C_{10}E_4$ micelles, and a semidilute (entangled) regime, consisting of a transient mesh or net of interpenetrating $C_{10}E_4$ micelles, as shown in Figure 5-3. This finding suggests that the solution structure of the two coexisting $C_{10}E_4$ micellar phases is indeed very different, with the top

(micelle-rich) phase containing a micellar net and the bottom (micelle-poor) phase containing individually dispersed micelles.

- A comparison between the experimentally obtained X^* values and those calculated according to the molecular-thermodynamic approach indicates a reasonable agreement, thus suggesting that the Kuhn length of $C_{10}E_4$ micelles, which is a measure of the flexibility of these micelles, is in the range of 100 - 150Å over the temperature range 5 - 20°C.

- Other experimental techniques, such as static light scattering and viscosity measurements, should be utilized in order to obtain a more complete and accurate picture of the micellar solution structure in the $C_{10}E_4$ aqueous micellar system.

In the next chapter, a summary of the results obtained in this thesis is presented, and possible extensions of the work presented in this thesis are also discussed.

Chapter 6

Summary and Possible Extensions of the Work Presented in This Thesis

6.1 Summary of the Central Results

The work presented in this thesis constitutes the first systematic experimental, theoretical, and practical study on the partitioning of biomolecules (hydrophilic proteins and viruses) in two phase aqueous micellar systems. The central results of this thesis are briefly summarized below:

- The partitioning behavior of several hydrophilic proteins in two-phase aqueous micellar systems, composed of the nonionic surfactant $C_{10}E_4$ or the zwitterionic surfactant C_8-lecithin, was investigated experimentally and theoretically, as described in Chapter 2. The partition coefficients of proteins, K_p, which is the ratio of the protein concentrations in the two coexisting micellar phases and constitutes a quantitative measure of the partitioning behavior, were found to be of order 1. The proteins were found to partition preferentially into the micelle-poor phase of the two-phase aqueous micellar systems. In addition, it was also found that the observed partitioning behavior becomes more extreme as (1) the

size of the biomolecules increases, or (2) the difference in the micellar concentrations of the two coexisting micellar phases becomes more pronounced. These findings strongly suggest that the interactions between the biomolecules and the non-charged micelles are primarily of the excluded-volume type. Accordingly, a theoretical formulation based on excluded-volume interactions between biomolecules and micelles was developed to describe the partitioning behavior of proteins in two-phase aqueous micellar systems. The theoretically predicted partitioning behavior was found to be in reasonable agreement with the experimental partitioning results. The theoretical formulation also provided useful information on how to achieve more extreme partitioning as well as optimize the partitioning operation.

- The partitioning behavior of virus particles in the two-phase aqueous $C_{10}E_4$ micellar system was subsequently investigated, as presented in Chapter 3, and the partition coefficients, K_v, were found to be of order 10^{-3}, indicating the much more extreme partitioning behavior of virus particles as compared to that of proteins. The theoretical formulation presented in Chapter 2, which is based on an excluded-volume picture of rigid micelles interacting with relatively small protein molecules, was generalized to incorporate the effect of micellar flexibility, which should play a more important role in the partitioning of the larger virus particles. However, the new theoretical formulation was found to over-predict the partitioning behavior of the larger virus particles examined when compared with the experimental results.

- As described in Section 3.5, an attempt was made to rationalize the observed deviation between the theoretically predicted virus partition coefficients, which should represent a true thermodynamic equilibrium condition, and the experimentally measured virus partition coefficients in terms of kinetic effects associated with the partitioning phenomenon. Specifically, the experimentally observed virus partitioning behavior may actually be complicated by kinetic effects, including the slow diffusion of virus particles and the convection of

the phase components. Accordingly, the experimentally observed partitioning behavior of large particles, such as viruses, may not represent a true thermodynamic equilibrium condition.

- Two-phase aqueous micellar systems may be utilized as a useful and practical separation or concentration method, and this possibility was investigated by simultaneously partitioning a protein (ovalbumin) and a virus (P22) in the two-phase aqueous $C_{10}E_4$ micellar system, as reported in Chapter 4. It was found that, by manipulating the volume ratio of the two coexisting micellar phases, the desired separation or concentration efficiency of these two biomolecules may be achieved.

- Dynamic light scattering studies were conducted to investigate the underlying solution structure of the $C_{10}E_4$ aqueous micellar system, as reported in Chapter 5. Using these measurements, it was possible to quantitatively deduce the crossover surfactant concentrations, X^*, denoting the transition of the micellar solution structure from the dilute to the semidilute (entangled) regimes, at various temperatures, T. An examination of the resulting X^* versus T data along with the coexistence (cloud-point) curve in the T versus $C_{10}E_4$ concentration phase diagram indicates that the solution structure of the two coexisting micellar phases in the $C_{10}E_4$ two-phase aqueous micellar system is different, with the bottom (micelle-poor) phase containing individually dispersed micelles, and the top (micelle-rich) phase containing a transient micellar mesh or net. This difference in the micellar solution structure may play a role in determining the observed partitioning behavior of biomolecules in such two-phase aqueous micellar systems.

6.2 Possible Extensions of the Work Presented in this Thesis

6.2.1 Partitioning at Different Conditions or in Different Two-Phase Aqueous Systems

1. Using other surfactants to generate the two-phase aqueous micellar systems

   In this thesis, only two surfactants — $C_{10}E_4$ and C_8-lecithin — were used to generate the two-phase systems. The possibility of using other surfactants to generate the two-phase aqueous systems should be investigated. As discussed in Section 4.5, a desirable surfactant should meet one or more of the following criteria:

   - It should generate two-phase aqueous micellar systems over a temperature range which is convenient and not detrimental to biomolecules, say, 15 - 35°C.
   - It should display a broad coexistence (cloud-point) curve, thus yielding a large difference in the surfactant concentrations of the two coexisting micellar phases. That is, it should display high $(\phi_t - \phi_b)$ values (see Eqs. (2.12) and (2.14)).
   - It should form spheroidal micelles, since the partitioning of biomolecules in such micellar systems is predicted to be more extreme (see Eq. (2.14)).
   - It should be commercially available and of relative low cost.

2. Investigating salt effects on the partitioning behavior

   The salt type and its concentration can have a direct influence on phase separation equilibrium of two-phase aqueous micellar systems [80], and, hence, can affect the partitioning behavior of biomolecules in these systems. In addition, the salt itself can partition between the two coexisting phases, thus generating an electric potential difference between the two phases. This has been observed

in two-phase aqueous polymer systems [13, 19]. Consequently, salt effects on the partitioning behavior may be pronounced, and may be utilized to effectively tune and optimize the partitioning of biomolecules in these systems.

3. Partitioning of biomolecules at solution pH's different from 7

   The net charge on a biomolecule (for example, a protein molecule) varies with the solution pH. Accordingly, the partitioning behavior of biomolecules can be manipulated by changing the solution pH. Indeed, partitioning of proteins at different solution pH's in two-phase aqueous polymer systems has been investigated [86, 87]. Similar partitioning studies should be conducted in two-phase aqueous micellar systems. However, one should keep in mind that there will be concomitant salt effects, since the solution pH is mainly manipulated by changing salt type and its concentration in the solution.

4. Utilizing mixed micelles to generate two-phase aqueous micellar systems

   Mixed-micellar systems represent an interesting extension of the non-charged micellar systems examined in this thesis. Indeed, incorporating different types of surfactants may induce different interaction patterns between the partitioned solutes and the mixed micelles. Hence, the selectivity of the two-phase systems may be improved. As discussed in Section 1.3, surfactant-type affinity ligands, which have specific binding affinity to certain biomolecules, can be used to form mixed micelles to enhance the separation or concentration efficiency of certain biomolecules. In addition, mixed micelles composed of charged (ionic or zwitterionic) and non-charged surfactants are expected to interact differently with biomolecules bearing different net charges, thus leading to different partitioning behavior of these biomolecules in two-phase aqueous mixed-micellar systems. An interesting possibility is to vary the solution pH in mixed-micellar systems. In so doing, the net charges on biomolecules may be varied, and the partitioning behavior may thus be further tuned. The latter method, which uses charged surfactants as part of the mixed micelles, may be more convenient than using affinity ligands, since it avoids the need to remove the ligands from the desired

biomolecules after partitioning is completed.

5. Using a mixture of micelles and polymers to generate two-phase aqueous systems

   Partitioning of biomolecules has been studied in both two-phase aqueous polymer and two-phase aqueous micellar systems. It will be interesting to investigate partitioning in two-phase systems composed of both micelles and polymers, since it is expected that a combination of micelles and polymers will add more degrees of freedom for manipulating the performance of the systems. Systems of this type include those composed of a surfactant and a polymer, or those composed of a polymer and a block copolymer which can form micellar structures in an aqueous environment [88]. In addition, electrostatic interactions can be exploited by utilizing ionic surfactants or polyelectrolytes to generate the two-phase systems.

6.2.2 Partitioning of Other Solute Species

In this thesis, only biomolecules — hydrophilic proteins and viruses — were considered as the partitioning solutes. The partitioning of other materials, not necessarily of biological origin, should also be attempted. This can not only expand the practical utilization of two-phase aqueous micellar systems as a useful separation or concentration method, but it can also aid in gaining a better understanding of some of the fundamental mechanisms responsible for the observed partitioning behavior. A few ideas on this issue are presented below:

1. Partitioning of other biological molecules or particles

   The partitioning behavior of other biological molecules or particles, such as DNA molecules, plasmids, cells, and cell organelles, in two-phase aqueous micellar systems should be investigated to expand the practical utilization of two-phase aqueous micellar systems.

2. Partitioning of colloidal particles with different sizes

The aims here are: (1) to further investigate the size effect of the partitioning solutes on the observed partitioning behavior when excluded-volume interactions between micelles and solute particles are the dominant factor, and (2) to provide information on kinetic effects associated with the partitioning phenomenon (see Section 6.2.5). The advantage of using colloidal particles, instead of the biological materials examined so far, is that one can control the surface properties and size of the colloidal particles in a systematic way. Particles with uniform surface properties and well-controlled sizes, such as colloidal gold particles, may be used for partitioning. Possibly, from a study of this type, the influence of particle size, micellar flexibility, micellar shape and size, and kinetic effects on the partitioning behavior may be elucidated more simply than in the biomolecule cases.

3. Partitioning of biomolecules with minor differences in their chemical structures

Minor differences in the chemical structures of biomolecules, for example, a difference in a single amino acid residue on protein molecules, or different lengths of hydrocarbon chains which are attached to protein molecules, may induce changes in the micelle-biomolecule interactions and hence in the resulting partitioning behavior. A study of this type may elucidate various types of micelle-biomolecule interactions in addition to those of the excluded-volume type. In other words, it may be possible to use *macroscopic* partitioning results in two-phase aqueous micellar systems to learn different *microscopic* interactions between biomolecules and micelles, which could be very valuable from a biochemical perspective.

4. Partitioning of materials with different hydrophobicity

As discussed in Section 1.3, in view of the dual nature of micelles (containing both hydrophilic and hydrophobic domains), separation of materials with different hydrophobicity using two-phase aqueous micellar systems is expected to be efficient and promising, and many studies have been conducted for investigating

the partitioning behavior of hydrophobic biomolecules in two-phase aqueous micellar systems [1, 2, 3, 4, 5, 6, 8, 9]. However, very few *systematic experimental studies* have been conducted on these systems, and no *fundamental theoretical work* has been done to describe the *partitioning behavior of hydrophobic solutes* in these systems. Consequently, it appears interesting to carry out more experimental and theoretical work on partitioning of materials with different hydrophobicity in order to improve the efficiency of two-phase aqueous micellar systems as a practical method for separation or extraction of hydrophobic materials.

5. Partitioning in Practically Relevant Systems

   The partitioning studies presented in this thesis have been restricted to "clean" systems, that is, systems composed of only one or two partitioning solutes. On the other hand, in most situations of practical importance, separation or concentration is usually conducted on "dirty" solutions containing many components or solutes, such as fermentation broths, blood serum, and sewage water. Accordingly, the application of two-phase aqueous micellar systems to these real and "dirty" solutions to achieve desired separation or concentration results should be investigated.

6.2.3 Developing Theoretical Formulations

Based on the derivation presented in Appendix A, the partition coefficient, K, was expressed in terms of the interactions between the partitioning solute and micelles and, hence, was expressed in terms of a virial series (see Eq. (A.27)). In the case considered in Appendix A, only the second virial coefficient, B_2, reflecting two-body interactions, was included in Eq. (A.27). In addition, only excluded-volume interactions between biomolecules and micelles were accounted for, since this was found to be the dominant factor controlling the observed partitioning behavior. However, other types of interactions may also be accounted for in the second virial coefficient, B_2, in order to describe the partitioning behavior of other solutes, if these solutes

are found to interact with micelles through different types of interactions, for example, the interactions between micelles and hydrophobic materials, or those between charged micelles and biomolecules. In addition, the effect of many-body interactions, as captured by B_3, B_4, ... (the third, fourth, ... virial coefficients) can also be included in the theoretical formulation of K.

6.2.4 Investigation of Micellar Solution Structure

In this thesis, dynamic light scattering measurements were conducted to examine the underlying micellar solution structure, as presented in Chapter 5. The information obtained so far is limited. Additional experimental techniques, including static light scattering and measurements of the viscoelastic properties of the micellar solutions, should be utilized to obtain more information on the micellar architecture (shape, size, and flexibility), as well as on the micellar solution structure. This can assist in developing a better theoretical formulation to describe the partitioning behavior in two-phase aqueous micellar systems, particularly in the case of larger solute particles, such as viruses, for which the current theoretical description may need refinement.

6.2.5 Investigation of Kinetic Aspects of Partitioning

The studies presented in Section 3.5 indicate that kinetic aspects of partitioning may play a role in the observed partitioning behavior of large particles, such as viruses. More experimental work should be conducted to further elucidate this issue. In view of the results and qualitative rationalization presented in Section 3.5, the following ideas for additional experimental work come to mind:

1. Stirring both of the coexisting micellar solution phases in order to enhance transport of partitioning solutes between the two phases.

2. Stirring the entire phase-separating solutions in order to delay the formation of macroscopic phases and increase the contact time between the microscopic phase domains.

3. Partitioning particles with well-defined size differences at the same temperature condition, as mentioned in 2 of Section 6.2.2, in order to examine how the particle size affects the extent of kinetic effects.

One should keep in mind, however, that these types of experiments are very sensitive to many factors and artifacts (see Section 3.5.3).

6.2.6 Removal of Micelles from the Desired Materials

After partitioning in the two-phase aqueous micellar systems is completed, it may be necessary to remove micelles from the desired materials in order to further purify these materials. A number of ideas on this issue are discussed below:

1. Dissociating micelles into surfactant monomers followed by filtration

   As discussed in Section 1.3, the self-assembling nature of micelles may be utilized to remove micelles. The surfactant monomers, usually of low molecular weight, should be easily removed from the desired materials by filtration.

2. Extracting micelles with organic solvents

   Some studies indicate [89] that Triton X-100 (a nonionic surfactant similar to those belonging to the C_iE_j series) micelles coexisting with biological molecules in aqueous solutions can be extracted and removed by an organic solvent, with the biological molecules remaining intact. The organic solvent used is of the alkyl alcohol type and possesses a long hydrocarbon chain as part of its molecular structure. Such long-chain alcohols are not soluble in water, and the solubility of Triton X-100 in such alcohols is high. As a result, the micelles can be efficiently removed using simple procedures. Similar methods may also be applied to remove micelles composed of other types of surfactants, such as $C_{10}E_4$.

3. Attaching magnetic substances to micelles for removal of micelles using magnetic forces

   Certain magnetic substances are known to be soluble in hydrophobic solvents, and such substances could possibly be solubilized in the hydrophobic interior

of micelles. By letting such a micellar solution flow through a magnetic field, the "magnetic micelles" will be retained by the magnetic field, while the desired solutes will flow away, resulting in efficient removal of micelles. In addition to incorporating magnetic substances into micelles, one can envision using "magnetic surfactants" to directly generate the two-phase systems. Needless to say, magnetic separations of this type should work best in systems in which the desired solutes do not associate and form complexes with micelles, for example, when the dominant interactions between the solutes and the micelles are of the excluded-volume type.

Appendix A

Derivation of Equation (2.6) in Chapter 2

In Chapter 2, the partition coefficient of protein molecules in two-phase aqueous micellar systems was expressed in terms of the excluded volume between a protein molecule and a micelle, as shown in Eq. (2.6) in Section 2.3.1. In this appendix, a detailed derivation of Eq. (2.6) is presented.

The Gibbs free energy, G, of a solution containing micelles, protein molecules, and water (the solvent) can be written as follows [16]:

$$G = G^{id} + G^{ex} \tag{A.1}$$

where G^{id} and G^{ex} are the ideal and excess Gibbs free energies of the solution respectively and can be expressed in terms of the solute and solvent properties as well as the solution conditions. Specifically [90],

$$G^{id} = N_w \mu_w^\circ + \sum_\alpha N_\alpha \mu_\alpha^\circ + k_B T \sum_\alpha N_\alpha (\ln m_\alpha - 1) \tag{A.2}$$

$$G^{ex} = A^{res} - k_B T \sum_\alpha N_\alpha \ln \frac{(V/N_w)}{\Omega_w} \tag{A.3}$$

where k_B is the Boltzmann constant, and T is the absolute temperature. The sub-

script w denotes the properties of water (the solvent), and α denotes those of the solutes, including protein molecules (for which $\alpha = p$) and micelles of aggregation number n (for which $\alpha = n$). In Eq. (A.2), μ_w° and μ_α° are the standard-state chemical potentials of the solvent and the solutes respectively, which depend solely on the solution temperature and pressure. Accordingly,

$$\sum_\alpha N_\alpha = N_p + \sum_n N_n \tag{A.4}$$

$$\sum_\alpha N_\alpha \mu_\alpha^\circ = N_p \mu_p^\circ + \sum_n N_n \mu_n^\circ \tag{A.5}$$

In Eq. (A.2), $m_\alpha = N_\alpha / N_w$ is the molality of solute α. In Eq. (A.3), V is the total volume of the solution. Under the assumption that the solution is incompressible, it follows that

$$V = N_w \Omega_w + \sum_\alpha N_\alpha \Omega_\alpha \tag{A.6}$$

where Ω_w and Ω_α are the volumes of a water molecule and a solute particle of type α respectively. In Eq. (A.3), A^{res} is the residual Helmholtz free energy denoting the difference in the Helmholtz free energy of a system in vacuum and that of an ideal gas, and it is a function of temperature T, total volume V, and the number of solute particles N_α (that is, N_p and N_n), but is not an explicit function of N_w. The explicit form of A^{res} is unknown and will be derived below.

The chemical potentials of the various components in the solution can be obtained by differentiating Eq. (A.1) with respect to the number of molecules of each component. For example, the chemical potential of the solvent, μ_w, is given by

$$\mu_w = \left(\frac{\partial G}{\partial N_w} \right)_{T,P,N_\alpha} \tag{A.7}$$

$$= \mu_w^\circ - k_B T \sum_\alpha \frac{N_\alpha}{N_w} + \left(\frac{\partial A^{res}}{\partial N_w} \right)_{T,N_\alpha} + k_B T \sum_\alpha \left(\frac{N_\alpha}{N_w} - \frac{N_\alpha \Omega_w}{V} \right) \tag{A.8}$$

$$= \mu_w^\circ + \left(\frac{\partial A^{res}}{\partial N_w} \right)_{T,N_\alpha} - k_B T \sum_\alpha C_\alpha \Omega_w \tag{A.9}$$

where $C_\alpha = N_\alpha/V$ is the concentration of solute α. Since A^{res} is a function of T, V, and N_α, A^{res} depends only indirectly on N_w through V (see Eq. (A.6)). Therefore, the differentiation of A^{res} with respect to N_w can be expressed as follows:

$$\left(\frac{\partial A^{res}}{\partial N_w}\right)_{T,N_\alpha} = \left(\frac{\partial A^{res}}{\partial V}\right)_{T,N_\alpha} \left(\frac{\partial V}{\partial N_w}\right)_{T,N_\alpha} = \left(\frac{\partial A^{res}}{\partial V}\right)_{T,N_\alpha} \cdot \Omega_w \tag{A.10}$$

where Eq. (A.6) has been utilized. Equation (A.9) thus becomes

$$\mu_w = \mu_w^\circ + \left[\left(\frac{\partial A^{res}}{\partial V}\right)_{T,N_\alpha} - k_B T \sum_\alpha C_\alpha\right] \Omega_w \tag{A.11}$$

By comparing Eq. (A.11) with the definition of the solution osmotic pressure, Π [27]:

$$\mu_w^\circ - \mu_w = \Pi \Omega_w \tag{A.12}$$

it follows that

$$\Pi = k_B T \left[\sum_\alpha C_\alpha - \frac{1}{k_B T}\left(\frac{\partial A^{res}}{\partial V}\right)_{T,N_\alpha}\right] \tag{A.13}$$

In analogy to the ideal-gas law, $P = \frac{n}{V} k_B T$, it follows that, in Eq. (A.13), the first term on the right-hand side represents the "ideal" contribution to Π, with the second term reflecting the "non-ideal" contribution.

In general, the osmotic pressure, Π, can be expressed as a virial series in the overall solute concentration, $C = \sum_\alpha C_\alpha$ [91, 92]. Specifically,

$$\frac{\Pi}{k_B T} = \sum_\alpha C_\alpha + \sum_{ij} B_{2,ij} C_i C_j + \sum_{ijk} B_{3,ijk} C_i C_j C_k + \cdots \tag{A.14}$$

where $B_{2,ij}$, $B_{3,ijk}, \cdots$ are the second, third, ..., virial coefficients, respectively. By comparing Eqs. (A.13) and (A.14), truncated at the second-virial coefficient level, it follows that

$$-\left(\frac{\partial A^{res}}{\partial V}\right)_{T,N_\alpha} = k_B T \sum_{ij} B_{2,ij} C_i C_j \tag{A.15}$$

$$= k_B T(\frac{1}{V^2}) \sum_{ij} B_{2,ij} N_i N_j \quad \text{(A.16)}$$

where $B_{2,ij}$ is the second-virial coefficient denoting the interactions between solutes i and j, which may either be a protein (p) or a micelle of aggregation number n (n). An expression for A^{res} can then be derived by integrating Eq. (A.16) with repsect to V. This yields

$$A^{res} = k_B T(\frac{1}{V}) \sum_{ij} B_{2,ij} N_i N_j \quad \text{(A.17)}$$

The protein chemical potential, μ_p, can be derived by differentiating the solution Gibbs free energy, G, with respect to N_p, that is,

$$\mu_p = \left(\frac{\partial G}{\partial N_p}\right)_{T,P,N_w,N_n} \quad \text{(A.18)}$$

$$= \mu_p^\circ + k_B T \ln \frac{N_p}{N_w} + \left(\frac{\partial A^{res}}{\partial N_p}\right)_{T,N_n} + k_B T \left[\ln \frac{N_w \Omega_w}{V} - \sum_\alpha \frac{N_\alpha}{V} \Omega_p\right] \quad \text{(A.19)}$$

$$= \mu_p^\circ + \left(\frac{\partial A^{res}}{\partial N_p}\right)_{T,N_n} + k_B T \ln(C_p \Omega_w) - k_B T \sum_\alpha C_\alpha \Omega p \quad \text{(A.20)}$$

From Eq. (A.17), it follows that

$$\left(\frac{\partial A^{res}}{\partial N_p}\right)_{T,N_n} = \frac{k_B T}{V}(2\sum_n B_{2,pn} N_n + 2B_{2,pp} N_p) - \frac{k_B T}{V^2}(\sum_{ij} B_{2,ij} N_i N_j) \cdot \Omega_p \quad \text{(A.21)}$$

where $B_{2,pn}$ is the second-virial coefficient denoting the interaction between a protein molecule and a micelle of aggregation number n, and $B_{2,pp}$ is the second-virial coefficient denoting the interaction between two protein molecules. In the case of protein partitioning in two-phase aqueous micellar systems, since the overall protein concentration (N_p/V) in the solution is low, the probability that two protein molecules interact with each other is very low, that is, $N_p/V \approx 0$. Accordingly, to a very good approximation, one can set the second-virial term characterizing protein-protein interactions, which is proportional to N_p/V, to zero. In this case, Eq. (A.21) simplifies to

$$\left(\frac{\partial A^{res}}{\partial N_p}\right)_{T,N_n} = 2k_B T \sum_n B_{2,pn} C_n - k_B T \Omega_p \sum_{ij} B_{2,ij} C_i C_j \quad \text{(A.22)}$$

By inserting Eq. (A.22) in Eq. (A.20), the protein chemical potential can be written as

$$\mu_p = \mu_p^\circ + 2k_BT\sum_n B_{2,pn}C_n - k_BT\Omega_p[\sum_\alpha C_\alpha + \sum_{ij} B_{2,ij}C_iC_j] + k_BT\ln(C_p\Omega_w) \quad \text{(A.23)}$$

Note that the square-bracketed term in Eq. (A.23) is exactly equal to Π/k_BT, as given by the virial expansion of the osmotic pressure (see Eq. (A.14) truncated at the second-virial coefficient level). Accordingly,

$$\mu_p = \mu_p^\circ + 2k_BT\sum_n B_{2,pn}C_n + k_BT\ln(C_p\Omega_w) - \Pi\Omega_p \quad \text{(A.24)}$$

An examination of Eq. (A.24) indicates that the protein chemical potential, μ_p, is determined by (1) the standard-state protein chemical potential, μ_p°, (2) the concentration of micelles, C_n, as well as the interaction between a protein molecule and a micelle, $B_{2,pn}$, (3) the protein concentration, C_p, and (4) the osmotic pressure of the solution, Π.

In the case of protein partitioning in two-phase aqueous micellar systems, there are two coexisting and equilibrated phases, in which the micelle and protein concentrations are different, but the solution conditions, such as temperature T and osmotic pressure Π, are the same. At equilibrium, the protein chemical potentials in the coexisting top (t) and bottom (b) phases should be the same, that is,

$$\mu_{p,t} = \mu_{p,b} \quad \text{(A.25)}$$

Since the standard-state protein chemical potential is only a function of temperature and pressure, which are the same in the two coexisting phases, it follows that $\mu_{p,t}^\circ = \mu_{p,b}^\circ$. Using Eq. (A.24) for $\mu_{p,t}$ and $\mu_{p,b}$, Eq. (A.25) thus becomes

$$2k_BT\sum_n B_{2,pn}C_{n,t} + k_BT\ln(C_{p,t}\Omega_w) = 2k_BT\sum_n B_{2,pn}C_{n,b} + k_BT\ln(C_{p,b}\Omega_w) \quad \text{(A.26)}$$

As mentioned earlier, since $B_{2,pn}$ represents the interaction between a protein molecule

and a micelle of aggregation number n, it does not depend on the concentration of proteins or micelles, and therefore $B_{2,pn}$ is the same in the top and bottom phases. In this case, the partition coefficient, K_p, can be deduced from Eq. (A.26) as

$$\ln K_p \equiv \ln \frac{C_{p,t}}{C_{p,b}} = -2 \sum_n B_{2,pn}(C_{n,t} - C_{n,b}) \tag{A.27}$$

Equation (A.27) clearly shows that the second-virial coefficient, $B_{2,pn}$, needs to be calculated in order to obtain K_p.

The second-virial coefficient is related to the interaction potential, $u(\vec{\mathbf{r}})$, between a particle at position $\vec{\mathbf{r}}_1$ and another particle at position $\vec{\mathbf{r}}_2$, where $\vec{\mathbf{r}} = \vec{\mathbf{r}}_2 - \vec{\mathbf{r}}_1$, and is given by [92]:

$$B_2 = -\frac{1}{2} \int [e^{-\beta u(\vec{\mathbf{r}})} - 1] d\vec{\mathbf{r}} \tag{A.28}$$

For example, for hard spheres of equal radius σ, the interaction potential is given by

$$u(r) = \begin{cases} \infty, & \text{for } r < 2\sigma \\ 0, & \text{for } r > 2\sigma \end{cases} \tag{A.29}$$

Using Eq. (A.29) in Eq. (A.28) yields

$$B_2 = -\frac{1}{2} \int_0^{\sigma} -d\mathbf{r} \tag{A.30}$$

$$B_2 = \frac{1}{2} U \tag{A.31}$$

where $U = \frac{4\pi}{3}(2\sigma)^3$ is the excluded volume between two hard spheres. In the case of protein-micelle interactions in the partitioning systems discussed in Chapter 2, it was assumed that the protein molecules and the micelles are mutually-impenetrable, non-associating, hard entities. To interpret the hard-entity interaction by following Eq. (A.29), the protein-micelle interaction potential is essentially infinite when a protein molecule and a micelle touch each other, and is zero when these two entities do not touch each other. Accordingly, similar to the derivation of Eq. (A.31), the second-virial coefficient associated with the hard-body protein-micelle interaction,

$B_{2,pn}$, is given by

$$B_{2,pn} = \frac{1}{2} U_{n,p} \tag{A.32}$$

where $U_{n,p}$ is the excluded volume between a protein molecule and a micelle of aggregation number n. Using Eq. (A.32) in Eq. (A.27), the partition coefficient, K_p, can be obtained as

$$\ln K_p = -\sum_n U_{n,p}(C_{n,t} - C_{n,b}) \tag{A.33}$$

$$K_p = \exp\left[-\sum_n U_{n,p}(C_{n,t} - C_{n,b})\right] \tag{A.34}$$

$$K_p = \exp\left[-\sum_n U_{n,p}\left(\frac{N_{n,t}}{V_t} - \frac{N_{n,b}}{V_b}\right)\right] \tag{A.35}$$

where $N_{n,t}$ and $N_{n,b}$ are the numbers of micelles of aggregation number n in the top and bottom phases respectively, and V_t and V_b are the volumes of the top and bottom phases respectively. Note that Eq. (A.35) is precisely Eq. (2.6) given in Section 2.3.1.

In order to further simplify the K_p expression, Eq. (A.35) can be written as

$$K_p = \frac{\Omega_t}{\Omega_b} \tag{A.36}$$

$$\text{where} \quad \Omega = \exp\left[-\sum_n U_{n,p}\frac{N_{n,t}}{V_t}\right] \tag{A.37}$$

and Ω represents the excluded-volume contribution to K_p from each of the two coexisting phases. Note that Eqs. (A.36) and (A.37) are precisely Eqs. (2.4) and (2.5) given in Section 2.3.1. Note also that Ω_t, Ω_b, and Ω_w (volume of a water molecule), Ω_α (volume of a solute of type α) have very different meanings and should not be confused.

The association of the protein partition coefficient, K_p, with the second-virial coefficient, $B_{2,pn}$, as expressed in Eq. (A.27), suggests that the protein partition behavior driven by non-excluded-volume type protein-micelle interactions can also be predicted from Eq. (A.27) by using the $B_{2,pn}$ expression corresponding to the specific type of interaction considered.

In addition to the above derivation, it is noteworthy that, by including more terms

in the virial expansion, as shown in Eq. (A.14), into Eq. (A.16), for example,

$$-\left(\frac{\partial A^{res}}{\partial V}\right)_{T,N_\alpha} = k_B T \sum_{ij} B_{2,ij} C_i C_j + k_B T \sum_{ijk} B_{3,ijk} C_i C_j C_k \tag{A.38}$$

it is possible to model the effect of more complicated many-body interactions, such as those resulting between a protein molecule and two micelles, on the protein partitioning behavior.

Appendix B

Bacteriophage Concentration Determination

This appendix describes detailed experimental procedures of the biological activity assay, which is used in this thesis for determining the bacteriophage concentrations (see Section B.1), as well as a discussion on the possible sources of the error in the virus concentration determination (see Section B.2).

B.1 Procedures Involved in the Biological Activity Assay

1. Preparation before conducting the assay

   Some materials, such as the host bacteria and the agar plates, need to be prepared before conducting the biological activity assay. Details of the preparation procedures include:

   (a) Growing the host bacteria for plating with viruses. See Appendix D for complete details.

   (b) Preparing the agar plates.

This involves pouring hot "hard agar" (in liquid state) into sterilized disposable petri dishes. Each dish should contain at least 30 mL of the hard agar. These dishes (or "plates") are then cooled down at room temperature at least overnight to allow the agar to gelate and solidify before use (see Appendix E for the composition of "hard agar").

(c) Prepare the "soft agar."

"Soft agar" (in solid form at room temperature) is heated up in a microwave oven until it boils. 2.5 mL of the liquid soft agar is then transferred into each of the test tubes which are kept in a constant temperature hood at 46°C (see Appendix E for the composition of "soft agar").

2. Conducting a serial dilution of the virus solution

This involves consecutively conducting several dilution steps, each yielding a 1:100 or 1:10 dilution. The 1:100 dilution is conducted as follows:

(a) The solution whose virus concentration needs to be determined (the "original solution") is vortexed to achieve thorough mixing.

(b) 0.05 mL of the solution is withdrawn using a 0.1-mL sterile pipet by mouth-pipeting method. The pipet is then wiped against the mouth of the test tube to ensure that no solution remains on the outside in order to avoid transferring more than 0.05 mL of the solution in the next step.

(c) 0.05 mL of the solution in the pipet is transferred into another test tube containing 5 mL of the fresh dilution fluid by blowing in the pipet lightly to ensure that all the solution in the pipet is transferred into the dilution fluid (see Appendix E for the composition of the dilution fluid). The solution is then vortexed.

In the case of a 1:10 dilution, the only difference with the above mentioned procedures is in the amount of solution withdrawn and in the amount of dilution fluid needed. Specifically, in step (b), a 1-mL pipet is used to extract 0.5 mL of

the solution; in step (c), 0.5 mL of the solution in the pipet is transferred into 4.5 mL of the dilution fluid.

One dilution step is completed by conducting steps (a) - (c) described above. If additional dilution steps are needed, steps (b) and (c) are implemented again on the solution obtained in (c), with a new and fresh dilution fluid used in (c). The final one or two solutions resulting from a dilution series are used for plating (see the next step).

3. Plating the virus solutions

0.1 mL of the solution, usually the final one of a dilution series, is withdrawn and mixed with host bacteria and soft agar, and the resulting mixture is incubated on the agar plate for generating plaques. This step is usually called "plating", and the details are as follows:

(a) Two drops of the plating bacteria solution (see Appendix D for preparation procedures) are added into a test tube containing 2.5 mL of the heated soft agar solution kept in the constant temperature hood of 46°C. Note that since the temperature, 46°C, is too high and thus fatal to bacterial cells, the two drops of bacteria solution should be added into the soft agar only immediately prior to adding the virus solution, so that the bacterial cells do not remain at the high-temperature condition for too long, and their viability can therefore be maintained.

(b) The virus solution to be plated is vortexed. 0.1 mL of the virus solution is withdrawn using a sterile 0.1-mL pipet and transferred into the soft agar solution in (a).

(c) The agar solution is vortexed briefly to achieve through mixing and then poured into an agar plate. The plate is then swirled to enable the soft agar solution to spread uniformly in the agar plate.

It is noteworthy that since agar solutions solidify and form gels at room temperature, handling of the soft agar solution after it is taken out of the

46°C hood should be performed quickly.

4. Incubating the plate overnight

   After the agar plates obtained in step 3 are kept at room temperature for about 15 - 30 minutes to allow the soft agar to solidify or "dry," the plates are inverted and placed in the 30°C incubator overnight. The purpose of inverting the plates and keeping the agar layer on the top is to prevent the plaques generated on the agar layer from being smeared off by moisture condensation in the plate.

5. Counting the number of plaques generated on the agar plates

   On the next day, the number of plaques on each plate is counted using a dark-field colony counter. In this device, the plaques appear as dark holes in the brightly illuminated bacterial layer on the agar plates. An automatic recording counting apparatus on the colony counter operates an electric recorder as it marks each plaque. After all the plaques in a plate are marked, the number of plaques can be obtained.

6. Calculating the virus concentration in the original solution

   According to the number of plaques counted in step 5, and the number and types of dilution steps performed in step 1, the virus concentration in the original virus solution can be calculated. For example, if a virus solution has undergone two 1:100 dilution steps before plating, and the number of resulting plaques on the agar plate is 200, the virus concentration in the original solution is

$$\frac{200 \times (100)^2}{0.1\text{mL}} = 2 \times 10^7 \text{ (phage particles/mL)}$$

   Note that the division by 0.1 mL reflects the fact that the number of plaques on the agar plate represents the number of phage particles in 0.1 mL of the final diluted solution (see step 3).

Usually, two or three sets of serial dilution were performed on one solution whose virus concentration was to be determined, and hence at least two or three plates were

made, in order to obtain a higher accuracy in determining the virus concentration in that solution.

The typical error of the biological activity assay is 20 - 30%. Therefore, counting results differing by about 10% are usually considered as being the same.

For a more detailed description of this assay, see Reference [93].

B.2 Possible Sources of Error in the Virus Concentration Determination

As mentioned in Section 3.3.2, the biological activity assay is a fairly accurate method for determining virus concentrations, but this assaying method is also sensitive to many factors, some of which are associated with the experimental operations. Possible sources of error in the determination of virus concentrations are discussed below:

1. The two coexisting micellar phases are mixed while being withdrawn after partitioning

   This will result in withdrawal of part of the other phase together with the desired phase. This sometimes occurs when the top phase of the two-phase aqueous $C_{10}E_4$ micellar system is withdrawn. Since, in the $C_{10}E_4$ micellar system, the top phase is more concentrated and viscous than the bottom phase, the interface between the two liquid phases is easily disturbed while the top phase is withdrawn. It is therefore possible to take out part of the bottom phase together with the top phase solution. This may result in a more serious problem in the virus partitioning experiments, since the virus concentration in the bottom $C_{10}E_4$ phase is about 3 orders of magnitude higher than that in the top $C_{10}E_4$ phase. Consequently, accidentally mixing the two phases, even to a small extent, may cause serious error in determining the virus concentrations, particularly in the top phase of the $C_{10}E_4$ two-phase micellar system.

   To avoid this type of error, one has to be very cautious while withdrawing the phase solutions after partitioning.

2. The graduations on the pipets are not accurate

Typically, on a pipet, only the largest amount is calibrated, and the others presenting smaller amounts are marked merely by equally dividing the length of the pipet. For example, in a 0.1-mL pipet with graduations marked for each 0.01 mL, only the 0.1-mL mark is calibrated and reliable, while the other graduations may not be accurate at all. As a result, the amount of solution which is measured to the 0.05-mL mark on the 0.1-mL pipet may not be exactly 0.05 mL, thus introducing error in the serial dilution procedure of the biological activity assay (see Section B.1).

This factor usually does not constitute a serious problem, but one should be aware of the limitations of the measuring instruments. For instance, for measuring 0.1 mL of a solution, a 0.1-mL pipet should be used, rather than using the 0.1-mL mark on a 1-mL pipet.

3. The solution remaining on the outside of pipets is not wiped off

This will make the amount of the virus solution transferred to the next test tube more than expected, resulting in the determined virus concentration being higher than the actual value. Specifically, the amount of virus solution taken out by a 0.1-mL pipet is typically 0.05 mL, which is very small, and hence the quantity of solution staying on the outside of the pipet cannot be ignored. In addition, since the top micelle-rich phase solutions are usually more viscous than typical aqueous solutions, top-phase solutions may cause a more serious problem. Consequently, one has to ensure that the solution remaining on the outside of the pipet is wiped off before transferring the content in the pipet into another test tube, and this can be done either by wiping the tip of the pipet against the mouth of the test tube from which the solution is withdrawn, or by using a clean tissue paper to wipe off the solution (although the latter is not recommended by biologists).

4. The time spent on vortexing the solution is not consistent in serial dilution

   The vortexing time of virus solutions will affect the uniformity of the solutions, from which aliquots will be withdrawn either during the dilution step or for plating. Vortexing each of the solutions for about the same amount of time is hence important, since this can ensure the consistency of uniformity in each of the solutions. This factor, however, does not constitute a serious problem.

5. Host bacteria are not fresh and healthy

   After being prepared, the host bacteria begin to degrade, and the cell density in the solution starts to decrease. If the host bacteria are not freshly-prepared, there are always some cells which are not healthy and viable, and the bacteriophage particles adsorbed onto such cells will not be able to generate clear plaques. The efficiency of plating viruses will therefore be reduced. This constitutes a more serious problem for large bacteriophages which usually generate small plaques, such as T4. Accordingly, only fresh cultures of bacteria should be used for plating.

   Typically, fresh and healthy cells will be suspended in the nutrient broth, and, as a result, the cell solution in the dropper bottles (for plating viruses, see Appendix D) looks turbid. As time goes on, some of the cells die and precipitate to the bottom of the bottle, and the turbidity of the solution will decrease gradually. This loss of turbidity is a clear indication that the bacteria are not healthy and fresh. Usually, the plating bacteria kept in dropper bottles are considered fresh within one week after preparation. A new batch of plating bacteria should be prepared each week to ensure that the bacterial cells are fresh and healthy for plating viruses.

6. The agar plates are not fresh

   After being kept at room temperature for more than one week, the hard agar in the agar plates will be dried and become wrinkled. Bacteria will not grow well on such agar plates, resulting in fussy phase plaques or low plating efficiency.

Therefore, fresh agar plates should be used for plating, or the agar plates should be consumed within one week (but not exceeding two weeks) after they are prepared.

Appendix C

Stability Test of Bacteriophages

Details of the stability test of the bacteriophages, P22, T4, and ϕX174, are presented in this appendix. This includes the solution conditions examined, experimental procedures, and a discussion of the results.

C.1 Solution Conditions Examined

The solution conditions used for testing the stability of each of the three bacteriophages are described below:

- P22 and T4

  Both P22 and T4 require the presence of magnesium ions (Mg^{+2}) in order to be stable in solutions. Accordingly, the stability of these viruses is tested in the following solution conditions:

  1. Dilution fluid (see Appendix C for its composition). Since the dilution fluid contains 2mM Mg^{+2}, it constitutes the most stable and "friendly" environment for P22 and T4. This is also the fluid in which P22 and T4 are typically stored.
  2. Dilution fluid + 2mM EDTA. Since EDTA chelates or binds magnesium ions, it reduces the concentration of available Mg^{+2} in the solution. Without sufficient Mg^{+2} in the solution, P22 or T4 particles are not stable and

may eventually decompose. Accordingly, this solution condition represents the most unstable condition for P22 and T4.

3. pH 7 McIlvaine buffer.
4. 10 wt% $C_{10}E_4$ in pH 7 McIlvaine buffer.
5. pH 7 McIlvaine buffer containing 2mM Mg^{+2}.

Note that solution conditions 3 - 5 are needed in order to examine the stability of P22 and T4 in the phase separating micellar systems.

- ϕX174

ϕX174 does not require the existence of any specific ions to be stable in solutions. In addition to the solution conditions 1, 3, and 4, as described above, the ϕX174 stability in solutions having different $C_{10}E_4$ concentrations was also tested, since the ϕX174 concentration in the $C_{10}E_4$ solution after incubation overnight was found to be lower than those in other solution conditions. Hence, the effect of the surfactant, specifically that of different surfactant concentrations, on the ϕX174 stability was further tested. Specifically, the following solution conditions were examined:

1. pH 7 McIlvaine buffer.
2. 1 wt% $C_{10}E_4$ in McIlvaine buffer.
3. 4 wt% $C_{10}E_4$ in McIlvaine buffer.
4. 10 wt% $C_{10}E_4$ in McIlvaine buffer.

Note that, although ϕX174 does not require Mg^{+2} ions to be stable in the solution, the dilution fluid is still used for dilution purposes.

C.2 Experimental Procedures

1. 1.5 - 2 mL of each of the solution conditions described in Section C.1 is prepared.

2. The original concentrated virus solution is added in each of the solutions prepared in step 1, followed by thorough mixing. The resulting virus concentration in each solution is of the order $10^7 \sim 10^8$ virus particles/mL. Note that this virus concentration is about the same as that used for the partitioning experiments.

3. A 0.05 mL aliquot of each of the virus solutions prepared in step 2 is withdrawn and transferred into a test tube containing 5 mL of the dilution fluid. This step is implemented in order to: (1) "quench" the possible detrimental effects of each solution condition on the virus, and (2) obtain a 1:100 dilution of these solutions, such as in step 2 (a) in Section 3.3.2.2. In order to assess the possible variation of the virus concentration with time, the 0.05 mL aliquots are withdrawn at various time intervals. For example, the time intervals adopted are listed below:

   5 minutes (or immediately after mixing), 15 minutes, 30 minutes, 1 hour, 2 hours, 4 hours, 6 hours, 8 hours, and overnight.

   Consequently, after completing this step, there are nine solutions for each of the solution conditions described in Section C.1.

4. The virus concentration in each of the nine solutions obtained in step 3 is determined as soon as possible. This concentration determination is conducted for each solution condition described in Section C.1 using the biological activity assay described in Section B.1 of Appendix B.

5. The measured virus concentrations versus time are plotted for each of the solution conditions in order to examine the virus stability and viability in each of these solution conditions.

C.3 Results and Discussion

Results of the stability test for each of the three bacteriophages examined are discussed below:

1. P22

Figure C-1 shows the P22 concentration in each of the solution conditions examined as a function of testing time. The P22 concentrations presented in Figure C-1 are normalized with respect to the initial P22 concentration, which is obtained at the 5-minute interval after adding P22 into that specific solution condition. The reason for examining the variation of the "normalized" P22 concentration with time, rather than that of the actual P22 concentration with time, is that, inevitably, the initial P22 concentrations in the five solution conditions (described in Section C.1) may be different from each other. By normalizing the P22 concentrations in a specific solution condition with respect to the initial P22 concentration in that solution condition, the variation of the virus concentration with time can be compared and contrasted to those corresponding to different solution conditions. Since, after 5 minutes, the P22 particles should not be affected by any possible damaging factors in the solution to any significant extent, the P22 concentration obtained at the 5-minute interval should represent the initial P22 concentration and is therefore used as the "standard" for normalization. Note that this implies that the initial normalized concentrations in all the solution conditions examined are unity (see Figure C-1).

In Figure C-1, only the initial concentrations, and those obtained at 5-minute, 1-hour, 4-hour, and overnight intervals are shown. Most of the normalized P22 concentrations are in the range of 1.0 ± 0.5, indicating the existence of fluctuations in the P22 concentrations at different solution conditions during the tested period of time. These fluctuations may reflect (1) an error in the P22 concentration determination, which can induce both positive and negative fluctuations, or (2) a reduction in the P22 concentrations due to the detrimental effect at certain solution conditions, which can lead to a decrease in the P22 concentrations. However, since the measured normalized P22 concentrations were found to be in the range of 1.0 ± 0.5, fluctuations in the P22 concentrations can still

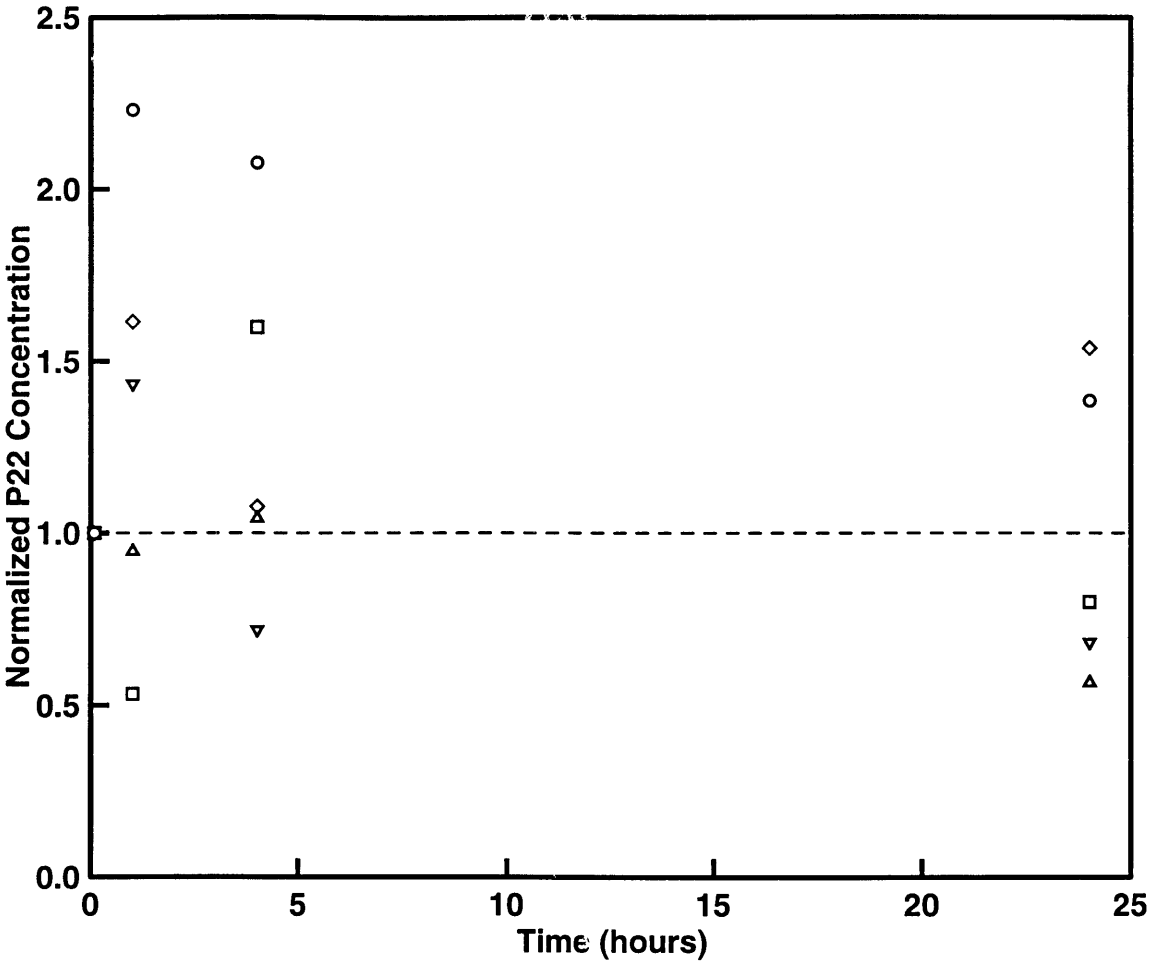

Figure C-1: Normalized P22 concentrations in various solution conditions as a function of testing time. The normalization is conducted with respect to the initial P22 concentration in each of the solution conditions. The symbols represent various solution conditions: (○) dilution fluid, (□) dilution fluid with 2mM EDTA, (△) pH 7 McIlvaine buffer, (◇) 10% $C_{10}E_4$ in pH 7 McIlvaine buffer, and (▽) pH 7 McIlvaine buffer with 2mM Mg^{+2}. The dashed horizontal line at a normalized concentration of unity is shown for reference purposes.

be considered reasonable.

The P22 concentrations in the EDTA solution (Solution 2, □), in the pH 7 McIlvaine buffer (Solution 3, △), and in the buffer solution containing Mg^{+2} ions (Solution 5, ▽) appear to decrease with time. Nevertheless, more than half of their initial concentrations are still retained after overnight incubation. This observed decay by a factor of about 2 in the P22 concentration after overnight incubation is considered by biologists to be a natural decay. In other words, the observed decay does not reflect any significant detrimental effect, and hence should not be viewed as being serious (this was stressed by Professor King). The decay should be considered significant if the concentration of virus particles is reduced by a factor of 10 after overnight incubation. Such a large decay may indeed denote the existence of damaging effects on the virus particles. However, it is expected that, since the given partitioning result reflects a ratio of virus concentrations in the top and bottom phases, the effect of the decay rate should cancel out, thus having a minimal influence on the partitioning results.

Note that the normalized P22 concentrations in the dilution fluid (○) seem to be quite high — about 2.25 at the 1-hour interval and then decreasing to about 1.4 after overnight incubation. These high P22 concentrations, as compared to that of the initial condition, may have been caused by an inaccurate determination of the initial P22 concentration at this solution condition. The reason is probably a lack of thorough mixing before withdrawing out the solution sample for concentration determinations. Note that even if the highest concentration (2.25 at the 1-hour interval) was used as the "standard" for normalization, the final P22 concentration after overnight incubation (1.4 in Figure C-1) would become about 0.6, which is still in the range of reasonable fluctuations (1.0 ± 0.5).

It can therefore be concluded that, since all the normalized P22 concentrations are of order unity (in the range of 1.0 ± 0.5), they can be assumed to be essentially the same. This, in turn, suggests that no significant damaging effects are induced by either the McIlvaine buffer or the $C_{10}E_4$ surfactant on the P22

virus particles. This also implies that P22 is a very stable virus in the solution conditions tested. Additional tests also revealed that the P22 concentration in the $C_{10}E_4$ solutions incubated overnight did not change very much when these solutions were kept in the refrigerator. Accordingly, it can be assumed that it is safe to leave P22-$C_{10}E_4$ surfactant solutions stored overnight. In view of this, the P22 partitioning experiments were conducted overnight, with the biological activity assay for measuring P22 concentrations conducted on the next day.

2. T4

Figure C-2 shows the normalized T4 concentrations in various solution conditions as a function of testing time. Within the first 8 hours, the normalized T4 concentrations were found to be of order 1 (in the range of 1.0±0.4). However, after overnight incubation, the T4 concentrations in all the solution conditions examined were found to reduce to lower than one half of the original concentrations. Although this reflects primarily the natural viral decay, this finding suggests that the assay of T4 concentrations should be completed within the same day of the partitioning experiments. Since it usually takes 3-4 hours to conduct the biological activity assay, the time involved in T4 partitioning experiments should not exceed 4-5 hours.

3. ϕX174

Figure C-3 shows the normalized ϕX174 concentrations as a function of testing time in McIlvaine buffer with $C_{10}E_4$ concentrations of 0, 1%, 4%, and 10%. Similar to Figure C-2, all the normalized ϕX174 concentrations were found to be of order 1 (1±0.5) within the first 8-hour period in all the solution conditions examined. However, beyond the 8-hour period, a reduction of the ϕX174 concentrations to about or lower than one half of the original concentrations was observed after overnight incubation. Nevertheless, as discussed in the T4 case, no significant effect of the surfactant concentrations on the ϕX174 stability was observed. As in the T4 case, the assay of ϕX174 concentrations should be completed in the same day of the partitioning experiments. In other words,

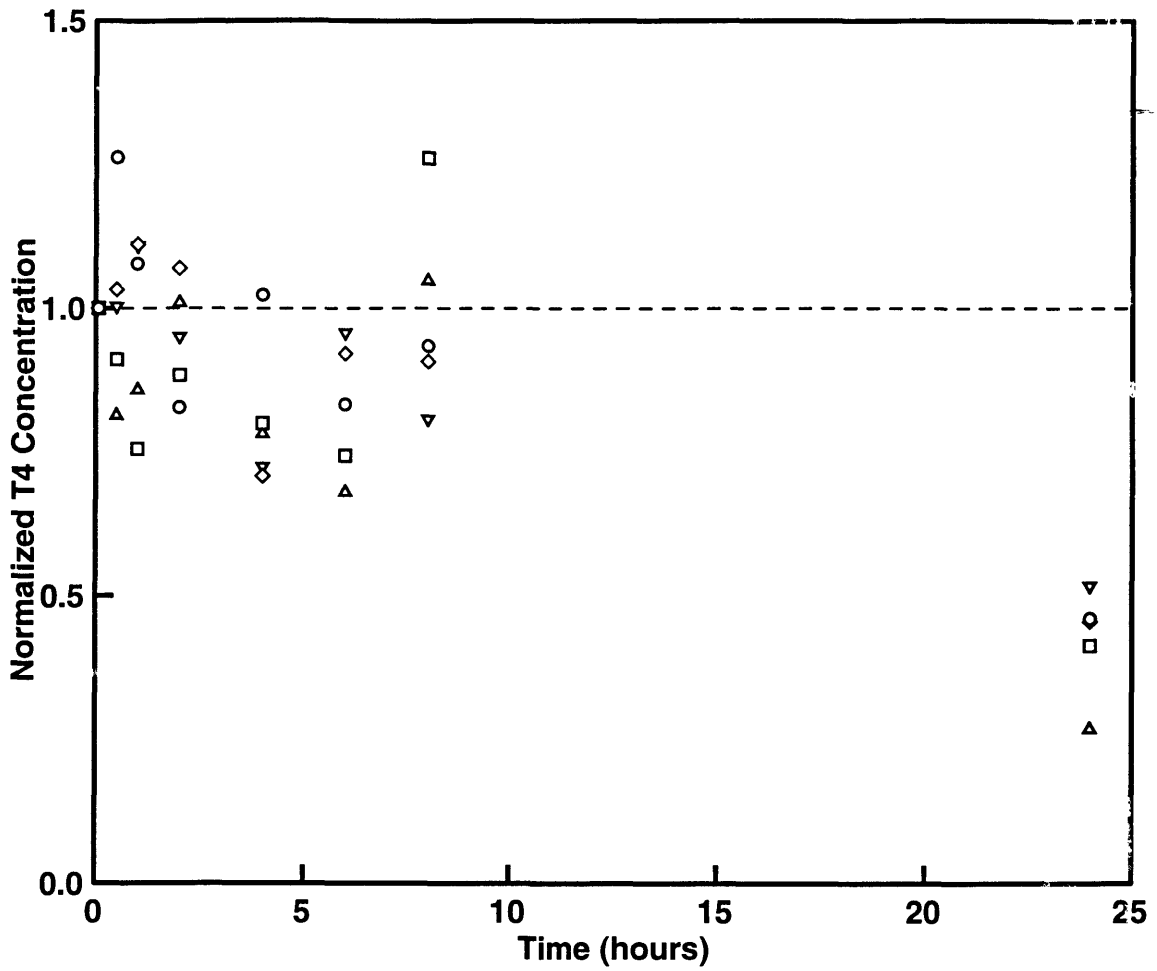

Figure C-2: Normalized T4 concentrations in various solution conditions as a function of testing time. The notation is the same as that in Figure C-1.

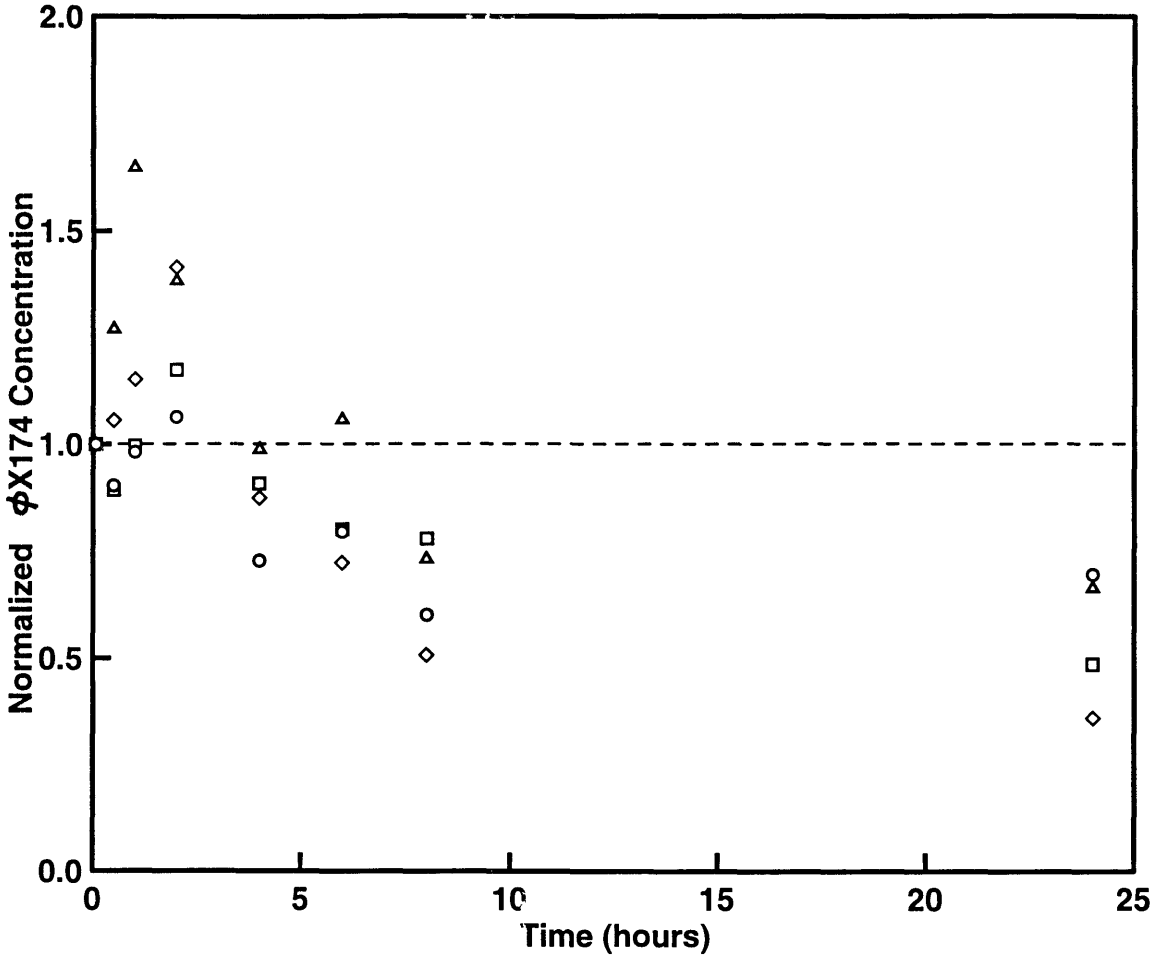

Figure C-3: Normalized ϕX174 concentrations in various solution conditions as a function of testing time. The symbols represent different solution conditions: (○) pH 7 McIlvaine buffer without $C_{10}E_4$, (□) 1% $C_{10}E_4$ in McIlvaine buffer, (△) 4% $C_{10}E_4$ in McIlvaine buffer, and (◇) 10% $C_{10}E_4$ in McIlvaine buffer. The dashed horizontal line at a normalized concentration of unity is for reference purposes.

the partitioning experiments involving ϕX174 should be conducted for no more than about 4 - 5 hours.

By comparing the results of these three bacteriophages, it can also be concluded that P22 possesses a somewhat higher stability than T4 and ϕX174.

Appendix D

Procedures for Growing Host Bacteria

Detailed procedures for preparing the host bacteria for plating viruses are described in this appendix. In principle, the bacteria are grown in the water bath set at the desired temperature overnight, with air bubbling through the cell solution, followed by centrifugation to concentrate and harvest the cells. The medium used for the bacteria culture varies with the bacteria species, but the Luria Broth (LB) is used for growing both *Salmonella* (the host bacteria of P22) and *Escherichia coli* B (the host bacteria of ϕX174 and T4). The ideal temperature for growing both bacteria is 35-37°C.

D.1 Growing the Bacteria Source Solution ("Overnight")

This is for preparing a concentrated cell solution from a bacteria colony (on an agar plate), and this solution is used as the source for growing the plating bacteria (see Section D.2). This concentrated bacteria solution is usually referred to as the "overnight."

1. Preparing the growing medium

Two culture solutions are prepared by pouring the medium (LB) into sterile test tubes, filled up to about 1/4 or 1/5 of the test tube volume. The test tubes used are of the type having a cap with a long thin glass tube inserting through the cap and stretching into the test tube. One of the solutions is used for growing bacteria, and the other is used as a "control" for checking whether the medium or the test tube is contaminated by other species. The growth of microbials is evidenced by the high turbidity of the medium solution after overnight incubation (see step 3 below).

2. Introducing the bacteria colony into the growing medium

   (a) A capillary tube is used to take out a bacteria colony from the agar plate on which the desired bacteria species grow. Typically, a small, round colony is favorable, and the "suspicious" colonies which are located out of the tracks of the cell should not be used, since such colonies may come from other species contaminating the plate. The capillary tube is inserted at the location of the desired colony into the bottom of the agar plate, and the tube is pulled out with the bacteria colony and agar inside.

   (b) The bacteria colony is then transferred into the medium solution by blowing air into the capillary tube to force the colony and agar to come out and fall into the test tube. One should ensure that the colony and agar stay in the medium solution instead of sticking to the test tube wall.

3. Incubating the bacteria overnight

The two test tubes containing the medium solution are subsequently placed in the water bath set at 35 - 37°C. Clean air is supplied to both solutions through the thin glass tubes on the caps of the test tubes. The ideal way to supply air to the culture medium is to make air flow gently along the wall of the test tubes. Vigorous bubbling should be avoided since it will cause overflow of the

solutions and loss of the bacteria. The two solutions are kept at this condition overnight.

4. Stopping cell growth on the next day

   On the next day, the two test tubes are taken out from the water bath and transferred into ice to quench further cell growth, with the air supply still turned on, for 20-30 minutes. The condition of the medium in the "control" tube should be examined. It is desirable that this medium be clear, indicating that no other microbials originally existed in the medium or test tube which may have contaminated the bacterial culture. The test tube containing the bacteria should look turbid because of the high cell concentration.

The cell concentration in this cultured medium is of order 10^{10} - 10^{11} cells/mL. The concentrated bacteria solution is stored in the refrigerator, and usually it should last for at most two weeks.

D.2 Growing the Plating Bacteria

The following steps are for preparing the cell solution in a dropper bottle for plating with the virus. This cell solution is prepared from the concentrated bacteria solution ("overnight") described in Section D.1.

1. Growing bacteria in the water bath

   (a) 3 mL of the concentrated bacteria solution (see Section D.1) is withdrawn with a sterile pipet and transferred into a bottle containing 300 mL LB broth. A cap with a thin glass tube inserted through it (such as those used with the test tubes in Section D.1) is placed on the LB broth bottle.

   (b) The bottle (containing bacteria and growing medium) is then placed in the water bath set at 35 - 37°C, with clean air supplied to the solution, as in step 3 of Section D.1. The solution is then incubated for 2-3 hours or until the solution becomes sufficiently turbid. The cell growth is then stopped

by placing the bottle in ice, with air still flowing through the solution, for 20-30 minutes.

2. Centrifuging to harvest the bacteria

   (a) The cell solution is poured into two centrifuge bottles (plastic, 250 mL, 8 oz.).

   (b) The two centrifuge bottles are weighed on a balance. The amounts of the cell solutions in the two bottles are adjusted by pouring the contents of the two bottles back and forth to make the final weights of the two bottles the same. Subsequently, the two bottles are closed tightly with their caps.

   (c) The two bottles are placed in the refrigerated centrifuge (whose temperature is set at about 4°C) to be centrifuged at a spinning speed of 5000 RPM for 10 minutes.

3. Resuspending the bacterial cell after centrifugation

   (a) After being taken out of the centrifuge, the supernatant in the two centrifuge bottles is poured into the original LB bottle used for cell growth.

   (b) 12.5 mL of the fresh LB broth is added into each of the two centrifuge bottles. The centrifuge bottles are vortexed or vigorously shaken to suspend the pellets (concentrated cells) in the LB broth. One has to ensure that the pellets are uniformly suspended, and that no aggregates or lumps of cells exist in the broth.

   (c) The cell suspension is poured from the centrifuge bottles into a dropper bottle. The resulting solution is the cell solution used for plating the virus in the biological activity assay (see Sections 3.3.2 and B.1 of Appendix B).

The cell concentration in the resulting bacteria solution is of order 10^9 cells/mL. This bacteria solution has to be stored in the refrigerator, and generally it should last for about a week.

Appendix E

Recipes for Preparing Various Media and Solutions Used in the Biological Activity Assay

This appendix describes the recipes and methods for preparing 1 L of the media or agar solutions in the biology laboratories, in particular, the media and solutions used in the partitioning experiments. In the Department of Biology at M.I.T., most of the media and solutions are prepared by those working in the media room. Therefore, all the media or solutions used in the biological activity assay for the partitioning experiments are from the media room.

1. Luria Broth (LB)

Material	Amount	Concentration
Tryptone	10 g	1%
Yeast Extract	5 g	0.5%
NaCl	5 g	0.5%
1N NaOH	4 mL	4 mM
Water	1 L	

After being well mixed, the LB broth is sterilized at 20 psi and 250°F for 30 - 40 minutes.

2. Dilution Fluid (DF)

Material	Amount	Concentration
Tryptone	1 g	0.1%
NaCl	7 g	0.7%
$MgSO_4 \cdot 7H_2O$	20 g	2%
Water	1 L	

After being well mixed, the dilution fluid is sterilized at 20 psi and 250°F for 30 - 40 minutes.

3. Hard Agar

This is the agar solution used for preparing agar plates. The agar content in this solution is 1%.

Material	Amount	Concentration
Tryptone	10 g	1 %
Yeast Extract	5 g	0.5%
NaCl	5 g	0.5%
1N NaOH	1 mL	1 mM
Agar	10 g	1%
Water	1 L	

First, the agar is heated for 30 minutes in order to be melted and mixed with other ingredients. After being well mixed, the agar solution is sterilized at 20 psi and 250°F for 40 - 45 minutes.

Typically, 30 mL of hard agar is poured into one petri dish to generate an agar plate. In the case of ϕX174, since Ca^{+2} ions are required for generating ϕX174 plaques on agar plates, 2 mL of 1.0 M $CaCl_2$ is added into 1 L hard agar before being poured for preparing agar plates.

4. Soft Agar

This is the agar solution used for mixing with bacteria and viruses and for forming the top agar layer on an agar plate. The agar content in this solution is 0.65%, lower than that in the hard agar.

Material	Amount	Concentration
LB Broth	8 g	0.8%
NaCl	5 g	0.5%
Agar	6.5 g	0.65%
Water	1 L	

Similar to the hard agar solution, the agar is heated for 30 minutes to be melted, and the resulting solution is sterilized at 20 psi and 250°F for 40 - 45 minutes after being well mixed.

Bibliography

[1] C. Bordier, "Phase separation of integral membrane proteins in Triton X-114 solution," *J. Biol. Chem.*, **256**, 1604-1607 (1981).

[2] J.G. Pryde, "Triton X-114: A detergent that has come in from the cold," *Trends Biochem. Sci.*, **11**, 160-163 (1986).

[3] J.G. Pryde and J.H. Phillips, "Fractionation of membrane proteins by temperature-induced phase separation in Triton X-114," *Biochem. J.*, **233**, 525-533 (1986).

[4] C. Holm, G. Fredrikson, and P. Belfrage, "Demonstration of the amphiphilic character of hormone-sensitive lipase by temperature-induced phase separation in Triton X-114 and charge-shift electrophoresis," *J. Biol. Chem.*, **261**, 15659-15661 (1986).

[5] R.A. Ramelmeier, G.C. Terstappen, and M.-R. Kula, "The partitioning of cholesterol oxidase in Triton X-114-based aqueous two-phase systems," *Bioseparation*, **2**, 315 (1991).

[6] T. Saitoh and W.L. Hinze, "Concentration of hydrophobic organic compounds and extraction of protein using alkylammoniosulfate zwitterionic surfactant mediated phase separations (cloud point extractions)," *Anal. Chem.*, **63**, 2520-2525 (1991).

[7] Y.J. Nikas, C.-L. Liu, T. Srivastava, N.L. Abbott, and D. Blankschtein, "Protein partitioning in two-phase aqueous nonionic micellar solutions," *Macromolecules*, **25**, 4797-4806 (1992).

[8] G.C. Terstappen, R.A. Ramelmeier, and M.-R. Kula, "Protein partitioning in detergent-based aqueous two-phase systems," *J. Biotechnol.*, **28**, 263-275 (1993).

[9] Á. Sánchez-Ferrer, R. Bru, and F. García-Carmona, "Phase separation of biomolecules in polyoxyethylene glycol nonionic detergents," *Crit. Rev. Biochem. Mol. Biol.*, **29**, 275-313 (1994).

[10] P.-Å. Albertsson, "1. History of aqueous polymer two-phase partition," in *Partitioning in Aqueous Two-Phase Systems: Theory, Methods, Uses, and Applications to Biotechnology*, edited by H. Walter, D.E. Brooks, and D. Fisher, p. 1-10, Academic Press, Orlando (1985).

[11] T.E. Treffry, P.T. Sharpe, H. Walter, and D.E. Brooks, "4. Thin-layer countercurrent distribution and apparatus," in *Partitioning in Aqueous Two-Phase Systems: Theory, Methods, Uses, and Applications to Biotechnology*, edited by H. Walter, D.E. Brooks, and D. Fisher, p. 132-148, Academic Press, Orlando (1985).

[12] I.A. Sutherland, "5. Other types of countercurrent distribution apparatus and continuous flow chromatography techniques," in *Partitioning in Aqueous Two-Phase Systems: Theory, Methods, Uses, and Applications to Biotechnology*, edited by H. Walter, D.E. Brooks, and D. Fisher, p. 149-160, Academic Press, Orlando (1985).

[13] P.-Å. Albertsson, *Partition of Cell Particles and Macromolecules*, 3rd edition, John Wiley and Sons, New York (1986).

[14] J. Huddleston, A. Veide, K. Köhler, J. Flanagan, S.-O. Enfors, and A. Lyddiatt "The molecular basis of partitioning in aqeuous two-phase systems," *Trends in Biotechnol.*, **9**, 381-388 (1991).

[15] P.J. Flory, *Principles of Polymer Chemistry*, Cornell University Press, Ithaca, New York (1953).

[16] M. Modell and R.C. Reid, *Thermodynamics and Its Applications*, 2nd edition, Prentice-Hall, New Jersey (1983).

[17] D.E. Brooks, K.A. Sharp, and D. Fisher, "2. Theoretical aspects of partitioning," in *Partitioning in Aqueous Two-Phase Systems: Theory, Methods, Uses, and Applications to Biotechnology*, edited by H. Walter, D.E. Brooks, and D. Fisher, p. 11-84, Academic Press, Orlando (1985).

[18] N.L. Abbott, D. Blankschtein, and T.A. Hatton, "On protein partitioning in two-phase aqueous polymer systems," *Bioseparation*, **1**, 191-225 (1990).

[19] N.L. Abbott, D. Blankschtein, and T.A. Hatton, "Protein partitioning in two-phase aqueous polymer systems. 1. Novel physical pictures and a scaling-thermodynamic formulation," *Macromolecules*, **24**, 4334-4348 (1991).

[20] N.L. Abbott, D. Blankschtein, and T.A. Hatton, "Protein partitioning in two-phase aqueous polymer systems. 2. On the free energy of mixing globular colloids and flexible polymers," *Macromolecules*, **25**, 3917-3931 (1992).

[21] N.L. Abbott, D. Blankschtein, and T.A. Hatton, "Protein partitioning in two-phase aqueous polymer systems. 3. A neutron scattering investigation of the polymer solution structure and protein-polymer interactions," *Macromolecules*, **25**, 3932-3941 (1992).

[22] N.L. Abbott, D. Blankschtein, and T.A. Hatton, "Protein partitioning in two-phase aqueous polymer systems. 4. Proteins in solutions of entangled polymers," *Macromolecules*, **25**, 5192-5200 (1992).

[23] N.L. Abbott, D. Blankschtein, and T.A. Hatton, "Protein partitioning in two-phase aqueous polymer systems. 5. Decoupling of the effects of protein concentration, salt type, and polymer molecular weight," *Macromolecules*, **26**, 825-828 (1993).

[24] Y. Chevalier and T. Zemb, "The structure of micelles and microemulsions," *Rep. Prog. Phys.*, **53**, 279-371 (1990).

[25] C. Tanford, *The Hydrophobic Effect: Formation of Micelles and Biological Membranes*, John Wiley and Sons, New York (1980).

[26] J.N. Israelachvili, *Intermolecular and Surface Forces*, 2nd edition, Academic Press, London and San Diego (1991).

[27] D. Blankschtein, G.M. Thurston, and G.B. Benedek, "Phenomenological theory of equilibrium thermodynamic properties and phase separation of micellar solutions," *J. Chem. Phys.*, **85**, 7268-7288 (1986).

[28] V. Degiorgio, "Nonionic micelles," in *Physics of Amphiphiles: Micelles, Vesicles, and Microemulsions*, edited by V. Degiorgio and M. Corti, p. 303-335, North-Holland Physics Publishing, The Netherlands (1985).

[29] J. Sjöblom, P. Stenius, and I. Danielsson, "Phase equilibria of nonionic surfactants and the formation of microemulsions," in *Nonionic Surfactants: Physical Chemistry*, edited by M.J. Schick, p. 369-434, Marcel Dekker Inc., New York (1987).

[30] D. Blankschtein, G.M. Thurston, and G.B. Benedek, "Theory of phase separation in micellar solutions," *Phys. Rev. Lett.*, **54**, 955-958 (1985).

[31] G. Briganti, S. Puvvada, and D. Blankschtein, "Effect of urea on micellar properties of aqueous solutions of nonionic surfactants," *J. Phys. Chem.*, **95**, 8989-8995 (1991).

[32] A. Yu. Grosberg and A.R. Khokhlov, *Statistical Physics of Macromolecules*, AIP Press, New York (1994).

[33] M.E. Cates and S.J. Candau, "Static and dynamic of worm-like surfactant micelles," *J. Phys.: Condens. Matter*, **2**, 6889-6892 (1990).

[34] T.R. Carale and D. Blankschtein, "Theoretical and experimental determinations of the crossover from dilute to semidilute regimes of micellar solutions," *J. Phys. Chem.*, **96**, 459-467 (1992).

[35] T.M. Kole, C.J. Richards, and M.R. Fisch, "Evolution of the diffusion coefficient and correlation length of aqueous solutions of $C_{12}E_6$," *J. Phys. Chem.*, **98**, 4949-4954 (1994).

[36] H. Wennerström and B. Lindman, "Micelles. Physical chemistry of surfactant association," in *Physics Reports*, **52**, p. 1-86, North-Holland Publishing Cmpany (1979).

[37] J. Steinhardt and J.A. Reynolds, *Multiple Equilibria in Proteins*, Academic Press, New York and London (1969).

[38] J.A. Reynolds and C. Tanford, "Binding of dodecyl sulfate to proteins at high binding ratios. Possible implications for the state of proteins in biological membranes," *Proc. Natl. Acad. Sci., U.S.A.*, **66**, 1002-1007 (1970).

[39] J.A. Reynolds and C. Tanford, "The gross conformation of protein-sodium dodecyl sulfate complexes," *J. Biol. Chem.*, **245**, 5161-5165 (1970).

[40] A. Ray, J.A. Reynolds, H. Polet, and J. Steinhardt, "Binding of large organic anions and neutral molecules by native bovine serum albumin," *Biochemistry*, **5**, 2606-2616 (1966).

[41] J.A. Reynolds, S. Herbert, H. Polet, and J. Steinhardt, "The binding of divers detergent anions to bovine serum albumin," *Biochemistry*, **6**, 937-947 (1967).

[42] Y. Nozaki, J.A. Reynolds, and C. Tanford, "The interaction of a cationic detergent with bovine serum albumin and other proteins," *J. Biol. Chem.*, **249**, 4452-4459 (1974).

[43] A. Helenius and K. Simons, "The binding of detergents to lipophilic and hydrophilic proteins," *J. Boil. Chem.*, **247**, 3656-3661 (1972).

[44] S. Makino, J.A. Reynolds, and C. Tanford, "The binding of deoxycholate and Triton X-100 to proteins," *J. Biol. Chem.*, **248**, 4926-4932 (1973).

[45] P. Pradipasena, O. Israeli, M. Lu, S.-H. Chen, G. Briganti, and C.K. Rha, "Conformational changes in globular proteins induced by a nonionic surface active agent," in *Proceedings of ACS Symposium* (1991).

[46] A. Helenius and K. Simons, "Solubilization of membranes by detergents," *Biochim. Biophys. Acta*, **415**, 29-79 (1975).

[47] L. Hammar, S. Eriksson, K. Malm, and B. Morein, "Concentration and purification of feline leukaemia virus (FeLV) and its outer envelope protein gp70 by aqueous two-phase systms", *J. Virol. Methods*, **24**, 91-102 (1989).

[48] C.A. Miller, R.-N. Hwan, W.J. Benton, and T. Fort, Jr., "Ultralow interfacial tensions and their relation to phase separation in micellar solutions," *J. Colloid Interface Sci.*, **61**, 554-568 (1977).

[49] G.M. Thurston, "Studies of phase separation in micellar solutions," Ph.D. Thesis, Dept. of Physics, M.I.T. (1986).

[50] I.D. Kuntz and E. Kauzmann, "Hydration of proteins and polypeptides," *Adv. Protein Chem.*, **28**, 239-345 (1974).

[51] P.L. Dubin and J.M. Principi, "Optimization of size-exclusion separation of proteins on a Superose column," *J. Chromatogr.*, **479**, 159-164 (1989).

[52] M. Kunitz, "Crystalline soybean trypsin inhibitor. II. General properties," *J. Gen. Physiol.*, **30**, 291-310 (1947).

[53] S.M. Read, "Techniques for determining protein concentration," in *Protein and Enzyme Biochemistry*, p. 1-34, Elsevier Scientific Publishers Ireland Ltd. (1984).

[54] P.C. Hiemenz, "Chapter 5: Light scattering " in *Principles of Colloid and Surface Chemistry*, 2nd edition, Marcel Dekker Inc., New York (1986).

[55] S. Puvvada and D. Blankschtein, "Molecular-thermodynamic approach to predict micellization, phase behavior and phase separation of micellar solutions. I. Application to nonionic surfactants," *J. Chem. Phys.*, **92**, 3710-3724 (1990).

[56] B. Lindman and H. Wennerström, "Nonionic micelles grow with increasing temperature," *J. Phys. Chem.*, **95**, 6053-6054 (1991).

[57] P.J. Flory, *Statistical Mechanics of Chain Molecules*, Hanser Publishers, Munich and New York (1988).

[58] A. Naor, S. Puvvada, and D. Blankschtein, "An analytical expression for the free energy of micellization," *J. Phys. Chem.*, **96**, 7830-7832 (1992).

[59] C. Sarmoria and D. Blankschtein, "Conformational characteristics of short poly(ethylene oxide) chains terminally attached to a wall and free in aqueous solution," *J. Phys. Chem.*, **96**, 1978-1983 (1992).

[60] G.S. Stent, *Molecular Biology of Bacterial Viruses*, W.H. Freeman and Company, San Francisco (1963).

[61] S.E. Luria, J.E. Darnell, Jr., D. Baltimore, and A. Campbell, *General Virology*, 3rd edition, John Wiley and Sons, New York (1978).

[62] W. Earnshaw, S. Casjens, and S.C. Harrison, "Assembly of the head of bacteriophage P22: X-ray diffraction from heads, proheads and related structures," *J. Mol. Biol.*, **104**, 387-410 (1976).

[63] A.R. Poteete, "Bacteriophage P22," in *The Bacteriophages*, Vol. 2, edited by R. Calendar, p. 647-682, Plenum Press, New York (1988).

[64] M. Hayashi, A. Aoyama, D.L. Richardson, Jr., and M.N. Hayashi, "Biology of the bacteriophage ϕX174," in *The Bacteriophages*, Vol. 2, edited by R. Calendar, p. 1-71, Plenum Press, New York (1988).

[65] F.A. Eiserling, "Structure of the T4 virion," in *Bacteriophage T4*, edited by C.K. Mathews, E.M. Kutter, G. Mosig, and P.B. Berget, p. 11-24, American Society for Microbiology, Washington, D.C. (1983).

[66] L. Lue, C.-L. Liu, and D. Blankschtein, Unpublished Results.

[67] K.M. Jansons and C.G. Phillips, "On the application of geometric probability theory to polymer networks and suspensions, I," *J. Colloid Interface Sci.*, **137**, 75-91 (1990).

[68] B.J. Berne and R. Pecora, *Dynamic Light Scattering, with Application to Chemistry, Biology, and Physics*, John Wiley and Sons, New York (1976).

[69] P.-Å. Albertsson, "Chapter 9: Biotechnical application," in *Partition of Cell Particles and Macromolecules*, 3rd edition, John Wiley and Sons, New York (1986).

[70] J.M. Smith and H.C. van Ness, "Chapter 8: Phase equilibria," in *Introduction to Chemical Engineering Thermodynamics*, McGraw-Hill Book Company, New York (1975).

[71] S.I. Sandler, *Chemical and Engineering Thermodynamics*, p. 238-240, John Wiley and Sons, New York (1977).

[72] L. Philipson, P.-Å. Albertsson, and G. Frick, "The purification and concentration of viruses by aqueous polymer phase systems," *Virology*, **11**, 553-571 (1960).

[73] P.-Å. Albertsson, "Chapter 10: Two-phase separation of viruses," in *Methods Virol.*, Vol. II, edited by K. Maramorosch and H. Koprowski, Academic Press, New York (1967).

[74] P.-Å. Albertsson, "Chapter 5: Biphasic separation of microbial particles," in *Methods Microbiol.*, Vol. 5B, edited by J.R. Norris and D.W. Ribbons, Academic Press, London and Orlando (1971).

[75] L. Walin, R. Tuma, G.J. Thomas, and D.H. Bamford, "Purification of viruses and macromolecular assemblies for structural investigations using a novel ion exchange method," *Virology*, **201**, 1-7 (1994).

[76] R.C. Williams and D. Fraser, "Morphology of the seven T-bacteriophages," *J. Bact.*, **66**, 458-464 (1953).

[77] B. Chu, *Laser Light Scattering*, 2nd edition, Academic Press, San Diego (1991).

[78] M. Born and E. Wolf, "Chapter 2: Electromagnetic Potentials and Polarization," in *Principle of Optics*, 6th edition, Pergamon Press, Oxford (1980).

[79] B. Chu, "Chapter 7: Methods of data analysis," in *Laser Light Scattering*, 2nd edition, Academic Press, San Diego (1991).

[80] T.R. Carale, Q.T. Pham, and D. Blankschtein, "Salt effects on intramicellar interactions and micellization of nonionic surfactants in aqueous solutions," *Langmuir*, **10**, 109-121 (1994).

[81] "Properties of water in the range 0 - 100°C,", in *CRC Handbook of Chemistry and Physics*, 71st edition, p. 6-8, CRC Press, Inc., Ann Arbor (1990).

[82] J.A. McDonald and A.R. Rennie, "A structural study of mixed micelles containing C_{16}TAB and $C_{12}E_6$ surfactants," *Langmuir*, **11**, 1493-1499 (1995).

[83] P.G. deGennes, *Scaling Concepts in Polymer Physics*, Cornell University Press, Ithaca, NY (1979).

[84] J. Rouch, P. Tartaglia, A. Safouane, and S.H. Chen, "Reexamination of the static and dynamic critical phenomena in water-amphiphile micellar solutions," *Physical Review A*, **40**, 2013-2021 (1989).

[85] S.H. Chen, J. Rouch, and P. Tartaglia, "Universality of critical phenomena in complex fliuds," *Physica A*, **204**, 134-151 (1994).

[86] P.-Å. Albertsson, S. Sasakawa, and H. Walter, "Cross partition and isoelectric points of proteins," *Nature*, **228**, 1329-1330 (1970).

[87] G. Johansson, "6. Partitioning of proteins," in *Partitioning in Aqueous Two-Phase Systems: Theory, Methods, Uses, and Applications to Biotechnology*, edited by H. Walter, D.E. Brooks, and D. Fisher, p. 161-226, Academic Press, Orlando (1985).

[88] M. Svensson, P. Linse, and F. Tjerneld, "Phase behavior in aqueous two-phase systems containing micelle-forming block copolymers," *Macromolecules*, **28**, 3597-3603 (1995).

[89] J. Leclerc and J. de Rudder, "Process for the isolation of viral glycoproteic antigens and its application to the preparation of vaccine," U.S. Patent 4,334,935 (1982).

[90] J.M. Smith and H.C. van Ness, "Chapter 7: Thermodynamic properties of homogeneous mixtures," in *Introduction to Chemical Engineering Thermodynamics*, McGraw-Hill Book Company, New York (1975).

[91] P.C. Hiemenz, "Chapter 3: Solution thermodynamics: Osmotic and Donnan equilibria, " in *Principles of Colloid and Surface Chemistry*, 2nd edition, Marcel Dekker Inc., New York (1986).

[92] D.A. McQuarrie, "Chapter 12: Imperfect gases," in *Statistical Mechanics*, Harper and Row Publishers, Inc., New York (1976).

[93] M.H. Adams, "Methods of study of bacterial viruses," in *Methods in Medical Research,* Vol. 2, edited by J.H. Comroe, Jr., p. 1-73, Year Book Publishers, Inc., Chicago (1950).